

A Critical Review of the Absorption Cross-Sections of O₃ and NO₂ in the 240–790 nm Region

Part 1. Ozone

ESA Technical Note MO-TN-ESA-GO-0302

March 15, 2002

Prepared by

Johannes Orphal,

Chargé de Recherche

Laboratoire de Photophysique Moléculaire,

CNRS, Orsay, France

for the

European Space Agency (ESA-ESTEC, Noordwijk, The Netherlands)

Technical Officer: Jörg Callies

Structure of this document

Chapter 1 is a brief introduction.

In Chapter 2, a few definitions are given.

The following text is divided in two parts:

Part I (Chapters 3–11) is a review of the O₃ cross-sections, Part II (Chapters 11–20) is a review of the NO₂ cross-sections.

In Chapter 3, the measurements that are available for the O₃ review are presented.

In Chapter 4, the overall structure of the O₃ spectrum in the region 240–790 nm is discussed.

In Chapter 5, the sensitivity of the O₃ cross-sections in the region 240–790 nm with respect to wavelength shifts and spectral resolution is investigated.

In Chapter 6, the available O₃ cross-sections at room temperature are compared.

- In Section 6.1., absolute values of the O₃ cross-sections at room temperature are compared at 10 discrete wavelengths between 253.65 nm and 263.82 nm.
- In Section 6.2., the available broad-band O₃ cross-sections at room temperature are compared at all available wavelengths. Systematic differences are discussed.
- In Section 6.3., integrated cross-sections in different spectral regions are calculated and compared.
- In Section 6.4, the cross-sections in the Huggins bands (323–343 nm) are evaluated using a non-linear least-squares fitting program, leading to conclusions about wavelength shifts and absolute cross-sections.

In Chapter 7, the available O₃ cross-sections at lower temperatures are compared and discussed using the same procedures as employed in Chapter 6.

In Chapter 8, some empirical models to reproduce the temperature-dependence of the O₃ cross-sections are compared.

In Chapter 9, the pressure-dependence of the O₃ cross-sections is discussed.

Chapter 10 contains some conclusions of the review of the O₃ cross-sections.

In Chapter 11, recommendations for remote-sensing of O₃ are proposed.

Acknowledgements

The author thanks J. Callies, M. Eisinger, A. Hahne, C. Readings, and T. Wehr from the Earth Science Division of ESA-ESTEC for initiating and supporting this work.

Helpful support by K. Bogumil, J. Brion, J. P. Burrows, M. Carleer, K. V. Chance, J.-M. Flaud, J. Malicet, M.-F. Mérienne, and A. C. Vandaele is gratefully acknowledged.

Thanks to all who have commented and reviewed the draft version.

Without the patience of my wife Annette this report would not have been produced.

Adress of the author

Johannes Orphal, Chargé de Recherche
Laboratoire de Photophysique Moléculaire
Centre National de la Recherche Scientifique
Bât. 350, Université de Paris-Sud
91405 Orsay Cedex, France
Phone +33 1 69157528
Fax +33 1 69157530
Johannes.Orphal@ppm.u-psud.fr

Contents

1. Introduction	6
2. Definitions	7
2.1. Absorption cross-section	7
2.2. Spectral resolution and instrumental line shape	7
2.3. Air-vacuum correction	8
2.4. Convolution	9
2.5. References for Chapter 2	10
3. Measurements of O ₃ absorption cross-sections in the 240–790 nm region	11
3.1. Description of the measurements	11
3.2. References for Chapter 3	17
4. The O ₃ absorption cross-sections in the 240–790 nm region	22
5. Sensitivity of the O ₃ cross-sections to wavelength shifts and resolution	25
6. Comparison of the O ₃ cross-sections at 298±5 K between 240–790 nm	31
6.1. Comparison of room temperature cross-sections at selected wavelengths	
6.1.1. 253.65 nm (Hg line)	31
6.1.2. 289.36 nm (Hg line)	32
6.1.3. 296.73 nm (Hg line)	34
6.1.4. 302.15 nm (Hg line)	35
6.1.5. 334.15 nm (Hg line)	36
6.1.6. 543.52 nm (HeNe laser line)	36
6.1.7. 576.96 nm (Hg line)	37
6.1.8. 594.10 nm (HeNe laser line)	38
6.1.9. 604.61 nm (HeNe laser line)	39
6.1.10. 611.97 nm (HeNe laser line)	40
6.1.11. 632.82 nm (HeNe laser line)	41
6.1.12. Summary of Section 6.1.	43

6.2. Comparison of room temperature cross-sections over large regions	45
6.2.1. Comparison of the O ₃ absorption cross-sections at room temperature at all available wavelengths	45
6.2.2. Integrated O ₃ cross-sections at room temperature	55
6.2.3. Comparison of the O ₃ cross-sections at room temperature in the Huggins bands using non-linear least-squares fits	56
6.2.4. Summary of Section 6.2.	60
7. Comparison of the O ₃ cross-sections between 230–790 nm at temperatures below room temperature (203–280 K)	61
7.1. Relative change of the O ₃ cross-sections with temperature	61
7.2. Comparison of the absolute O ₃ cross-sections at all available wavelengths at temperatures below ambient: 276±4 K, 243±3 K, 221±3 K, and 203±1 K	70
7.3. Comparison of the integrated O ₃ cross-sections at temperatures below ambient: 276±4 K, 243±3 K, 221±3 K, and 203±1 K	103
7.4. Non-linear least-squares fits of the O ₃ cross-sections in the Huggins bands at temperatures below ambient: 276±4 K, 243±3 K, 221±3 K, and 203±1 K	111
8. Empirical models for the temperature-dependence of the O ₃ cross-sections in the 240–790 nm region	114
9. Pressure-dependence of the O ₃ cross-sections in the 240–790 nm region	117
10. Conclusions of the O ₃ review	118
11. Recommendations for atmospheric remote-sensing	122
Annex A: Influence of the convolution and the ILS in the Huggins bands	126

1. Introduction

In the past decade, a new generation of multi-spectral remote-sensing instruments using medium-resolution diode-array spectrometers in the ultraviolet, visible, and near-infrared has been developed. Since the successful launch of the first of these new experiments, GOME onboard ERS-2, in 1995, it is possible to study global O₃ concentrations using the full spectral information in the 240–790 nm region. Besides the improved accuracy for the O₃ measurements that results from this broad spectral coverage at medium resolution (including O₃ profile retrieval), it is possible to detect many other species of atmospheric relevance (NO₂, H₂O, BrO, OCIO, SO₂, H₂CO, NO₃) as well as atmospheric properties such as cloud coverage, cloud optical depth, aerosols distributions, surface albedo, etc.

GOME will be followed by the SCIAMACHY instrument (launched in march 2001 onboard ENVISAT-1), by the GOME-2 instruments onboard the METOP satellites (first launch in 2005), by the OMI instruments onboard EOS-Aura (launch in 2003) and by other UV-visible spectrometers using diode-array detectors. For GOME and these equivalent sensors, accurate knowledge of the absorption strengths of the target species at atmospheric conditions (temperature, pressure) is required.

In this report, an attempt is made to review the available laboratory measurements of the absorption cross-sections of O₃ and NO₂ for the new atmospheric remote-sensing instruments. It is a difficult task to compare laboratory measurements. We have used several methods to take into account possible sources for systematic errors: studying the influence of resolution and wavelength accuracy on the cross-sections, comparing the cross-sections at single wavelengths, comparing the cross-sections over broad spectral regions, comparing integrated cross-sections, studying the influence of temperature, using non-linear least-squares fits in regions where the cross-sections vary rapidly with wavelength, comparing different approaches to model the cross-sections. This list is probably not complete, and we are open for any comments, questions, and suggestions for future work: please send an e-mail to Johannes.Orphal@ppm.u-psud.fr – always with a copy to Joerg.Callies@esa.int.

The present report was prepared upon action of the GOME Science Advisory Group during its 30. Meeting at ESRIN (Frascati, Oct. 2000), presented to the GOME Science Advisory Group during its 31. Meeting (Bremen, Feb. 2001), and delivered to ESA-ESTEC in March, 2001 (Part 1) and in July, 2001 (Part 2). It was reviewed in 2001 by the GOME groups and other scientists involved in UV-visible cross-section measurements and applications for atmospheric remote-sensing. It was accepted by the GOME Science Advisory Group in October, 2001 during its 32. Meeting.

2. Definitions

2.1. Absorption cross-section

The absorption cross-section $\sigma(\lambda, T, p)$ (in $\text{cm}^2 \text{ molecule}^{-1}$) is a molecule-specific quantity to characterize its absorption strength, a quantity that generally changes with wavelength λ (in nm), with temperature T (in K), and with total pressure p (in Pa).

In order to determine this quantity, laboratory measurements need to be performed. The most common method is to measure the spectral intensity $I(\lambda, T, p)$ after passing a sample of the molecular species of interest that is kept in a cell of length L (in cm) at temperature T and total pressure p , having previously measured the spectral intensity $I_0(\lambda)$ of the white-light source without any absorber in the cell. The absorption cross-section can then be calculated as

$$\sigma(\lambda, T, p) = -\ln [I(\lambda, T, p) / I_0(\lambda)] \times 1 / (\rho(p, T) \times L)$$

where $\rho(p, T)$ (in molecules/cm^3) is the molecular density defined as

$$\rho(p, T) = p/P_0 \times T_0/T \times N_L$$

with N_L being the Loschmidt constant ($N_L = 2.6868 \times 10^{19} \text{ molecules/cm}^3$) which is defined as the Avogadro constant ($N_A = 6.0221 \times 10^{23} \text{ molecules/mole}$) divided by the molar volume ($V_{mol} = 22414.1 \text{ cm}^3/\text{mole}$) at normal temperature $T_0 = 273.15 \text{ K}$ and normal pressure $p_0 = 101325 \text{ Pa}$.

The absorption cross-sections need to be measured at a spectral resolution that is sufficiently high to eliminate any influence of the instrumental line shape, and with a sampling grid that is sufficiently dense to avoid undersampling effects (at least two independent sampling points over the spectral interval corresponding to the spectral resolution). The wavelength accuracy must be high enough to eliminate any artefacts due to wavelength calibration errors.

Generally, the requirements on spectral resolution, spectral sampling, and on wavelength accuracy depend on the molecular species and on the spectral region, and can also change as for different temperatures and/or pressures of the sample.

2.2. Spectral resolution and instrumental line shape

The spectral resolution depends on the experimental set-up employed for measuring the absorption cross-sections.

For dispersive spectrometers, the spectral resolution is commonly given as the full width at half maximum of the instrumental line shape (ILS) which depends generally on the optical configuration of the spectrometer and which is also a function of the

wavelength. The instrumental line shape is only analytically defined for ideal dispersive spectrometers. In real life it needs to be measured with an independent method, e.g. by using a narrow-band line source that is scanned over the spectral region of interest.

For absorption measurements using lasers or atomic emission lines (Hg or others) the spectral resolution depends on the intrinsic linewidth of the source and needs to be measured with an independent method, e.g. a high-resolution spectrometer. In most cases where atomic emission lines are used, it is necessary to use narrow optical filters to eliminate parasitic lines emitting at different wavelengths.

For interferometric measurements (e. g. Michelson interferometers) the spectral resolution depends on the maximum optical path difference between the interfering beams. Note that in this case the instrumental line shape (which can be extremely narrow when using large path differences but is only well defined for ideal interferometers) is generally constant in units of wavenumbers ($1/\lambda$ in cm^{-1}) and therefore varies with wavelength. The product of the wavelength λ (in nm) and of the wavenumber k (in cm^{-1}) is

$$\lambda \times k = 10^7$$

e.g. a wavelength of 250 nm corresponds to exactly 40000 cm^{-1} . A useful relation for converting a wavenumber interval Δk (in cm^{-1}) at a given wavenumber k (in cm^{-1}) into a wavelength interval $\Delta\lambda$ (in nm) at the corresponding wavelength λ is

$$\Delta\lambda = 10^7 \times \Delta k / k^2 = \lambda \times \Delta k / k$$

For example, a spectral resolution of 1.0 cm^{-1} at 40000 cm^{-1} (250 nm) corresponds to a spectral resolution of 0.00625 nm. The same spectral resolution of 1.0 cm^{-1} but at 20000 cm^{-1} (500 nm) corresponds to a spectral resolution of 0.025 nm.

2.3. Air-vacuum correction

The wavelength depends on the medium in which the measurements are performed. For the transformation of wavelengths measured in air λ_{air} (in nm) into wavelengths in vacuum λ_{vac} (in nm), the formula proposed by *Edlén* in 1966 is applied:

$$\lambda_{vac} = \lambda_{air} \times (1.0000834213 + 2.40603 \times 10^{-2} / (130 - 10^6 / \lambda_{air}^2) + 1.5997 \times 10^{-4} / (38.9 - 10^6 / \lambda_{air}^2))$$

Note that wavelengths in vacuum are always larger than in air. The above formula is given for “standard” air (dry air, 15°C, 760 Torr). For different conditions (other mixtures, temperatures, pressures, ...) the above formula is not applicable. For the remainder of this report, standard conditions are assumed when using the *Edlén* formula of 1966. All wavelengths in this report are given in air.

2.4. Convolution

The convolution is a mathematical operation that creates a new data set $g(x)$ which was obtained by calculating the point-wise averages over the original data $f(x)$ with a weighting function $h(x)$ that can be selected arbitrarily:

$$g(x) = f(x) \otimes h(x) = \int \{ f(x-k) \times g(k) \} dk$$

For instance, measuring a spectrum which has sharp spectral features with a lower experimental resolution than required corresponds to the convolution of the real spectrum $I_{real}(\lambda)$ with an instrumental line shape $ILS(\lambda)$, yielding a convoluted spectrum $I_{conv}(\lambda)$:

$$I_{conv}(\lambda) = I_{real}(\lambda) \otimes ILS(\lambda) = \int \{ I_{real}(\lambda-\lambda') \times ILS(\lambda') \} d\lambda'$$

It is important to note that, because laboratory spectra are always measured using the ratio between a spectrum without and a spectrum with an absorber in the cell, the convolution with the ILS always takes place on the spectrum and not on the cross sections, i.e.

$$\sigma_{conv}(\lambda) = \sigma_{real}(\lambda) \otimes ILS(\lambda)$$

does not produce cross sections which necessarily correspond to those obtained from the ratio

$$\sigma(\lambda, T, p) = -\ln [I(\lambda, T, p) / I_0(\lambda)] \times 1 / (p(p, T) \times L)$$

In general, therefore, comparing cross-sections recorded at different spectral resolutions is not straightforward, and the correctness of the results depend on the sharpness of the spectral features in the original spectrum, the shape of the white light source employed, and the instrumental line shape. Even worse, using cross sections which were recorded at high resolution to resolve all structures in the real spectrum, and convoluted with the ILS before calculating the transmission will always lead to systematic errors, in particular in regions with sharp spectral features. And equally, using cross-sections recorded at low spectral resolution will not fully reproduce atmospheric spectra – except in the case that the O_3 amount in the atmospheric spectrum is the same as during the laboratory measurement.

This problem is a serious one. It means that only laboratory spectra that were recorded at sufficiently high spectral resolution to resolve all structures without influence of the ILS can be compared to obtain the best agreement. If spectra at lower resolutions are compared, they must have been recorded at exactly the same experimental conditions, in particular concerning the amount of absorbers and the shape of the light source. This is in general not the case. Therefore, in regions with sharp spectral features, the comparison of low-resolution absorption cross-sections with those recorded at high resolution, even after convolution of the high-resolution

cross-sections (which is wrong) or convolution of the high-resolution transmission spectrum (except for reproducing exactly the conditions during recording of the low-resolution spectrum), will produce systematic differences which are only due to the convolution problem.

The difficulties arising from this problem are presented in a recent paper by *Vandaele and Carleer*, who propose an iterative algorithm to circumvent the artefacts produced by the recording of low- or medium-resolution spectra.

Fortunately, for spectra with broad spectral features (i.e. when the ILS is narrow compared to width of the spectral structures) the convolution problem is negligible.

Also, for weak absorptions (less than 1% change in transmission), the convolution that takes place on the transmission spectrum is commutable with the logarithm function, due to the linearity of the latter function for small arguments. Only then, no systematic errors due to the convolution procedure occur. For all strong absorbers (e.g. H₂O or O₂ in the visible and O₃ in the UV) this is however not the case.

2.5. References for Chapter 2

E. R. Cohen and B. N. Taylor: "The Fundamental Physical Constants", *Physics Today* 49 Supplement, 9–13, 1996.

F. A. Jenkins and H. E. White: "Fundamentals of Optics", 4th Edition, McGraw-Hill, Singapore, 1981.

B. Edlén, "The Refractive Index of Air", *Metrologia* 2, 71–80, 1966.

A. C. Vandaele and M. Carleer, "Development of Fourier transform spectrometry for UV-visible differential optical absorption spectroscopy measurements of tropospheric minor constituents", *Appl. Opt.* 38, 2630–2639, 1999.

M. Young, "Optics and Lasers", 5th Revised and Enlarged Edition, Springer, Berlin, 2000.

3. Available laboratory O₃ absorption cross-sections in the 240–790 nm region

3.1. Description of the measurements

For the present review, the following measurements were considered:

A) Measurements of absolute O₃ cross-sections at single wavelengths

1. Hearn (Proc. Phys. Soc. 78, 932–940, 1961):

Instrument: Cary recording spectrophotometer

Spectral resolution: 0.01 nm and 0.09 nm (line at 253.7 nm)

Wavelengths: 6 lines between 253.7–577.0 nm

Wavelength uncertainty: 0.1 nm

Temperatures: 295 K

Temperature uncertainty: not indicated

Light source reference spectra: recorded rapidly before and after the ozone spectra using a rotating shutter

Absolute scaling: measurements of the decomposition of pure O₃ into O₂

Stated cross-section uncertainty: 0.4–2.1%

2. Yoshino et al. (Planet. Space Sci. 36, 395–398, 1988):

Instrument: 0.3 m Czerny–Turner vacuum monochromator, and 6.65 m photoelectric scanning spectrometer

Spectral resolution: 0.13 nm (below 264 nm) and 0.003 nm (above 264 nm)

Wavelengths: 13 lines between 238.3–344.4 nm

Wavelength uncertainty: 0.001 nm

Temperatures: 295 K, 228 K, 195 K

Temperature uncertainty: not indicated

Light source reference spectra: recorded after the ozone spectra

Absolute scaling: measurements of total pressure

Stated cross-section uncertainty: 0.7%

3. Mauersberger et al. (Geophys. Res. Lett. 13, 671–673, 1986; J. Geophys. Res. D 92, 8480–8482, 1987; J. Geophys. Res. D 92, 14861–14864, 1987):

Instrument: Hg lamp

Spectral resolution: not stated

Wavelengths: 1 line at 253.65 nm

Wavelength uncertainty: not stated

Temperatures: 195 K, 221 K, 237 K, 253 K, 273 K, 297 K, 318 K, 335 K, 351 K

Temperature uncertainty: 0.1 K

Light source reference spectra: recorded after the ozone spectra

Absolute scaling: measurements of total pressure and temperature

Stated cross-section uncertainty: 0.5%–0.7%

4. Malicet et al. (Chem. Phys. Lett. 158, 293–296, 1989):

Instrument: 1.5 m Czerny-Turner spectrometer

Spectral resolution: not stated

Wavelengths: 1 line at 253.65 nm

Wavelength uncertainty: not stated

Temperatures: 229 K, 295 K

Temperature uncertainty: 0.05 K.

Light source reference spectra: recorded before and after the ozone spectra

Absolute scaling: measurements of total pressure

Stated cross-section uncertainty: 1.8%

5. Anderson and Mauersberger (Geophys. Res. Lett. 19, 933–936, 1992):

Instrument: HeNe laser

Spectral resolution: not stated

Wavelengths: 5 lines between 543.5–632.8 nm

Wavelength uncertainty: not stated

Temperatures: 295 K

Temperature uncertainty: 0.5 K.

Light source reference spectra: recorded before and after the ozone spectra

Absolute scaling: measurements of total pressure

Stated cross-section uncertainty: 0.8%

B) Measurements of absolute O₃ cross-sections over large spectral regions

6. Inn and Tanaka (J. Opt. Soc. Am. 43, 870–873, 1953)

Instrument: Cary recording double-beam spectrophotometer

Spectral resolution: 0.1 (below 350 nm) and 0.5 nm (above 400 nm)

Wavelength range: 200–350 nm and 400–750 nm

Wavelength uncertainty: 0.01 nm

Data format: not available in digital form, values at single wavelengths can be found in the literature (*Hearn, Griggs*)

Temperatures: 300 K

Temperature uncertainty: not indicated

Light source reference spectra: recorded simultaneously

Absolute scaling: measurements of total pressure

Stated cross-section uncertainty: 5% (*Hearn* writes 2% stated by the authors)

7. Griggs (J. Chem. Phys. 49, 857–859, 1968)

Instrument: Beckman DK-1A dual-beam spectrometer

Spectral resolution: 0.1 (below 350 nm) and 0.5 nm (above 400 nm)

Wavelength range: 200–360 nm and 450–850 nm
Wavelength uncertainty: 0.2 nm (below 360 nm) and 1.5 nm (above 450 nm)
Data format: not available in digital form, values at single wavelengths are given in the paper
Temperatures: 303 K
Temperature uncertainty: not indicated
Light source reference spectra: recorded simultaneously
Absolute scaling: measurements of total pressure
Stated cross-section uncertainty: 1.5% except for the regions 350–360 nm (6%), 450–480 nm (5%) and 830–850 nm (5%)

8. Vigroux (Ann. Géophys. 25, 169–172, 1969)

Instrument: Hilger medium
Spectral resolution: not stated
Wavelength range: 230–270 nm
Wavelength uncertainty: not stated
Data format: not available in digital form, values at single wavelengths are given in the paper
Temperatures: 291K
Temperature uncertainty: 1 K
Light source reference spectra: recorded simultaneously
Absolute scaling: chemical titration
Stated cross-section uncertainty: 1.3%

9. Molina and Molina (J. Geophys. Res. D 91, 14501–14508, 1986):

Instrument: Cary 219 double-beam spectrophotometer
Spectral resolution: 0.07 nm
Wavelength range: 185–350 nm
Wavelength uncertainty: 0.05 nm
Data format: in steps of 0.5 nm (modified data)
Temperatures: 298 K, 263 K, 226 K
Temperature uncertainty: 1 K
Light source reference spectra: recorded before and after two ozone spectra
Absolute scaling: measurements of total pressure
Stated cross-section uncertainty: 1%

10. Cacciani et al. (J. Geophys. Res. D 94, 8485–8490, 1989):

Instrument: 1 m Jobin Yvon double monochromator
Spectral resolution: 0.012 nm
Wavelength range: 339–355 nm
Wavelength uncertainty: not indicated
Data format: in steps of 0.1 nm

Temperatures: 220 K, 293 K
Temperature uncertainty: not indicated
Light source reference spectra: recorded simultaneously
Absolute scaling: measurements of total pressure
Stated cross-section uncertainty: 3-4%

11. *Amoruso et al. (J. Geophys. Res. D 95, 20565–20568, 1990):*

Instrument: 1 m Jobin Yvon double monochromator
Spectral resolution: 0.05 nm
Wavelength range: 590–610nm
Wavelength uncertainty: not indicated
Data format: in steps of 0.1 nm (not available but values at selected wavelengths are given in the paper)
Temperatures: 230 K, 299 K
Temperature uncertainty: not indicated
Light source reference spectra: recorded simultaneously
Absolute scaling: measurements of total pressure
Stated cross-section uncertainty: 2%

12. *Johnston (unpublished data, 1990):*

Instrument: –
Spectral resolution: –
Wavelength range: 408–600 nm
Wavelength uncertainty: –
Data format: in steps of 0.4 nm
Temperatures: 295 K
Temperature uncertainty: –
Light source reference spectra: –
Absolute scaling: –
Stated cross-section uncertainty: –

13. *Brion et al. (J. Atm. Chem. 15, 145–155, 1992; Chem. Phys. Lett. 213, 610–612, 1993; J. Atm. Chem. 21, 263–273, 1995):*

Instrument: Jobin Yvon THR1500 and THR 640 spectrometers
Spectral resolution: 0.01 nm
Wavelength range: 195–345 nm (except at 273 K: 300–345 nm)
Wavelength uncertainty: not stated
Data format: in steps of 0.01 nm
Temperatures: 218 K, 228 K, 243 K, 273 K, 295 K
Temperature uncertainty: 0.3 K
Light source reference spectra: recorded before and after the ozone spectra
Absolute scaling: measurements of total pressure

Stated cross-section uncertainty: 1.3–2.5%

14. *Brion et al.* (J. Atm. Chem. 30, 291–299, 1998):

Instrument: Jobin Yvon THR 640 spectrometer

Spectral resolution: 0.02 nm

Wavelength range: 345–830 nm

Wavelength uncertainty: not stated

Data format: in steps of 0.01 nm

Temperatures: 218 K, 228 K, 243 K, 273 K, 295 K

Temperature uncertainty: 0.3 K

Light source reference spectra: recorded simultaneously

Absolute scaling: measurements of total pressure

Stated cross-section uncertainty: 1.5% (420–830 nm), 1.5–4% (350–420 nm)

15. *Burrows et al.* (J. Quant. Spectrosc. Rad. Transf. 61, 50–517, 1999):

Instrument: GOME-FM (monochromator with 4 diode-array detectors)

Spectral resolution: 0.2–0.4 nm

Wavelength range: 231–794 nm

Wavelength uncertainty: 0.03 nm

Data format: in steps of 0.12–0.21 nm

Temperatures: 202 K, 221 K, 241 K, 273 K, 293 K

Temperature uncertainty: 2 K

Light source reference spectra: recorded before and after the ozone spectra

Absolute scaling: using a chemical titration at 293 K assuming temperature-independent cross-sections for all lower temperatures

Stated cross-section uncertainty: 2.6–4.6%

C) Measurements of relative O₃ absorption spectra over large spectral regions

16. *Freeman et al.* (Planet. Space Sci. 32, 239–248, 1984):

Instrument: 6.65 m photoelectric scanning spectrometer

Spectral resolution: 0.003 nm

Wavelength range: 254–350 nm

Wavelength uncertainty: less than 0.001 nm

Data format: in steps of 0.006–0.0012 nm

Temperatures: 195 K

Temperature uncertainty: not indicated

Light source reference spectra: recorded before and after the ozone spectra

Absolute scaling: using the values of *Yoshino et al.* at 195 K

Stated cross-section uncertainty: 1.0%.

17. Bass and Paur (J. Photochem. 17, 141–144, 1981; Geophys. Res. Lett. 9, 227–230, 1982; Proc. Quadr. Ozone Sympos., 606–614, 1985):

Instrument: 1.8 m Ebert scanning monochromator

Spectral resolution: less than 0.025 nm

Wavelength range: 245–343 nm

Wavelength uncertainty: less than 0.025 nm

Data format: in steps of 0.05 nm (quadratic coefficients for each wavelength)

Temperatures: 203K, 218 K, 228 K, 243 K, 273 K, 298 K

Temperature uncertainty: 0.25 K

Light source reference spectra: recorded simultaneously

Absolute scaling: using the value of *Hearn* at 253.65 nm and a 1% increase at this wavelength between 298 K and 203 K

Stated cross-section uncertainty: 1.0%.

18. Burkholder and Talukdar (Geophys. Res. Lett. 21, 581–584, 1994):

Instrument: grating spectrograph with a diode-array detector

Spectral resolution: not stated

Wavelength range: 407–763 nm

Wavelength uncertainty: 0.2 nm

Data format: in steps of 1.0 nm

Temperatures: 220 K, 240 K, 260 K, 280 K, 298 K

Temperature uncertainty: 1–3 K

Light source reference spectra: recorded simultaneously

Absolute scaling: using the values of *Anderson and Mauersberger* at 298 K

Stated cross-section uncertainty: 1–5%.

19. Richter et al. (unpublished data, 1996):

Instrument: GOME-FM (monochromator with 4 diode-array detectors)

Spectral resolution: 0.2–0.4 nm

Wavelength range: 231–794 nm

Wavelength uncertainty: not stated

Data format: in steps of 0.12–0.21 nm

Temperatures: 202 K, 221 K, 241 K, 273 K, 293 K

Temperature uncertainty: 2 K

Light source reference spectra: recorded before and after the ozone spectra

Absolute scaling: using the values of *Bass and Paur* at all temperatures in the 304.5–305.5 nm window

Stated cross-section uncertainty: not stated

20. Voigt et al. (J. Photochem. Photobiol. A 143, 1-9, 2001):

Instrument: Bruker IFS-120HR Fourier-transform spectrometer

Spectral resolution: 5 cm⁻¹

Wavelength range: 231–851 nm
Wavelength uncertainty: less than 0.1 cm⁻¹
Data format: in steps of 0.08–0.14 nm
Temperatures: 203 K, 223 K, 246 K, 280 K, 293 K
Temperature uncertainty: 2 K
Light source reference spectra: recorded before and after the ozone spectra
Absolute scaling: using the values of *Burrows et al.* at all temperatures
Stated cross-section uncertainty: 3–6%.

21. Bogumil et al. (Proc. ERS-ENVISAT Sympos., 2000 ; Chem. Phys. Lett. 349, 241-248, 2001):

Instrument: SCIAMACHY PFM (monochromator with 8 diode-array detectors)
Spectral resolution: 0.2–0.4 nm
Wavelength range: 230–1070 nm
Wavelength uncertainty: less than 0.01 nm
Data format: in steps of 0.14–0.20 nm
Temperatures: 203 K, 223 K, 243 K, 273 K, 293 K
Temperature uncertainty: 2 K
Light source reference spectra: recorded before and after the ozone spectra
Absolute scaling: using the values of *Bass and Paur* at all temperatures
Stated cross-section uncertainty: 3.1%.

An extensive list of publications related to laboratory measurements of O₃ cross-sections in the 240–790 nm region is given below.

3.2. References for Chapter 3

G. L. Humphrey and R. M. Badger, "The Absorption Spectrum of Ozone in the Visible", *J. Chem. Phys.* 15, 794-798, 1947.

A. Vassy and E. Vassy, "Effect of Temperature on the Absorption Spectrum of Ozone: Chappuis bands", *J. Chem. Phys.* 16, 1163-1164, 1948.

E. Vigroux, "Contribution à l'Étude Expérimentale de l'Absorption de l'Ozone", *Ann. Phys.* 8, 709-762, 1953.

E. C. Y. Inn and Y. Tanaka, "Absorption Coefficients of Ozone in the Ultraviolet and Visible Regions", *J. Opt. Soc. Am.* 43, 870-873, 1953.

E. C. Y. Inn and Y. Tanaka, "Ozone Absorption Coefficients in the Visible and Ultraviolet Regions", *Adv. Chem. Ser.* 21, 263–268, 1958.

- A. G. Hearn, "The Absorption of Ozone in the Ultraviolet and Visible Regions of the Spectrum", *Proc. Phys. Soc.* 78, 932-940, 1961.
- W. B. De More and O. Raper, "Hartley Band Extinction Coefficients of Ozone in the Gas Phase and in Liquid Nitrogen, Carbon Monoxide, and Argon", *J. Phys. Chem.* 68, 412-414 (1964).
- E. Vigroux, "Détermination des Coefficients Moyens de l'Absorption de l'Ozone en Vue des Observations Concernant l'Ozone Atmosphérique à l'Aide du Spectromètre Dobson", *Ann. Phys.* 2, 209-215, 1967.
- M. Griggs, "Absorption Coefficients of Ozone in the Ultraviolet and Visible Regions", *J. Chem. Phys.* 49, 857-859, 1968.
- E. Vigroux, "Coefficients d'absorption de l'ozone dans la bande de Hartley", *Ann. Géophys.* 25, 169-172, 1969.
- J. W. Simons, R. J. Paur, H. A. Webster, and E. J. Bair, "Ozone Ultraviolet Photolysis, VI, The Ultraviolet Spectrum", *J. Chem. Phys.* 59, 1203-1208, 1973.
- R. D. Hudson, "Absorption Cross Sections of Stratospheric Molecules", *Can. J. Chem.* 52, 1465-1478, 1974.
- W. B. De More and M. Patapoff, "Comparison of Ozone Determination by Ultraviolet Photometry and Gas-Phase Titration", *Environ. Sci. Technol.* 10, 897, 1976.
- C. M. Penny, "Study of Temperature Dependence of the Chappuis Band Absorption of Ozone", NASA Contract Rep. 158977, 1979.
- W. D. Komhyr, "Dobson Spectrophotometer Systematic Total Ozone Measurement Error", *Geophys. Res. Lett.* 7, 161-163, 1980.
- K. F. Klenk, "Absorption Coefficients of Ozone for the Backscatter UV Experiment", *Appl. Opt.* 19, 236-242, 1980.
- A. M. Bass and R. J. Paur, "UV Absorption Cross-Sections for Ozone: The Temperature Dependence", *J. Photochem.* 17, 141, 1981.
- R. D. McPeters and A. M. Bass, "Anomalous Atmospheric Spectral Features Between 300 and 310 nm Interpreted in Light of New Ozone Absorption Coefficient Measurements", *Geophys. Res. Lett.* 9, 227, 1982.
- D. Daumont, J. Brion, and J. Malicet, "Measurement of Total Atmospheric Ozone: Consequences Entailed by the New Value of O₃ Absorption Cross-Sections at 223 K in the 310-350 nm Spectral Range", *Planet. Space Sci.* 31, 1229-1234, 1983.
- J. Brion, D. Daumont, and J. Malicet, "New Measurements of the Absolute Absorption Cross-Sections of Ozone at 294 and 223 K in the 310-350 nm Spectral Range", *J. Phys. (Paris) Lett.* 45, L57-L60, 1984.

- J. Brion, D. Daumont, J. Malicet, and P. Marché, "Sections Efficaces Absolues de l'Ozone à 298 K aux Longueurs d'Onde de la Lampe au Mercure: Etude Critique des Données Expérimentales Existantes", *J. Phys. (Paris) Lett.* 46, L105-L110, 1985.
- D. E. Freeman, K. Yoshino, J. R. Esmond, and W. H. Parkinson, "High-Resolution Absorption Cross-Section Measurements of Ozone at 195 K in the Wavelength Region 240-350 nm", *Planet. Space Sci.* 32, 239-248, 1984.
- A. M. Bass and R. J. Paur, "The Ultraviolet Cross-Sections of Ozone, I, The Measurements", in: *Atmospheric Ozone*, edited by C. S. Zerefos and A. Ghazi, pp. 606-610, D. Reidel, Norwell, Mass., 1985.
- R. J. Paur and A. M. Bass, "The Ultraviolet Cross-Sections of Ozone, II, Result and Temperature Dependence", in: *Atmospheric Ozone*, edited by C. S. Zerefos and A. Ghazi, pp. 611-616, D. Reidel, Norwell, Mass., 1985.
- K. Mauersberger, D. Hanson, and J. Morton, "A New Ozone Standard: The Vapor Pressure of Ozone at Liquid Argon Temperatures", *Geophys. Res. Lett.* 12, 89-92, 1985.
- L. T. Molina and M. J. Molina, "Absolute Absorption Cross Sections of Ozone in the 185- to 350-nm Wavelength Range", *J. Geophys. Res. D* 91, 14501-14508, 1986.
- K. Mauersberger, D. Hanson, and J. Morton, "Measurement of the Ozone Absorption Cross-Section at the 253.7 nm Mercury Line", *Geophys. Res. Lett.* 13, 671-673, 1986.
- K. Mauersberger, D. Hanson, J. Barnes, and J. Morton, "Ozone Vapor Pressure and Absorption Cross-Section Measurements: Introduction of an Ozone Standard", *J. Geophys. Res.* 91, 8480-8482, 1987.
- J. Barnes and K. Mauersberger, "Temperature Dependence of the Ozone Absorption Cross Section at the 253.7-nm Mercury Line", *J. Geophys. Res. D* 92, 14861-14864, 1987.
- J. I. Steinfeld, S. M. Adler-Golden, and J. W. Gallagher, "Critical Survey of Data on the Spectroscopy and Kinetics of Ozone in the Mesosphere and Thermosphere", *J. Phys. Chem. Ref. Data* 16, 911-951, 1987.
- J. B. Kerr, I. A. Asbridge, and W. F. J. Evans, "Intercomparison of Total Ozone Measured by the Brewer and Dobson Spectrophotometers in Toronto", *J. Geophys. Res. D* 93, 11129-11140, 1988.
- K. Yoshino, D. E. Freeman, J. R. Esmond, and W. H. Parkison, "Absolute Absorption Cross-Section Measurements of Ozone in the Wavelength Region 238-335 nm and the Temperature Dependence", *Planet. Space Sci.* 36, 395-398, 1989.

- J. Malicet, J. Brion, and D. Daumont, "Temperature Dependence of the Absorption Cross-Section of Ozone at 254 nm", *Chem. Phys. Lett.* 158, 293-296, 1989.
- M. Cacciani, A. Di Sarra, G. Fiocco, and A. Amoruso. "Absolute Determination of the Cross-Sections of Ozone in the Wavelength Region 339-355 nm at Temperature 220-293 K", *J. Geophys. Res. D* 94, 8485-8490, 1989.
- A. Amoruso, M. Cacciani, A. Di Sarra, and G. Fiocco, "Absorption Cross Sections of Ozone in the 590- to 610-nm Region at T=230K and T=299K", *J. Geophys. Res.* 95, 20565-20568, 1990.
- S. M. Anderson and K. Mauersberger, "Laser Measurements of Ozone Absorption Cross Sections in the Chappuis Band", *Geophys. Res. Lett.* 19, 933-936, 1992.
- D. Daumont, J. Brion, J. Charbonnier, and J. Malicet, "Ozone UV Spectroscopy I: Absorption Cross-Sections at Room Temperature", *J. Atm. Chem.* 15, 145-155, 1992.
- J. Brion, A. Chakir, D. Daumont, J. Malicet, and C. Parisse, "High-Resolution Laboratory Absorption Cross Section of O₃. Temperature Effect", *Chem. Phys. Lett.* 213, 610-612, 1993.
- K. Yoshino, J. R. Esmond, D. E. Freeman, and W. H. Parkinson, "Measurements of Absolute Absorption Cross Sections of Ozone in the 185- to 254-nm Wavelength Region", *J. Geophys. Res. D* 98, 5205-5211, 1993.
- W. D. Komhyr, C. L. Mateer, and R. D. Hudson, "Effective Bass-Paur 1985 Ozone Absorption Coefficients for Use With Dobson Spectrophotometers", *J. Geophys. Res. D* 98, 20451-20465, 1993.
- J. B. Burkholder and R. K. Talukdar, "Temperature Dependence of the Ozone Absorption Spectrum Over the Wavelength Range 410 to 760 nm", *Geophys. Res. Lett.* 21, 581-584, 1994.
- J. Malicet, D. Daumont, J. Charbonnier, C. Parisse. A. Chakir, and J. Brion, "Ozone UV Spectroscopy II: Absorption Cross-Sections and Temperature Dependence", *J. Atm. Chem.* 21, 263-273, 1995.
- J. Brion, A. Chakir, J. Charbonnier, D. Daumont, C. Parisse, and J. Malicet, "Absorption Spectra Measurements for the Ozone Molecule in the 350-830 nm Region", *J. Atm. Chem.* 30, 291-299, 1998.
- S. Voigt, J. Orphal, and J. P. Burrows: "A Study of Absorption Cross-Sections in the UV and Visible: High-Resolution Absorption Cross-Sections of NO₂ and O₃ at Atmospheric Temperatures", Final Report for the European Space Agency ESA, prepared by SERCO Europe Ltd., London, 1998.

J. P. Burrows, A. Richter, A. Dehn, B. Deters, S. Himmelmann, S. Voigt, and J. Orphal, "Atmospheric Remote-Sensing Reference Data from GOME: 2. Temperature-Dependent Absorption Cross Sections of O₃ in the 231–794 nm Range", *J. Quant. Spectrosc. Rad. Transf.* 61, 509–517, 1999.

S. Voigt, J. Orphal, and J. P. Burrows: "UV-Visible Absorption Cross-Sections of NO₂ and O₃ at Atmospheric Temperatures and Pressures by FTS", *Proc. Europ. Sympos. Atm. Meas. Space, ESA WPP-161 Vol. II*, 471-475, 1999.

K. Bogumil, J. Orphal, S. Voigt, H. Bovensmann, O. C. Fleischmann, M. Hartmann, T. Homann, P. Spietz, and J. P. Burrows: "Reference Spectra of Atmospheric Trace Gases Measured with the SCIAMACHY PFM Satellite Spectrometer", *Proc. Europ. Sympos. Atm. Meas. Space, ESA WPP-161 Vol. II*, 443-446, 1999.

K. Bogumil, J. Orphal, and J. P. Burrows: "Temperature-Dependent Absorption Cross-Sections of O₃, NO₂, and Other Atmospheric Trace Gases Measured with the SCIAMACHY Spectrometer", *Proc. ERS-ENVISAT Sympos.*, ESA-ESTEC, 2000.

K. Bogumil, J. Orphal, J.-M. Flaud, and J. P. Burrows: "Vibrational Progressions in the Visible and Near-Ultraviolet Absorption Spectrum of Ozone", *Chem. Phys. Lett.* 349, 241-248, 2001.

S. Voigt, J. Orphal, K. Bogumil, and J. P. Burrows: "The Temperature Dependence (203-293 K) of the Absorption Cross-Sections of O₃ in the 230-850 nm region Measured by Fourier-Transform Spectroscopy", *J. Photochem. Photobiol. A* 143, 1-9, 2001.

4. The O₃ absorption cross-sections in the 240–790 nm region

The O₃ absorption cross-sections in the 240–790 nm region can be separated into four systems: the Hartley band, the Huggins bands, the Chappuis band, and the Wulf bands extending towards longer wavelengths (see Figure 4-1).

The Hartley band is the strongest band extending from about 200–320 nm and peaks around 255 nm. Although its overall shape is smooth and determined by the short lifetime of O₃ in the upper electronic state due to rapid photodissociation, there is a residual vibrational structure (see Figure 4-2), due to quasiperiod orbits of the electronic wavepacket before dissociation in the upper state, which is slightly temperature-dependent (due to the change of Franck-Condon point with temperature). Although the overall structure of the Hartley band is today theoretically well understood, there is currently no theoretical calculation that predicts the absorption cross-sections of O₃ within experimental accuracy or better. The Hartley band is extremely important for atmospheric photochemistry.

The Huggins bands consists of a series of individual peaks extending from about 300–390 nm (see Figure 4-3), showing a strong temperature dependence due to the varying slope of the Hartley band and to the sharpening of the individual bands at lower temperatures. Due to the drastic change of the cross-sections with wavelength over more than five orders of magnitude, it is impossible to measure this system at once (with the same combination of absorption path and O₃ pressure) at high accuracy. In the past, several analytical expressions have been proposed to interpolate the temperature-dependence of the absorption cross-sections in this region. The Huggins bands are currently used for spectroscopic remote-sensing of O₃ by many experimental techniques (Dobson spectrometers, Brewer spectrometers, TOMS, DOAS, ...).

The Chappuis band is a broad structure in the visible region between about 380–800 nm which is more than thousand times weaker than the Hartley band (see Figure 4-1). The residual structures (similar to those observed in the Hartley band), see Figure 4-4, arise from quantum mechanical interferences between two interacting excited electronic states and show only little variation with temperature. The region between 400–500 nm is very important for atmospheric remote-sensing from ground.

For all these bands in the 240–790 nm region, there are many new laboratory measurements using different spectrometers and experimental conditions. It is important to provide a detailed comparison of these measurements and the resulting cross-sections. In the following sections, several approaches will be used for these comparisons: absolute values at selected wavelengths, absolute values over large regions, integrated cross-sections, and non-linear least-squares fits.

Figure 4-1: The O₃ spectrum at room temperature (source: *Richter et al.*)

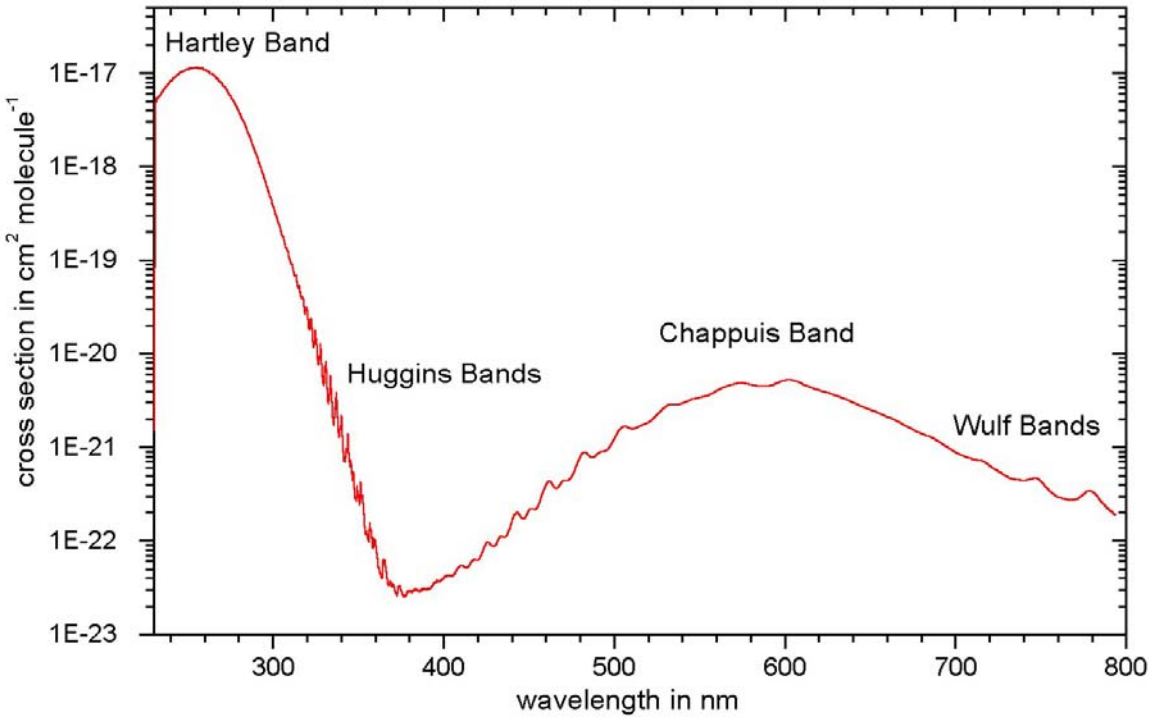


Figure 4-2: The O₃ cross-sections at the peak of the Hartley band (source: *Richter et al.*)

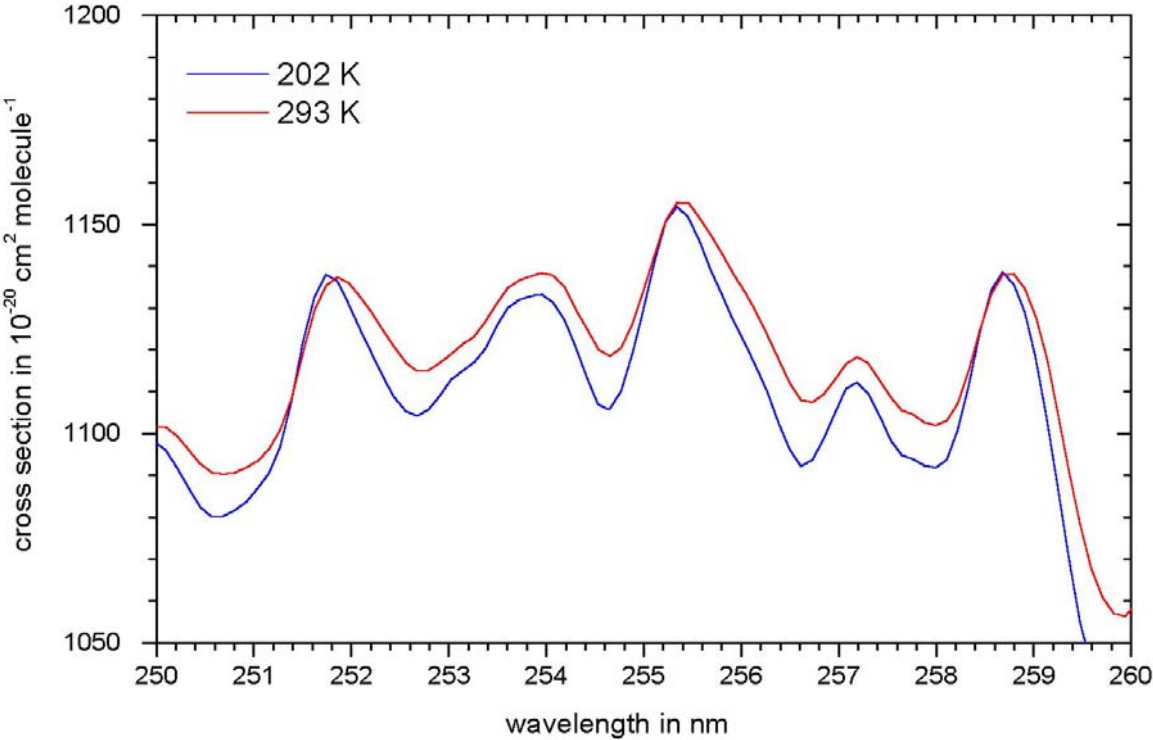


Figure 4-3: The O₃ cross-sections in the Huggins bands (source: *Richter et al.*)

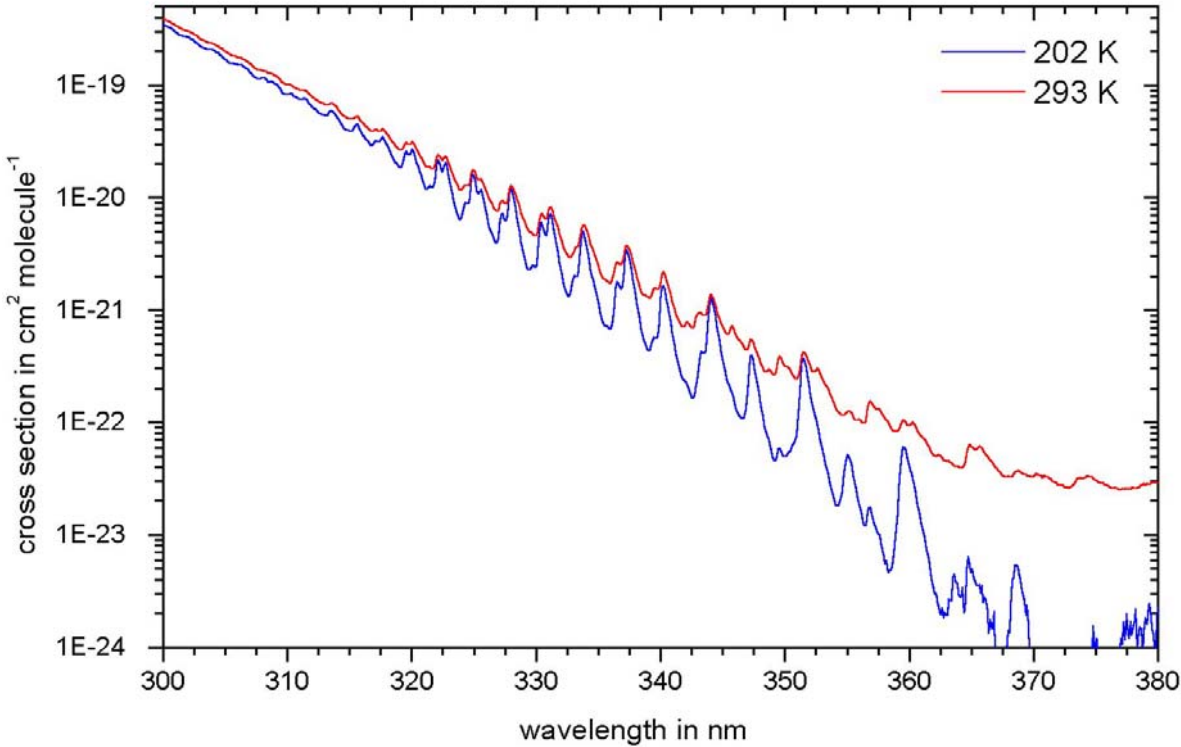
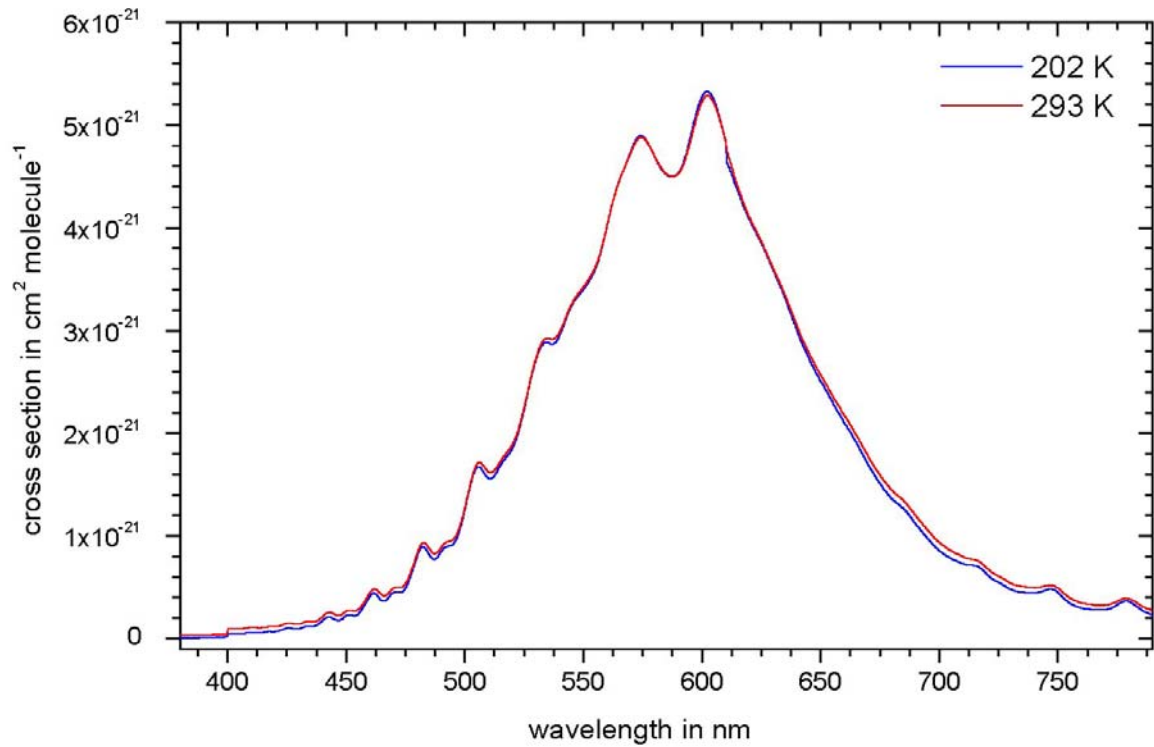


Figure 4-4: The O₃ cross-sections in the Chappuis band (source: *Richter et al.*)



5. Sensitivity of the O₃ cross-sections to wavelength shifts and resolution

First we propose to investigate the sensitivity of the spectrum to wavelength calibration and spectral resolution, in order to assess their influence on the absorption cross-sections which will be compared afterwards.

In order to determine the influence of wavelength calibration and spectral resolution on the O₃ spectrum (before starting to compare experimental data recorded with different instruments), the following comparisons were made:

A) Sensitivity of the O₃ spectrum to wavelength shifts (see Figures 5-1 to 5-5)

1. relative change of the O₃ spectrum (*Brion et al.*, spectral resolution ca. 0.01 nm) after a wavelength shift of –0.05 nm
2. relative change of the O₃ spectrum (*Brion et al.*, spectral resolution ca. 0.01 nm) after a wavelength shift of –0.01 nm
3. relative change of the O₃ spectrum (*Bass and Paur*, spectral resolution less than 0.025 nm) after a wavelength shift of –0.05 nm
4. relative change of the O₃ spectrum (*Bass and Paur*, spectral resolution less than 0.025 nm) after a wavelength shift of –0.01 nm
5. relative change of the O₃ spectrum (*Burrows et al.*, spectral resolution ca. 0.2–0.4 nm) after a wavelength shift of –0.05 nm
6. relative change of the O₃ spectrum (*Burrows et al.*, spectral resolution ca. 0.2–0.4 nm) after a wavelength shift of –0.01 nm

B) Sensitivity of the O₃ spectrum to the spectral resolution (see Figures 5-6 to 5-8)

7. relative change of the O₃ spectrum (*Bass and Paur*, spectral resolution less than 0.025 nm) after convolution with a Gaussian function of 0.1 nm FWHM
8. relative change of the O₃ spectrum (*Brion et al.*, spectral resolution ca. 0.01 nm) after convolution with a Gaussian function of 0.1 nm FWHM
9. relative change of the O₃ spectrum (*Brion et al.*, spectral resolution ca. 0.01 nm) after convolution with a Gaussian function of 0.01 nm FWHM
10. relative change of the O₃ spectrum (*Bass and Paur*, spectral resolution less than 0.025 nm) after convolution with a Gaussian function of 0.01 nm FWHM

It is important to stress the fact that, since relative changes are studied, the differing absolute values of the cross-sections and the wavelength calibration errors in the experimental data are not showing up in these comparisons. This will become clear from the comparison of the results from different data (see below). However, the

spectral resolution of the experimental data is important (see below), and therefore, three different data sets have been used:

- *Brion et al.* because of the high spectral resolution and the broad spectral coverage of this data set,
- *Bass and Paur* because of the high spectral resolution and the fact that this data set is the current remote-sensing standard for O₃,
- *Burrows et al.* because of the lower resolution (see below) which is somewhat representative for most remote-sensing experiments in the UV-visible.

Note that these comparisons are presented only for spectra at room temperature. For lower temperatures, similar results are obtained. Below are several figures which shall illustrate the results. On the basis of these plots, the observations will be summarized and conclusions will be drawn which are useful for the comparisons of the ozone cross-sections.

Figure 5-1: relative change of the O₃ spectrum (source: *Brion et al.*, spectral resolution ca. 0.01 nm) after a wavelength shift of -0.05 nm

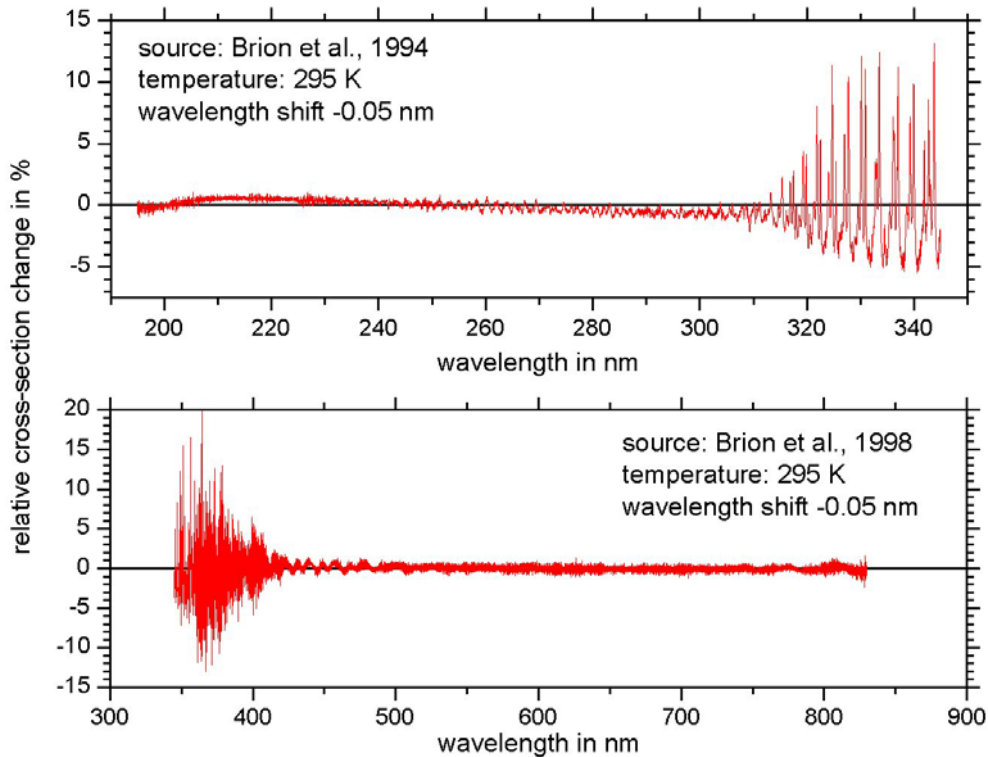


Figure 5-2: relative change of the O₃ spectrum (source: *Brion et al.*, spectral resolution ca. 0.01 nm) after a wavelength shift of -0.01 nm

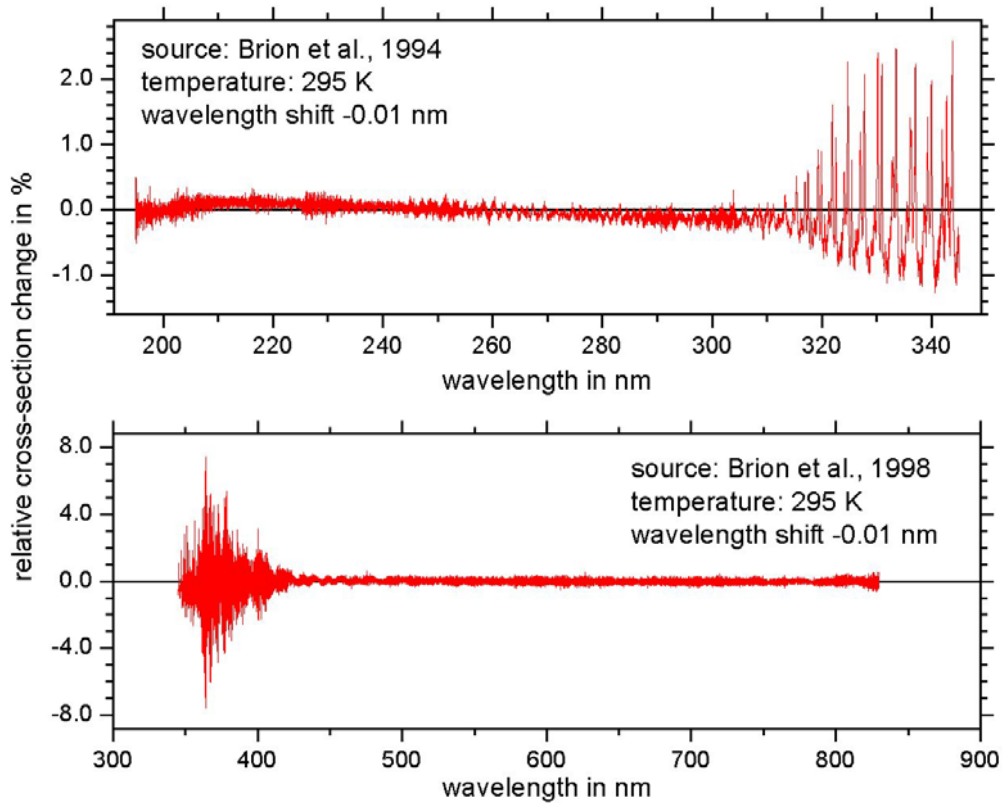


Figure 5-3: relative change of the O₃ spectrum (source: *Bass and Paur*, spectral resolution less than 0.025 nm) after wavelength shifts of -0.05 nm and -0.01 nm, respectively

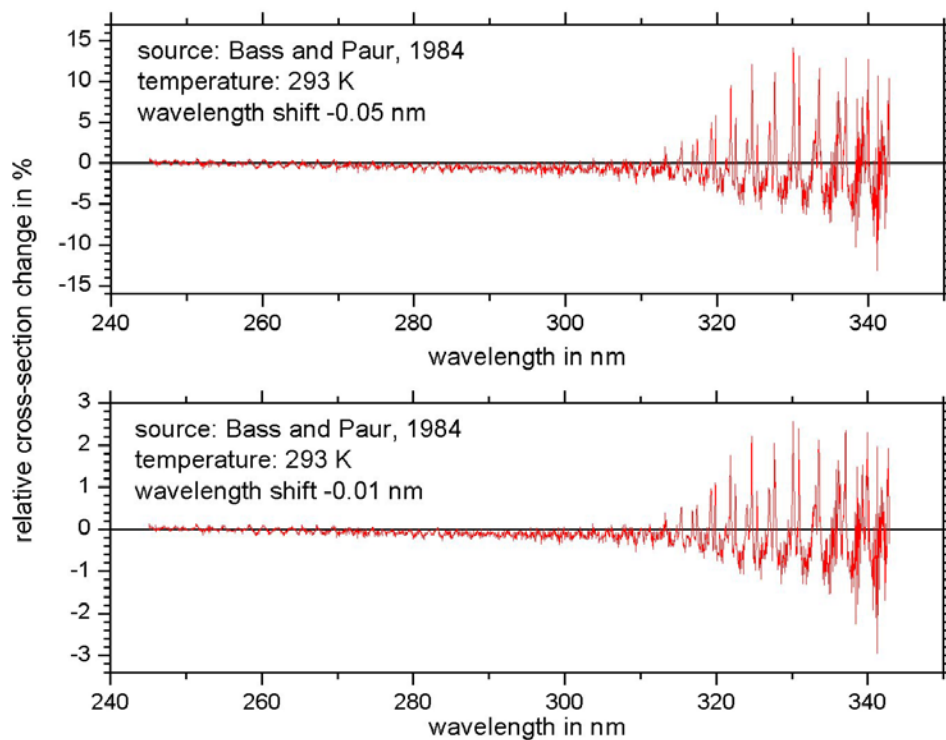


Figure 5-4: relative change of the O₃ spectrum (source: *Burrows et al.*, spectral resolution ca. 0.2–0.4 nm) after a wavelength shift of –0.05 nm

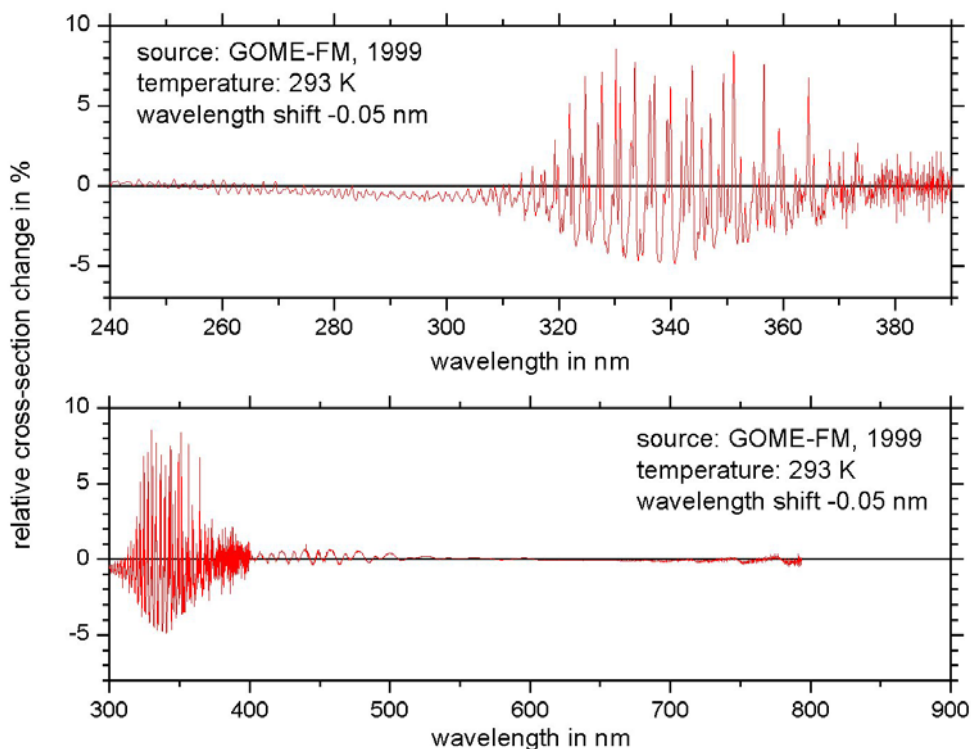


Figure 5-5: relative change of the O₃ spectrum (source: *Burrows et al.*, spectral resolution ca. 0.2–0.4 nm) after a wavelength shift of –0.01 nm

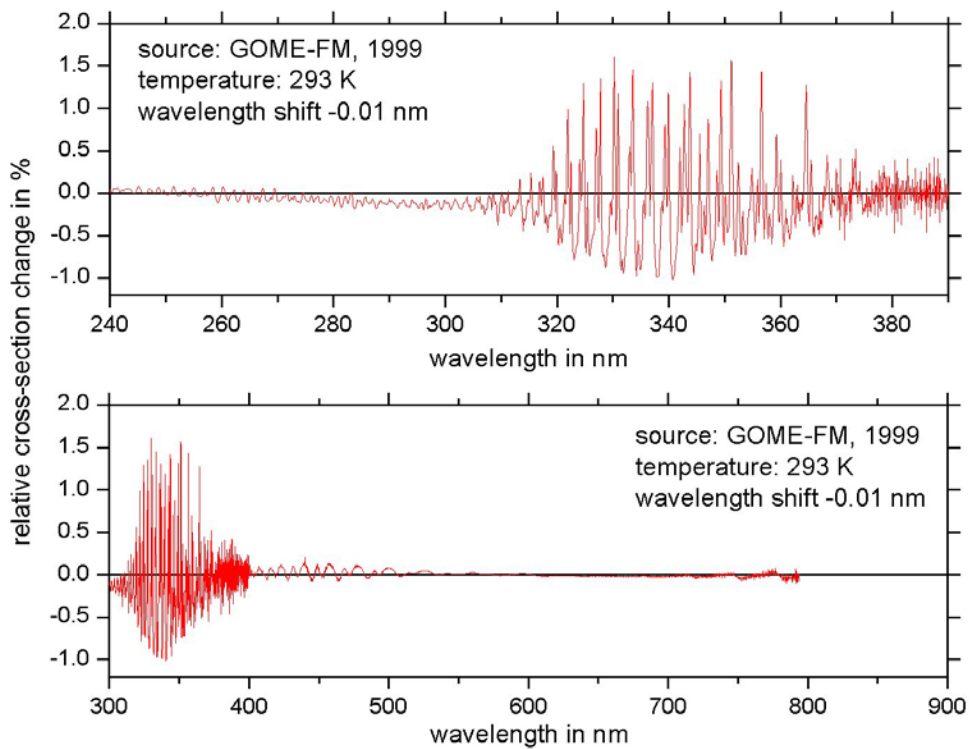


Figure 5-6: relative change of the O₃ spectrum (source: *Bass and Paur*, spectral resolution less than 0.025 nm, and *Brion et al.*, spectral resolution ca. 0.01 nm) after convolution with a Gaussian function of 0.1 nm FWHM

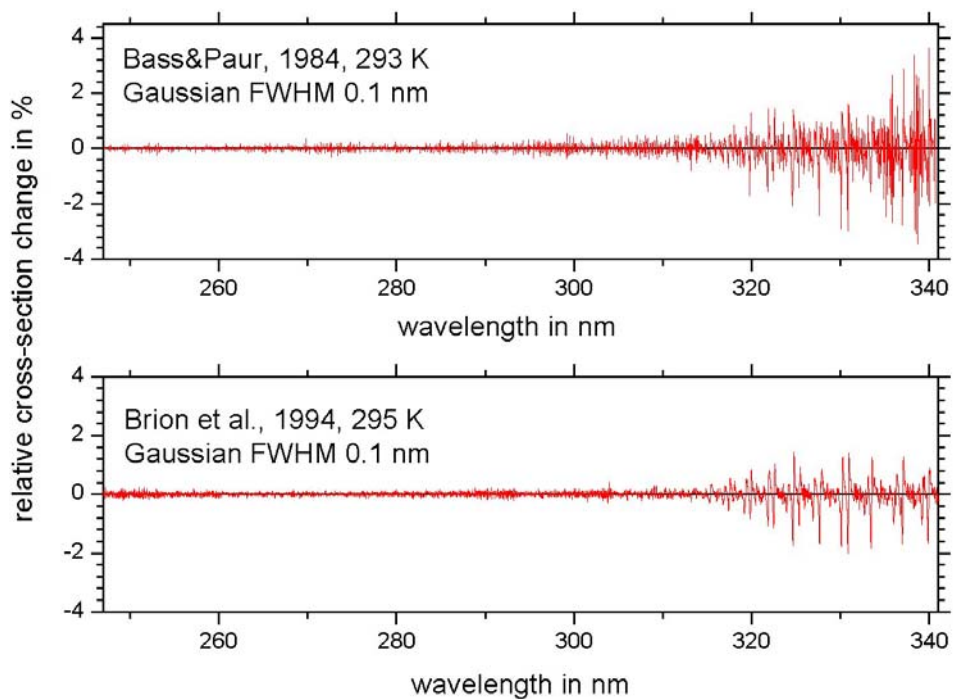


Figure 5-7: relative change of the O₃ spectrum (source: *Bass and Paur*, spectral resolution less than 0.025 nm, and *Brion et al.*, spectral resolution ca. 0.01 nm) after convolution with a Gaussian function of 0.01 nm FWHM

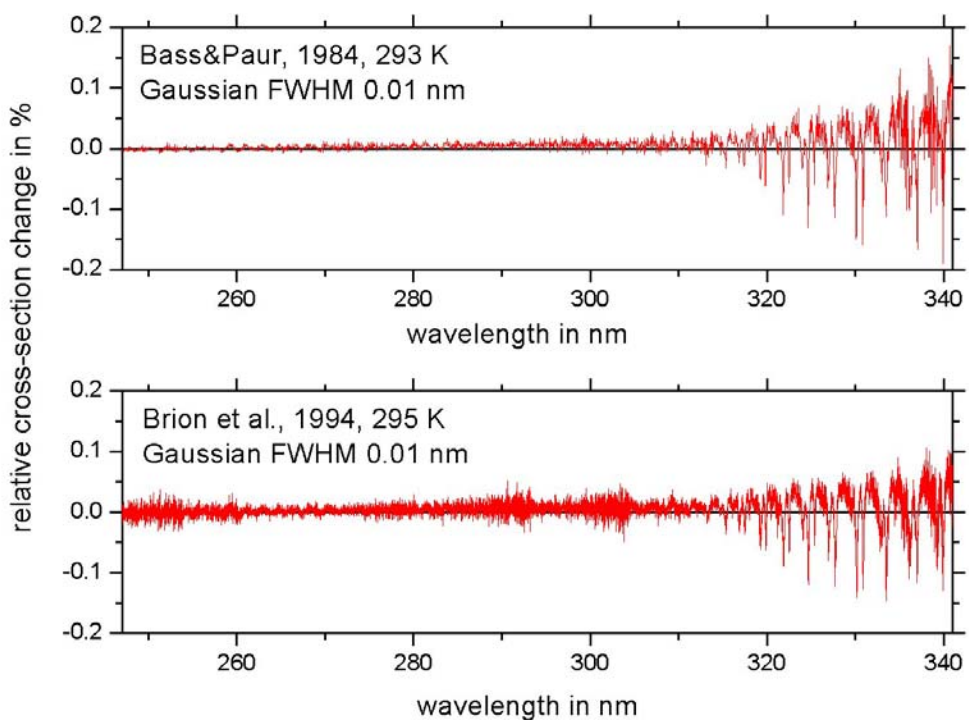
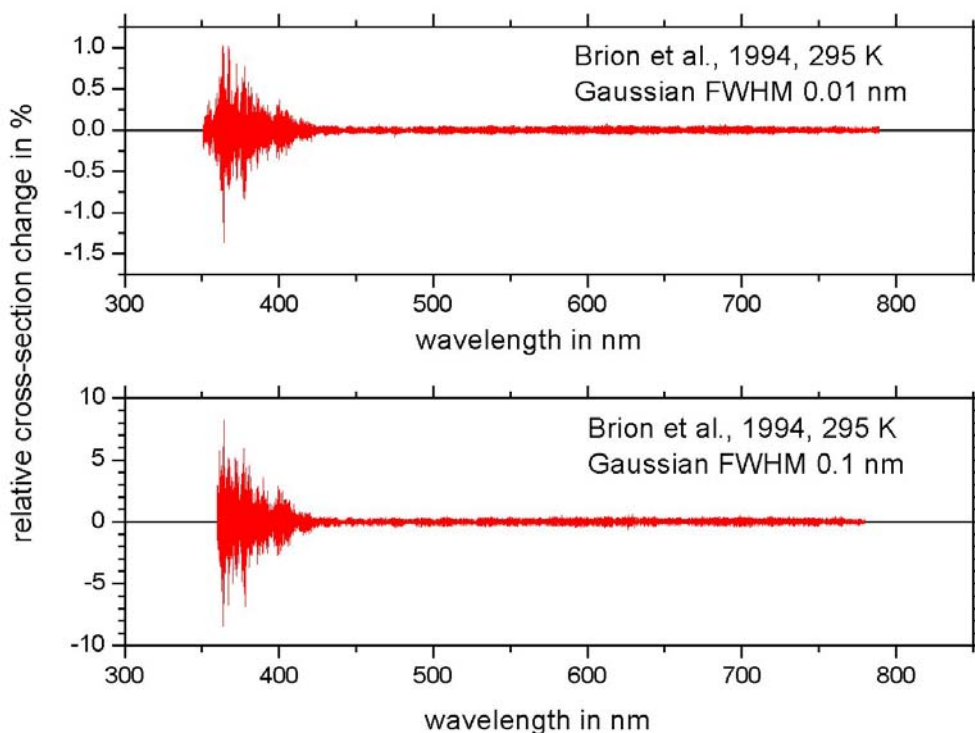


Figure 5-8: relative change of the O₃ spectrum (source: *Brion et al.*, spectral resolution ca. 0.01 nm) after convolution with a Gaussian function of 0.01 nm FWHM and of 0.1 nm FWHM



In the 240–790 nm region (except between 310–410 nm), the O₃ spectrum changes by less than 1% for wavelength shifts of 0.05 nm or less.

In the 240–790 nm region (except between 310–410 nm), the O₃ spectrum changes by less than 0.2% when the spectrum is convoluted with a Gaussian of 0.1 nm FWHM, and by less than 0.05% when the spectrum is convoluted with a Gaussian of 0.01 nm FWHM.

In the 310–410 nm region, the O₃ spectrum (at spectral resolutions of 0.025 nm or better) changes by up to 20% for wavelength shifts of 0.05 nm and by up to 7% for wavelength shifts of 0.01 nm. In this region (310–410 nm) the changes in the O₃ spectrum for different wavelength shifts are resolution-dependent: For lower resolution (e.g. for the GOME-FM spectra at a spectral resolution of about 0.2 nm) wavelength shifts of 0.05 nm introduce changes in the O₃ spectrum of up to 9% and even shifts of only 0.01 nm still introduce changes of up to 1.5%.

In the 310–410 nm region, the O₃ spectrum changes by up to 9% after convolution with a Gaussian of 0.1 nm FWHM by up to 0.2% after convolution with a Gaussian of 0.01 nm.

6. Comparison of the O₃ cross-sections between 230–790 nm at 298±5 K

6.1. Comparison of room temperature cross-sections at selected wavelengths

From the previous investigations concerning the sensitivity of the O₃ cross-sections to wavelength shifts and spectral resolution, we concluded that values in the 240–310 and 410–790 nm region can be compared if the measurements were conducted at a spectral resolution of about 0.1 nm and with a wavelength accuracy of 0.05 nm or better. We will now compare such measurements at selected wavelengths, and attempt to find an average value at each wavelength, for O₃ cross-sections recorded at room temperature (298 K) or at temperatures close to it (293–303 K).

Where no digital data are available, we take the values as given in the literature.

6.1.1. 253.65 nm (Hg line)

Table 6-1: Comparison of the O₃ cross-sections at 298±5K at 253.65 nm

Value in 10 ⁻²⁰ cm ²	Uncertainty in 10 ⁻²⁰ cm ²	Temperature in K	Deviation from mean value	Reference
1140	57 (5.0%)	300	-0.1%	Inn & Tanaka
1147	24 (2.1%)	295	+0.5%	Hearn
1156	46 (4.0%)	298	+1.3%	De More & Raper
1129	17 (1.5%)	303	-1.0%	Griggs
1145	24 (2.1%)	293	+0.4%	Bass&Paur
1157	12 (1.0%)	298	+1.4%	Molina & Molina
1137	6 (0.5%)	297	-0.4%	Mauersberger et al.
1131	8 (0.7%)	297	-0.9%	Mauersberger et al.
1136	6 (0.5%)	297	-0.4%	Mauersberger et al.
1145	8 (0.7%)	295	+0.4%	Yoshino et al.
1143	11 (1.0%)	295	+0.2%	Yoshino et al.
1126	20 (1.8%)	295	-1.3%	Malicet et al.
1130.5	11 (1.0%)	295	-0.9%	Brion et al.
1137	30 (2.6%)	293	-0.4%	Richter et al.
1150	30 (2.6%)	293	+0.8%	Burrows et al.

1137	46 (4.0%)	293	-0.4%	Voigt et al.
1145	11 (2.0%)	293	+0.4%	Bogumil et al.

Mean value of all measurements:	1141 ± 9 (1σ = 0.8%)	No: 17
Mean without IUP data: ⁽¹⁾	1140 ± 10 (1σ = 0.9%)	No: 13
Mean without “scaled” data: ⁽²⁾	1141 ± 10 (1σ = 0.9%)	No: 13

⁽¹⁾ without Richter et al., Burrows et al., Voigt et al., and Bogumil et al.

⁽²⁾ without Bass&Paur, Richter et al., Voigt et al., and Bogumil et al.

Data in the interval [-1.5%, -1.0%]:	1
Data in the interval [-1.0%, -0.5%]:	3
Data in the interval [-0.5%, ±0.0%]:	5
Data in the interval [±0.0%, +0.5%]:	5
Data in the interval [±0.5%, +1.0%]:	1
Data in the interval [±1.0%, +1.5%]:	2

At 253.65 nm, a total of 17 measurements of the O₃ cross-sections at room temperature is available. The mean value of the independent measurements is found to be $1141 \times 10^{-20} \text{ cm}^2$, with a standard deviation (1σ) of $10 \times 10^{-20} \text{ cm}^2$ (0.9%). Of all available measurements, 10 fall in the interval [-0.5%, +0.5%], 4 lie below and 3 above. Concerning the “scaled” cross sections, only one data set (Bass&Paur) was calibrated to absolute values at 253.65 nm, the other three were either calibrated to absolute values at longer wavelengths (Richter et al., Bogumil et al.) or using the assumption of constant integrated cross-sections (Voigt et al.). All of these four measurements provide values with less than 0.5% difference to the mean value.

Only two data sets have slightly larger deviations from the mean value than the stated accuracy of the measurements: Molina and Molina (deviation +1.4%, stated accuracy 1.0%) and Mauersberger et al. (deviation -0.9%, stated accuracy 0.7%).

Different approaches to calculate the mean value at this and other wavelengths have been proposed, e.g. using the inverse of the uncertainty squared as weight for each value, and Student-T testing.¹ With other approaches one obtains values close to that given above, e.g. 1136 ± 40 (2σ = 3.5%) after elimination of some measurements.²

¹ E. Shettle, personal communication, 2001.

² J. Malicet, personal communication, 2001.

6.1.2. 289.36 nm (Hg line)

Table 6-2: Comparison of the O₃ cross-sections at 298±5K at 289.36 nm

Value in 10 ⁻²⁰ cm ²	Uncertainty in 10 ⁻²⁰ cm ²	Temperature in K	Deviation from mean value	Reference
147	7 (5.0%)	300	-1.3%	Inn & Tanaka
147	3 (2.0%)	292	-1.3%	Hearn
148	6 (4.0%)	298	-0.7%	De More & Raper
148	2 (1.5%)	303	-0.7%	Griggs
150	3 (2.1%)	293	+0.7%	Bass&Paur
149	1 (0.7%)	295	±0.0%	Freeman et al.
154	2 (1.0%)	298	+3.4%	Molina & Molina
144	3 (1.8%)	295	-3.4%	Malicet et al.
151	2 (1.0%)	295	+1.3%	Brion et al.
150	4 (2.6%)	293	+0.7%	Richter et al.
151	4 (2.6%)	293	+1.3%	Burrows et al.
154	6 (4.0%)	293	+3.4%	Voigt et al.
151	2 (2.0%)	293	+1.3%	Bogumil et al.

Mean value of all measurements: 150 ± 3 (1σ = 1.9%) No: 13

Mean without IUP data:⁽¹⁾ 149 ± 3 (1σ = 2.0%) No: 9

Mean without “scaled” data:⁽²⁾ 149 ± 3 (1σ = 2.0%) No: 9

⁽¹⁾ without Richter et al., Burrows et al., Voigt et al., and Bogumil et al.

⁽²⁾ without Bass&Paur, Richter et al., Voigt et al., and Bogumil et al.

Data in the interval [-1.5%, +1.5%]: 10

Data outside the interval [-1.5%, +1.5%]: 3

At 289.36 nm, a total of 13 measurements of the O₃ cross-sections at room temperature is available. The mean value of the independent measurements is found to be 149×10⁻²⁰ cm², with a standard deviation (1σ) of 3×10⁻²⁰ cm² (2.0%). Of all

available measurements, 10 fall in the interval $[-1.5\%, +1.5\%]$, 2 lie below and 1 lies above. 3 measurements have larger deviations from the mean value than the stated accuracy, however the mean value and the dispersion do not change when eliminating these measurements.

6.1.3. 296.73 nm (Hg line)

Table 6-3: Comparison of the O₃ cross-sections at 298±5K at 296.73 nm

Value in 10 ⁻²⁰ cm ²	Uncertainty in 10 ⁻²⁰ cm ²	Temperature in K	Deviation from mean value	Reference
56.7	2.8 (5.0%)	300	-5.2%	Inn & Tanaka
59.7	2.6 (4.4%)	295	-0.2%	Hearn
58.7	2.3 (4.0%)	298	-1.8%	De More & Raper
60.0	0.9 (1.5%)	303	+0.3%	Griggs
60.7	1.3 (2.1%)	293	+1.5%	Bass&Paur
59.7	0.4 (0.7%)	295	-0.2%	Freeman et al.
62.3	0.6 (1.0%)	298	+4.2%	Molina & Molina
58.3	1.0 (1.8%)	295	-2.5%	Malicet et al.
61.5	0.6 (1.0%)	295	+2.8%	Brion et al.
60.7	1.6 (2.6%)	293	+1.5%	Richter et al.
61.0	1.6 (2.6%)	293	+2.0%	Burrows et al.
61.7	2.5 (4.0%)	293	+3.2%	Voigt et al.
61.4	0.6 (2.0%)	293	+2.7%	Bogumil et al.

Mean value of all measurements: 60.2 ± 1.6 ($1\sigma = 2.7\%$) No: 13

Mean without IUP data:⁽¹⁾ 59.7 ± 1.7 ($1\sigma = 2.8\%$) No: 9

Mean without “scaled” data:⁽²⁾ 59.8 ± 1.7 ($1\sigma = 2.9\%$) No: 9

⁽¹⁾ without Richter et al., Burrows et al., Voigt et al., and Bogumil et al.

⁽²⁾ without Bass&Paur, Richter et al., Voigt et al., and Bogumil et al.

Data in the interval $[-2.0\%, +2.0\%]$: 8

Data outside the interval $[-2.0\%, +2.0\%]$: 5

At 296.73 nm, a total of 13 measurements of the O₃ cross-sections at room temperature is available. The mean value of the independent measurements is found to be $59.8 \times 10^{-20} \text{ cm}^2$, with a standard deviation (1σ) of $1.7 \times 10^{-20} \text{ cm}^2$ (2.9%). Of all available measurements, 8 fall in the interval $[-2.0\%, +2.0\%]$, 1 lies below and 4 lies above. 4 measurements have larger deviations from the mean value than the stated accuracy. When eliminating these measurements, the mean value changes to $60.3 \times 10^{-20} \text{ cm}^2$, with a standard deviation (1σ) of $0.9 \times 10^{-20} \text{ cm}^2$ (1.6%).

6.1.4. 302.15 nm (Hg line)

Table 6-4: Comparison of the O₃ cross-sections at $298 \pm 5\text{K}$ at 302.15 nm

Value in 10^{-20} cm^2	Uncertainty in 10^{-20} cm^2	Temperature in K	Deviation from mean value	Reference
28.4	1.4 (5.0%)	300	-2.7%	Inn & Tanaka
28.6	0.1 (0.4%)	293	-2.1%	Hearn
28.4	0.4 (1.5%)	303	-2.7%	Griggs
29.4	0.6 (2.1%)	293	+0.7%	Bass&Paur
29.1	0.2 (0.7%)	295	-0.3%	Freeman et al.
30.1	0.3 (1.0%)	298	+3.1%	Molina & Molina
28.9	0.5 (1.8%)	295	-1.0%	Malicet et al.
29.8	0.3 (1.0%)	295	+2.1%	Brion et al.
29.5	0.8 (2.6%)	293	+1.0%	Richter et al.
29.9	0.8 (2.6%)	293	+2.4%	Burrows et al.
30.4	1.2 (4.0%)	293	+4.1%	Voigt et al.
29.8	0.3 (2.0%)	293	+2.1%	Bogumil et al.

Mean value of all measurements: 29.4 ± 0.7 ($1\sigma = 2.3\%$) No: 12

Mean without IUP data:⁽¹⁾ 29.1 ± 0.6 ($1\sigma = 2.2\%$) No: 8

Mean without "scaled" data:⁽²⁾ 29.2 ± 0.7 ($1\sigma = 2.4\%$) No: 8

⁽¹⁾ without Richter et al., Burrows et al., Voigt et al., and Bogumil et al.

⁽²⁾ without Bass&Paur, Richter et al., Voigt et al., and Bogumil et al.

Data in the interval [−2.5 %, +2.5%]: 8

Data outside the interval [−2.5%, +2.5%]: 4

At 302.15 nm, a total of 12 measurements of the O₃ cross-sections at room temperature is available. The mean value of the independent measurements is found to be $29.2 \times 10^{-20} \text{ cm}^2$, with a standard deviation (1σ) of $0.7 \times 10^{-20} \text{ cm}^2$ (2.4%). Of all available measurements, 8 fall in the interval [−2.5%, +2.5%], 2 lie below and 2 lie above. 5 measurements have larger deviations from the mean value than the stated accuracy. When eliminating these measurements, the mean value remains at $29.2 \times 10^{-20} \text{ cm}^2$, with a standard deviation (1σ) of $0.5 \times 10^{-20} \text{ cm}^2$ (1.8%).

6.1.5. 334.15 nm (Hg line)

This wavelength corresponds to an emission line of Hg. In the past, a number of comparisons have shown large dispersion (up to 6%) of the experimental values for the O₃ cross section at room temperature at this wavelength. This is obviously due to the high sensitivity of the O₃ spectrum to wavelength accuracy and to the ILS in this spectral region. This wavelength can therefore not be used for comparison of absolute cross-section values without taking into account the different wavelength accuracies and spectral resolutions employed in the experiments.

6.1.6. 543.52 nm (HeNe laser line)

Table 6-5: Comparison of the O₃ cross-sections at 298±5K at 543.52 nm

Value in 10^{-22} cm^2	Uncertainty in 10^{-22} cm^2	Temperature in K	Deviation from mean value	Reference
30.75	0.3 (0.9%)	295	−1.4%	Anderson
30.8	0.3 (1.0%)	298	−1.4%	Burkholder
31.2	0.5 (1.5%)	295	±0.0%	Brion et al.
30.7			+0.7%	Johnston
31.8	0.8 (2.6%)	293	+1.9%	Richter et al.
31.7	0.8 (2.6%)	293	+1.6%	Burrows et al.

31.5	1.2 (4.0%)	293	+1.0%	Voigt et al.
31.5	0.3 (2.0%)	293	+1.0%	Bogumil et al.

Mean value of all measurements:	31.2 ± 0.4 ($1\sigma = 1.4\%$)	No: 8
Mean without IUP data: ⁽¹⁾	30.9 ± 0.2 ($1\sigma = 0.7\%$)	No: 4
Mean without “scaled” data: ⁽²⁾	31.1 ± 0.5 ($1\sigma = 1.5\%$)	No: 4

⁽¹⁾ without Richter et al., Burrows et al., Voigt et al., and Bogumil et al.

⁽²⁾ without Burkholder, Richter et al., Voigt et al., and Bogumil et al.

Data in the interval [−2.0%, −1.0%]:	3
Data in the interval [−1.0 %, +1.0%]:	4
Data in the interval [+1.0%, +2.0%]:	1

At 543.52 nm, a total of 8 measurements of the O₃ cross-sections at room temperature is available. The mean value of the independent measurements is found to be 31.1×10^{-22} cm², with a standard deviation (1σ) of 0.5×10^{-22} cm² (1.5%). Of all available measurements, 4 fall in the interval [−1.0%, +1.0%], 3 lie below and 1 lies above. 2 measurements (one of them is “scaled” to the other one) have larger deviations from the mean value than the stated accuracy. When eliminating these measurements, the mean value changes to 31.4×10^{-22} cm², with a standard deviation (1σ) of 0.4×10^{-22} cm² (1.3%).

6.1.7. 576.96 nm (Hg line)

Table 6-6: Comparison of the O₃ cross-sections at 298±5K at 576.96 nm

Value in 10 ⁻²² cm ²	Uncertainty in 10 ⁻²² cm ²	Temperature in K	Deviation from mean value	Reference
44.6	2.2 (5.0%)	300	−6.1%	Inn&Tanaka
47.6	0.9 (1.9%)	294	+0.2%	Hearn
47.4			−0.2%	Vigroux
46.9	0.5 (1.0%)	298	−1.2%	Burkholder
47.7	0.7 (1.5%)	295	+0.4%	Brion et al.

47.3			-0.4%	Johnston
48.4	1.3 (2.6%)	293	+1.9%	Richter et al.
48.3	1.3 (2.6%)	293	+1.7%	Burrows et al.
48.3	1.6 (3.0%)	293	+1.7%	Voigt et al.
48.4	0.5 (2.0%)	293	+1.9%	Bogumil et al.

Mean value of all measurements: 47.5 ± 1.1 ($1\sigma = 2.4\%$) No: 10

Mean without IUP data:⁽¹⁾ 46.9 ± 1.2 ($1\sigma = 2.5\%$) No: 6

Mean without “scaled” data:⁽²⁾ 47.2 ± 1.3 ($1\sigma = 2.7\%$) No: 6

⁽¹⁾ without Richter et al., Burrows et al., Voigt et al., and Bogumil et al.

⁽²⁾ without Burkholder, Richter et al., Voigt et al., and Bogumil et al.

Data in the interval [-2.0%, -1.0%]: 1

Data in the interval [-1.0 %, +1.0%]: 4

Data in the interval [+1.0%, +2.0%]: 4

Data outside the interval [-2.0%, +2.0%]: 1

At 576.96 nm, a total of 10 measurements of the O₃ cross-sections at room temperature is available. The mean value of the independent measurements is found to be 47.2×10^{-22} cm², with a standard deviation (1σ) of 1.3×10^{-22} cm² (2.7%). Of all available measurements, 9 fall in the interval [-2.0%, +2.0%], and only 1 lies above. 2 measurements have larger deviations from the mean value than the stated accuracy. When eliminating these measurements, the mean value changes to 47.7×10^{-22} cm², with a standard deviation (1σ) of 0.4×10^{-22} cm² (0.8%).

6.1.8. 594.10 nm (HeNe laser line)

Table 6-7: Comparison of the O₃ cross-sections at 298±5K at 594.10 nm

Value in 10 ⁻²² cm ²	Uncertainty in 10 ⁻²² cm ²	Temperature in K	Deviation from mean value	Reference
45.7	0.4 (0.9%)	298	-0.9%	Anderson
46.4	0.5 (1.0%)	298	+0.7%	Burkholder

46.8	0.7 (1.5%)	295	+1.5%	Brion et al.
46.2			+0.2%	Johnston
44.0	0.4 (0.8%)	299	-4.6%	Amoruso et al.
47.5	1.2 (2.6%)	293	+1.9%	Richter et al.
47.6	1.2 (2.6%)	293	+2.1%	Burrows et al.
47.5	1.4 (3.0%)	293	+1.9%	Voigt et al.
47.3	0.9 (2.0%)	293	+1.5%	Bogumil et al.

Mean value of all measurements: 46.6 ± 1.2 ($1\sigma = 2.5\%$) No: 9

Mean without IUP data:⁽¹⁾ 45.8 ± 1.1 ($1\sigma = 2.4\%$) No: 5

Mean without “scaled” data:⁽²⁾ 46.1 ± 1.4 ($1\sigma = 2.9\%$) No: 5

⁽¹⁾ without Richter et al., Burrows et al., Voigt et al., and Bogumil et al.

⁽²⁾ without Burkholder, Richter et al., Voigt et al., and Bogumil et al.

Data in the interval [-2.0%, -1.0%]: 1

Data in the interval [-1.0 %, +1.0%]: 3

Data in the interval [+1.0%, +2.0%]: 3

Data outside the interval [-2.0%, +2.0%]: 2

At 594.10 nm, a total of 9 measurements of the O₃ cross-sections at room temperature is available. The mean value of the independent measurements is found to be 46.1×10^{-22} cm², with a standard deviation (1σ) of 1.4×10^{-22} cm² (2.9%). Of all available measurements, 7 fall in the interval [-2.0%, +2.0%], and only 2 lie above. Two measurement have a larger deviation from the mean value than the stated accuracy. When eliminating these measurements, the mean value changes to 47.0×10^{-22} cm², with a standard deviation (1σ) of 0.6×10^{-22} cm² (1.2%).

6.1.9. 604.61 nm (HeNe laser line)

Table 6-8: Comparison of the O₃ cross-sections at 298±5K at 604.61 nm

Value in 10 ⁻²² cm ²	Uncertainty in 10 ⁻²² cm ²	Temperature in K	Deviation from mean value	Reference
51.3	0.4 (0.8%)	298	-0.4%	Anderson

50.9	0.5 (1.0%)	298	-2.5%	Burkholder
51.8	0.8 (1.5%)	295	-0.4%	Brion et al.
52.3	1.4 (2.6%)	293	-0.4%	Richter et al.
52.4	1.4 (2.6%)	293	+0.9%	Burrows et al.
52.6	1.6 (3.0%)	293	+0.6%	Voigt et al.
52.6	1.1 (2.0%)	293	+0.9%	Bogumil et al.

Mean value of all measurements: 52.0 ± 0.7 ($1\sigma = 1.3\%$) No: 7

Mean without IUP data:⁽¹⁾ 51.3 ± 0.5 ($1\sigma = 0.9\%$) No: 3

Mean without “scaled” data:⁽²⁾ 51.8 ± 0.6 ($1\sigma = 1.1\%$) No: 3

⁽¹⁾ without Richter et al., Burrows et al., Voigt et al., and Bogumil et al.

⁽²⁾ without Burkholder, Richter et al., Voigt et al., and Bogumil et al.

Data in the interval [-1.0 %, +1.0%]: 6

Data outside the interval [-1.0%, +1.0%]: 1

At 604.61 nm, a total of 7 measurements of the O₃ cross-sections at room temperature is available. The mean value of the independent measurements is found to be 51.8×10^{-22} cm², with a standard deviation (1σ) of 0.6×10^{-22} cm² (1.1%). Of all available measurements, 6 fall in the interval [-1.0%, +1.0%], and only 1 lies below. One measurement has a larger deviation from the mean value than the stated accuracy. When eliminating this single measurement, the mean value changes to 52.2×10^{-22} cm², with a standard deviation (1σ) of 0.5×10^{-22} cm² (1.0%).

6.1.10. 611.97 nm (HeNe laser line)

Table 6-9: Comparison of the O₃ cross-sections at 298±5K at 611.97 nm

Value in 10 ⁻²² cm ²	Uncertainty in 10 ⁻²² cm ²	Temperature in K	Deviation from mean value	Reference
46.3	0.3 (0.7%)	298	-0.4%	Anderson
45.3	0.5 (1.0%)	298	-2.5%	Burkholder
46.3	0.8 (1.5%)	295	-0.4%	Brion et al.

46.3	1.2 (2.6%)	293	-0.4%	Richter et al.
46.9	1.2 (2.6%)	293	+0.9%	Burrows et al.
46.8	1.4 (3.0%)	293	+0.6%	Voigt et al.
46.9	0.9 (2.0%)	293	+0.9%	Bogumil et al.

Mean value of all measurements: 46.4 ± 0.5 ($1\sigma = 1.2\%$) No: 7

Mean without IUP data:⁽¹⁾ 46.0 ± 0.6 ($1\sigma = 1.3\%$) No: 3

Mean without “scaled” data:⁽²⁾ 46.5 ± 0.4 ($1\sigma = 0.7\%$) No: 3

⁽¹⁾ without Richter et al., Burrows et al., Voigt et al., and Bogumil et al.

⁽²⁾ without Burkholder, Richter et al., Voigt et al., and Bogumil et al.

Data in the interval [-1.0 %, +1.0%]: 6

Data outside the interval [-1.0%, +1.0%]: 1

At 611.97 nm, a total of 7 measurements of the O₃ cross-sections at room temperature is available. The mean value of the independent measurements is found to be 46.0×10^{-22} cm², with a standard deviation (1σ) of 0.6×10^{-22} cm² (1.3%). Of all available measurements, 6 fall in the interval [-1.0%, +1.0%], and only 1 lies below. One measurement has a larger deviation from the mean value than the stated accuracy. When eliminating this single measurement, the mean value changes to 46.6×10^{-22} cm², with a standard deviation (1σ) of 0.3×10^{-22} cm² (0.7%).

6.1.11. 632.82 nm (HeNe laser line)

Table 6-10: Comparison of the O₃ cross-sections at 298±5K at 632.82 nm

Value in 10 ⁻²² cm ²	Uncertainty in 10 ⁻²² cm ²	Temperature in K	Deviation from mean value	Reference
33.8	0.2 (0.7%)	298	-1.2%	Anderson
33.5	0.3 (1.0%)	298	-2.0%	Burkholder
33.9	0.5 (1.5%)	295	-0.9%	Brion et al.
34.6	0.9 (2.6%)	293	+1.2%	Richter et al.
35.0	0.9 (2.6%)	293	+2.3%	Burrows et al.

34.7	1.0 (3.0%)	293	+1.5%	Voigt et al.
34.9	0.7 (2.0%)	293	+2.0%	Bogumil et al.

Mean value of all measurements:	34.3 ± 0.6 ($1\sigma = 1.7\%$)	No: 7
Mean without IUP data: ⁽¹⁾	33.7 ± 0.2 ($1\sigma = 0.6\%$)	No: 3
Mean without “scaled” data: ⁽²⁾	34.2 ± 0.7 ($1\sigma = 1.9\%$)	No: 3

⁽¹⁾ without Richter et al., Burrows et al., Voigt et al., and Bogumil et al.

⁽²⁾ without Burkholder, Richter et al., Voigt et al., and Bogumil et al.

Data in the interval [−2.0%, −1.0%]:	2
Data in the interval [−1.0 %, +1.0%]:	1
Data in the interval [+1.0%, +2.0%]:	3
Data outside the interval [−2.0%, +2.0%]:	1

At 632.82 nm, a total of 7 measurements of the O₃ cross-sections at room temperature is available. The mean value of the independent measurements is found to be 34.2×10^{-22} cm², with a standard deviation (1σ) of 0.7×10^{-22} cm² (1.9%). Of all available measurements, 6 fall in the interval [−2.0%, +2.0%], and only 1 lies above. Two measurements (one of them is “scaled” to the other one) have a larger deviation from the mean value than the stated accuracy. When eliminating these measurements, the mean value changes to 34.6×10^{-22} cm², with a standard deviation (1σ) of 0.4×10^{-22} cm² (1.2%).

6.1.12. Summary of Section 6.1.

From the comparisons above using from different experiments, average O₃ cross-sections at room temperature (298 ± 3 K) were calculated at 10 single wavelengths between 253.65 and 632.82 nm, with uncertainties between 0.7–2.0%.

In the table below the results at these wavelengths are summarized:

Table 6-11: Average absorption cross-sections of O₃⁽¹⁾ at 298±5 K

Wavelength in nm	Value in 10 ⁻²⁰ cm ²	Uncertainty in 10 ⁻²⁰ cm ²	Uncertainty in %	Number of exp. data	Dispersion of exp. data
253.65	1141	10	0.9	17	[-1.3%, +1.4%]
289.36	149	3	2.0	13	[-3.4%, +3.4%]
296.73	60.3	0.9	1.6	13	[-5.2%, +4.2%]
302.15	29.2	0.5	1.8	12	[-2.7%, +4.1%]
543.52	0.0314	4×10 ⁻⁴	1.4	8	[-1.4%, +1.9%]
576.96	0.0477	4×10 ⁻⁴	0.8	10	[-6.1%, +1.9%]
594.10	0.0470	6×10 ⁻⁴	1.2	8	[-1.9%, +2.1%]
604.61	0.0522	5×10 ⁻⁴	0.9	7	[-2.5%, +0.9%]
611.97	0.0466	4×10 ⁻⁴	0.7	7	[-2.5%, +0.9%]
632.82	0.0346	4×10 ⁻⁴	1.2	7	[-1.2%, +2.3%]

⁽¹⁾ The cross sections are given in units of 10⁻²⁰ cm².

The average values given in this table are those determined after eliminating measurements having larger deviations than the stated experimental uncertainties.

Clearly, there is a large gap between 302–543 nm, which cannot be “filled” by simple comparisons of the experimental data.

Before proceeding further, we will compare the deviations of the experimental data (covering large spectral regions and available and different temperatures) with respect to the mean values as given in the table above, for each data set individually.

Table 6-12: Absorption cross-sections⁽¹⁾ of O₃ at room temperature (298±5 K) and comparison to average values (differences in %)

wavelength in nm	Mean value	<i>Bass and Paur</i>	<i>Molina and Molina</i>	<i>Brion et al.</i>	<i>Brion et al.</i>	<i>Burkholder and Talukdar</i>	<i>Richter et al.</i>	<i>Burrows et al.</i>	<i>Voigt et al.</i>	<i>Bogumil et al.</i>
253.65	1141 ±0.9%	1145 +0.4%	1157 +1.4%	1130.5 -0.9%	–	–	1137 -0.4%	1150 +0.8%	1137 -0.4%	1145 +0.4%
289.36	149 ±2.0%	150 +0.7%	154 +3.4%	151 +1.3%	–	–	150 +0.7%	151 +1.3%	154 +3.4%	151 +1.3%
296.73	60.3 ±1.6%	60.7 +0.7%	62.3 +3.3%	61.5 +2.0%	–	–	60.7 +1.5%	61.0 +2.0%	61.7 +3.2%	61.4 +2.7%
302.15	29.2 ±1.8%	29.4 +0.7%	30.1 +3.1%	29.8 +2.1%	–	–	29.5 +1.0%	29.9 +2.4%	30.4 +4.1%	29.8 +2.1%
543.52	0.0314 ±1.3%	–	–	–	0.0312 ±0.0%	0.0308 -1.9%	0.0318 +1.3%	0.0317 +1.0%	0.0315 +0.3%	0.0315 +0.3%
576.96	0.0477 ±0.8%	–	–	–	0.0477 ±0.0%	0.0469 -1.2%	0.0484 +1.5%	0.0483 +1.3%	0.0483 +1.3%	0.0484 +1.5%
594.10	0.0470 ±1.2%	–	–	–	0.0468 -0.4%	0.0464 -1.3%	0.0475 +1.1%	0.0476 +1.3%	0.0475 +1.1%	0.0473 +0.6%
604.61	0.0522 ±1.0%	–	–	–	0.0518 -0.8%	0.0509 -2.5%	0.0523 +0.2%	0.0524 +0.4%	0.0526 +0.8%	0.0526 +0.8%
611.97	0.0466 ±0.7%	–	–	–	0.0463 -0.6%	0.0453 -2.8%	0.0463 -0.6%	0.0469 +0.6%	0.0468 +0.4%	0.0469 +0.6%
632.82	0.0346 ±1.2%	–	–	–	0.0339 -2.0%	0.0335 -3.2%	0.0346 ±0.0%	0.0350 +1.1%	0.0347 +0.3%	0.0349 +0.9%
Mean deviations :		+0.6%	+2.8%	+1.1%	-0.6%	-2.2%	+0.6%	+1.2%	+1.5%	+1.1%

⁽¹⁾ The cross sections are given in units of 10⁻²⁰ cm².

6.2. Comparison of room temperature cross-sections over large regions

6.2.1. Comparison of the absolute values at all available wavelengths

On the next pages, we will plot the data and the relative differences with respect to the cross-sections of *Bogumil et al.* The latter data set was selected only because it covers the largest spectral range (230–1070 nm). We selected the following plot windows:

1. The entire region 240–790 nm on a logarithmic scale.
2. The 240–270 nm region (top of the Hartley band).
3. The 270–310 nm region (the “red” wing of the Hartley band).
4. The 310–340 nm region (the low-wavelength part of the Huggins bands).
5. The 340–380 nm region (the long-wavelength part of the Huggins bands).
6. The 380–510 nm region (the “blue” wing of the Chappuis band).
7. The 510–650 nm region (top of the Chappuis band).
8. The 650–800 nm region (the “red” wing of the Chappuis band).

From the plots on the next pages, systematic differences between the available measurements are observed:

- The data show large differences in the region 360–450 nm, a region where the O_3 cross-sections are small (less than 10^{-22} cm²).
- In the 240–270 nm region, the relative differences are smaller than 2%, except for the data of *Voigt et al.* who show a strong baseline drift below 255 nm. The data of *Brion et al.* show a jump of about +1% at 260 nm. The data of *Bogumil et al.* seem to contain periodic artefacts of the order of 0.5–1.0%.
- In the 270–310 nm region, the relative differences are smaller than 2%. The data of *Bass and Paur* show a jump of about –1% at 285 nm. The data of *Bogumil et al.* contain a straylight feature of the order of 2% around 305 nm.
- In the 310–340 nm, large differences due to differences spectral resolutions and wavelength shifts are observed, between –10% and +12%. The data of *Voigt et al.* show a strong baseline drift between 310–320 nm.
- In the 340–510 nm region, the data differ considerably, due to the small cross-sections in this region. The differences increase towards longer wavelengths. From this observation together with the fact that the O_3 still spectral features still remain in the relative differences, we conclude that the differences arise

mainly from straylight or baseline drifts in the different experiments. The data of *Richter et al.* show a sudden jump of +200% at 400 nm.

- In the 510–650 nm region, the data differ by up to 4%. The cross-sections of *Bogumil et al.* contain an artefact of about 1% around 595 nm, and some small structures of about 0.2% in the entire region. The data of *Brion et al.* show a broad structure of about –2% around 640 nm. The data of *Richter et al.* show a small jump of about –1% around 610 nm.
- In the 650–800 nm region, the differences increase again towards longer wavelengths, probably due to baseline drifts or straylight. At 762 nm, the data of *Voigt et al.* and *Bogumil et al.* clearly contain residual O₂ structures.

Figure 6-1: Comparison of O₃ absorption cross-sections at 298±5 K: 240–800 nm

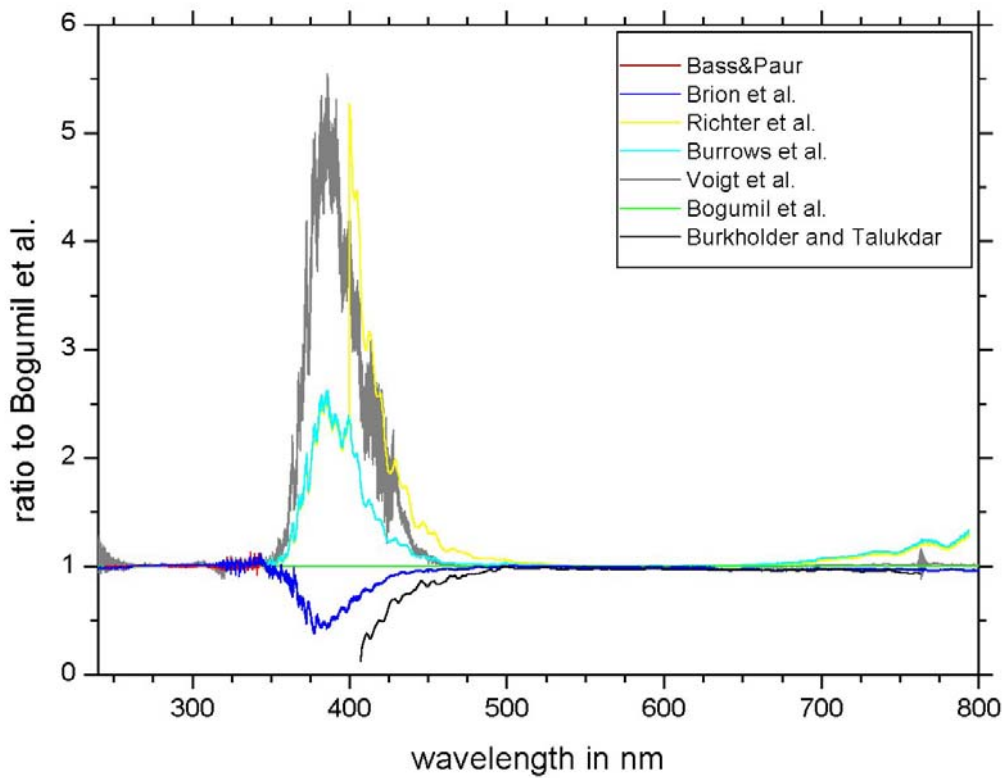
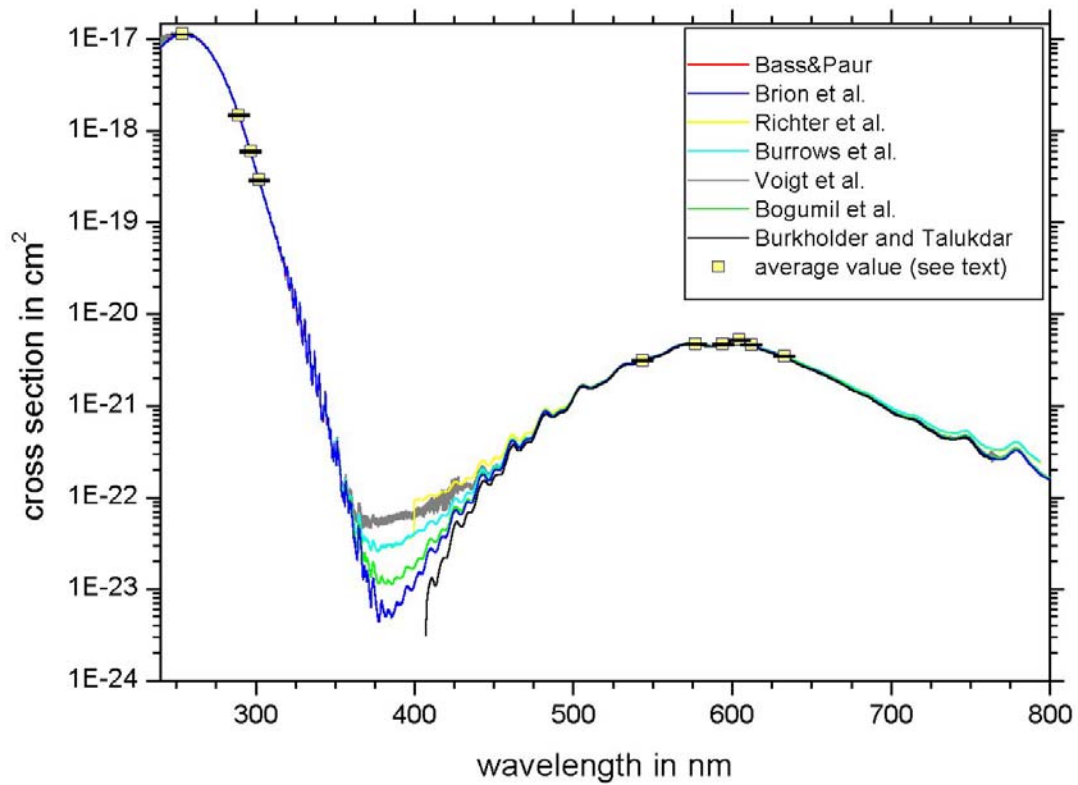


Figure 6-2: Comparison of O₃ absorption cross-sections at 298±5 K: 240–270 nm

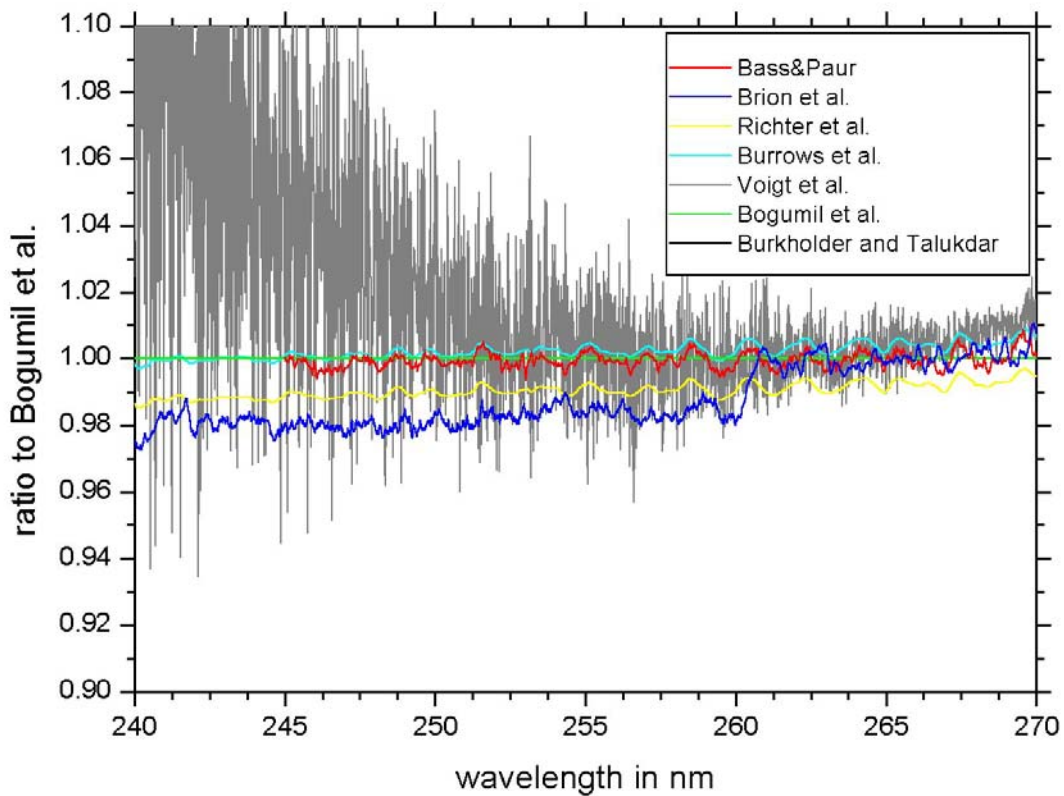
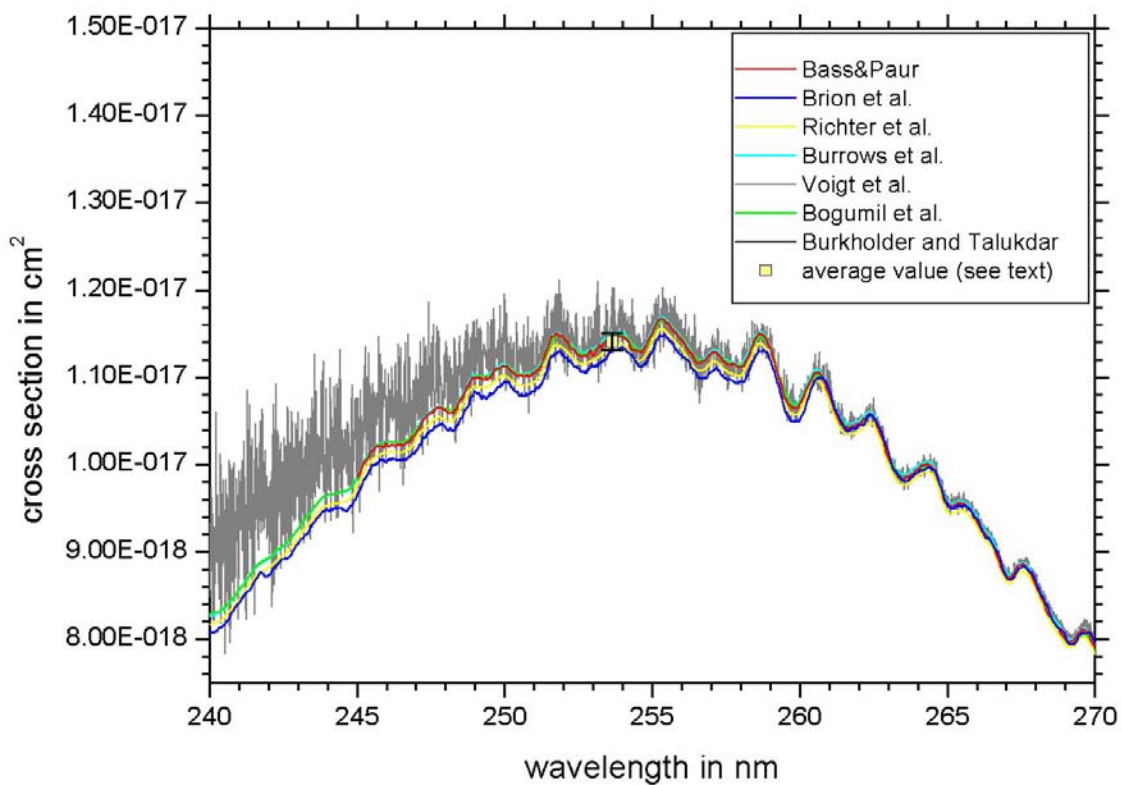


Figure 6-3: Comparison of O₃ absorption cross-sections at 298±5 K: 270–310 nm

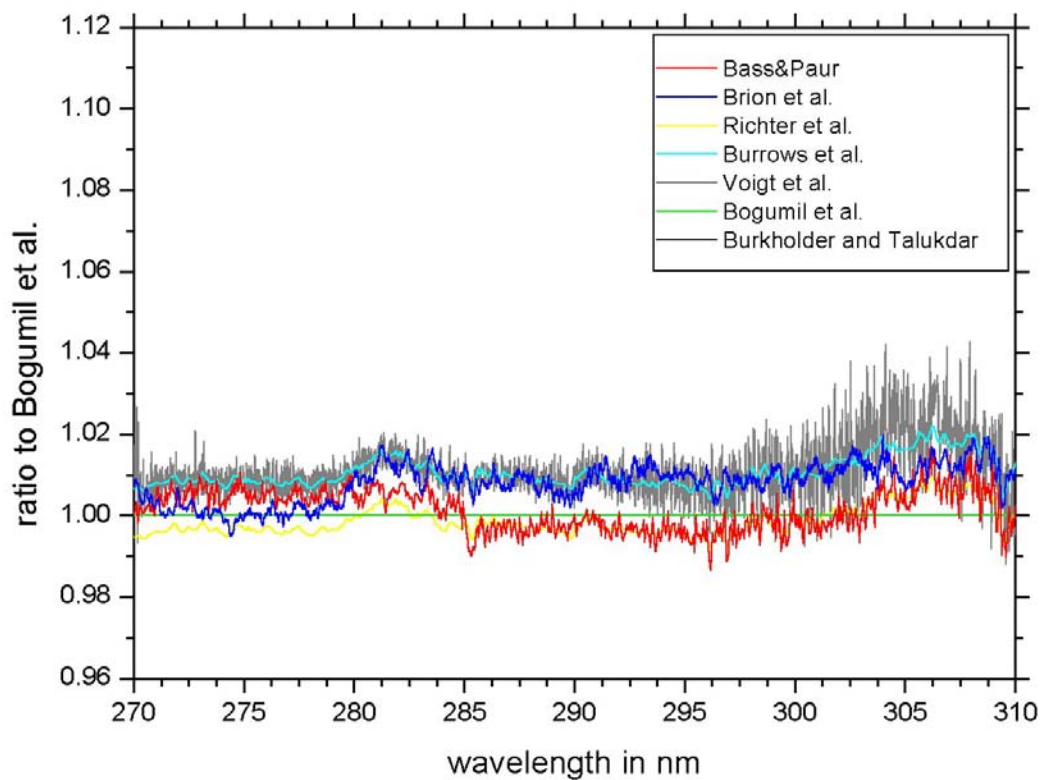
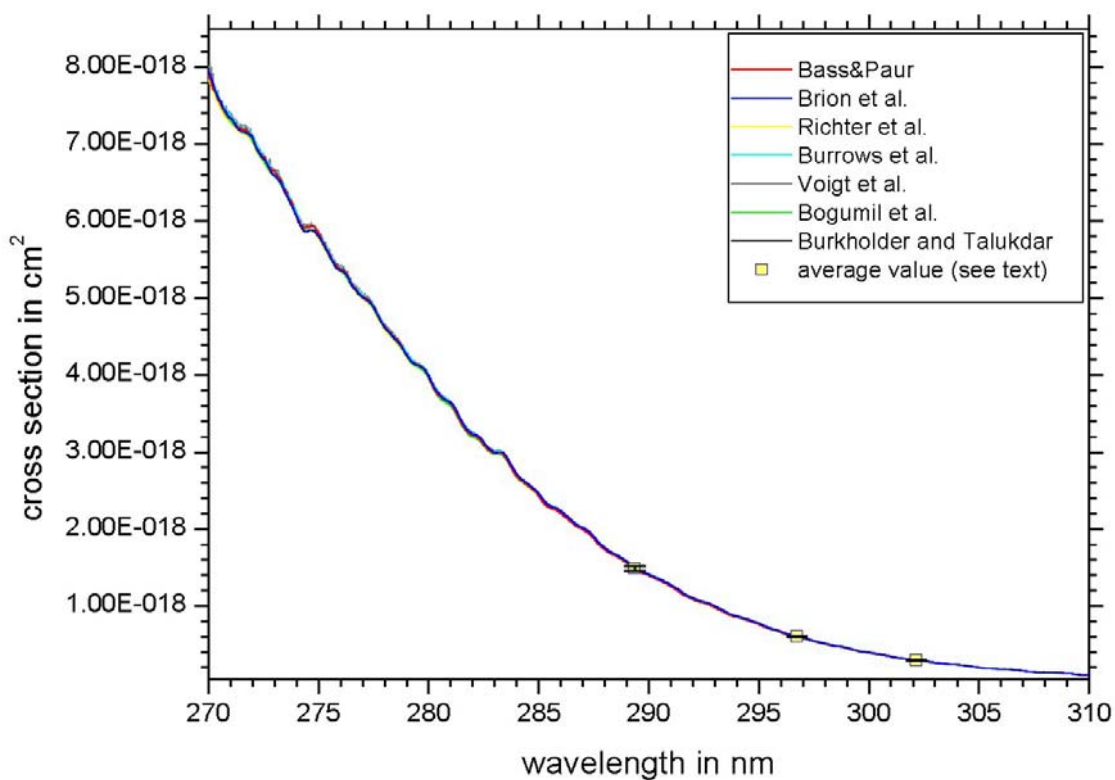


Figure 6-4: Comparison of O₃ absorption cross-sections at 298±5 K: 310–340 nm

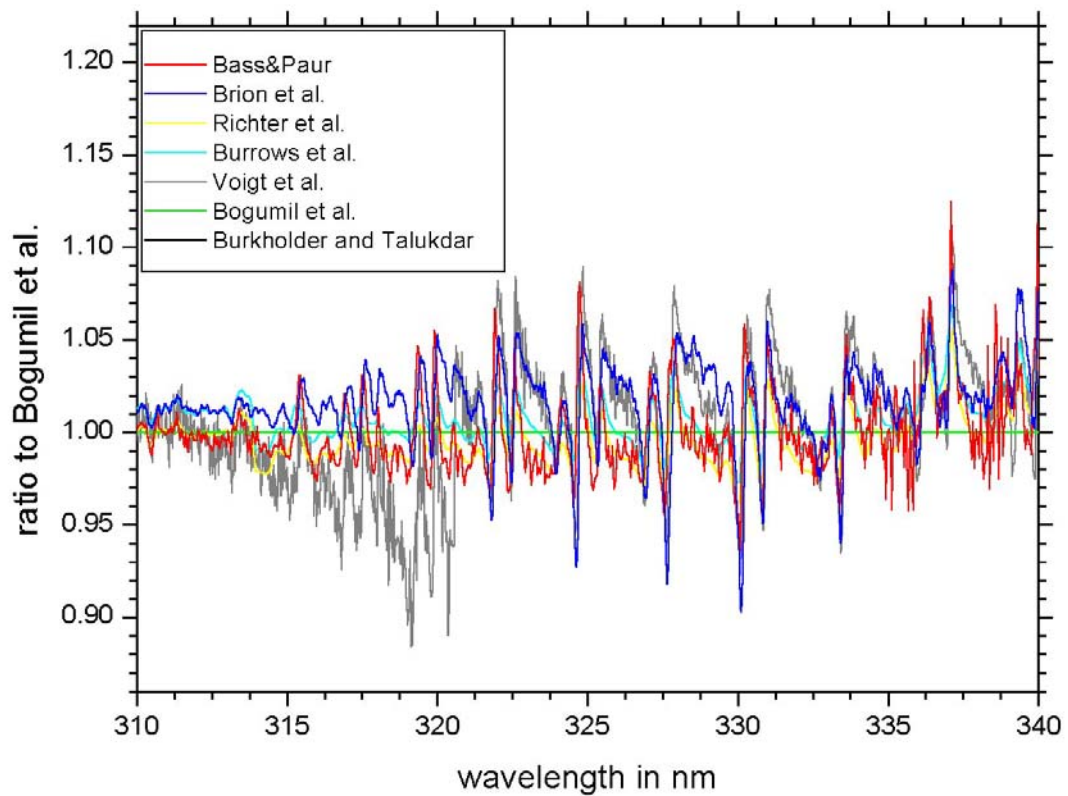
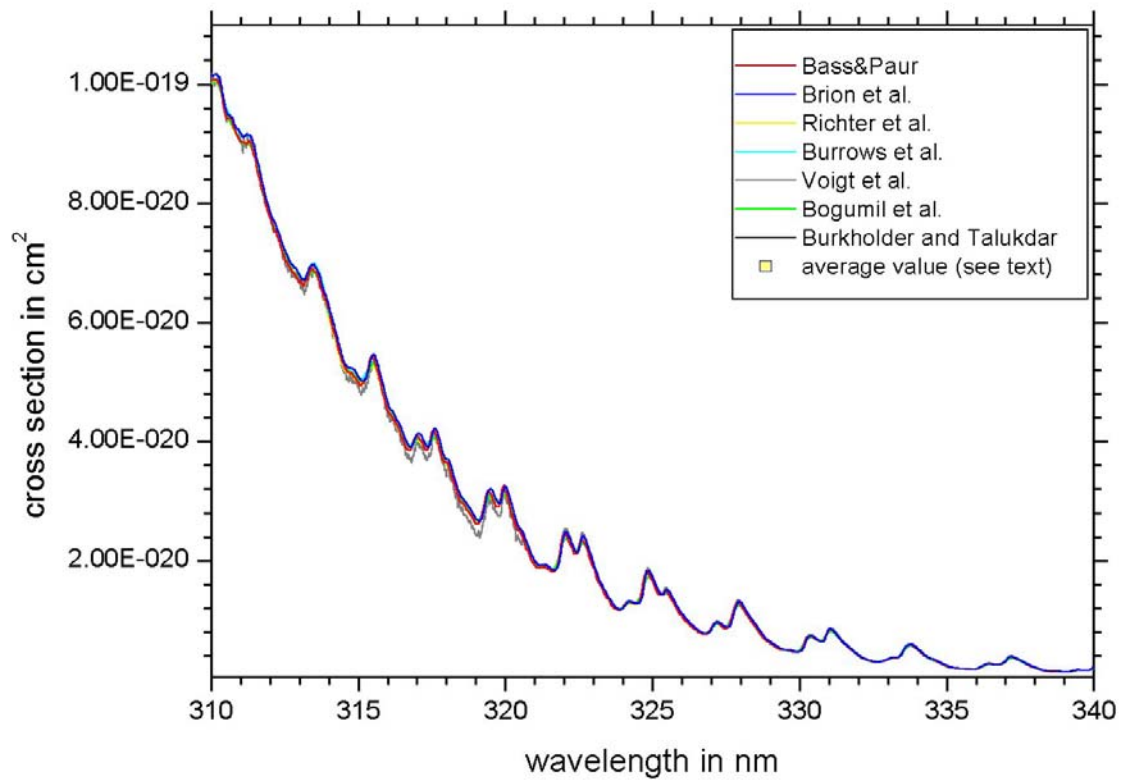


Figure 6-5: Comparison of O₃ absorption cross-sections at 298±5 K: 340–380 nm

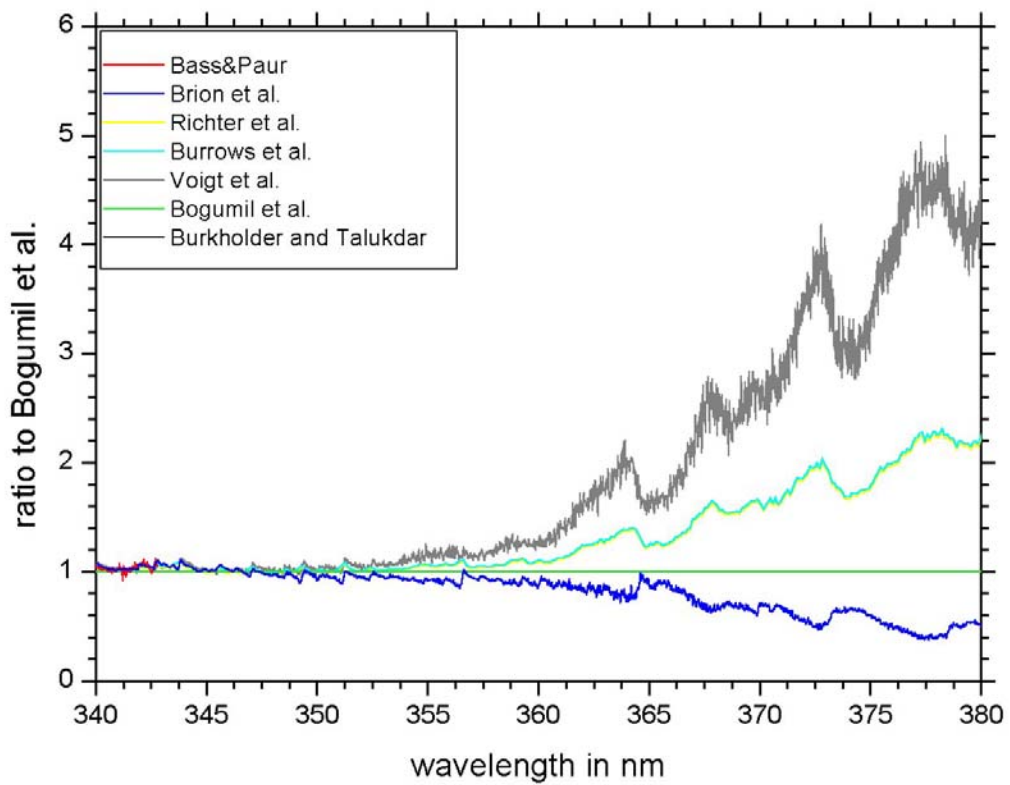
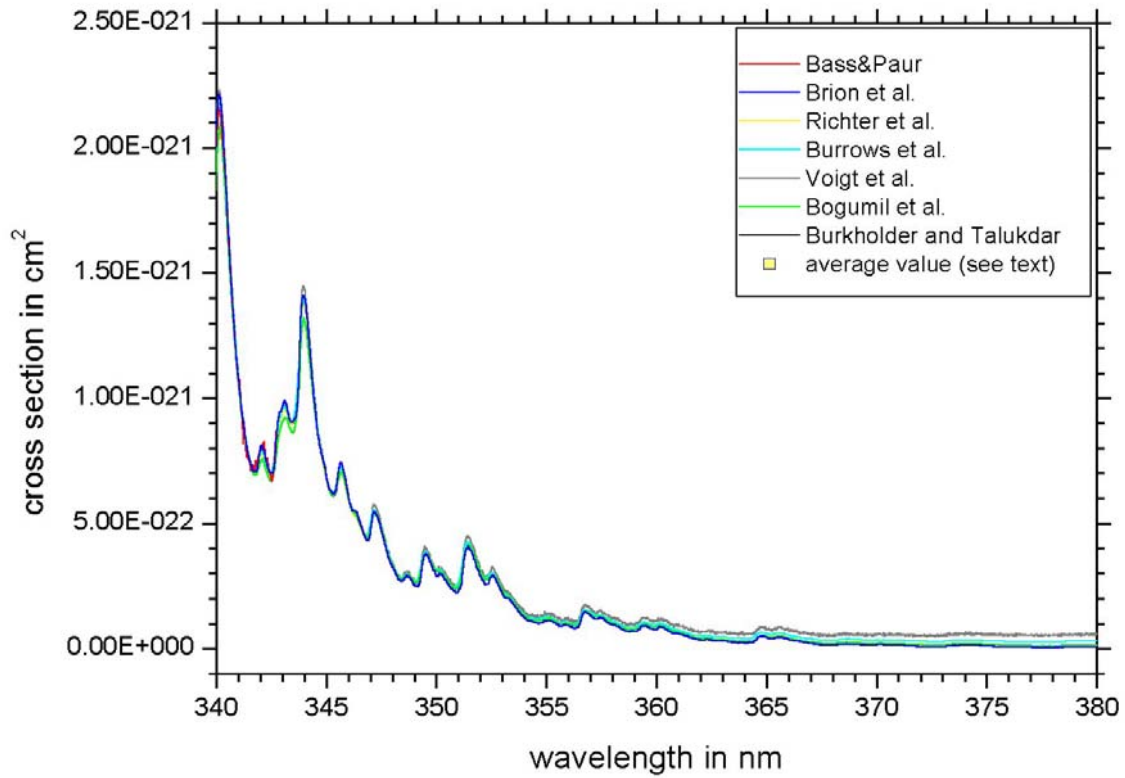


Figure 6-6: Comparison of O₃ absorption cross-sections at 298±5 K: 380–510 nm

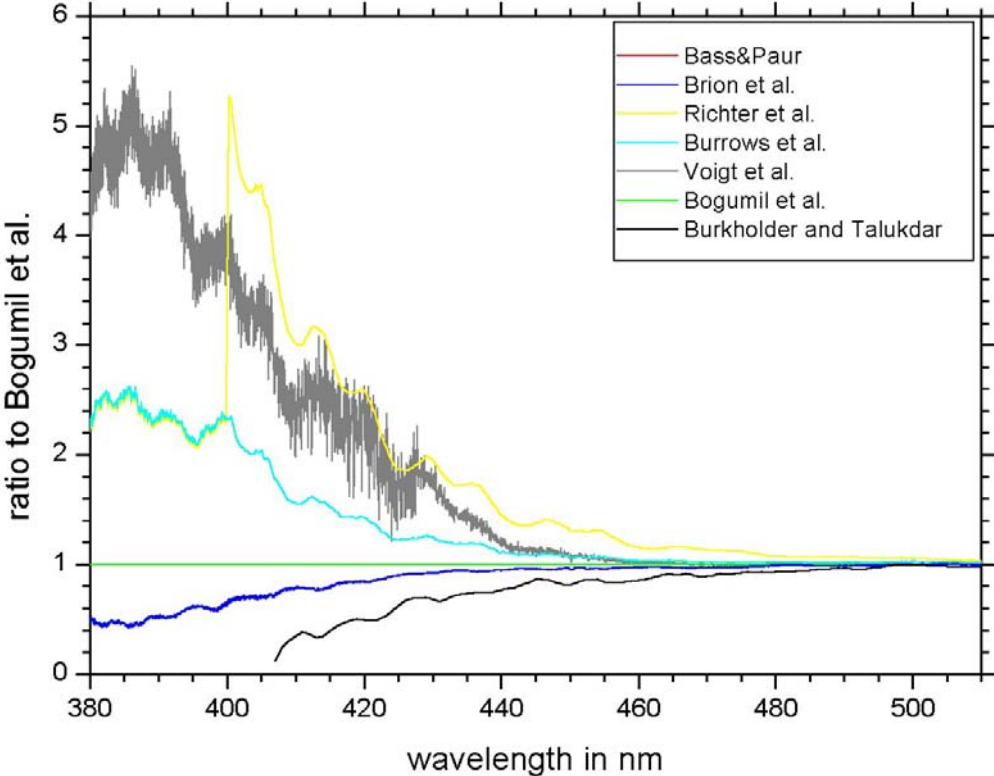
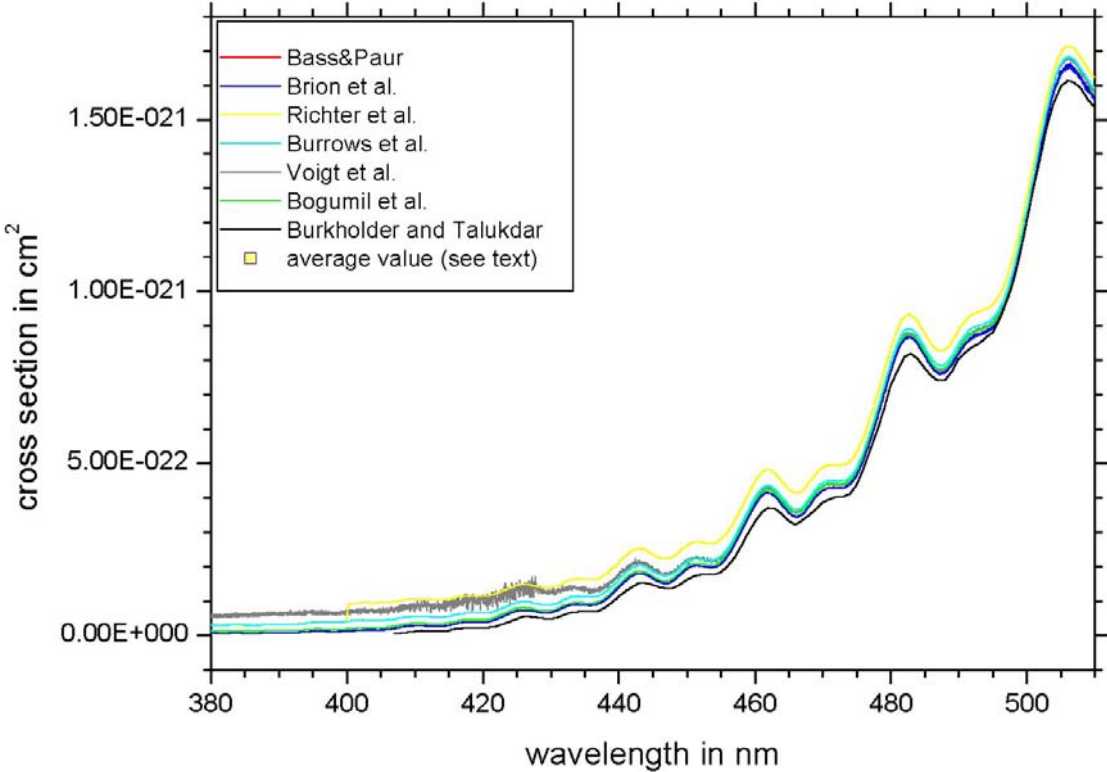


Figure 6-7: Comparison of O₃ absorption cross-sections at 298±5 K: 510–650 nm

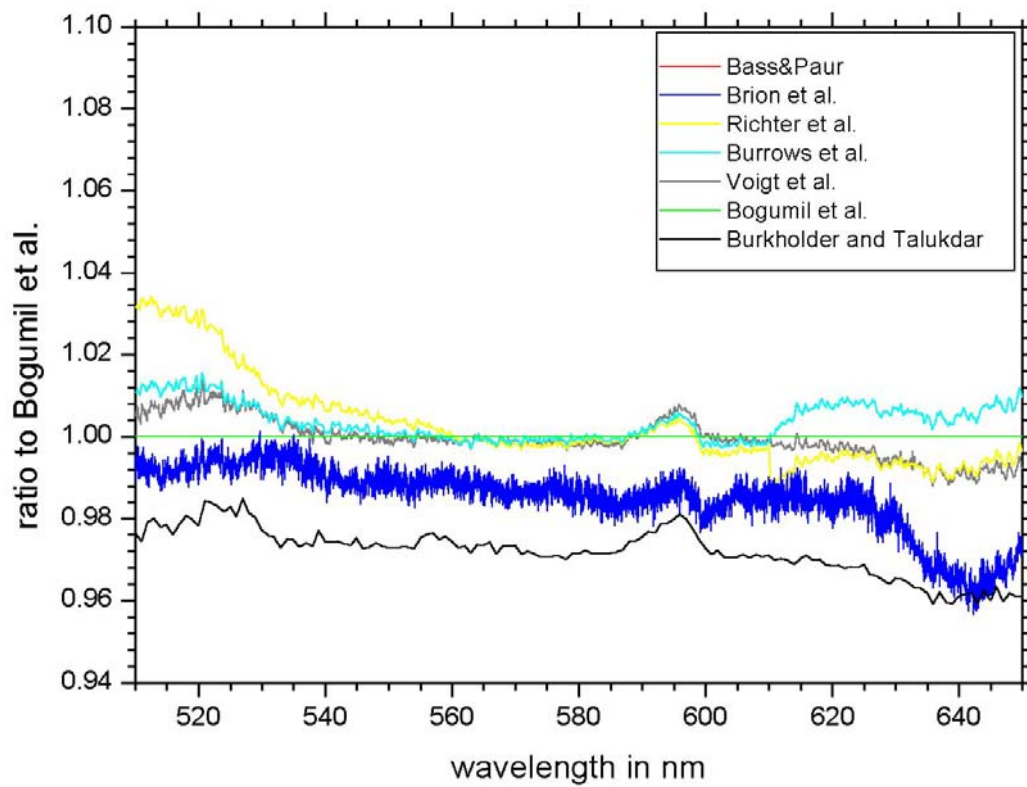
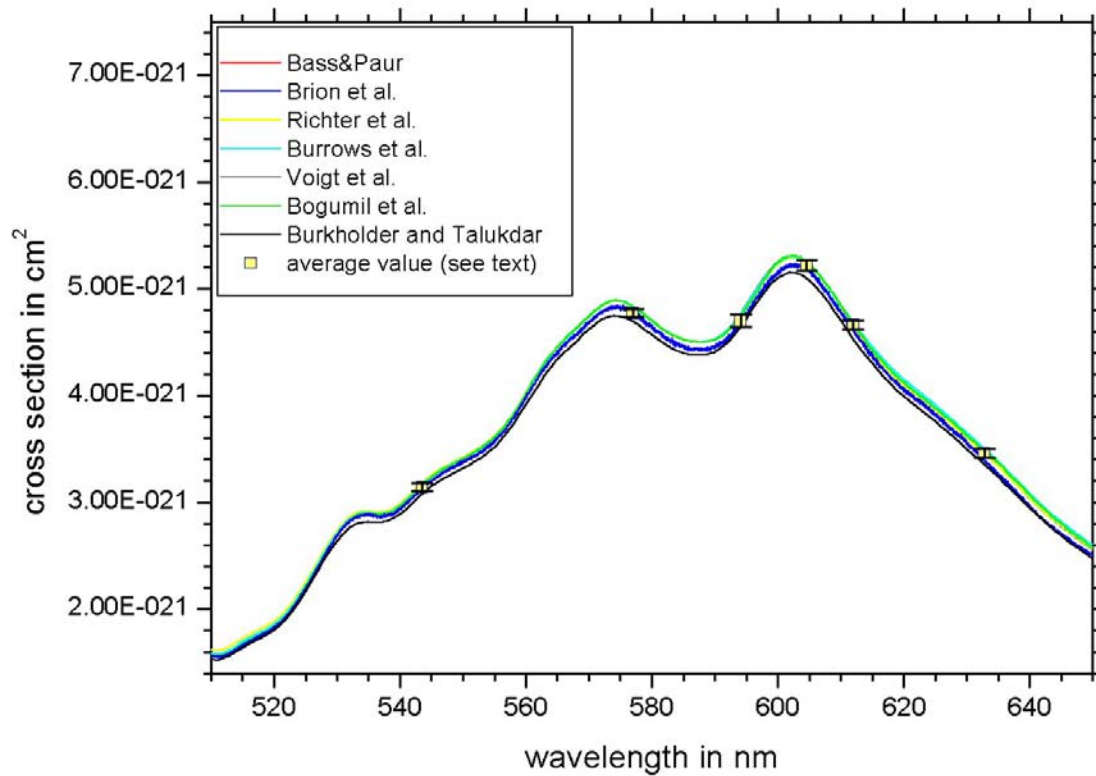
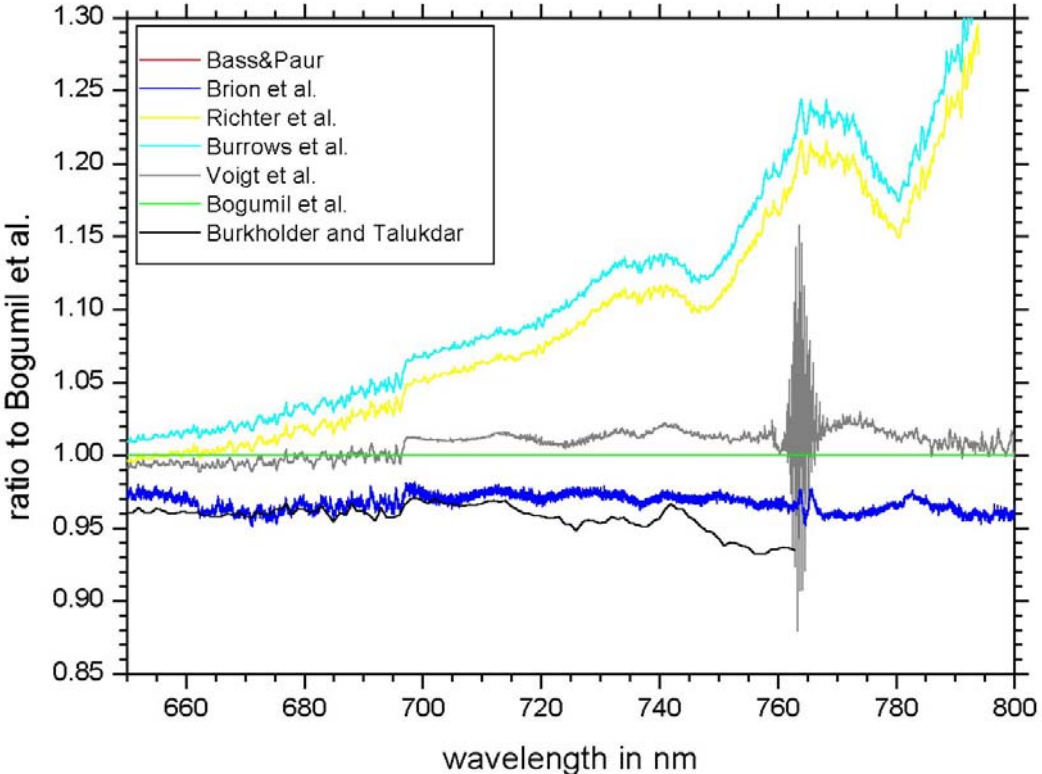
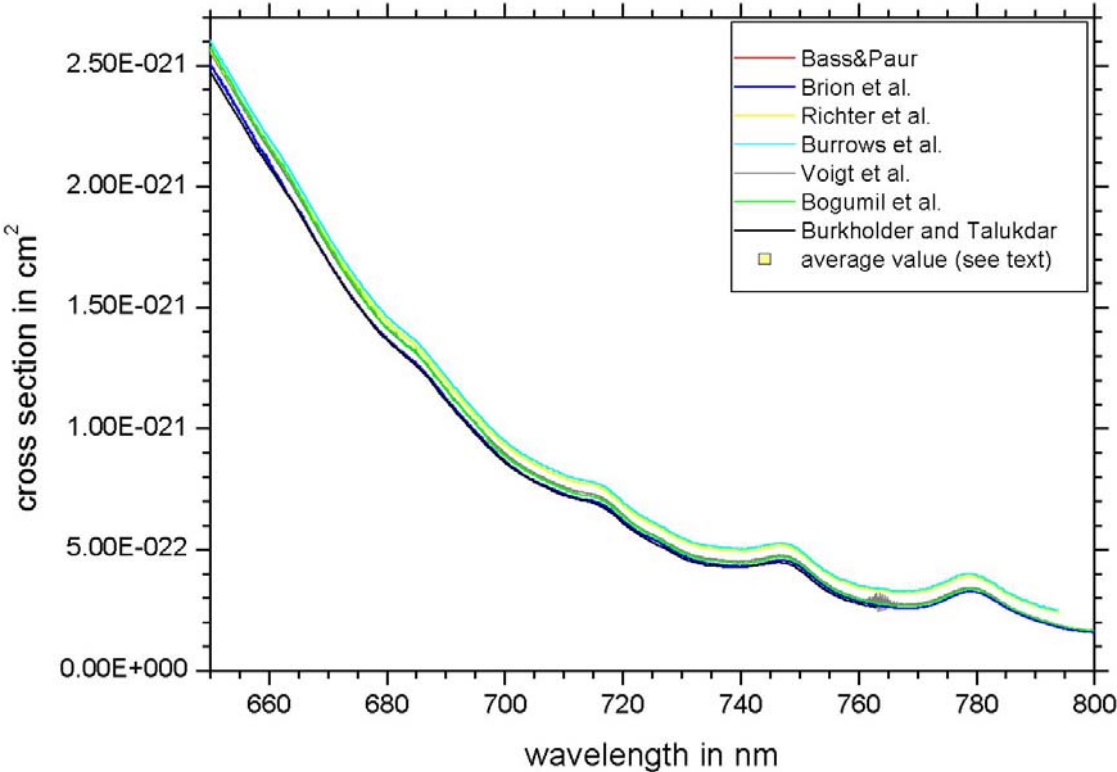


Figure 6-8: Comparison of O₃ absorption cross-sections at 298±5 K: 650–800 nm



6.2.2. Integrated O₃ absorption cross-sections at room temperature

Because the integrated absorption cross-sections are rather insensitive to differences in small spectral intervals, we have calculated these values for the following regions:

- in the Hartley band between 245–340 nm,
- in the Chappuis band between 410–690 nm,
- in the Huggins bands between 325–340 nm,
- in the blue tail of the Chappuis band between 410–520 nm.

Table 6-13: Integrated absorption cross-sections of O₃⁽¹⁾ at 298±5 K

Reference	Hartley band	Chappuis band	Huggins band	Blue tail of the Chappuis band
<i>Bass and Paur</i>	3.55×10 ⁻¹⁶ ±0.0%	–	8.20×10 ⁻²⁰ –1.2%	–
<i>Brion et al.</i>	3.52×10 ⁻¹⁶ –0.8%	–	8.32×10 ⁻²⁰ +0.3%	–
<i>Richter et al.</i>	3.53×10 ⁻¹⁶ –0.6%	6.47×10 ⁻¹⁹ +1.6%	8.25×10 ⁻²⁰ –0.6%	7.23×10 ⁻²⁰ +8.4%
<i>Burrows et al.</i>	3.57×10 ⁻¹⁶ +0.6%	6.45×10 ⁻¹⁹ +1.2%	8.35×10 ⁻²⁰ +0.6%	6.75×10 ⁻²⁰ +1.1%
<i>Voigt et al.</i>	3.58×10 ⁻¹⁶ +0.8%	6.42×10 ⁻¹⁹ +0.7%	8.35×10 ⁻²⁰ +0.6%	6.75×10 ⁻²⁰ +1.1%
<i>Bogumil et al.</i>	3.55×10 ⁻¹⁶ ±0.0%	6.41×10 ⁻¹⁹ +0.5%	8.33×10 ⁻²⁰ +0.4%	6.52×10 ⁻²⁰ –2.2%
<i>Burkholder and Talukdar</i>	–	6.21×10 ⁻¹⁹ –2.6%	–	6.35×10 ⁻²⁰ –4.8%
<i>Brion et al.</i>	–	6.29×10 ⁻¹⁹ –1.3%	–	6.43×10 ⁻²⁰ –3.6%
Average value	3.55×10 ⁻¹⁶	6.38×10 ⁻¹⁹	8.30×10 ⁻²⁰	6.67×10 ⁻²⁰
Relative uncertainty	±0.6%	±1.6%	±0.7%	±4.8%

⁽¹⁾ The integrated cross sections are given in units of cm²×nm.

One can state that the agreement between the different data is better than 1.2% for the Hartley and Huggins bands, but less (up to 2.7%) for the Chappuis band, and much less for the blue tail of the Chappuis band. The data of *Burrows et al.* and *Voigt et al.* are always higher than the average.

6.2.3. Comparison of the O₃ cross-sections in the Huggins bands

To evaluate the O₃ cross-sections in the Huggins bands, more work is required.

Because of the strong influence of small wavelength shifts and of the spectral resolution, we have used the following procedure, in the region 323–343 nm:

- all spectra were convoluted with a Gaussian with a 0.4 nm FWHM
- the spectra were compared with a non-linear least-squares fitting program, with five fitting parameters: a quadratic baseline polynomial (3 parameters), a scaling coefficient for the magnitude of the cross-sections (1 parameter), and a linear wavelength shift coefficient (1 parameter).

The convolution is employed to minimize the influence of spectral resolution when comparing cross-sections recorded at rather high resolution (*Bass and Paur*, *Brion et al.*, and *Voigt et al.*) with cross-sections recorded at lower resolution (*Richter et al.*, *Burrows et al.*, and *Bogumil et al.*). The non-linear least-squares fitting program is employed to minimize the influence of wavelength shifts and of baseline drifts or straylight. We have verified that the convolution does not change the scaling and shifting parameters within the experimental uncertainties.

Figure 6-9: NLS-fit of O₃ absorption cross-sections at 298±5 K in the Huggins bands (323–343 nm): *Bass and Paur* compared to *Brion et al.*

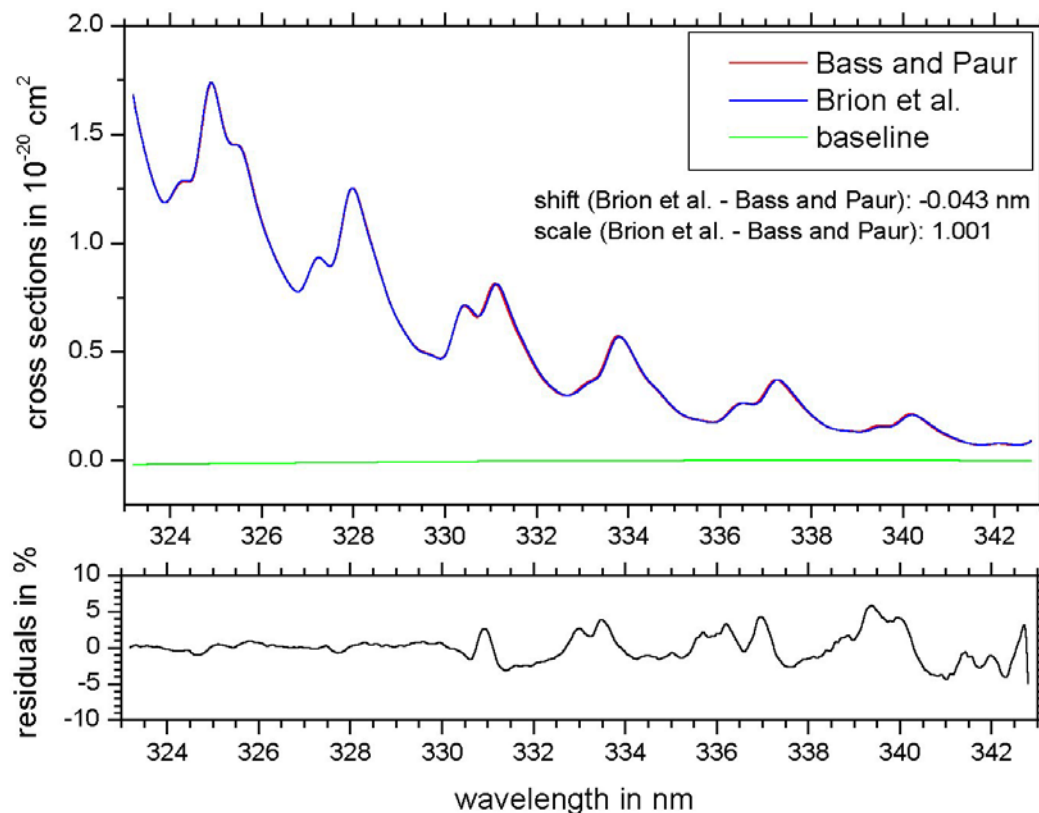


Figure 6-10: NLS-fit of O₃ absorption cross-sections at 298±5 K in the Huggins bands (323–343 nm): *Bass and Paur* compared to *Richter et al.*

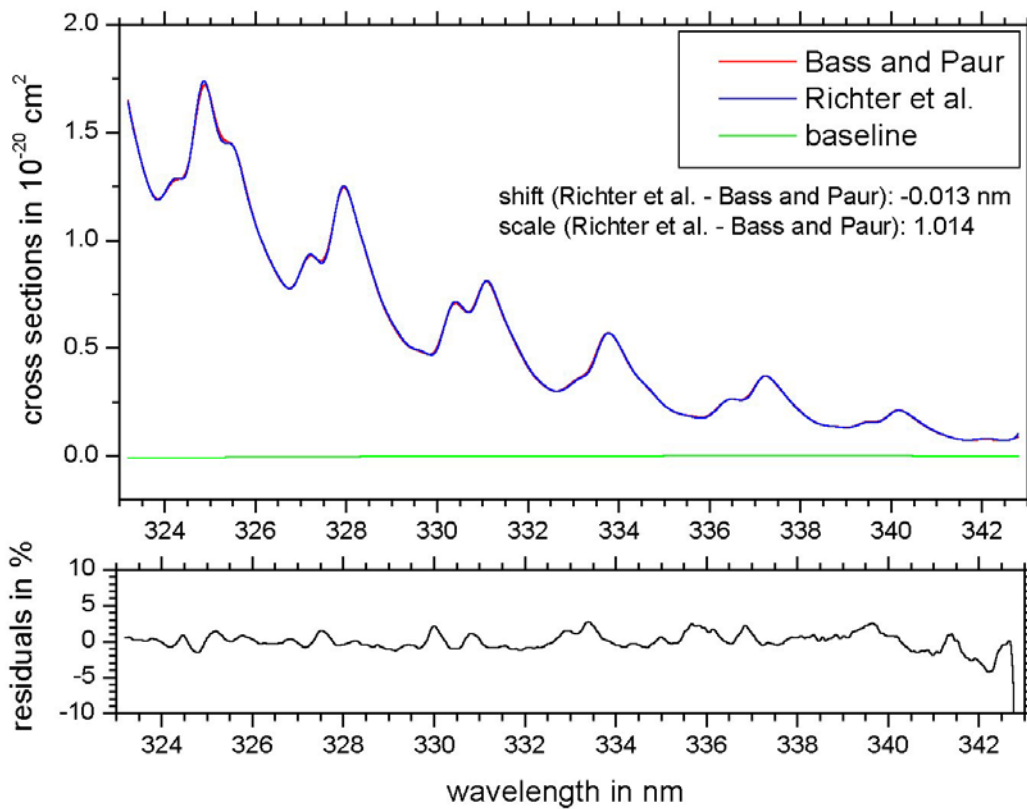


Figure 6-11: NLS-fit of O₃ absorption cross-sections at 298±5 K in the Huggins bands (323–343 nm): *Bass and Paur* compared to *Burrows et al.*

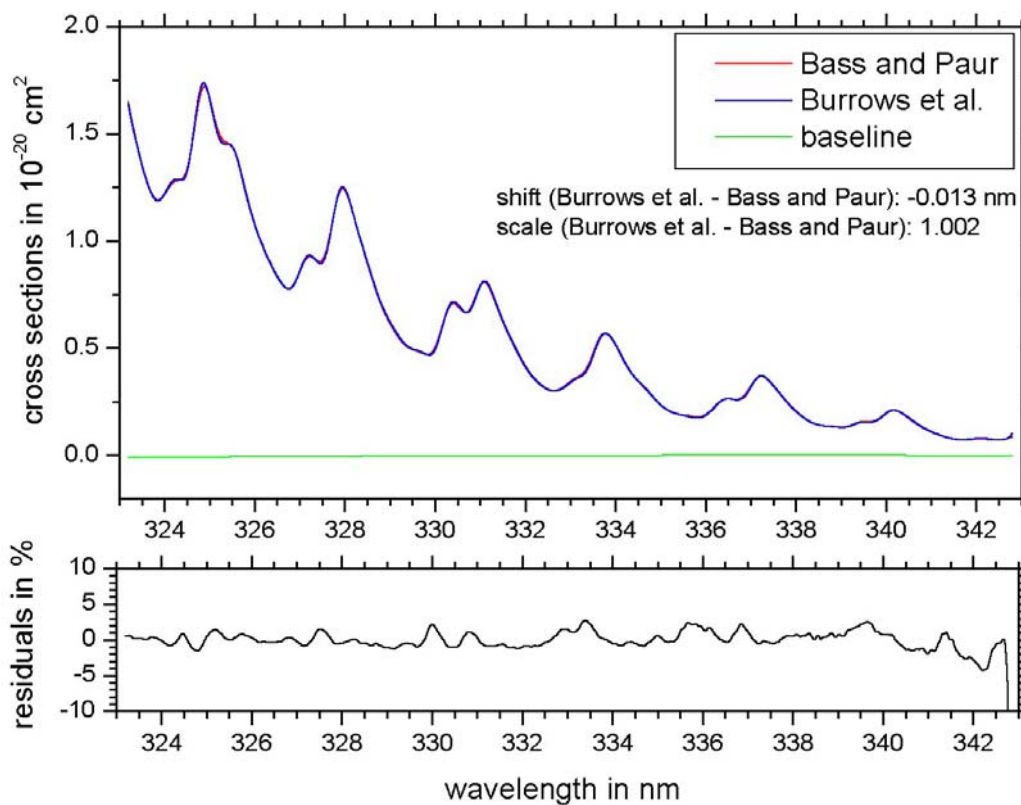


Figure 6-12: NLS-fit of O₃ absorption cross-sections at 298±5 K in the Huggins bands (323–343 nm): *Bass and Paur* compared to *Voigt et al.*

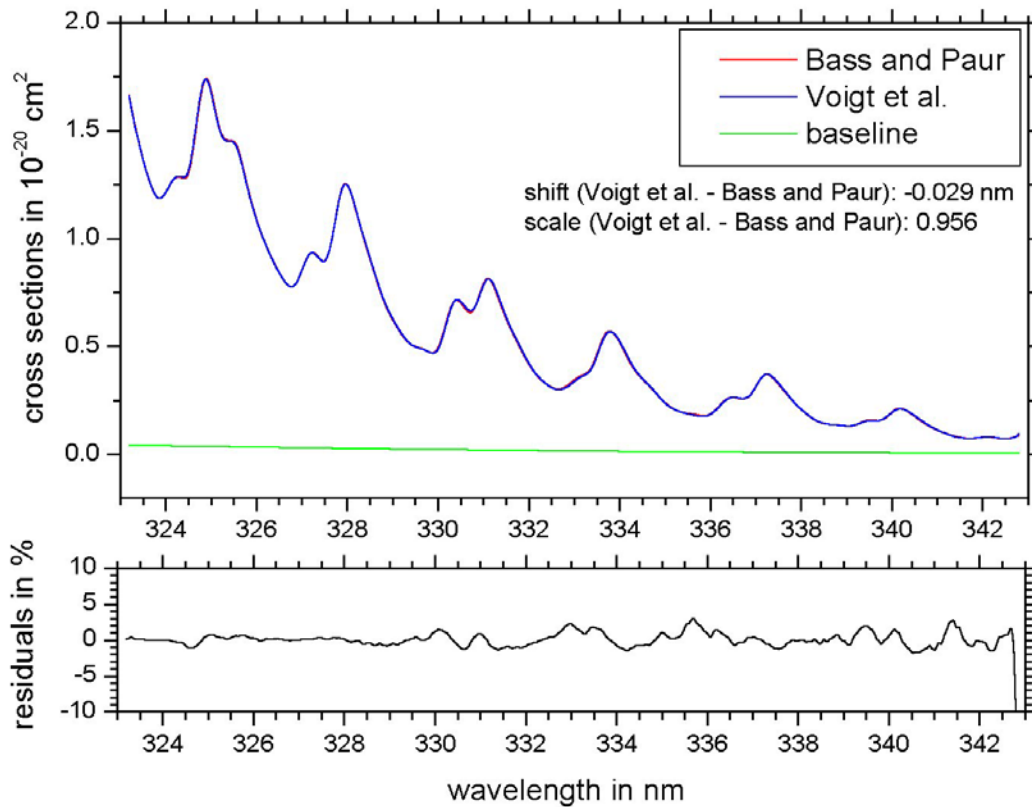
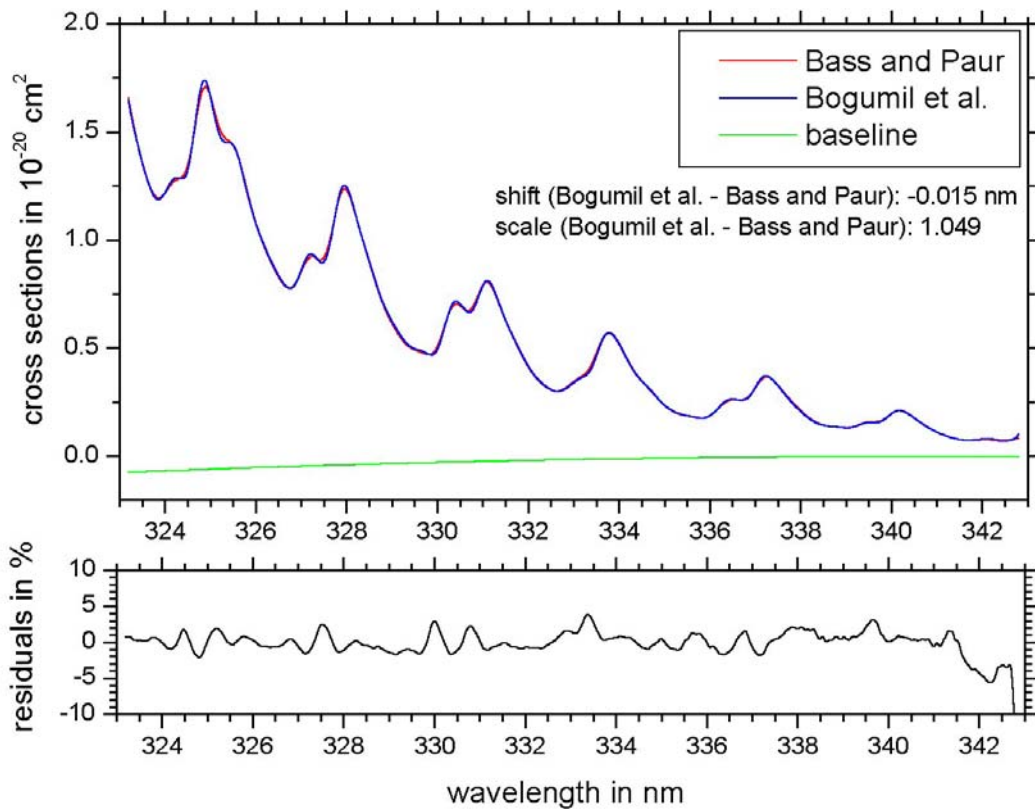


Figure 6-13: NLS-fit of O₃ absorption cross-sections at 298±5 K in the Huggins bands (323–343 nm): *Bass and Paur* compared to *Bogumil et al.*



From the fits, one can draw the following conclusions:

- Despite the rather good agreement in the other regions of the spectrum, the O₃ cross-sections from the different experiments show deviations of up to 5% concerning the magnitude of the O₃ cross-sections between 323–343 nm, after correction for baseline effects and wavelength shifts.
- The remaining residuals are in the order of 2-5%, and are due to non-linear wavelength differences (we used only a linear shift), to the differences in the ILS of the laboratory spectra, and partly also to the non-linearity of the convolution (see Chapter 2).
- The data of *Bass and Paur*, *Brion et al.*, *Richter et al.*, and *Burrows et al.* show only small baseline differences.
- The data of *Bass and Paur*, *Brion et al.*, *Richter et al.*, and *Burrows et al.* show good agreement concerning the magnitude of the cross-sections: the relative difference between *Bass and Paur* and *Brion et al.* is 0.1%, the relative difference between *Bass and Paur* and *Richter et al.* is 1.5%, and the relative difference between *Richter et al.* and *Burrows et al.* is 1.1%.
- The data of *Bass and Paur* show systematic wavelength differences, and need to be shifted to higher wavelengths. The shift required is +0.029 nm compared to the FTS data of *Voigt et al.*
- The data of *Brion et al.* show systematic wavelength differences, and need to be shifted to lower wavelengths. There is a jump in the wavelength calibration of *Brion et al.* around 331 nm, making it difficult to determine a single shift coefficient. If a linear shift is assumed one has to use –0.014 nm compared to the FTS data of *Voigt et al.*
- The data of *Voigt et al.* show a systematic baseline drift towards lower wavelengths, and are higher than the cross-sections of *Bass and Paur*, *Brion et al.*, *Richter et al.*, and *Burrows et al.* by about 5%.
- The data of *Bogumil et al.* are lower than the cross-sections of *Bass and Paur*, *Brion et al.*, *Richter et al.*, and *Burrows et al.* by about 5%, and show a systematic baseline drift towards smaller wavelengths.
- The data of *Bogumil et al.* and of *Richter et al.* (which have exactly the same wavelength scale as *Burrows et al.*) agree very well between each other (shift of 0.002 nm) but are systematically too low by 0.014 nm (*Bogumil et al.*) and by 0.016 nm (*Richter et al.* and *Burrows et al.*) compared to *Voigt et al.*

Using the relative differences obtained from the non-linear least-squares fits, we have determined the relative differences of each individual spectrum to the average values (taking into account the different wavelength shifts and the baseline differences) for the O₃ cross-sections in this region (323–343 nm) at 298±5 K.

Table 6-14: Comparison of O₃ cross-sections in the Huggins bands at 298±5 K using a non-linear least-squares fit approach

Reference 1	Reference 2	Shift in nm	Scaling Factor	Scale to Mean
–	<i>Bass and Paur</i>	–	1.000	0.996
<i>Bass and Paur</i>	<i>Brion et al.</i>	–0.043	1.001	0.997
<i>Bass and Paur</i>	<i>Voigt et al.</i>	–0.029	0.956	0.953
<i>Bass and Paur</i>	<i>Richter et al.</i>	–0.013	1.014	1.010
<i>Bass and Paur</i>	<i>Burrows et al.</i>	–0.013	1.002	0.965
<i>Bass and Paur</i>	<i>Bogumil et al.</i>	–0.015	1.049	1.045
Mean: 1.004 ± 0.030				

It is very important to take into account these systematic differences when comparing O₃ columns determined from the different cross-sections.

6.2.4 Summary of Section 6.2

In this section, we have compared the available laboratory measurements of O₃ cross sections at room temperature, in the entire 240–790 nm region.

We have observed several systematic artefacts (baseline drifts, jumps from the concatenation of different spectra) and differences in the magnitude of the cross sections. The integrated cross-sections agree well in the Hartley and Huggins bands but less in the Chappuis band and in the blue wing of the Chappuis band. In the Huggins bands, non-linear least-squares fits can take into account the differences in the baseline and in the wavelength calibration.

In the following Chapters, we will apply the same procedure (comparisons over broad regions, comparisons of integrated cross-sections, and comparisons of the results of least-squares fits in the Huggins bands) to the O₃ cross-sections that are available at lower temperatures.

7. Comparison of the O₃ cross-sections between 230–790 nm at temperatures below room temperature (203–280 K)

In order to study the absorption cross-sections at temperatures below ambient, we have used the same approaches as for the comparisons at room temperature, at four selected temperatures where sufficient laboratory measurements are available:

- 276±4 K,
- 243±3 K,
- 221±3 K, and
- 203±1 K.

The following O₃ cross-sections were available in digital form over large spectral intervals:

- *Bass and Paur* (245–343 nm),
- *Brion et al.* (300–345 nm and 515–650 nm)¹,
- *Burkholder and Talukdar* (407–763 nm),
- *Richter et al.* (231–794 nm),
- *Burrows et al.* (231–794 nm),
- *Voigt et al.* (231–851 nm),
- *Bogumil et al.* (230–1070 nm).

Note that *Burkholder et al.* and *Brion et al.* did not measure the cross-sections at temperatures below 218 K.

7.1. Relative change of the O₃ absorption cross-sections with temperature

For each set of laboratory cross-sections at different temperatures, we have studied the relative change of the O₃ absorption cross-sections with temperature. This approach allows the identification of regions where the effect of temperature is dominant, and reduces systematic errors due to the determination of O₃ amounts during the laboratory measurements.

We will later quantify the absolute changes in the most important regions.

The first series of plots shows the relative changes in the region 240–350 nm.

¹ There are measurements of *Brion et al.* between 340–519 nm at lower temperatures (243 K and 218 K) that were not available in digital format when this report was written. However the authors state that their data agree with those of *Burkholder et al.* [*J. Malicet et al.*, personal communication, 2001].

Figure 7-1: Relative changes of the O₃ cross-sections compared to the values at room temperature in the region 240–350 nm (source: *Bass and Paur*)

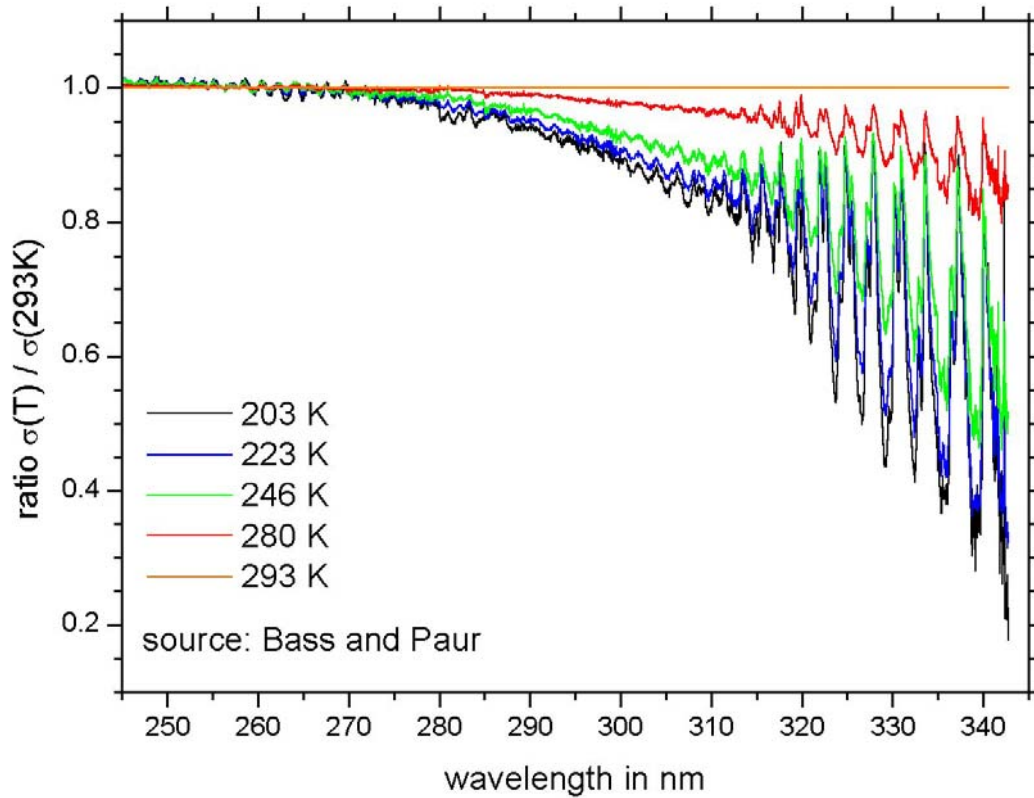


Figure 7-2: Relative changes of the O₃ cross-sections compared to the values at room temperature in the region 240–350 nm (source: *Brion et al.*)

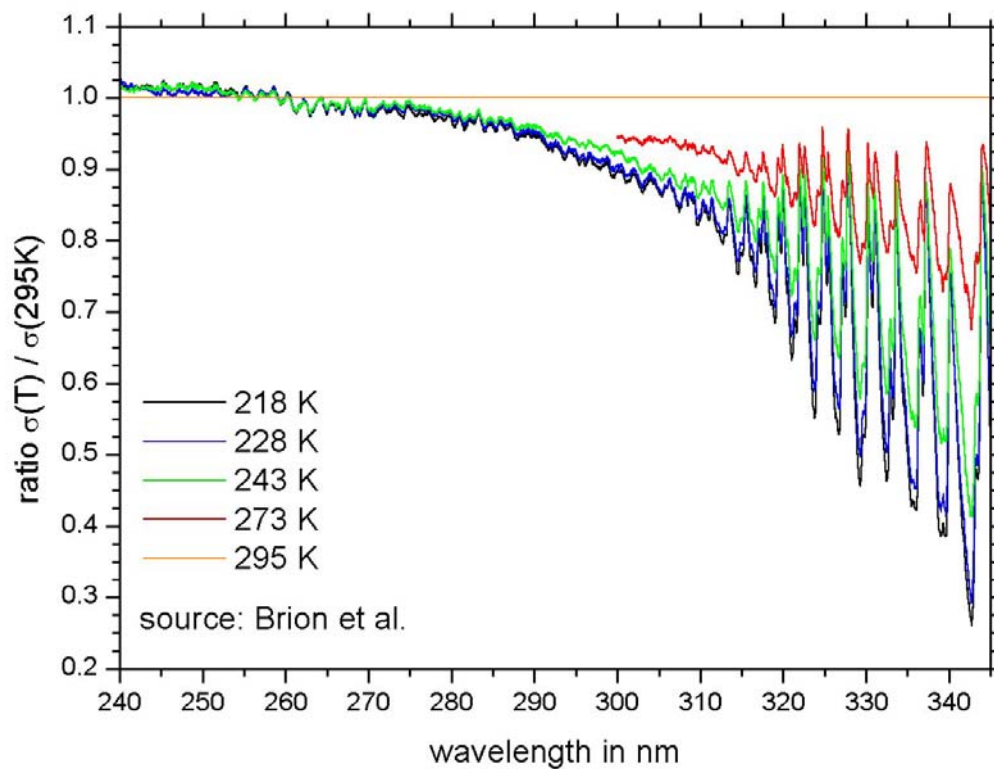


Figure 7-3: Relative changes of the O₃ cross-sections compared to the values at room temperature in the region 240–350 nm (source: *Richter et al.*)

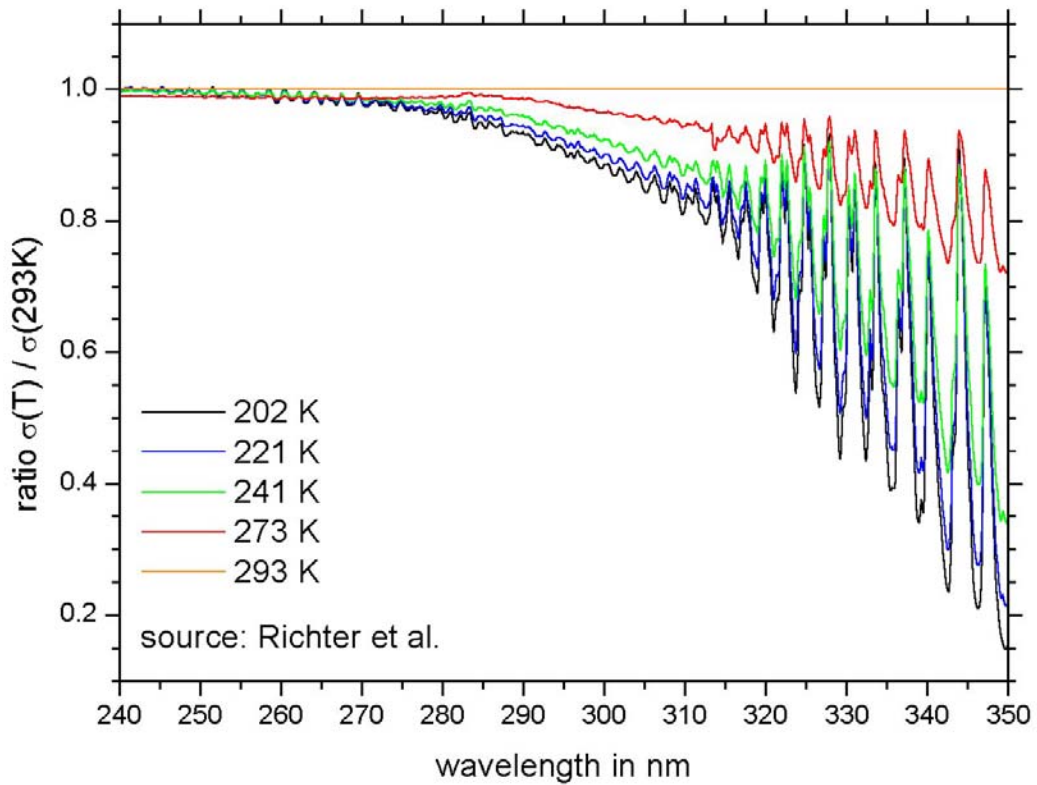


Figure 7-4: Relative changes of the O₃ cross-sections compared to the values at room temperature in the region 240–350 nm (source: *Burrows et al.*)

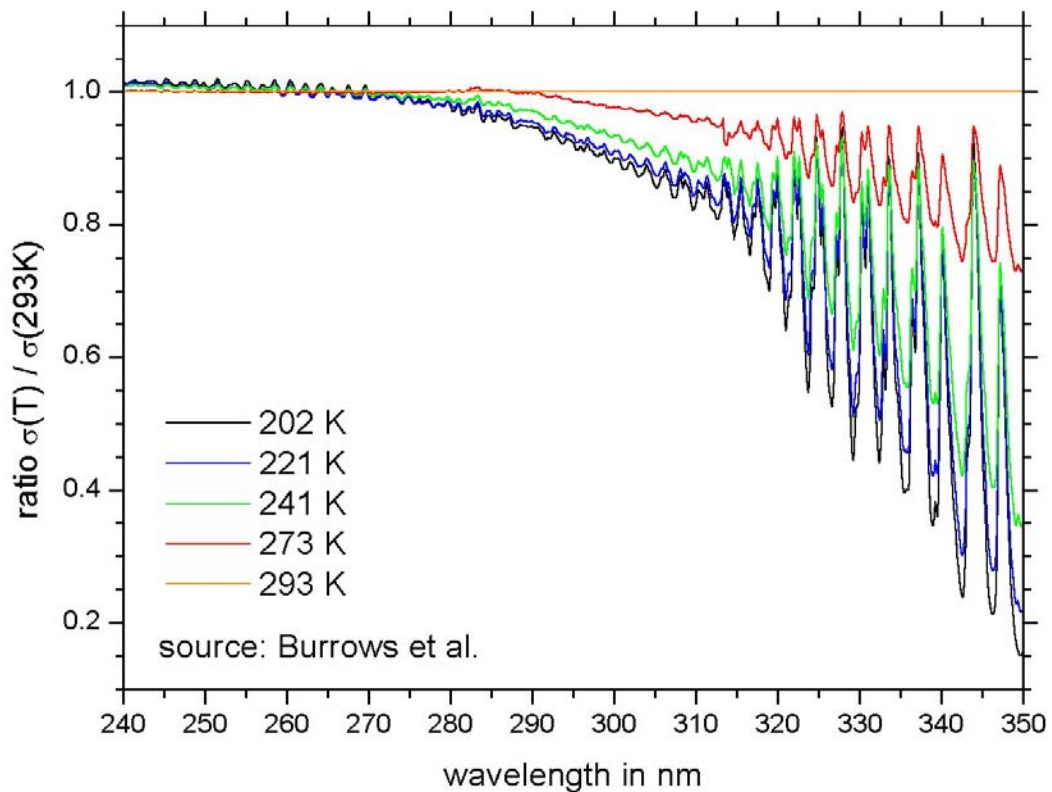


Figure 7-5: Relative changes of the O₃ cross-sections compared to the values at room temperature in the region 240–350 nm (source: *Voigt et al.*)

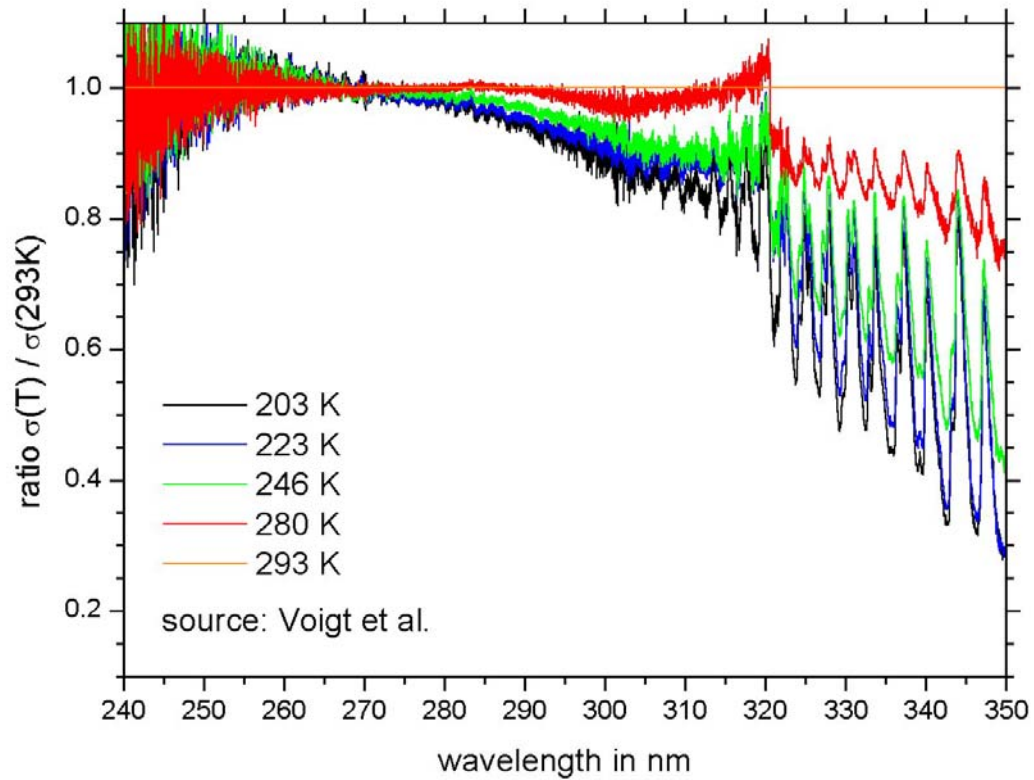
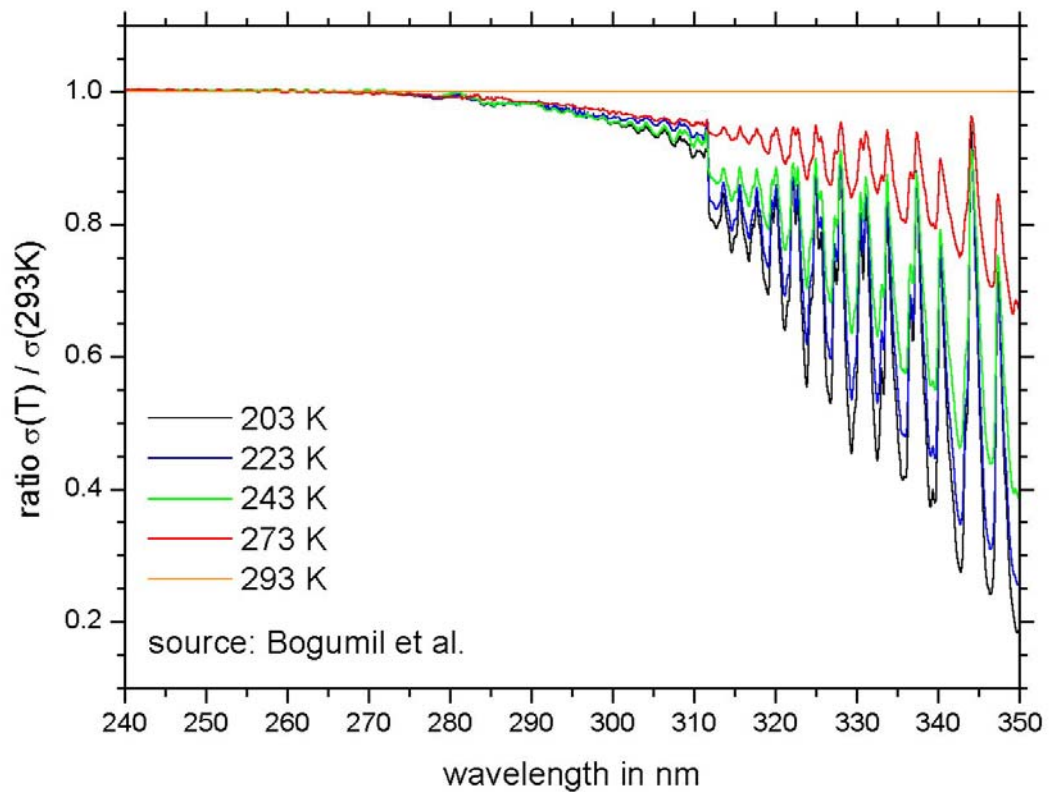


Figure 7-6: Relative changes of the O₃ cross-sections compared to the values at room temperature in the region 240–350 nm (source: *Bogumil et al.*)



From these plots, one can draw the following conclusions:

- In the Hartley band (240–310 nm), the cross sections increase only slightly with decreasing temperature at wavelengths below 260 nm, and start to decrease significantly at lower temperatures at wavelengths above 260 nm. There is agreement between most of the laboratory measurements concerning the “inversion” point around 260 nm and concerning the appearance and amplitude of small periodic features in the ratio between the cross-sections at low and at ambient temperatures. Although there is currently no theoretical explanation for these observations, we want to stress the fact that this is basically the same effect as observed upon a small wavelength shift of the absorption cross-sections towards longer wavelengths when the temperature decreases.
- There are clearly wavelengths where data from different measurements were concatenated: small jumps in the cross-sections of Bass and Paur (around 280 nm) and of *Brion et al.* (around 257 nm), and large jumps in the cross-sections of *Voigt et al.* (around 320 nm) and of *Bogumil et al.* (around 310 nm). Note that in the vicinity of these wavelengths, there are also important differences in the baselines of the different cross-sections. Some baseline effects are also observed in the spectra recorded with GOME (*Richter et al.* and *Burrows et al.*) between 280–290 nm. The cross-section ratios of *Voigt et al.* show the strongest noise in the Hartley bands.
- The cross-sections of *Richter et al.* that were scaled to those of *Bass and Paur* in the window 304.5–305.5 nm are always below the latter cross-sections at all wavelengths below 290 nm. This can be due to uncorrected straylight or due to some residual O₃ absorption in the light source reference spectra.
- In the Huggins bands (310–350 nm), the changes of the cross-sections with decreasing temperature are very strong. Additionally, they seem to depend on the instrumental line shape (e.g. compare the data of *Brion et al.* and *Burrows et al.*). The cross-section ratios of *Bass and Paur* show the strongest noise in the Huggins bands.
- The Huggins bands clearly need to be studied independently taking into account the differences in spectral resolution and wavelength calibration. This will be carried out using the same procedure as at room temperature (non-linear least-squares fitting of different laboratory data recorded at the same temperature, after convolution with a Gaussian ILS).

The second series of plots shows the relative changes in the region 400–790 nm.

Figure 7-7: Relative changes of the O₃ cross-sections compared to the values at room temperature in the region 400–790 nm (source: *Burkholder and Talukdar*)

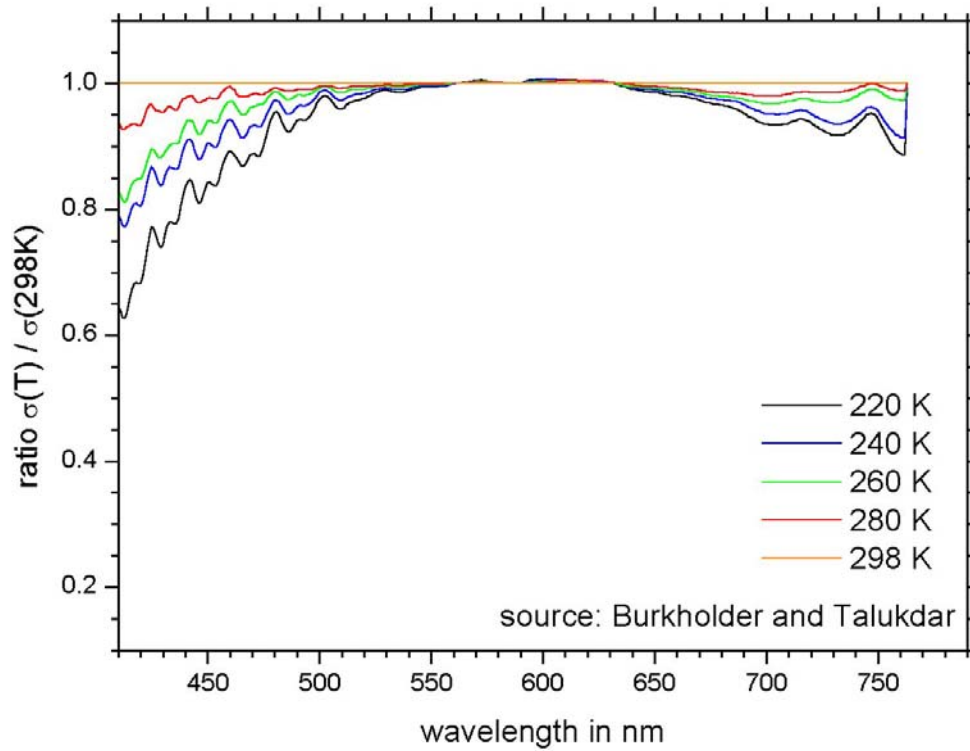


Figure 7-8: Relative changes of the O₃ cross-sections compared to the values at room temperature in the region 515–650 nm (source: *Brion et al.*)

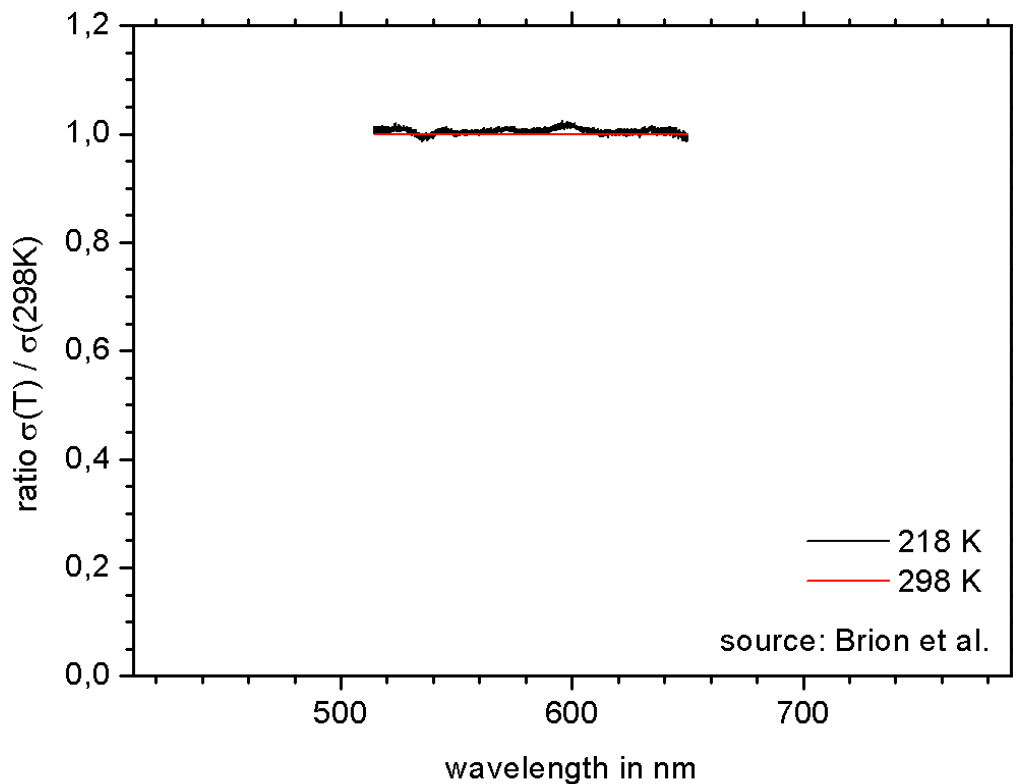


Figure 7-9: Relative changes of the O₃ cross-sections compared to the values at room temperature in the region 400–790nm (source: *Richter et al.*)

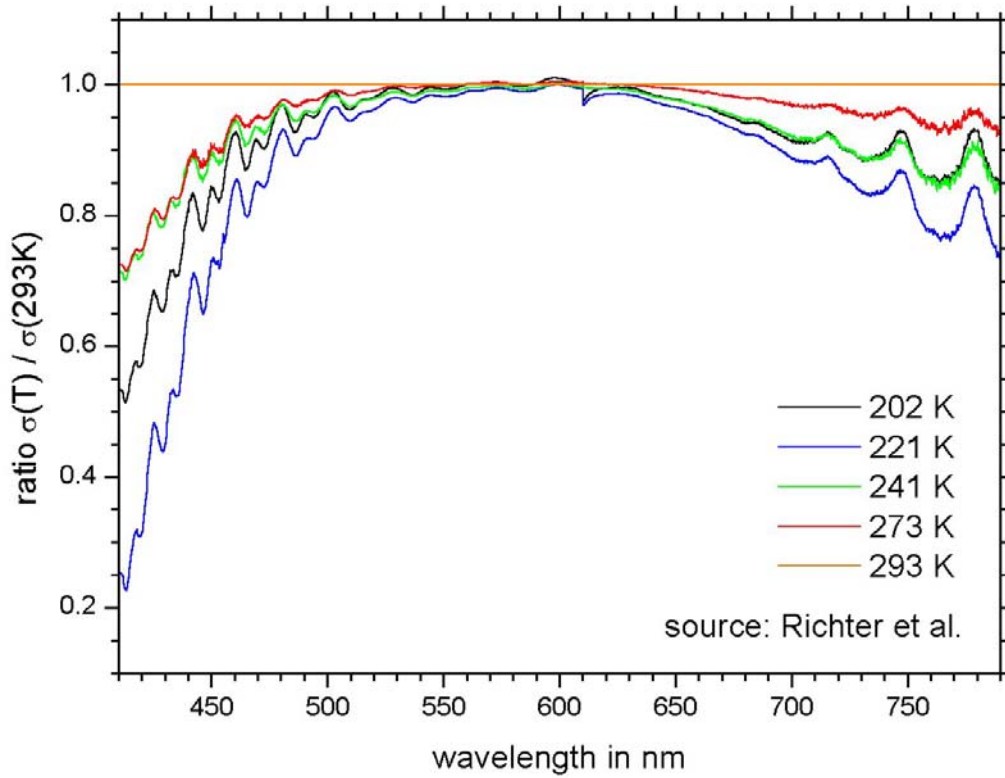


Figure 7-10: Relative changes of the O₃ cross-sections compared to the values at room temperature in the region 400–790nm (source: *Burrows et al.*)

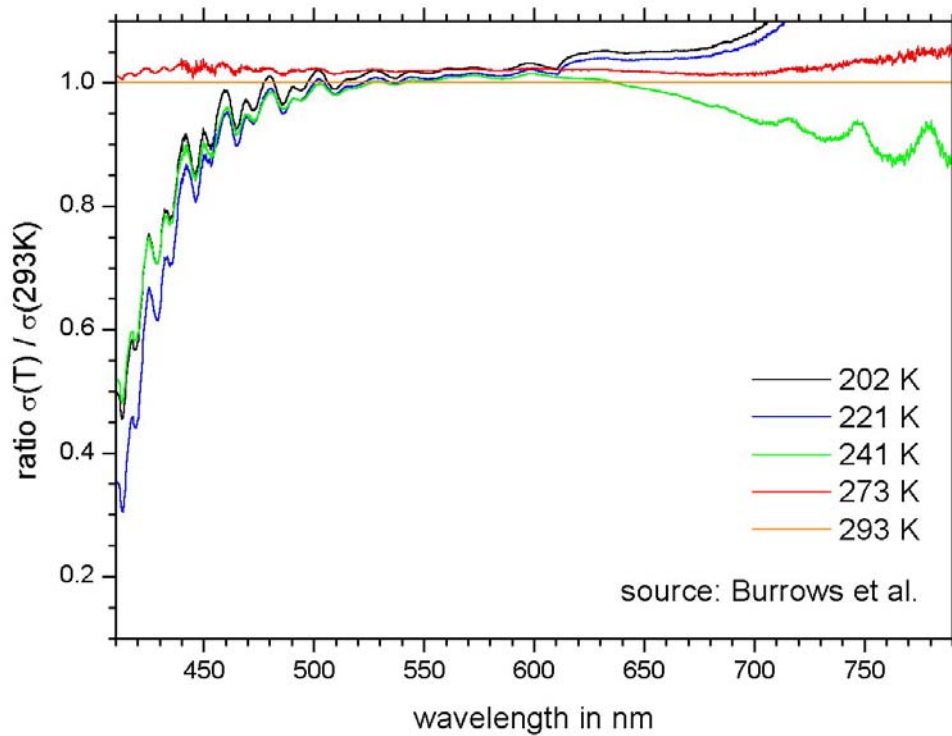


Figure 7-11: Relative changes of the O₃ cross-sections compared to the values at room temperature in the region 400–790nm (source: *Voigt et al.*)

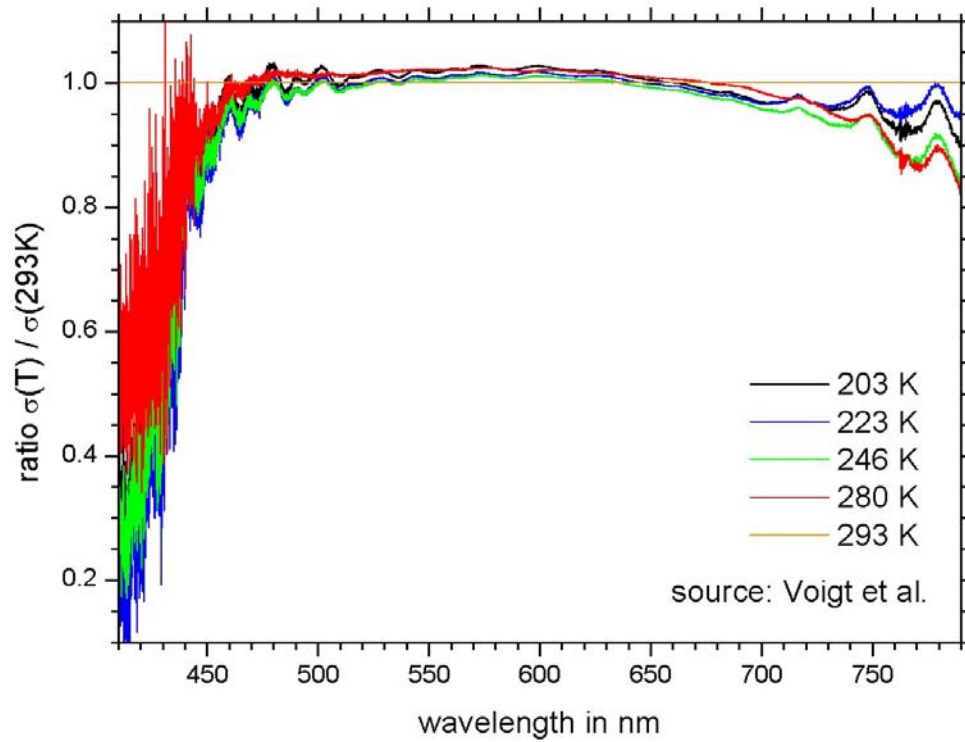
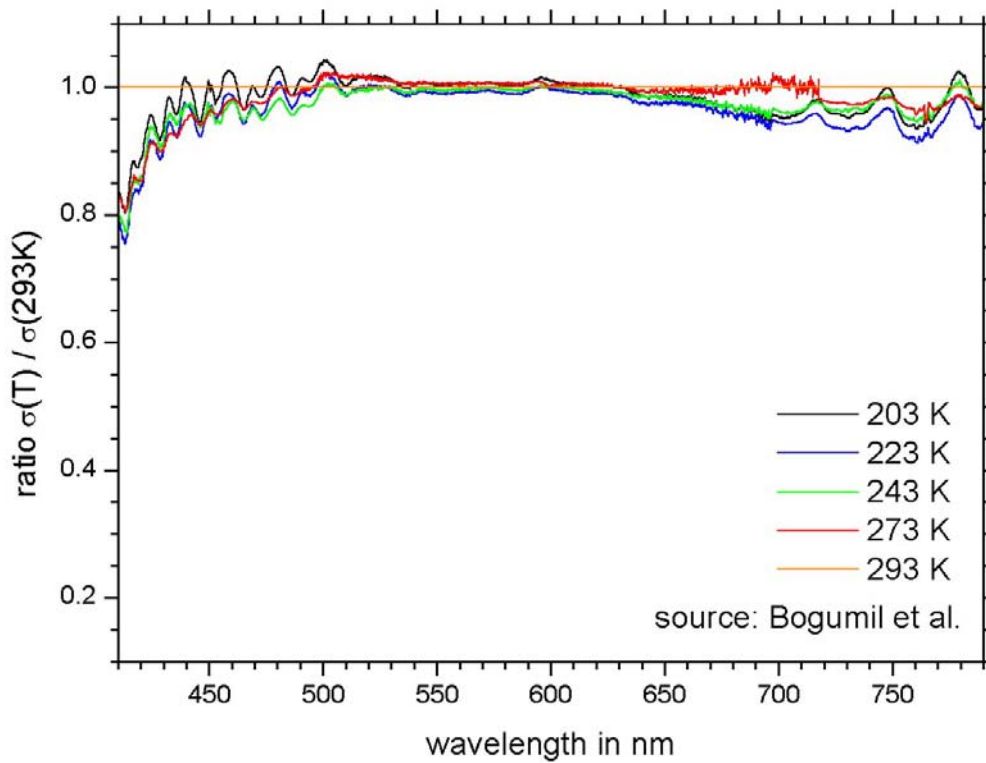


Figure 7-12: Relative changes of the O₃ cross-sections compared to the values at room temperature in the region 400–790nm (source: *Bogumil et al.*)



From these plots, one can draw the following conclusions:

- In the Chappuis band (400–790 nm), the available laboratory cross sections agree in showing a very small or no change of the peak cross-sections (between ca. 550–650 nm) with temperature. There is also good agreement concerning the increase of differential structure with decreasing temperature, which shows up as quasi-periodic features in the ratio of the cross-sections. The magnitude of these features is also in general agreement but needs to be quantified by another method (e.g. non-linear least-squares fits taking into account different baselines, as used for the Huggins bands).
- However, there is strong disagreement between the available laboratory cross sections concerning the relative temperature dependence of the baseline in the regions 400–550 nm and 650–790 nm. In these regions, the overall temperature dependence of the baseline is rather unsystematic except for the cross-sections of *Burkholder and Talukdar*.² This could be due to baseline problems due to the small cross-sections in these regions, but it is difficult to draw conclusions from experimental data with such a large dispersion.
- *Malicet et al.* state that their new measurements in the 340–519 nm region at 218 K and 243 K are in “reasonable good agreement” with the cross-sections of Burkholder et al. They explain the differences to the other cross-sections (*Burrows et al.*, *Richter et al.*, *Voigt et al.*, *Bogumil et al.*) are due to the difficulties of these authors of measuring small cross-sections at low temperatures.³
- While the most recent IUPAC evaluation⁴ states that “... ozone cross-sections in the Chappuis bands (450-750 nm) ... are independent of temperature” (this statement is clearly only valid for low-resolution data and for the centre of the Chappuis band), there are important temperature effects in the wings of the Chappuis band.
- These temperature effects are quasi-period features appearing in the blue and red wings of the Chappuis band (400–550 nm and 650–790 nm) which are clearly visible in all available data. The features are related to an increase in the differential cross-sections of up to 10 % between 298 K and 203 K.
- In addition to this differential effect, the band structures between 400–500 nm show shifts towards shorter wavelengths with decreasing temperature, see the figures by *Burrows et al.* and *Voigt et al.* in the relevant papers. This effect was first observed by *Richter*⁵ and is rather important for atmospheric retrievals.

² It should be noted, however, that these spectra were measured with a double setup comparing the low-temperature spectra directly to those at room temperature. This could explain why they obtained a systematic temperature dependence whereas the other measurements did not [E. Shettle, personal communication, 2001].

³ J. Brion, personal communication, 2001.

⁴ IUPAC "Subcommittee on Gas Kinetic Data", Data Sheet POx2, updated Oct. 2, 2001.

⁵ A. Richter, personal communication, 1995.

7.2. Comparison of the absolute O₃ cross-sections at all available wavelengths at temperatures below ambient: 276±4 K, 243±3 K, 221±3 K, and 203±1 K

On the following pages, we will show a number of plots of the available O₃ cross-sections at temperatures below ambient: 276±4 K, 243±3 K, 221±3 K, and 203±1 K, together with the ratio to the data of *Bogumil et al.*

These plots lead to the same observations as already made by inspecting the data at room temperature, namely

- significant baseline differences which are most important in the regions with small cross-sections (i.e. between 350–450 nm and above 700 nm),
- an overall agreement between the different cross-sections within about 2% in the Hartley band,
- sudden jumps of the cross-sections and smooth baseline differences (between a few % and several 100%) around such wavelengths where laboratory data with different O₃ amounts had to be concatenated,
- large discrepancies of up to 20% in the Huggins bands (310–350 nm) due to the different instrumental line shapes and due to differences in the wavelength calibration, which require a non-linear least squares fitting approach,
- a systematic disagreement between the broad-band spectra (GOME-FM, FTS, SCIAMACHY-PFM) and the cross-sections of *Burkholder and Talukdar* in the Chappuis bands at all temperatures considered (the latter values lie always below the broad-band values by 3–5% in the centre of the Chappuis band and much more in the wings of the Chappuis band),
- residual O₂ absorption features around 760 nm in some of the spectra.

Although these plots are difficult to interpret since most of the observed differences are due to measurement errors, they indicate the current accuracy of the laboratory cross-sections of O₃ at temperatures below 298 K, and they might be useful for the elimination of spectral artefacts, which can play an important role in the analysis of atmospheric spectra.

We use the same spectral regions as for the plots comparing the room-temperature cross-sections: the full region 240–790 nm, the top of the Hartley band (240–270 nm), the red wing of the Hartley band (270–310 nm), the short-wavelength part of the Huggins bands (310–340 nm), the long-wavelength part of the Huggins bands (340–380 nm), the blue tail of the Chappuis band (380–510 nm), the top of the Chappuis band (510–650 nm), and the red tail of the Chappuis band (650–790 nm).

Figure 7-13: Comparison of O₃ absorption cross-sections at 276±4 K: 240–800 nm

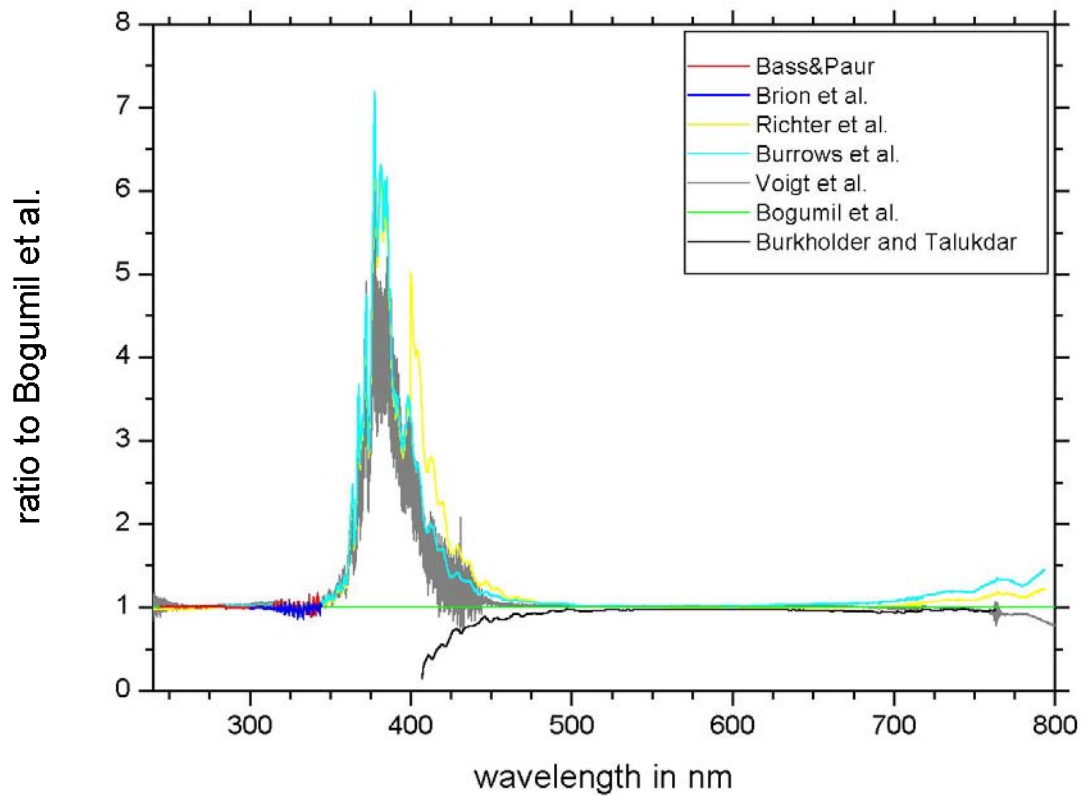
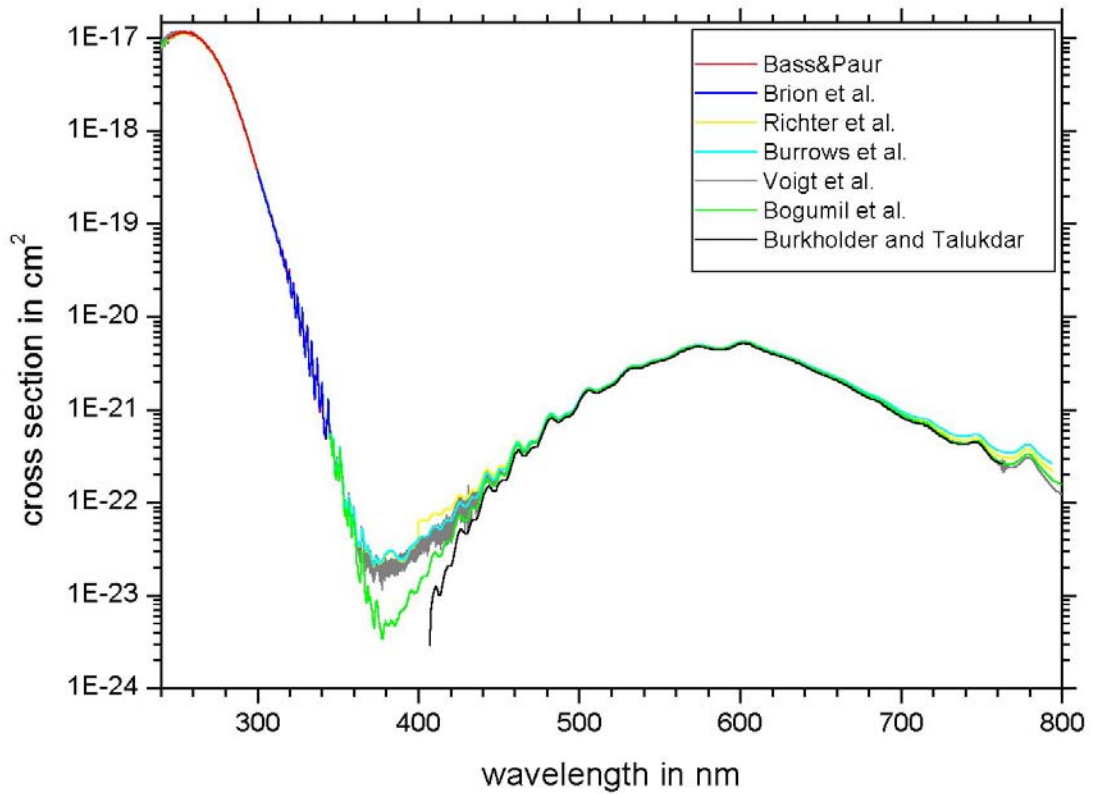


Figure 7-14: Comparison of O₃ absorption cross-sections at 276±4 K: 240–270 nm

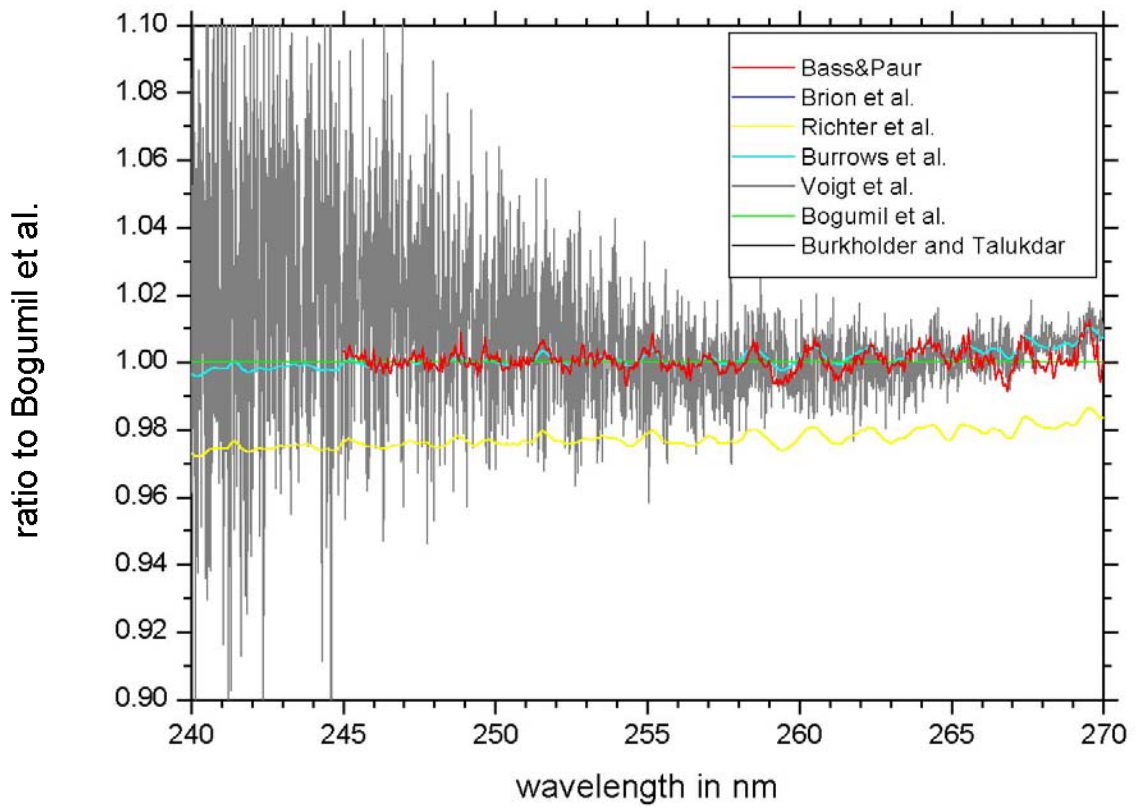
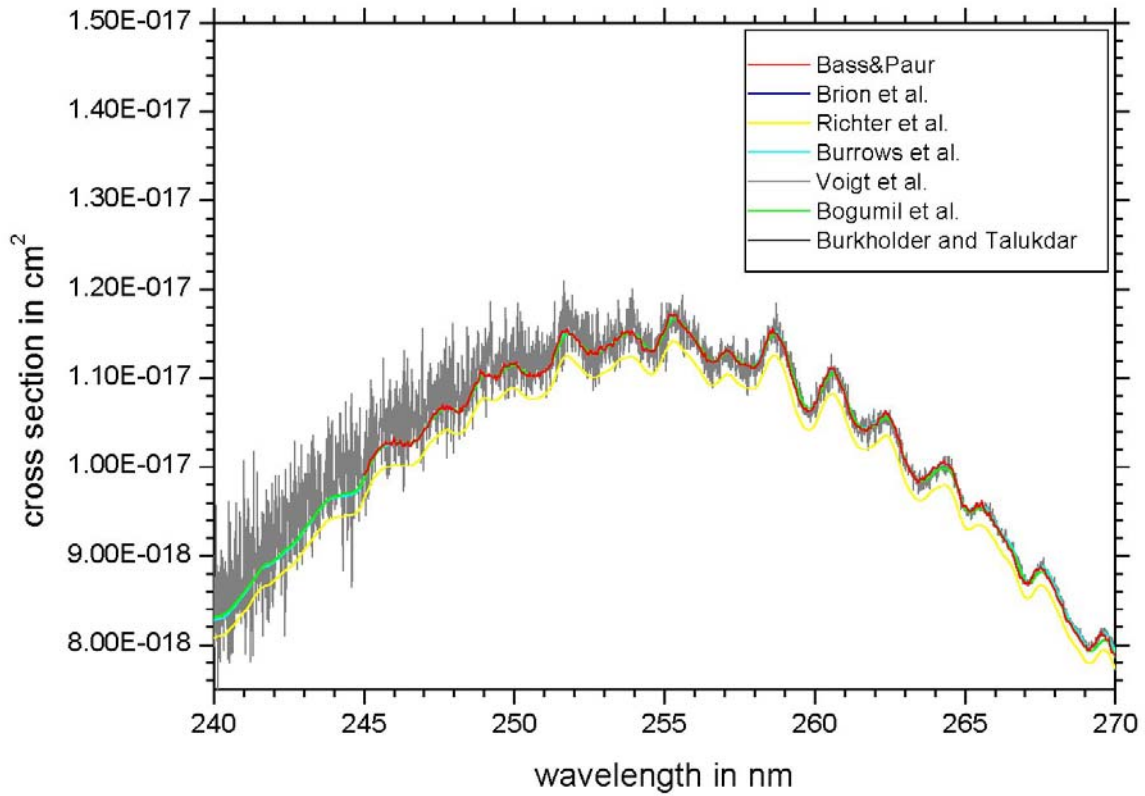


Figure 7-15: Comparison of O₃ absorption cross-sections at 276±4 K: 270–310 nm

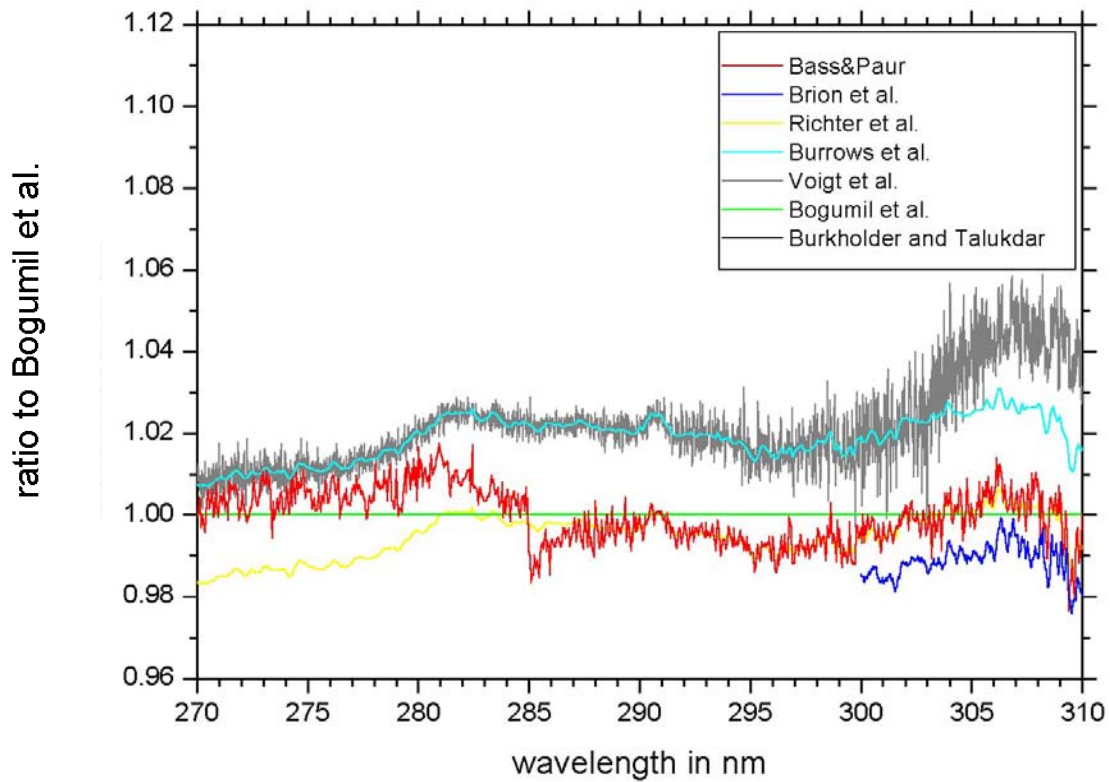
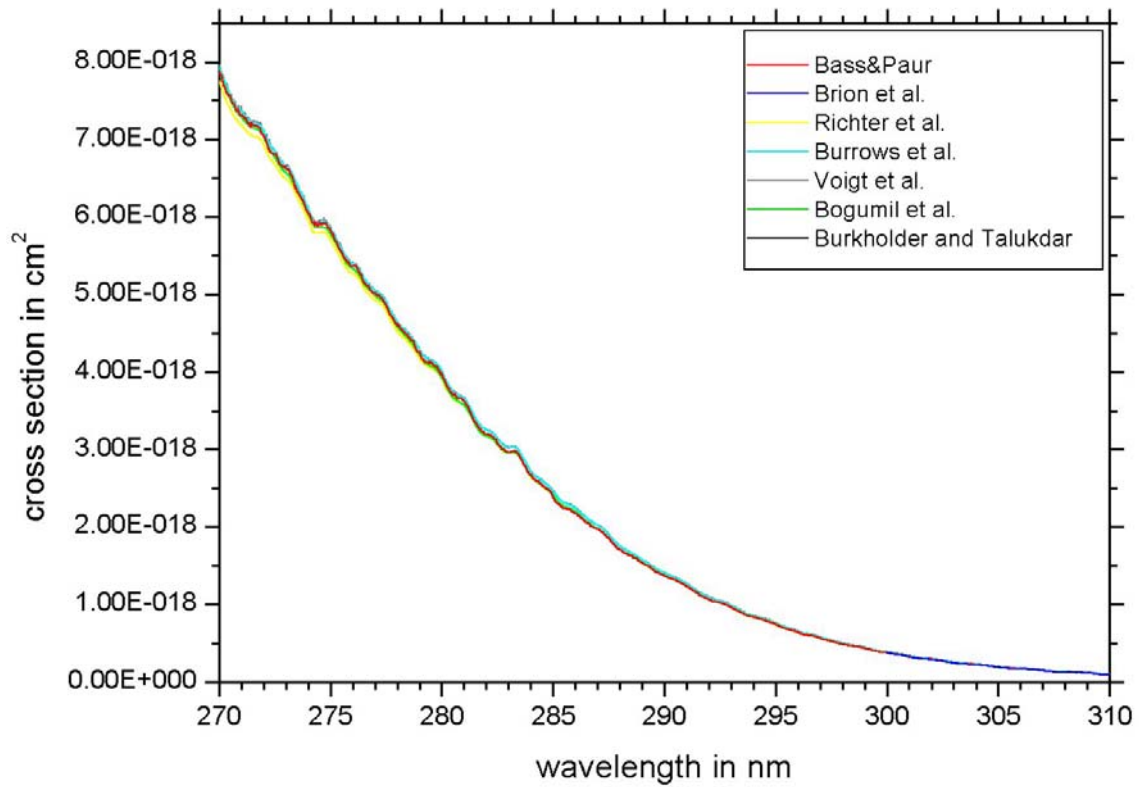


Figure 7-16: Comparison of O₃ absorption cross-sections at 276±4 K: 310–340 nm

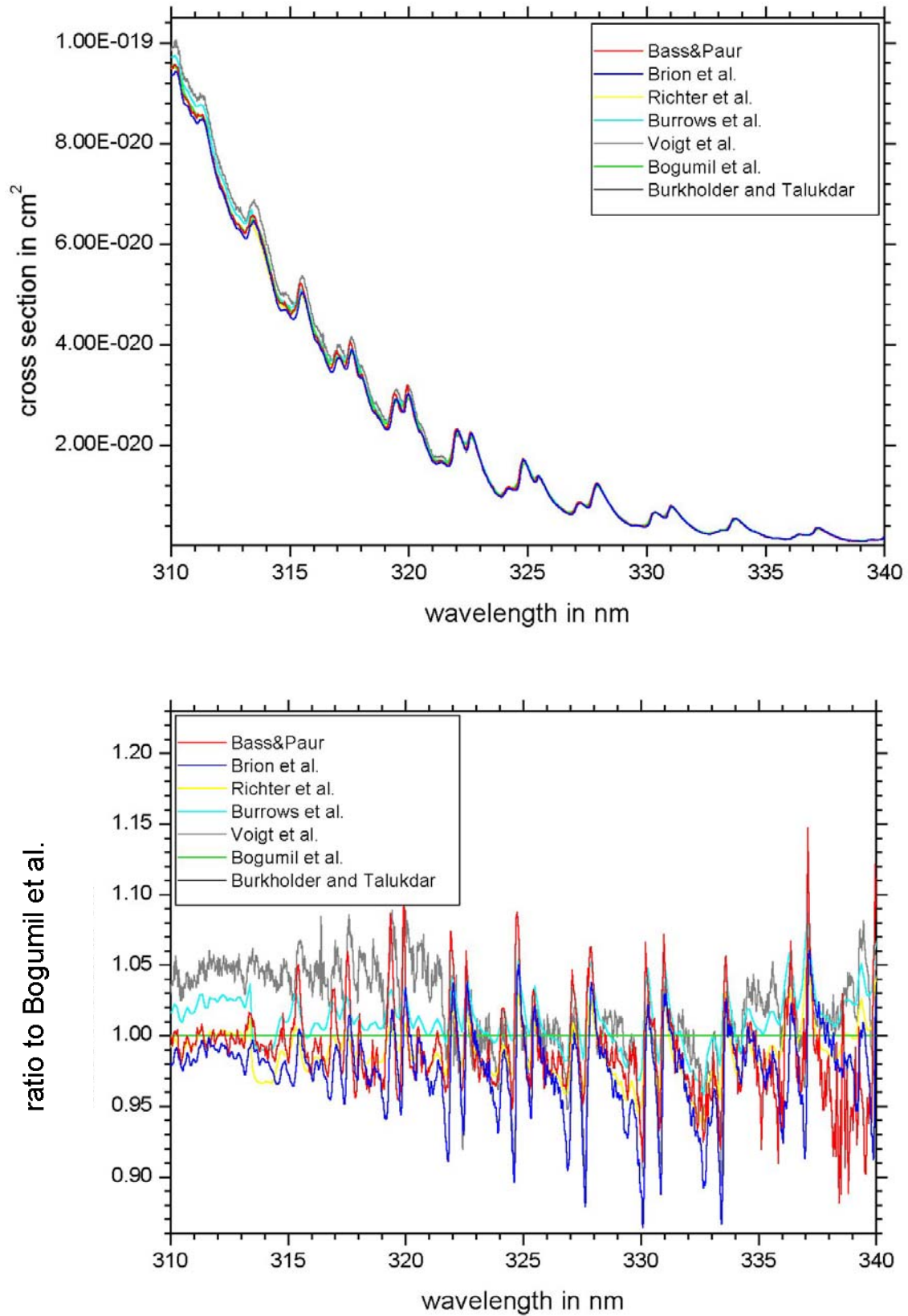


Figure 7-17: Comparison of O₃ absorption cross-sections at 276±4 K: 340–380 nm

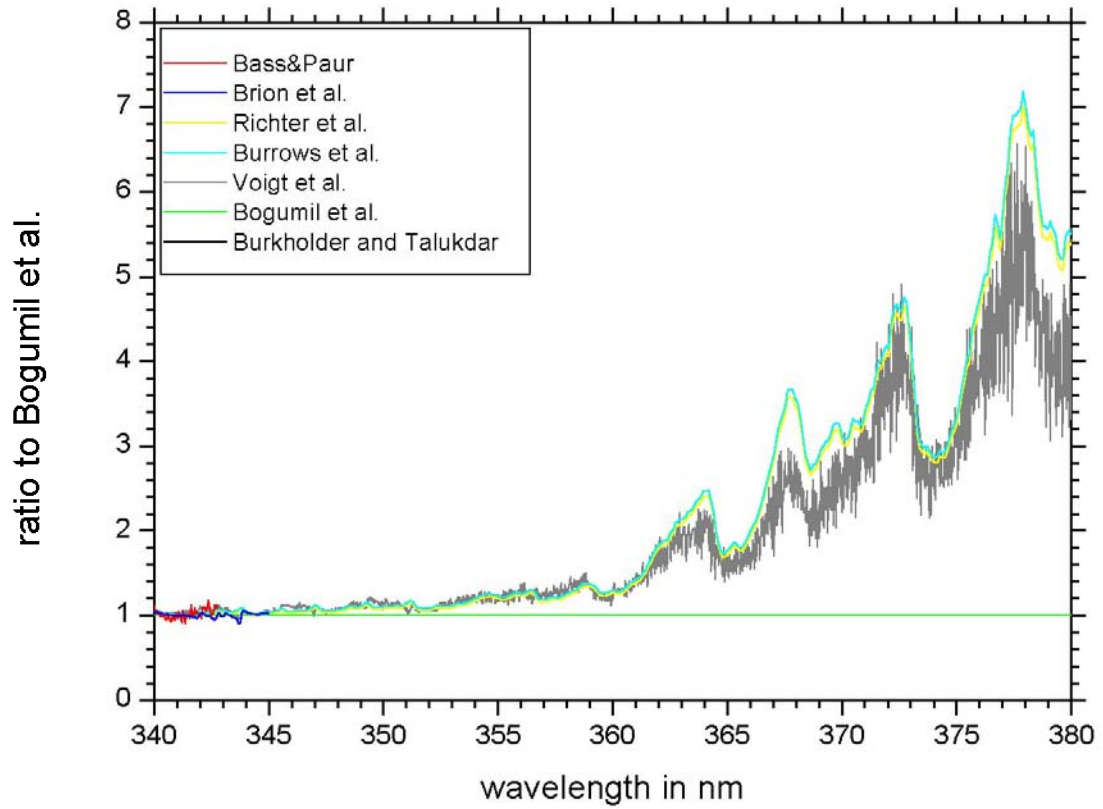
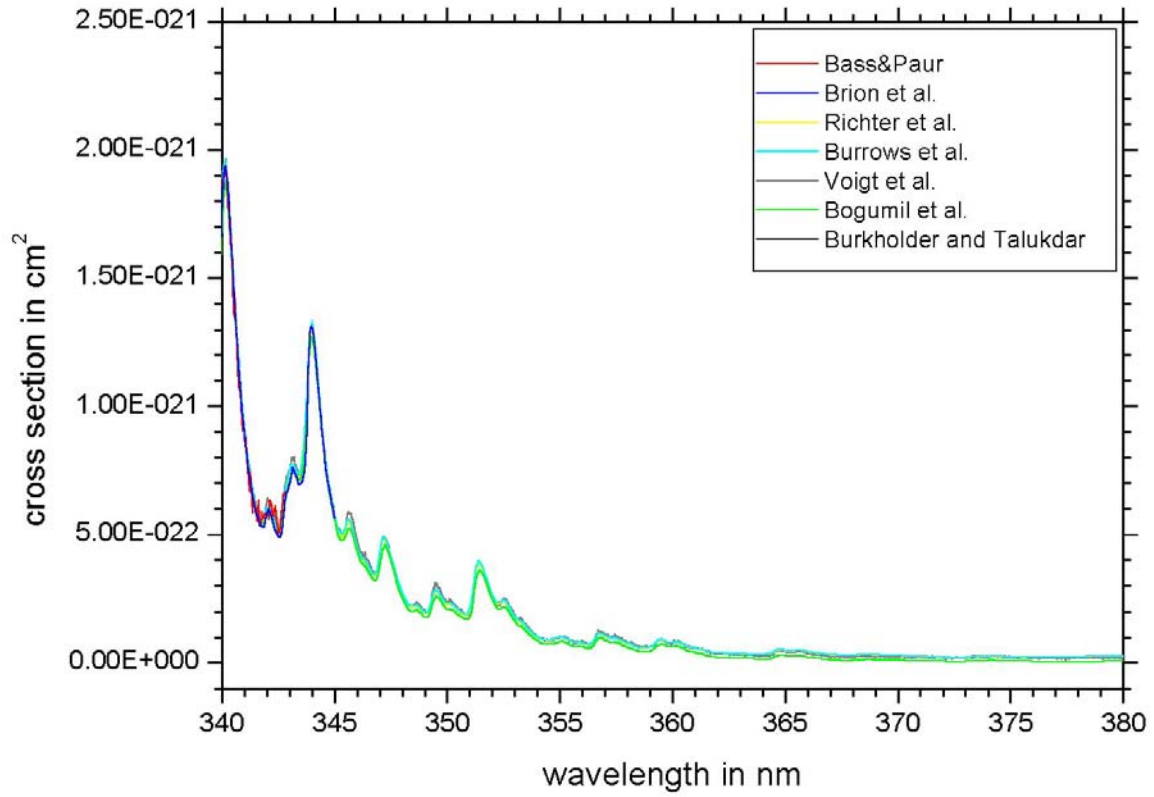


Figure 7-18: Comparison of O₃ absorption cross-sections at 276±4 K: 380–510 nm

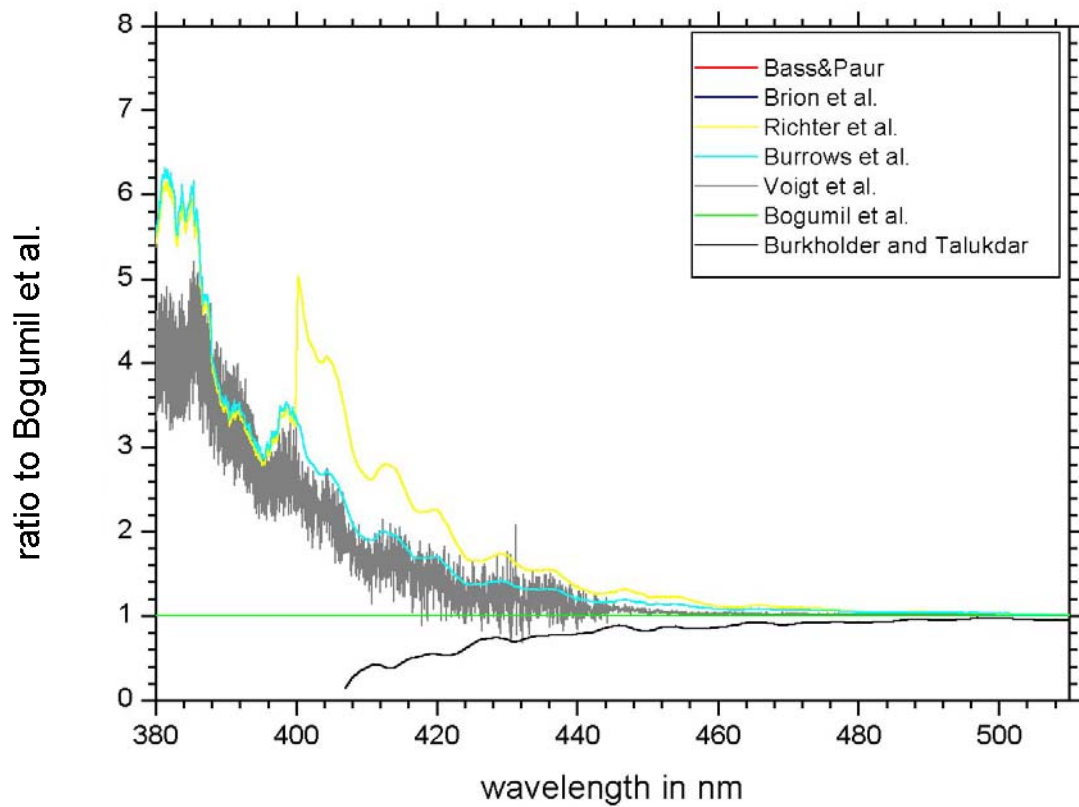
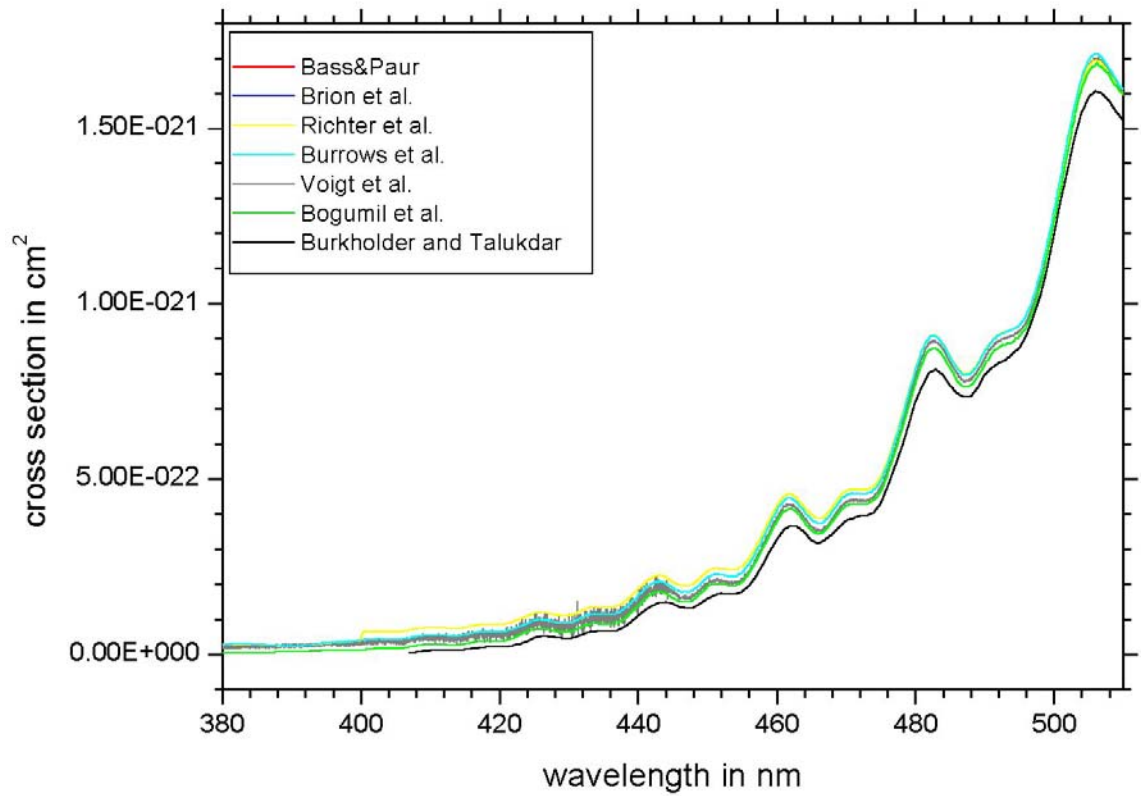


Figure 7-19: Comparison of O₃ absorption cross-sections at 276±4 K: 510–650 nm

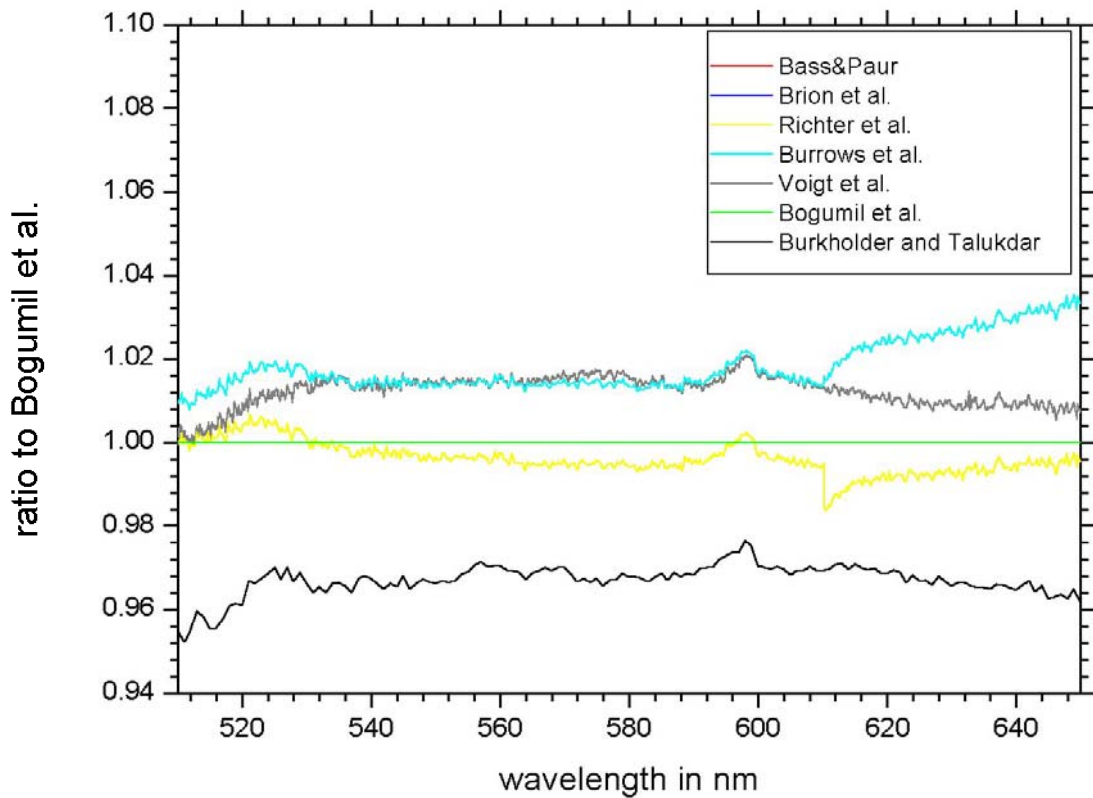
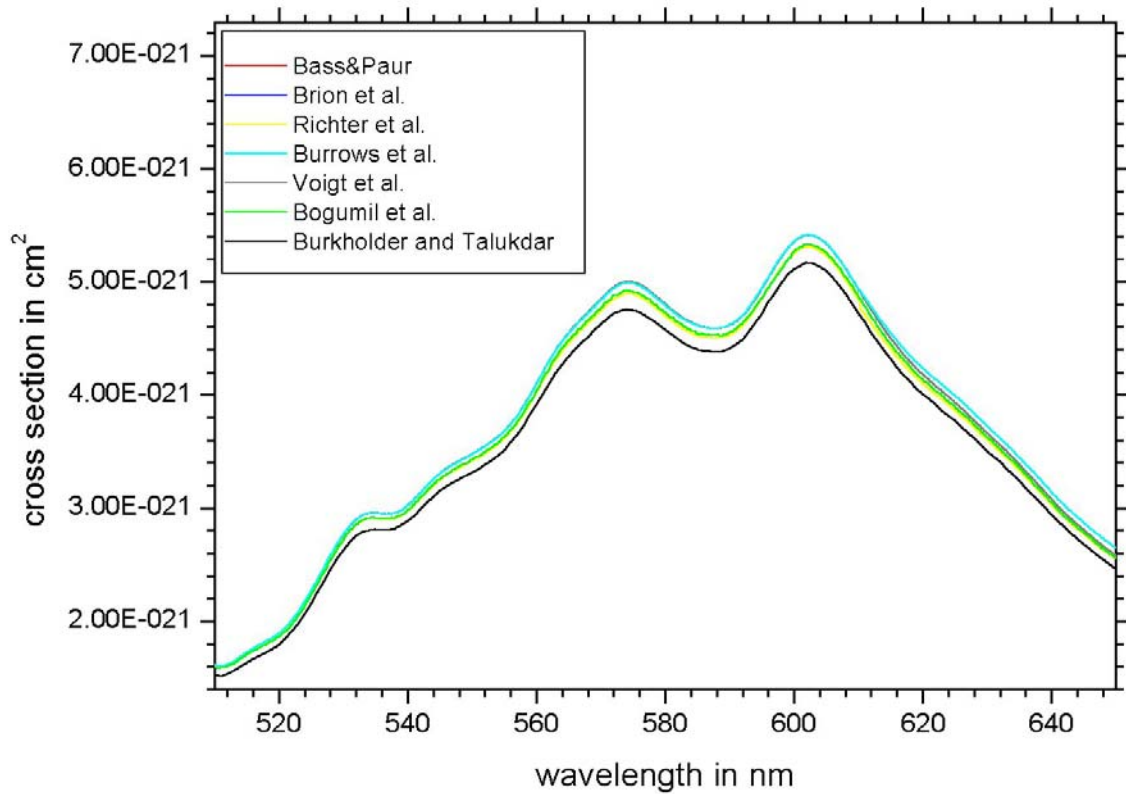


Figure 7-20: Comparison of O₃ absorption cross-sections at 276±4 K: 650–800 nm

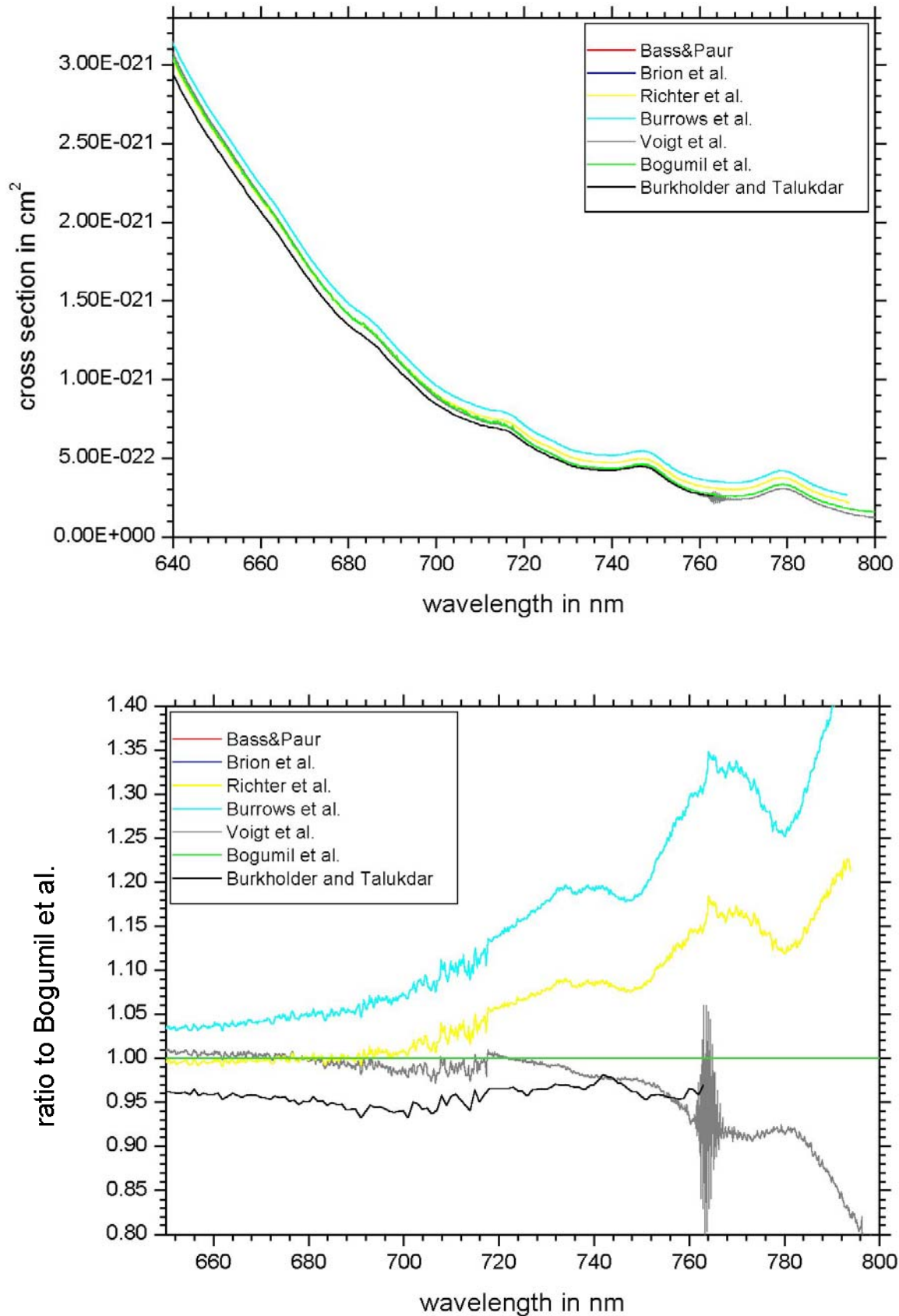


Figure 7-21: Comparison of O₃ absorption cross-sections at 243±3 K: 240–800 nm

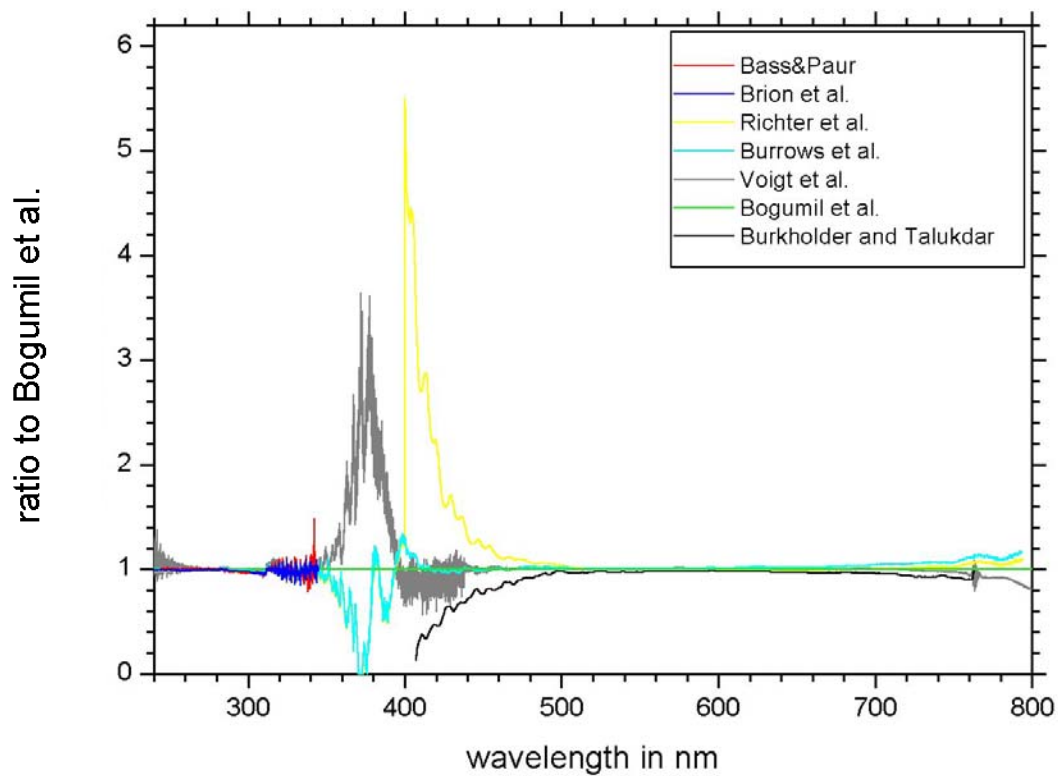
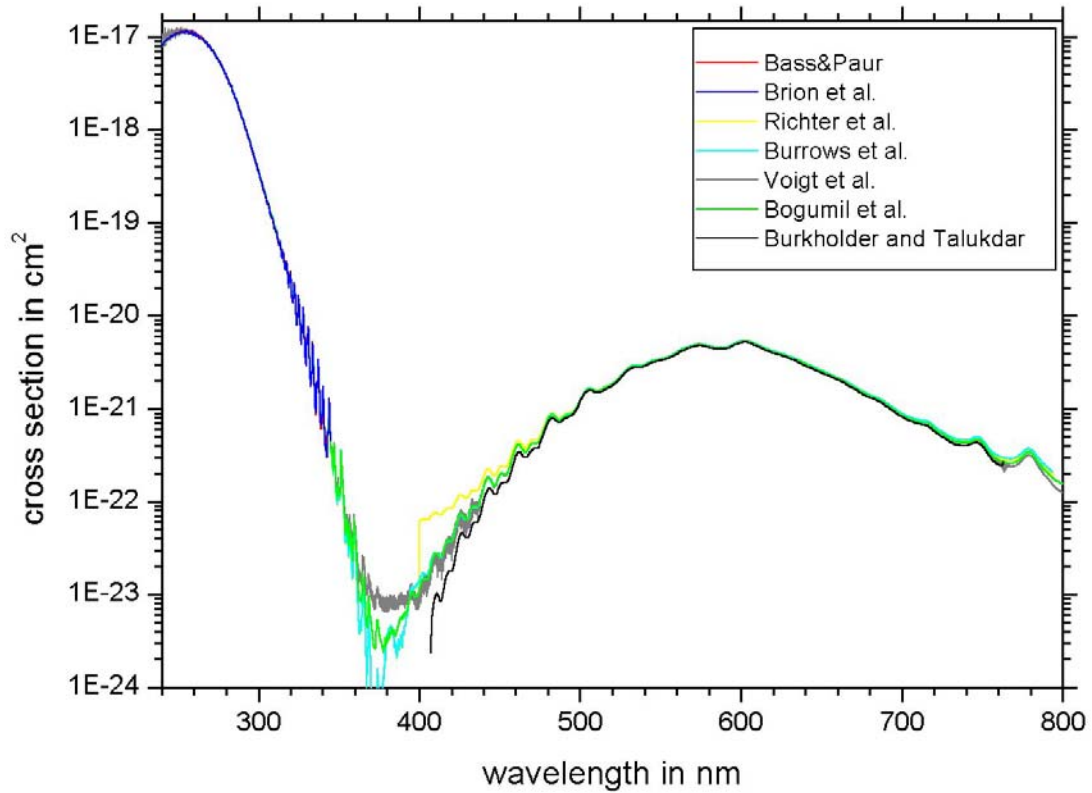


Figure 7-22: Comparison of O₃ absorption cross-sections at 243±3 K: 240–270 nm

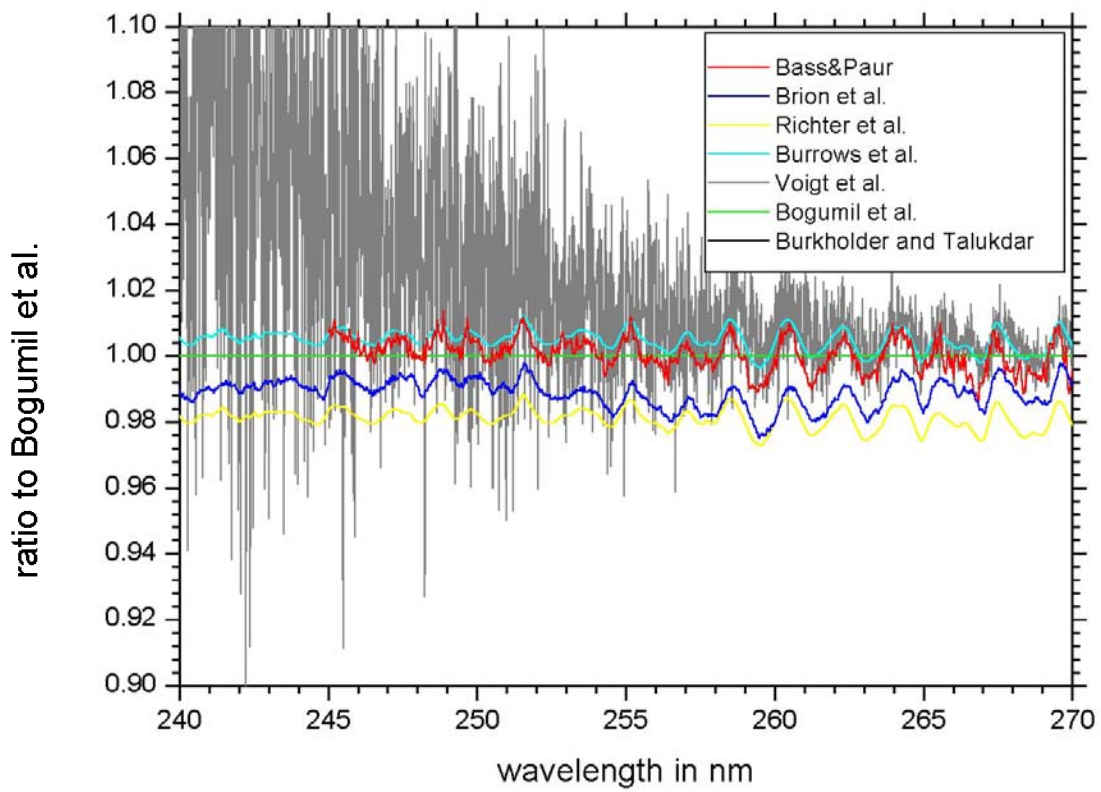
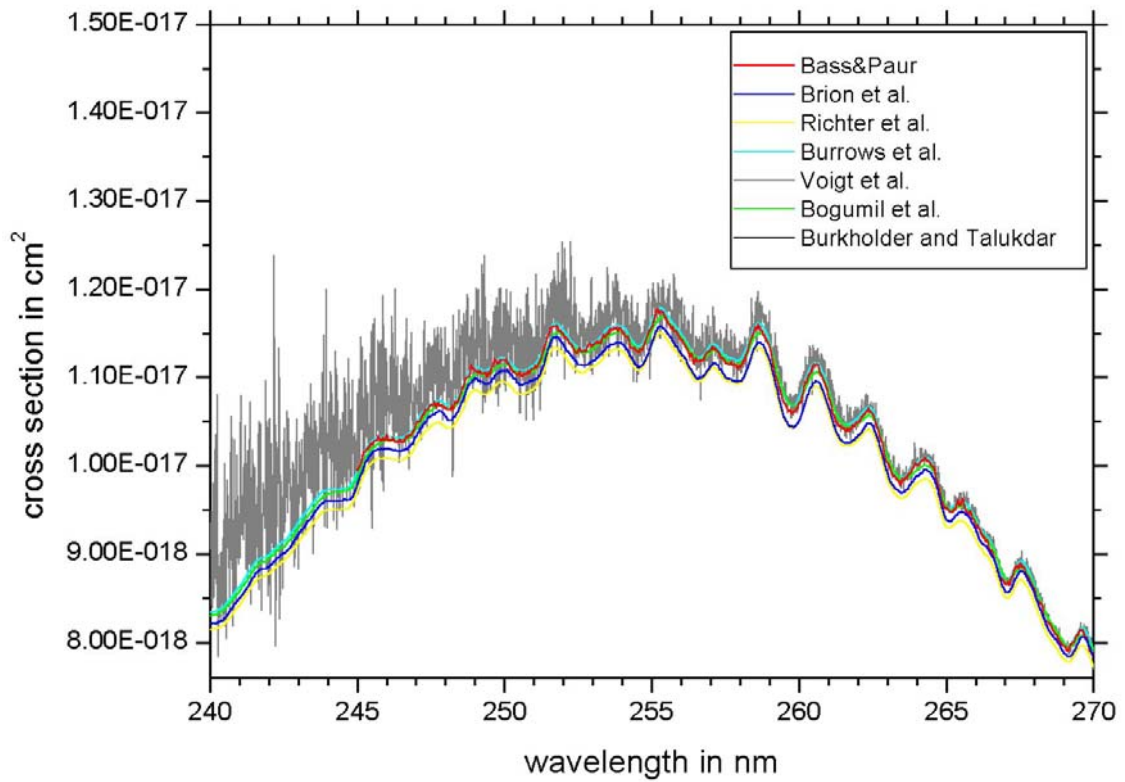


Figure 7-23: Comparison of O₃ absorption cross-sections at 243±3 K: 270–310 nm

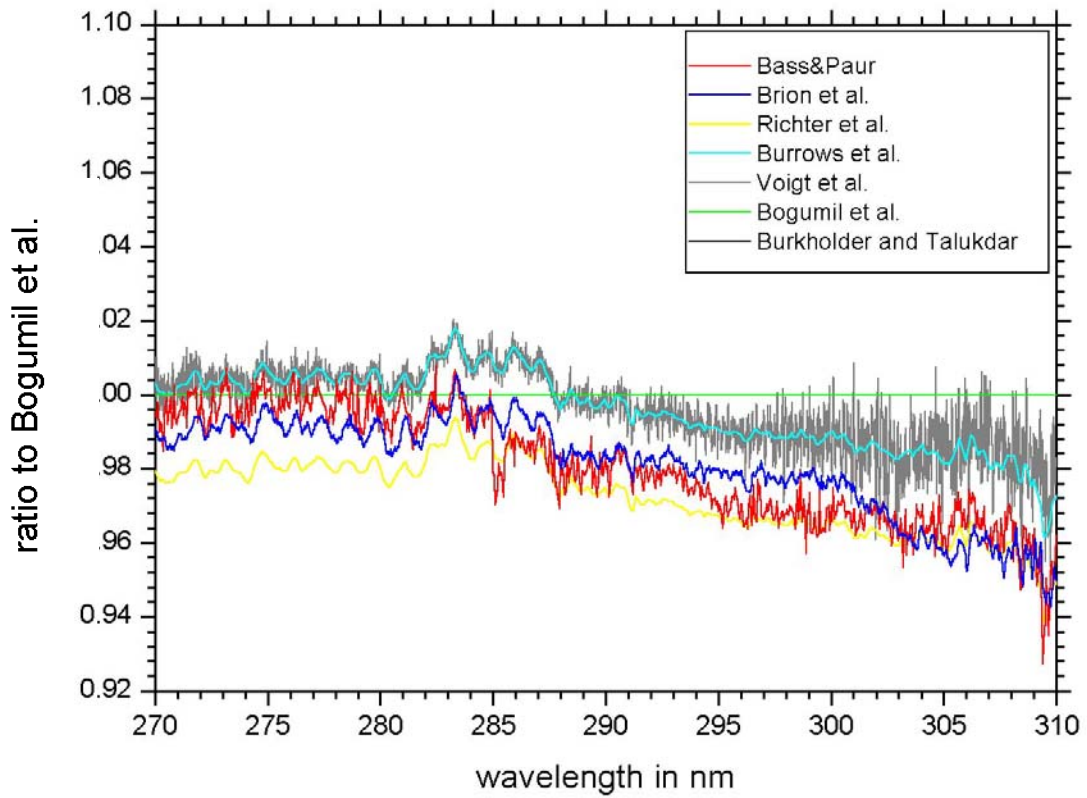
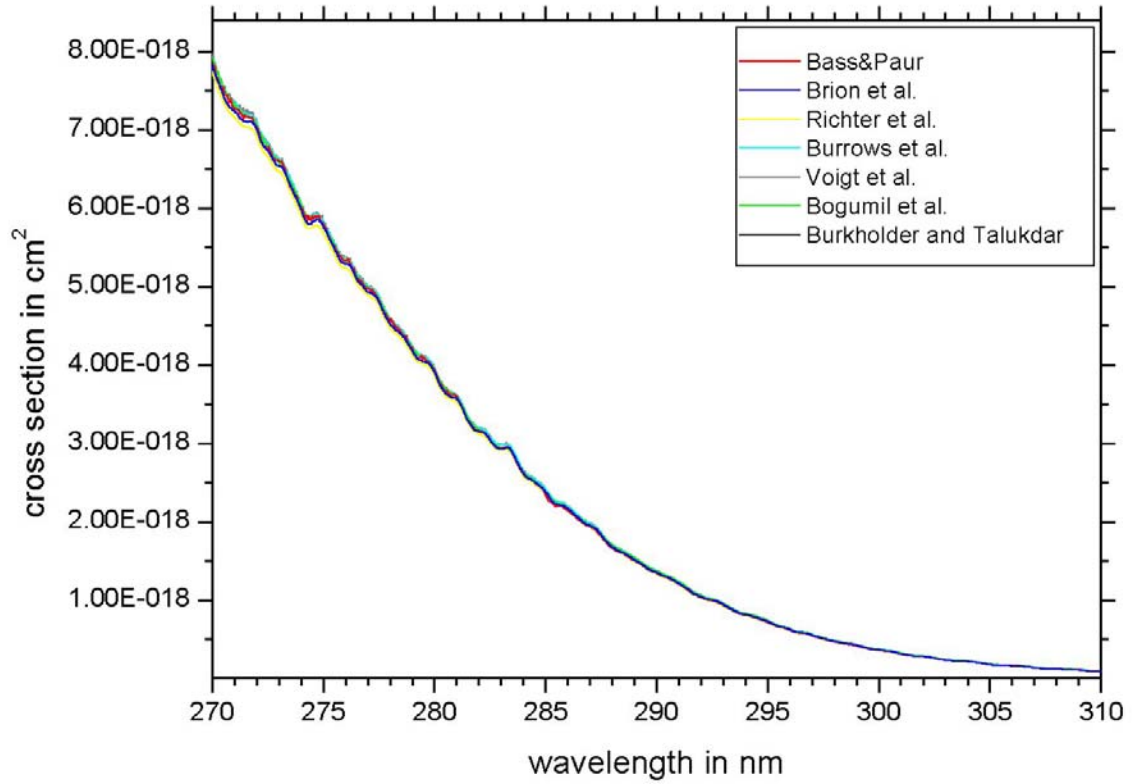


Figure 7-24: Comparison of O₃ absorption cross-sections at 243±3 K: 310–340 nm

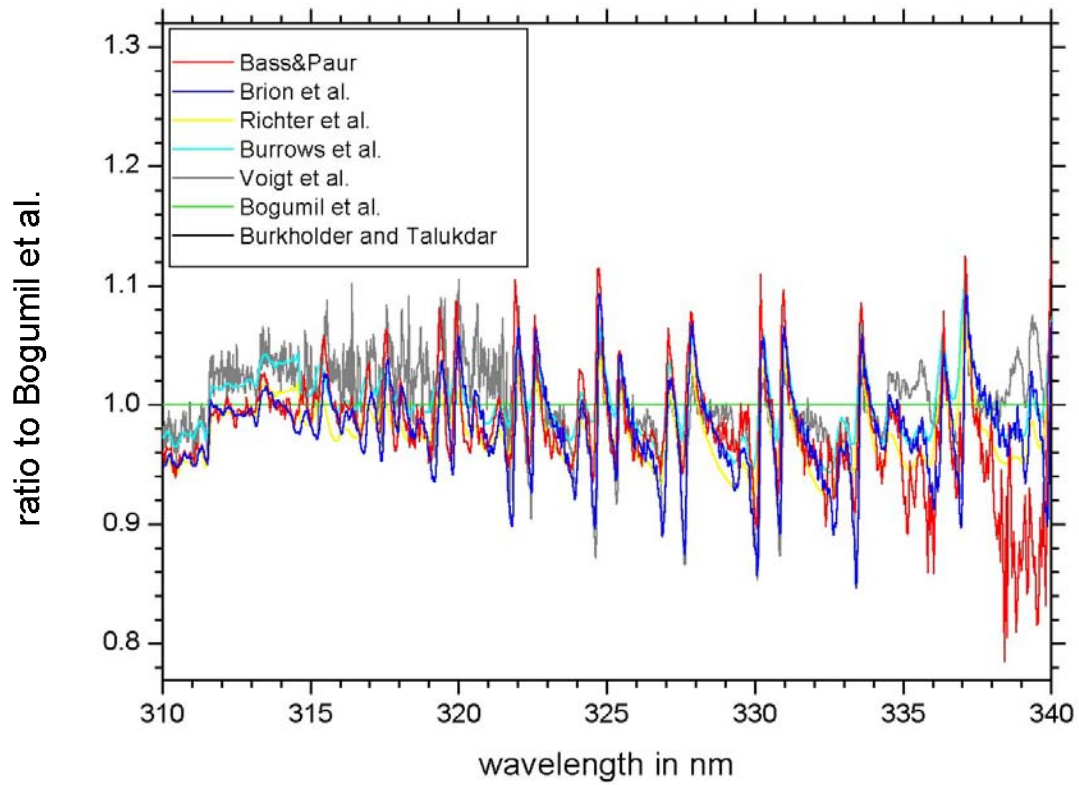
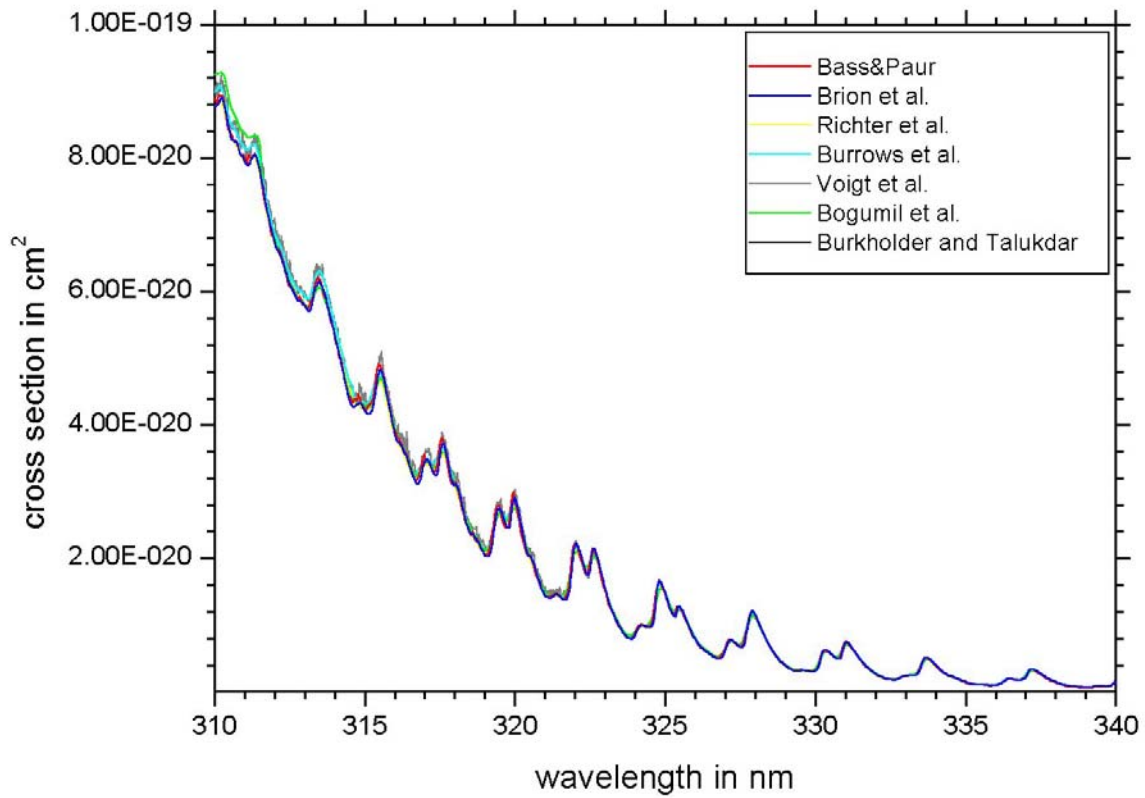


Figure 7-25: Comparison of O₃ absorption cross-sections at 243±3 K: 340–380 nm

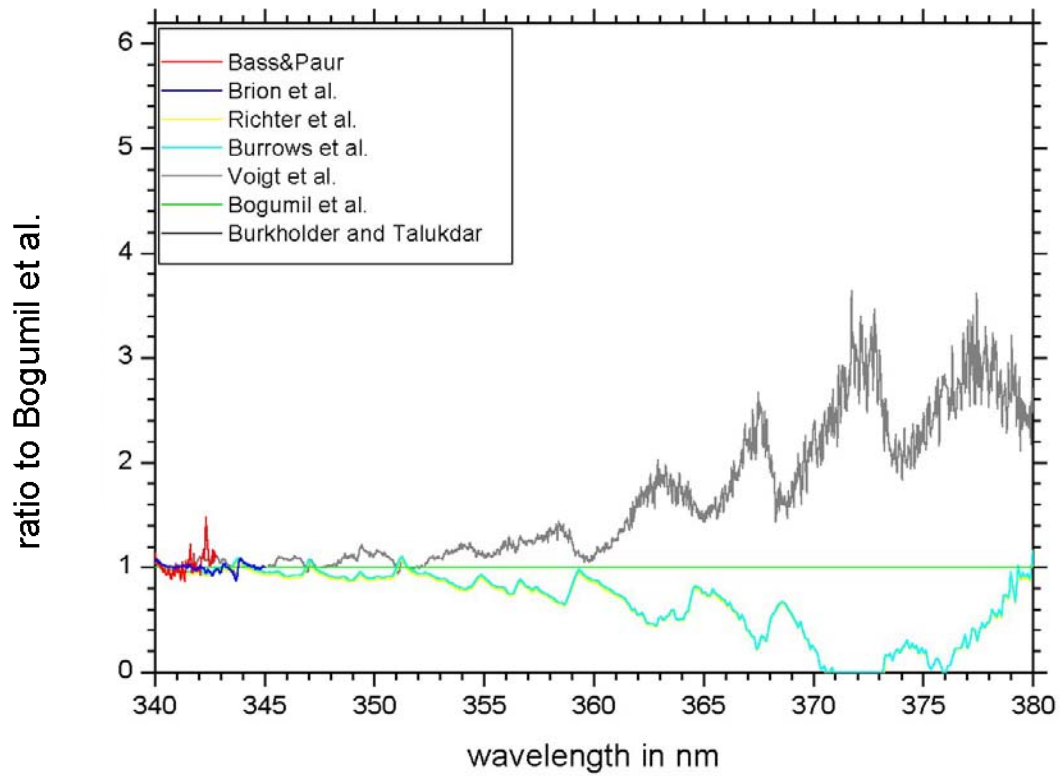
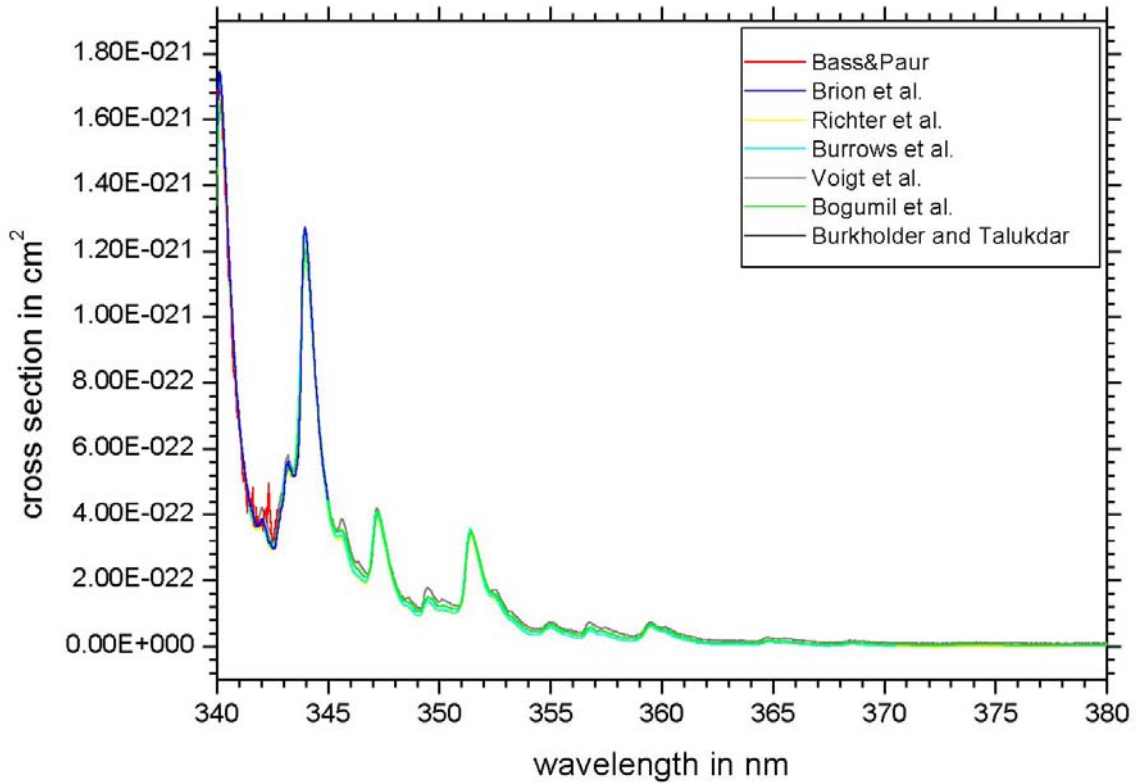


Figure 7-26: Comparison of O₃ absorption cross-sections at 243±3 K: 380–510 nm

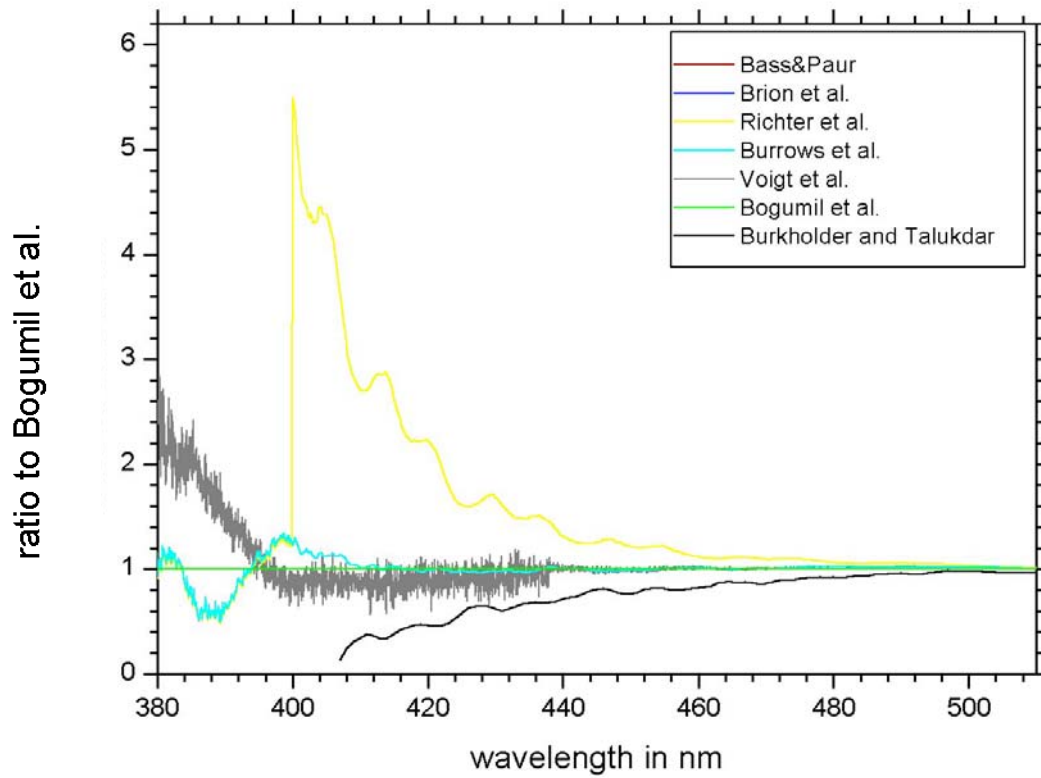
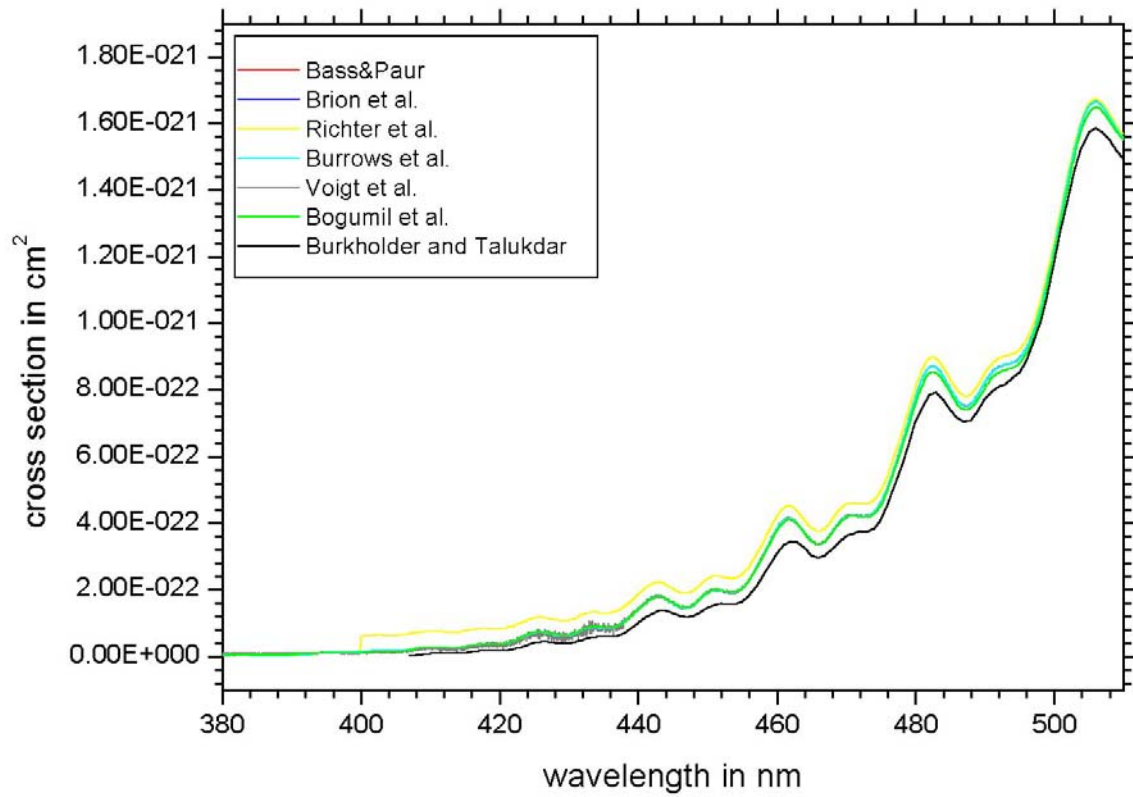


Figure 7-27: Comparison of O₃ absorption cross-sections at 243±3 K: 510–650 nm

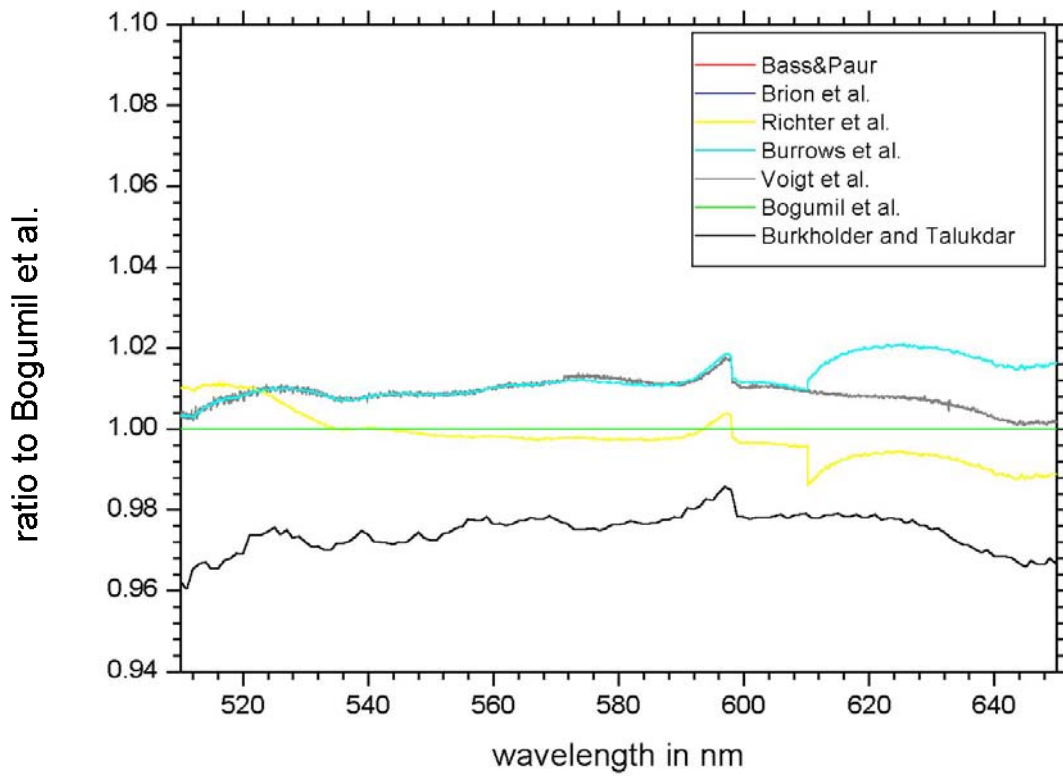
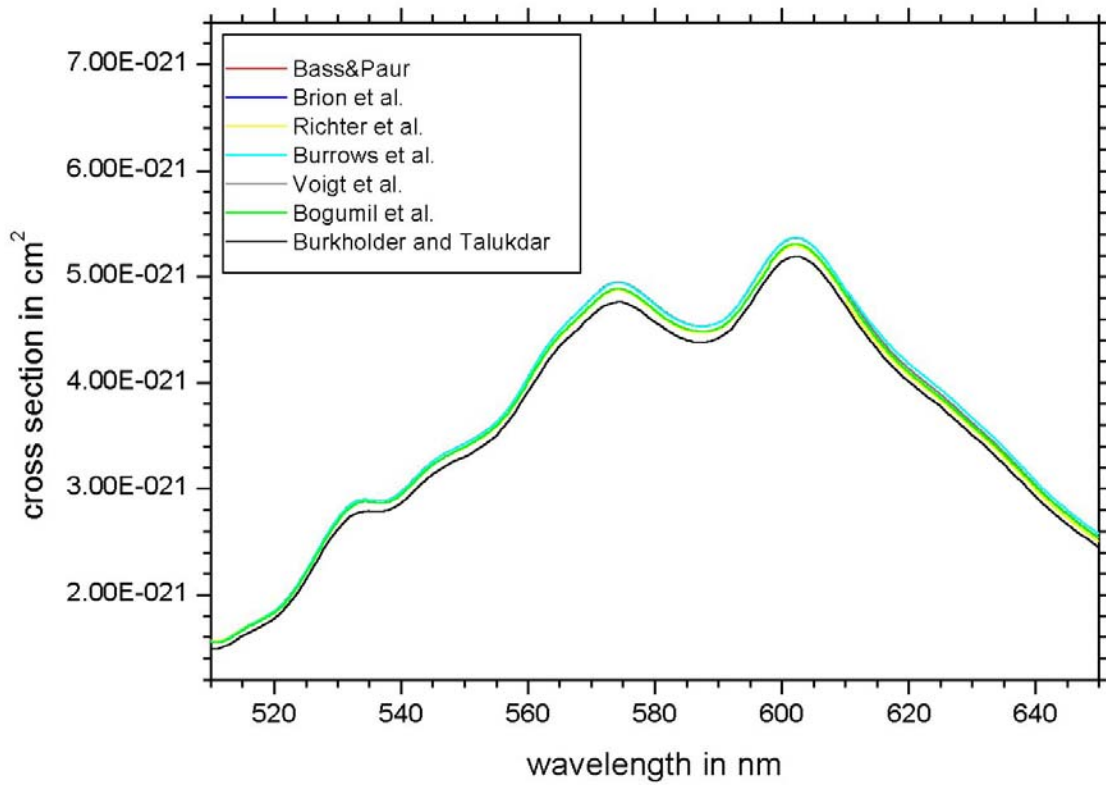


Figure 7-28: Comparison of O₃ absorption cross-sections at 243±3 K: 650–800 nm

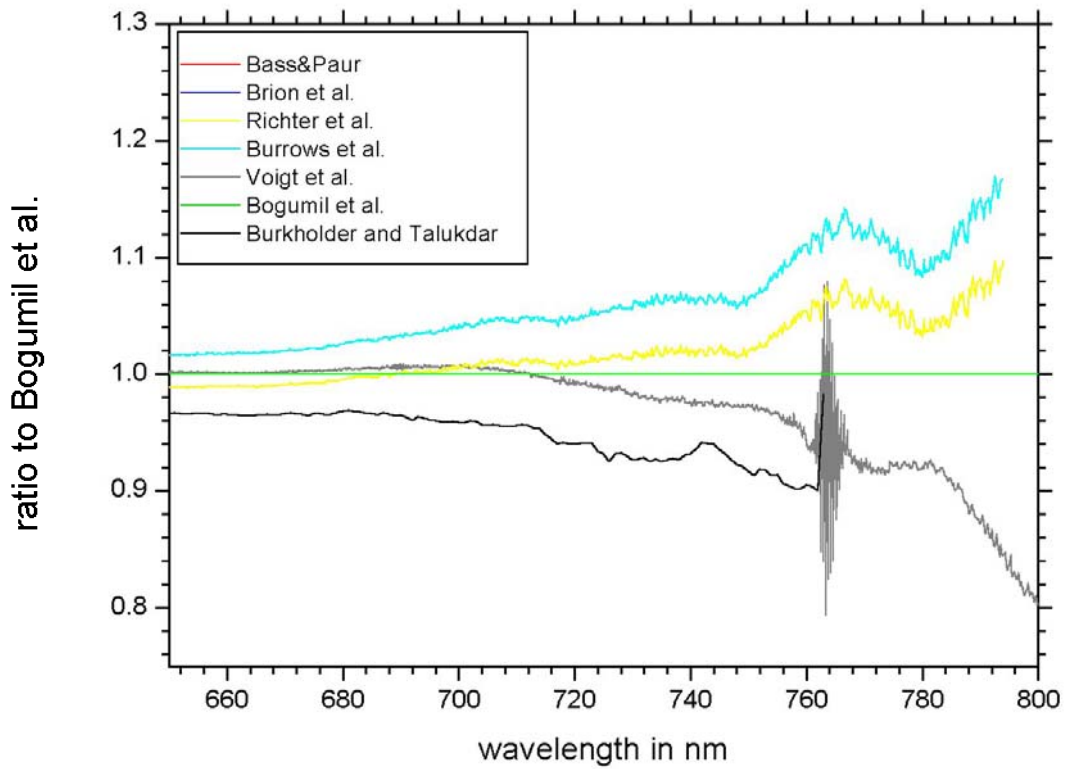
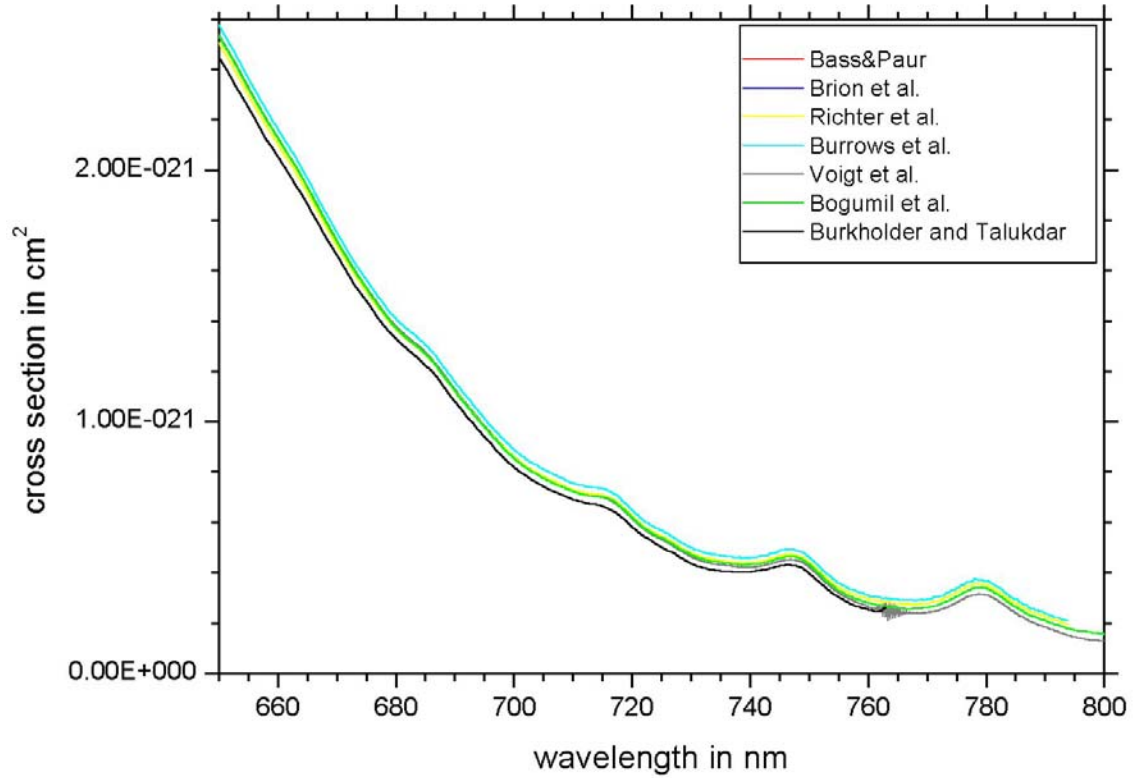


Figure 7-29: Comparison of O₃ absorption cross-sections at 221±3 K: 240–800 nm

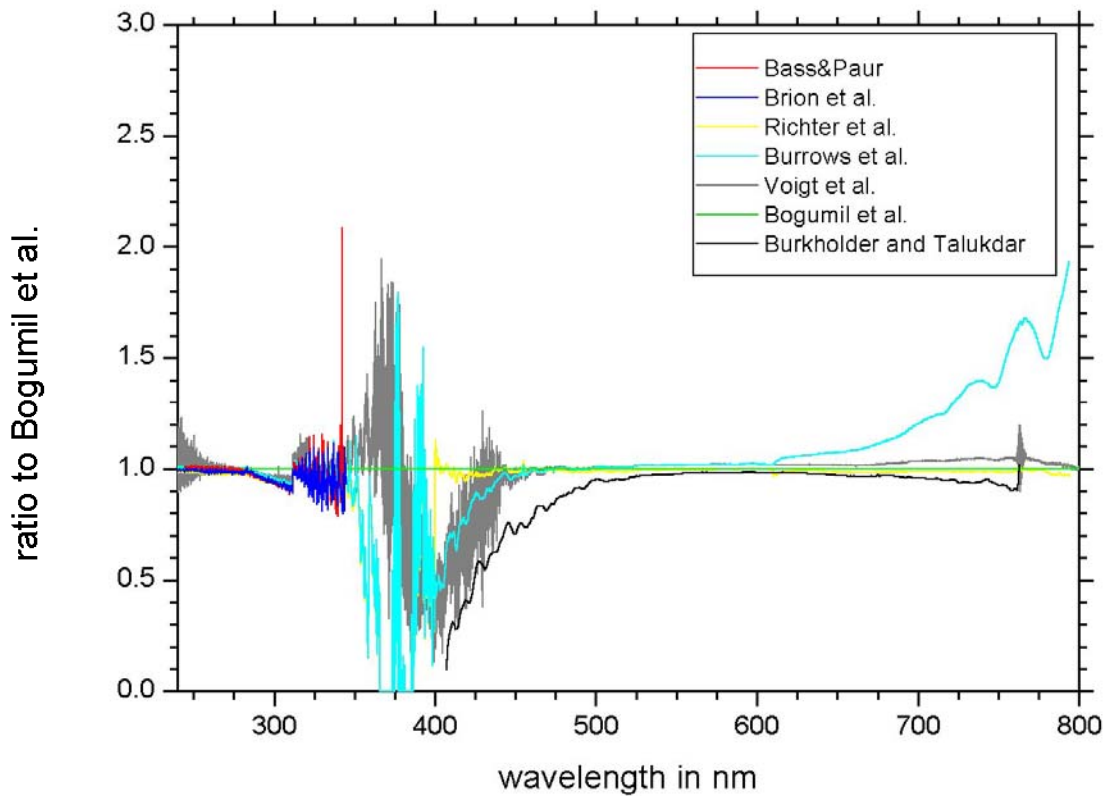
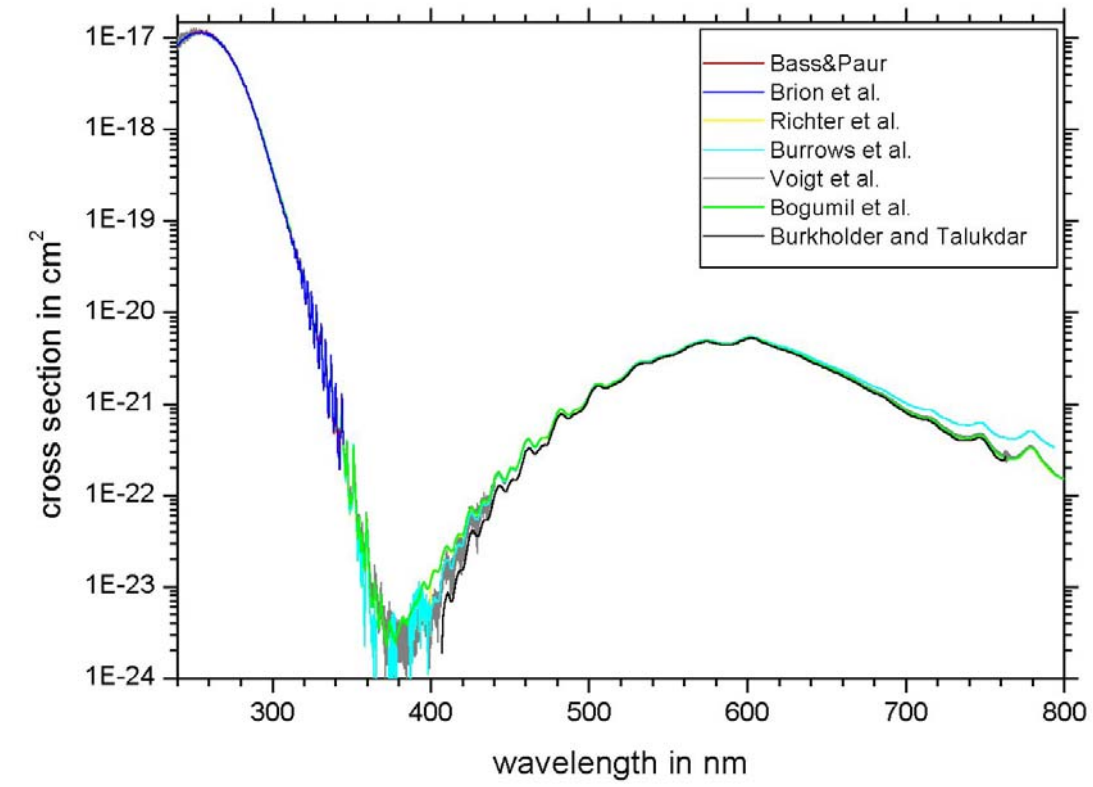


Figure 7-30: Comparison of O₃ absorption cross-sections at 221±3 K: 240–270 nm

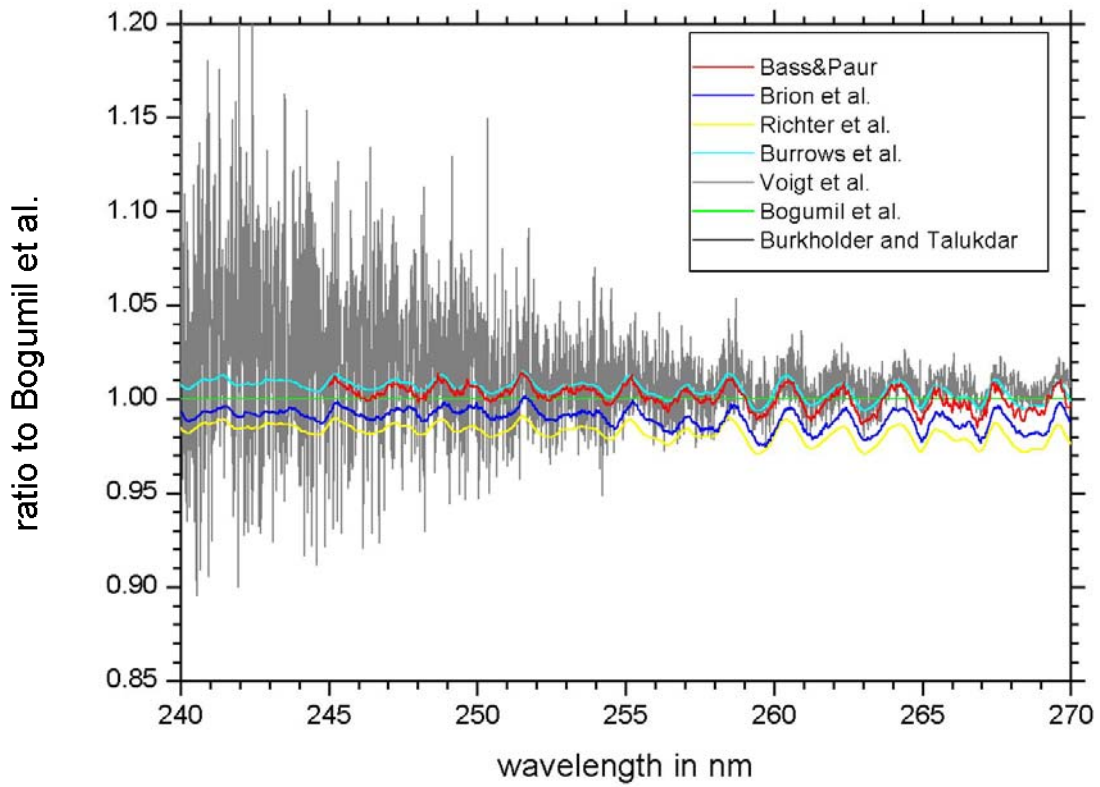
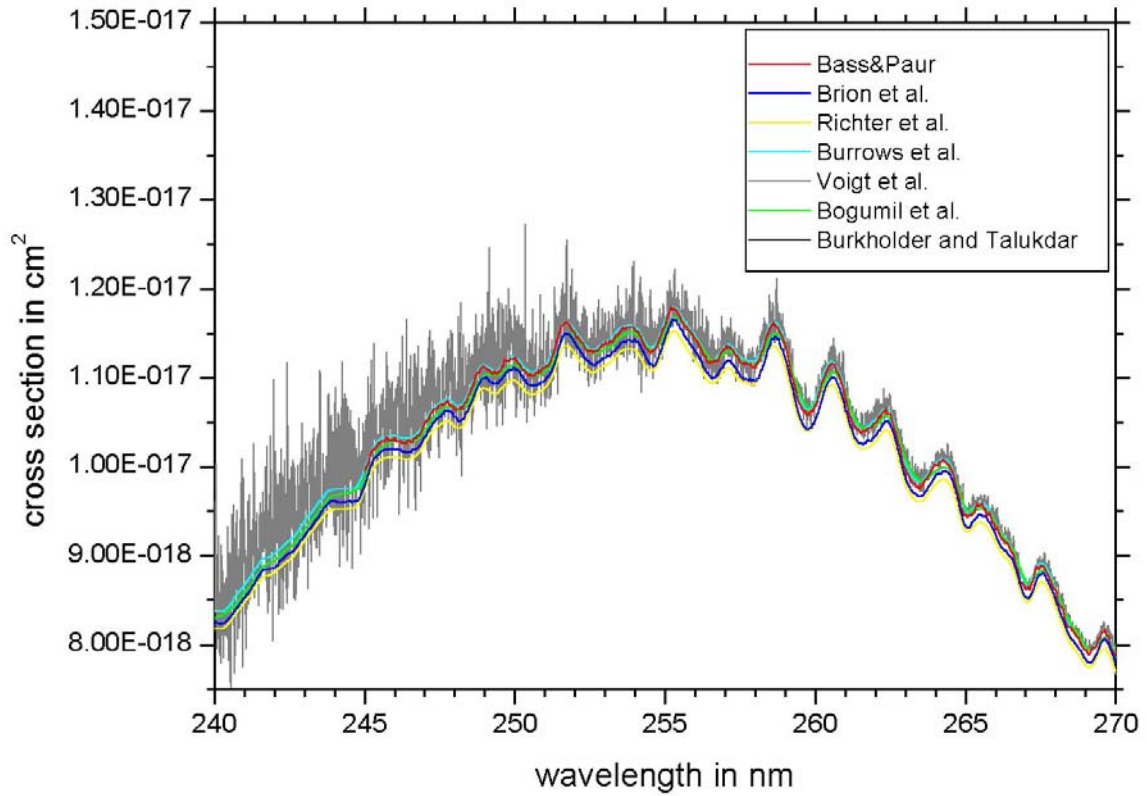


Figure 7-31: Comparison of O₃ absorption cross-sections at 221±3 K: 270–310 nm

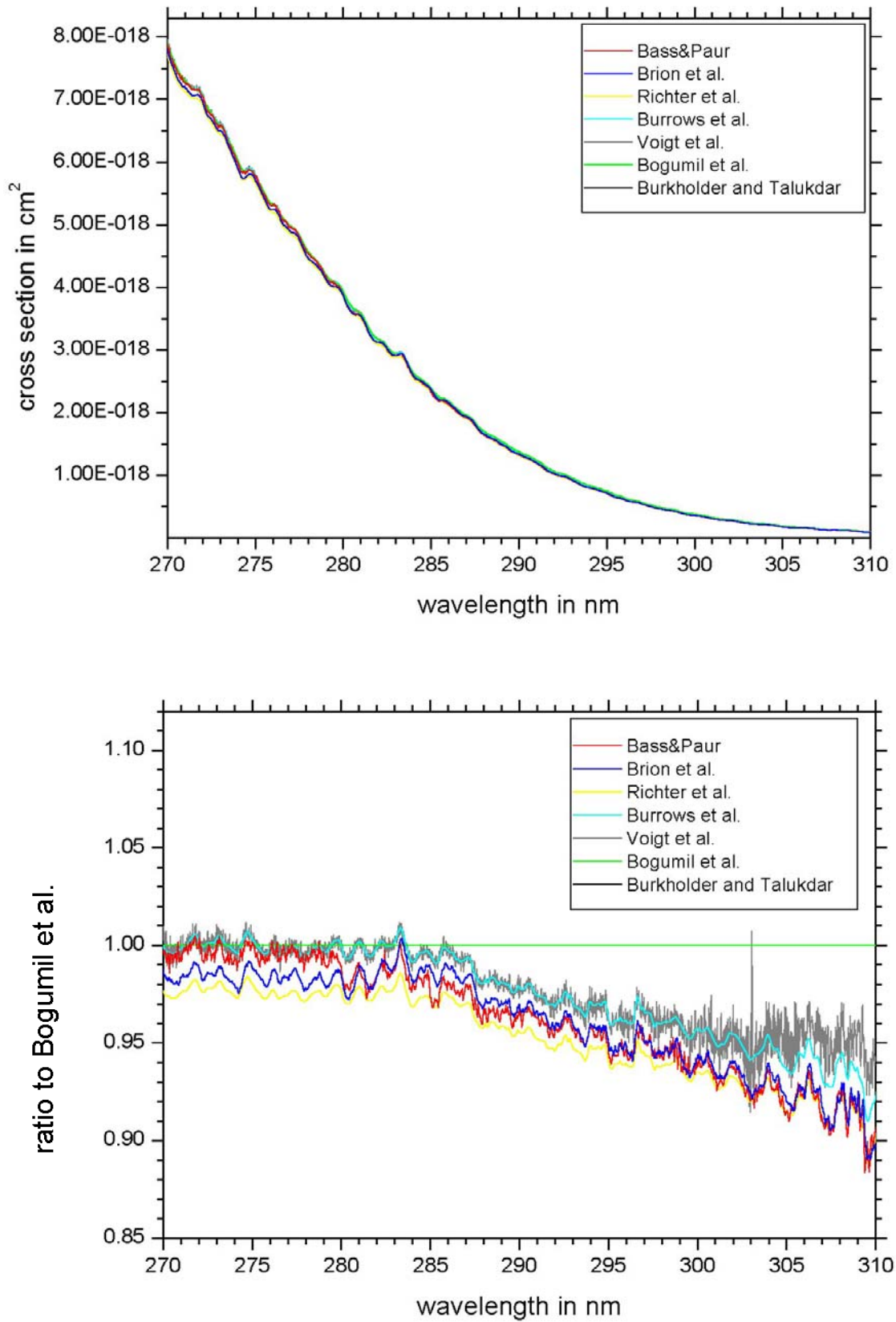


Figure 7-32: Comparison of O₃ absorption cross-sections at 221±3 K: 310–340 nm

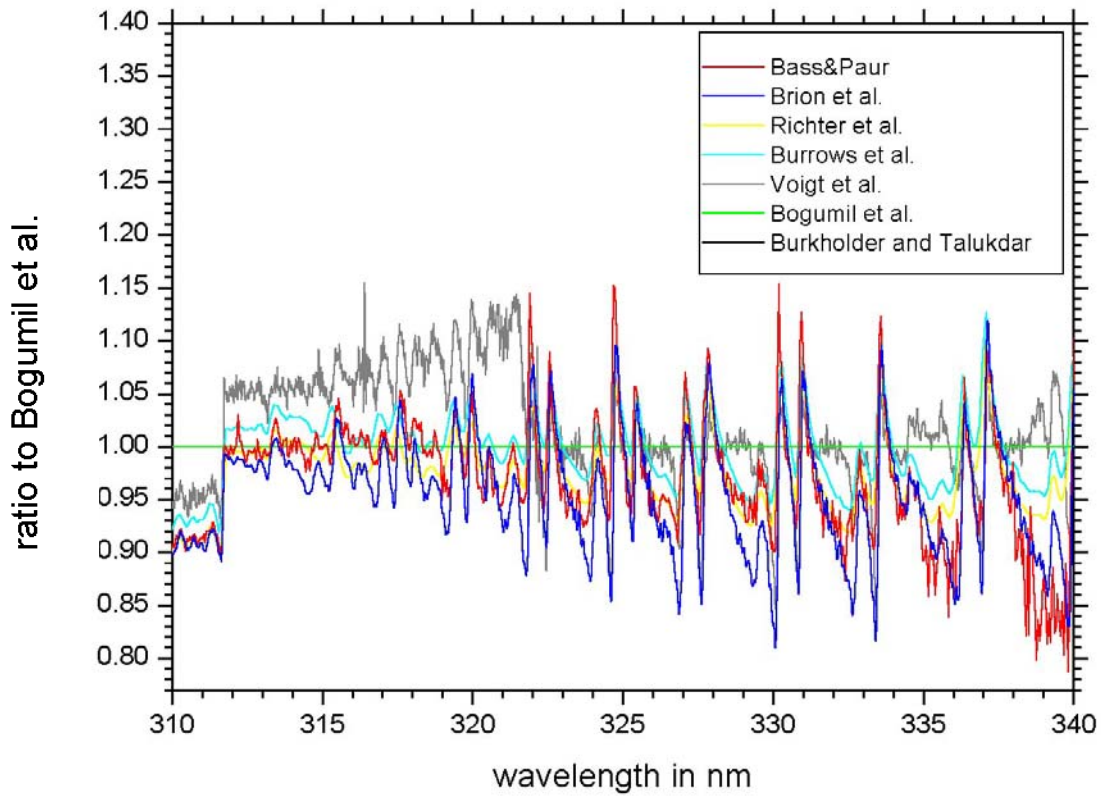
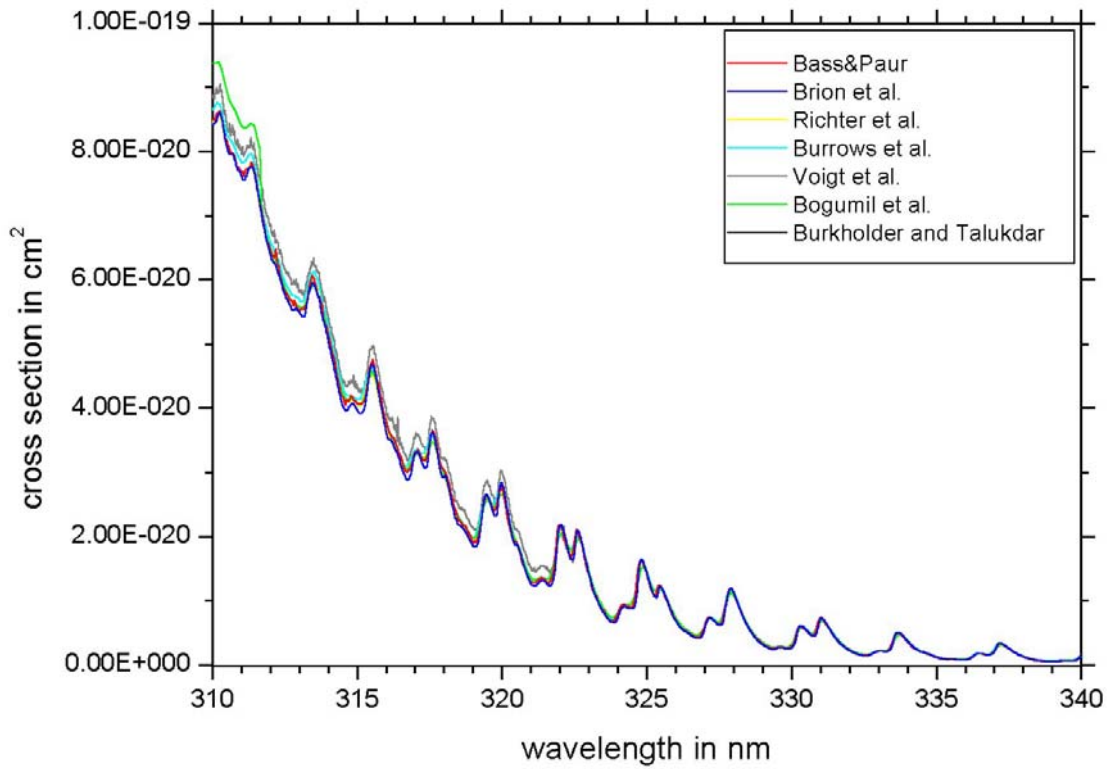


Figure 7-33: Comparison of O₃ absorption cross-sections at 221±3 K: 340–380 nm

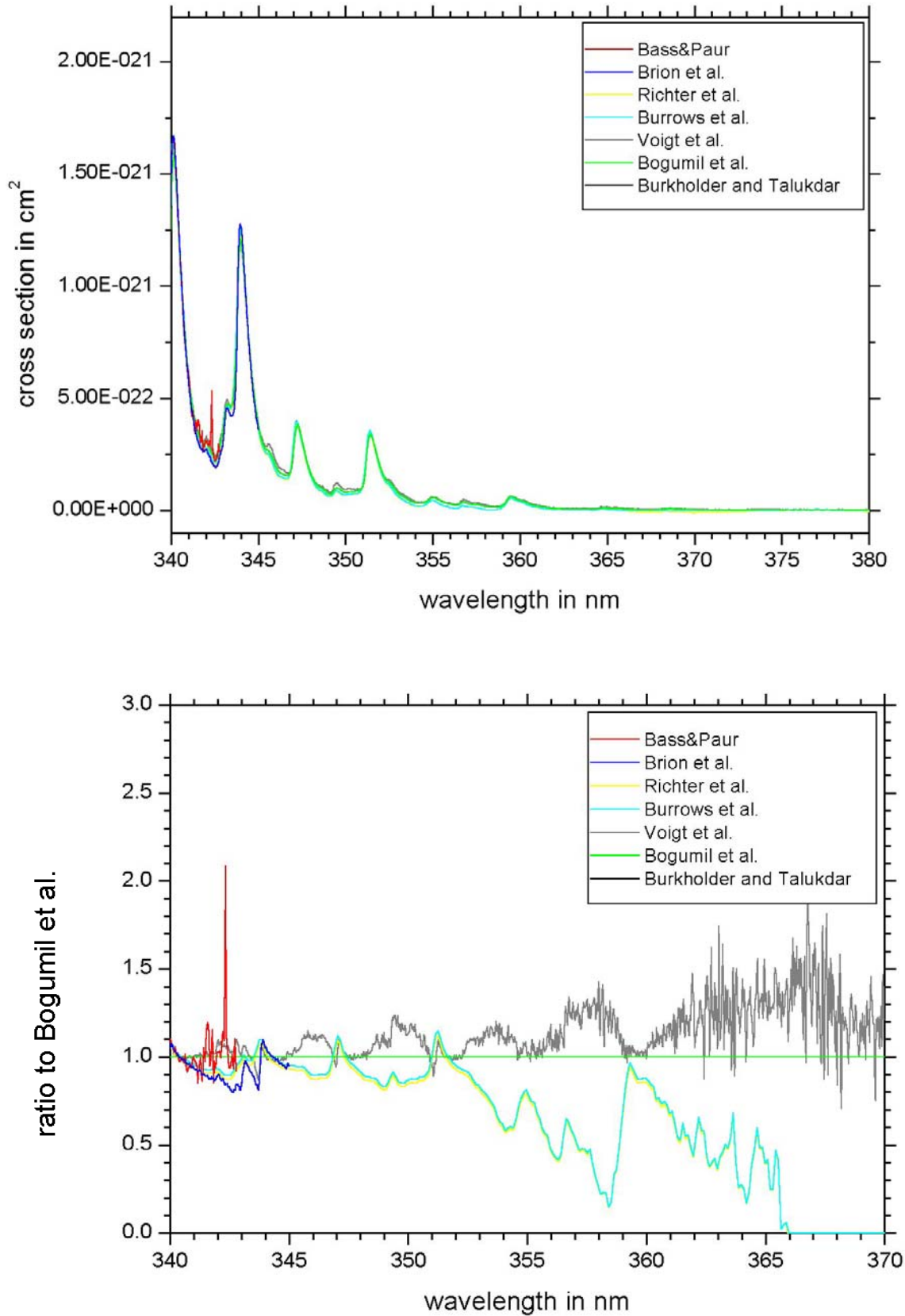


Figure 7-34: Comparison of O₃ absorption cross-sections at 221±3 K: 380–510 nm

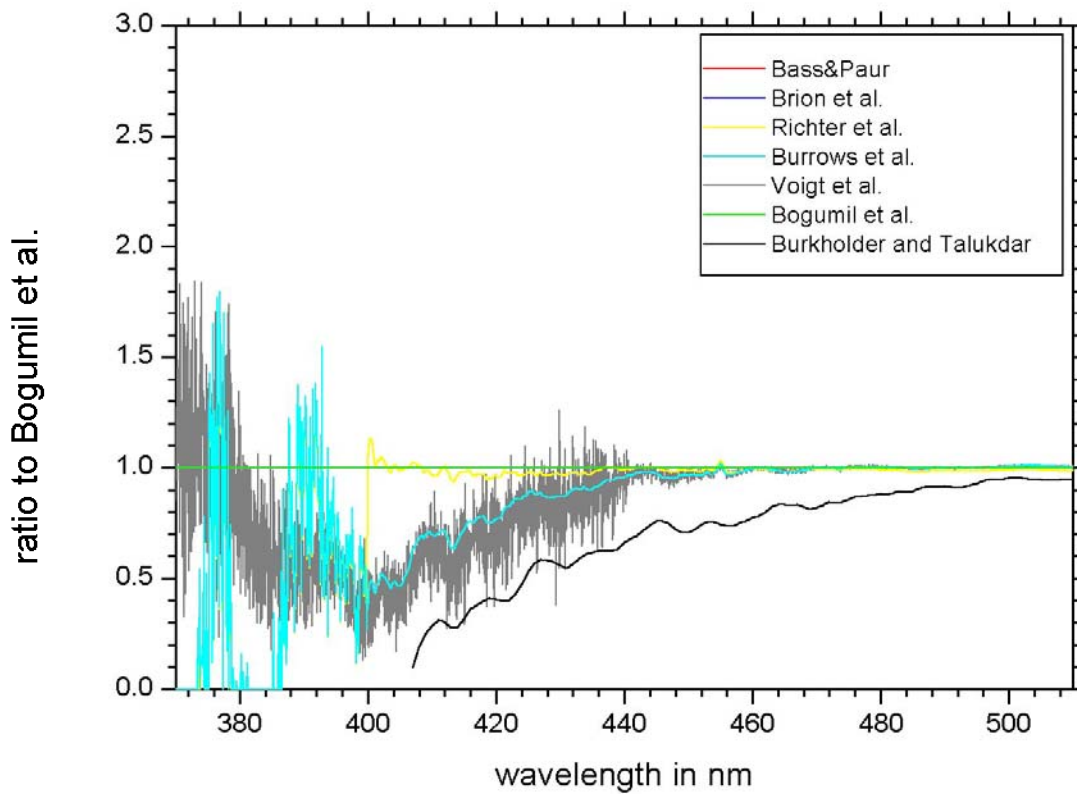
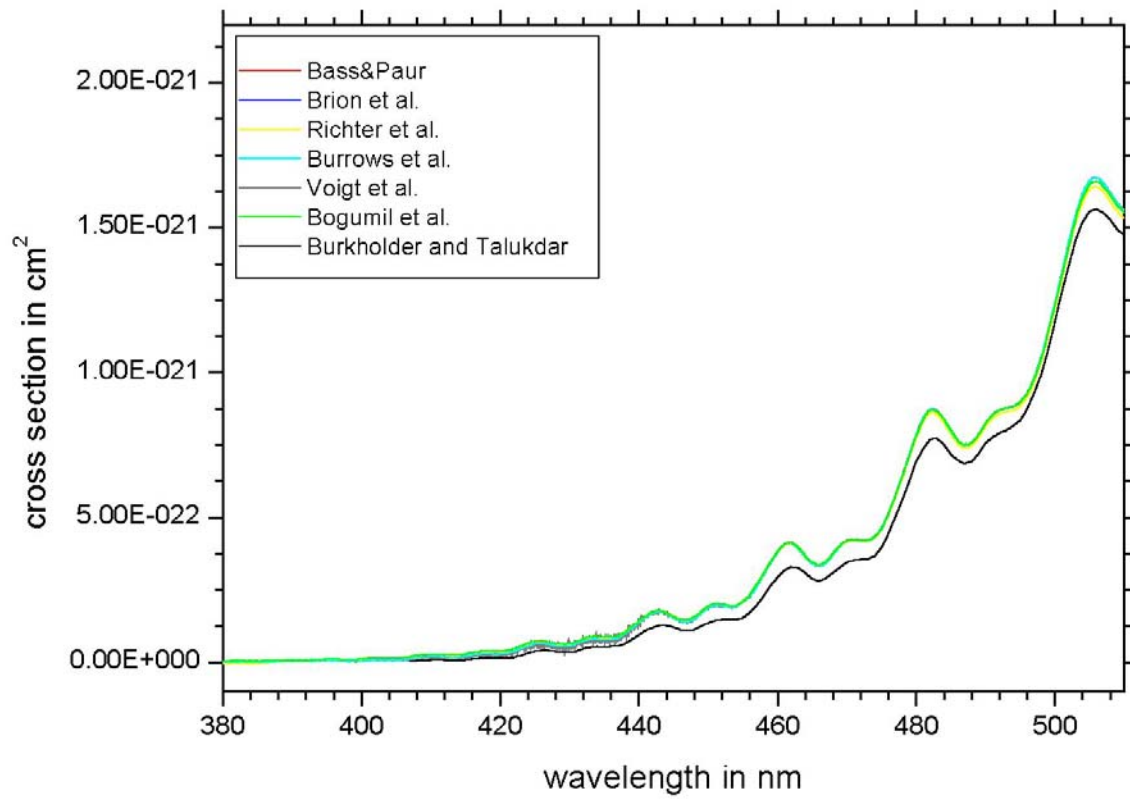


Figure 7-35: Comparison of O₃ absorption cross-sections at 221±3 K: 510–650 nm

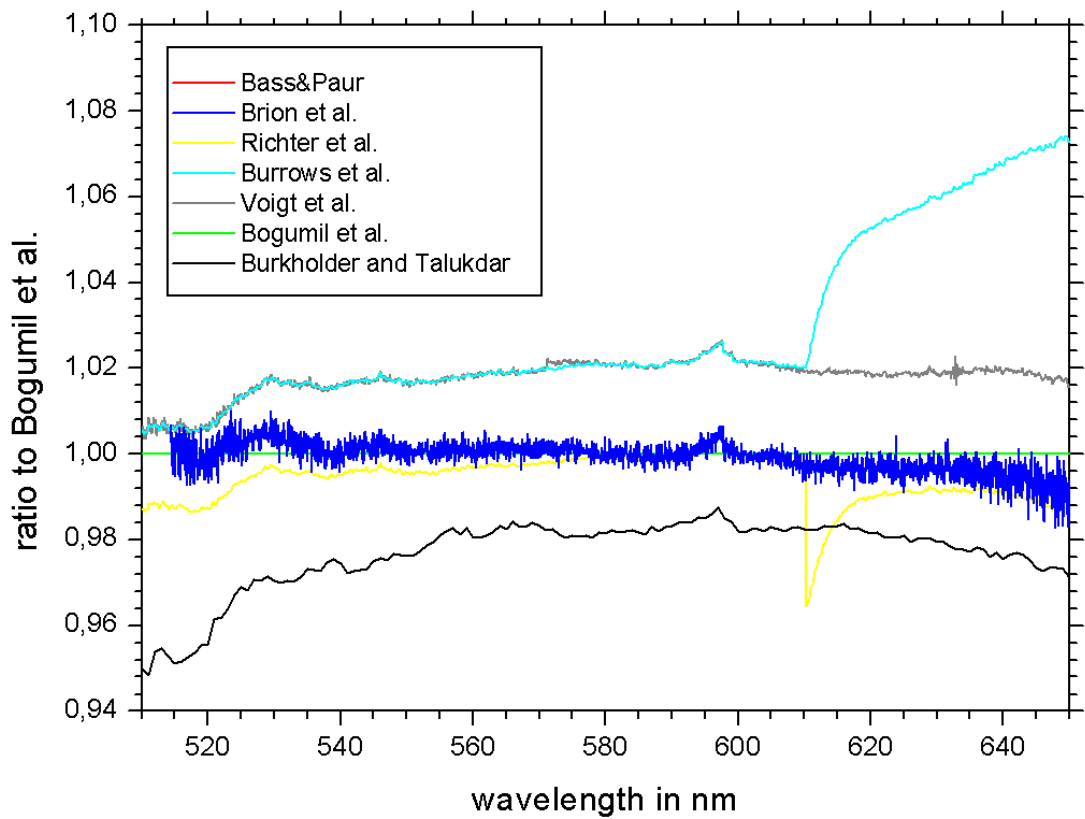
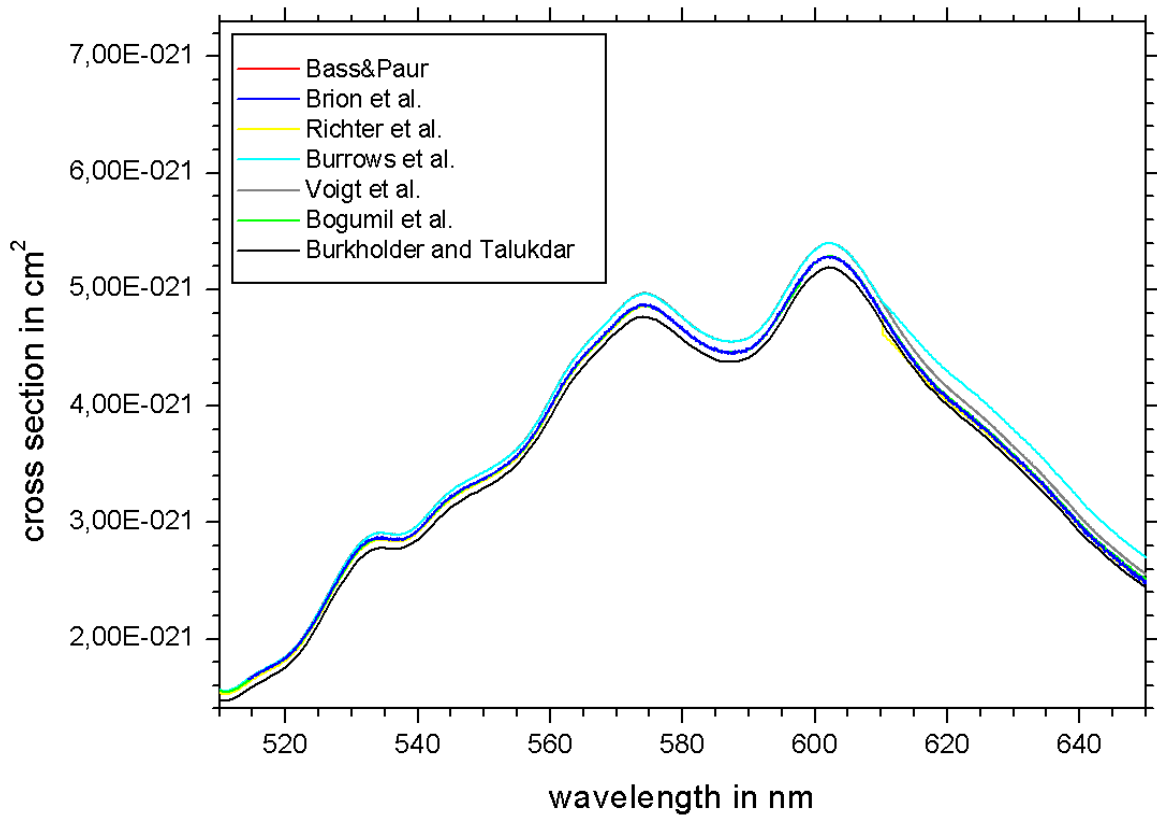


Figure 7-36: Comparison of O₃ absorption cross-sections at 221±3 K: 650–800 nm

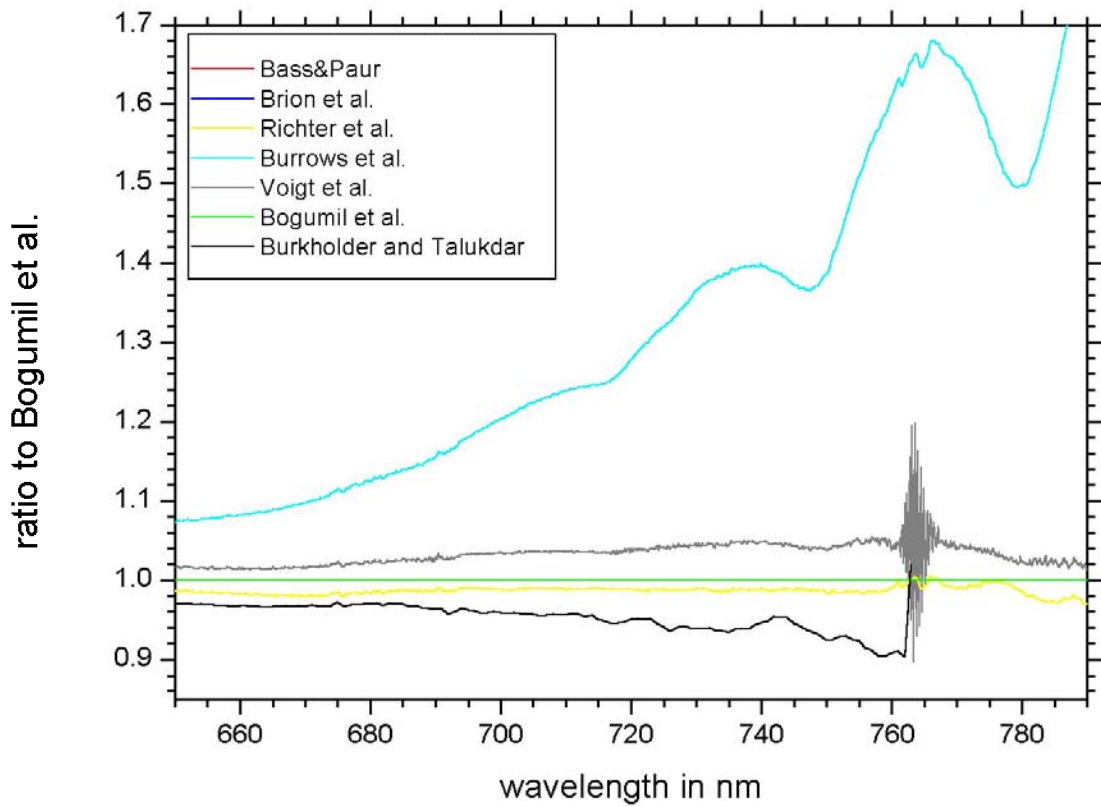
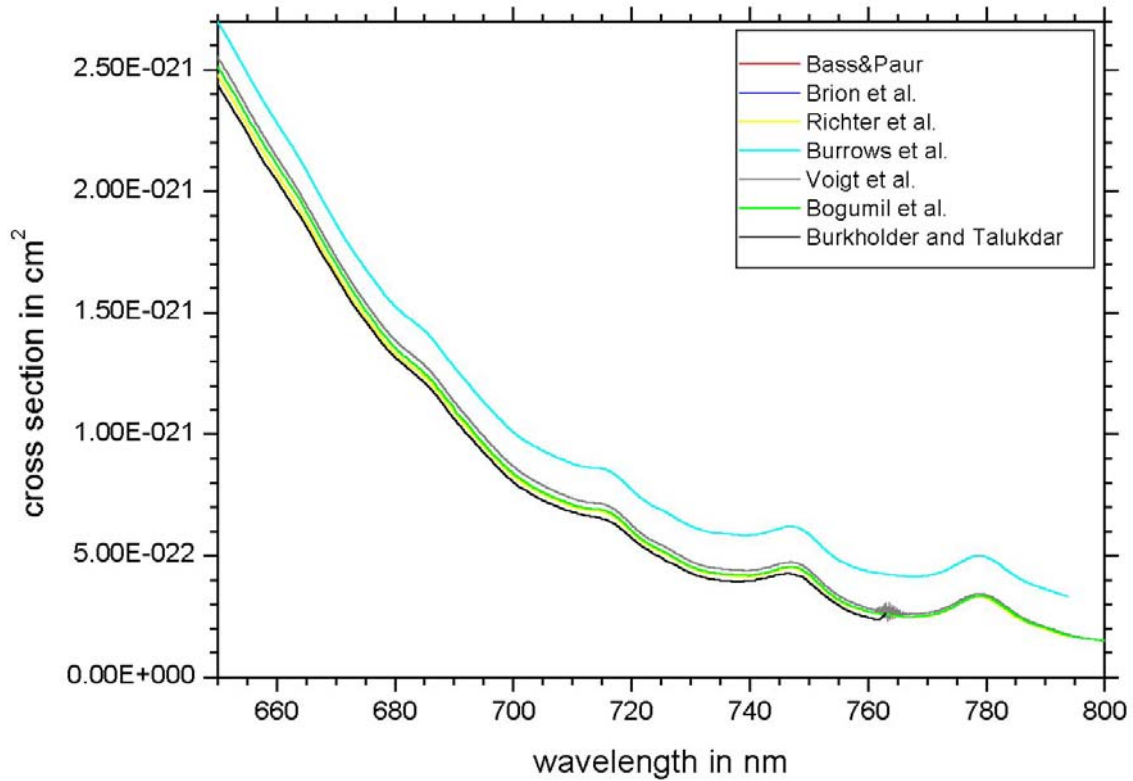


Figure 7-37: Comparison of O₃ absorption cross-sections at 203±1 K: 240–800 nm

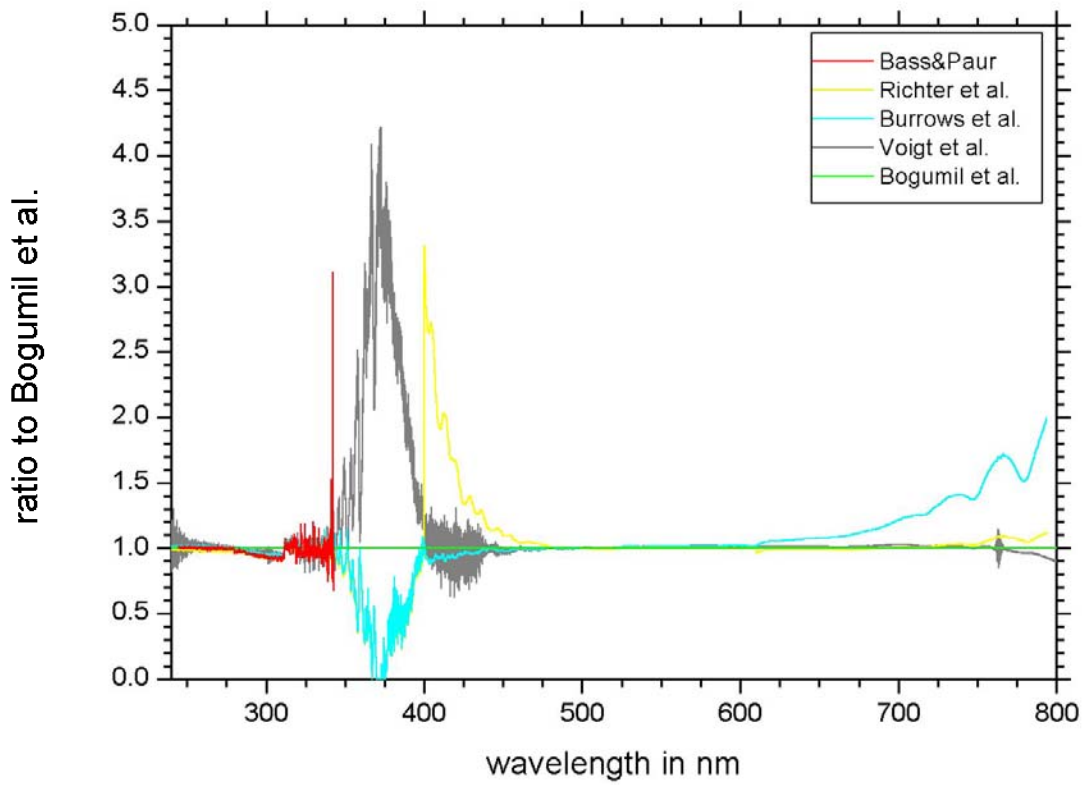
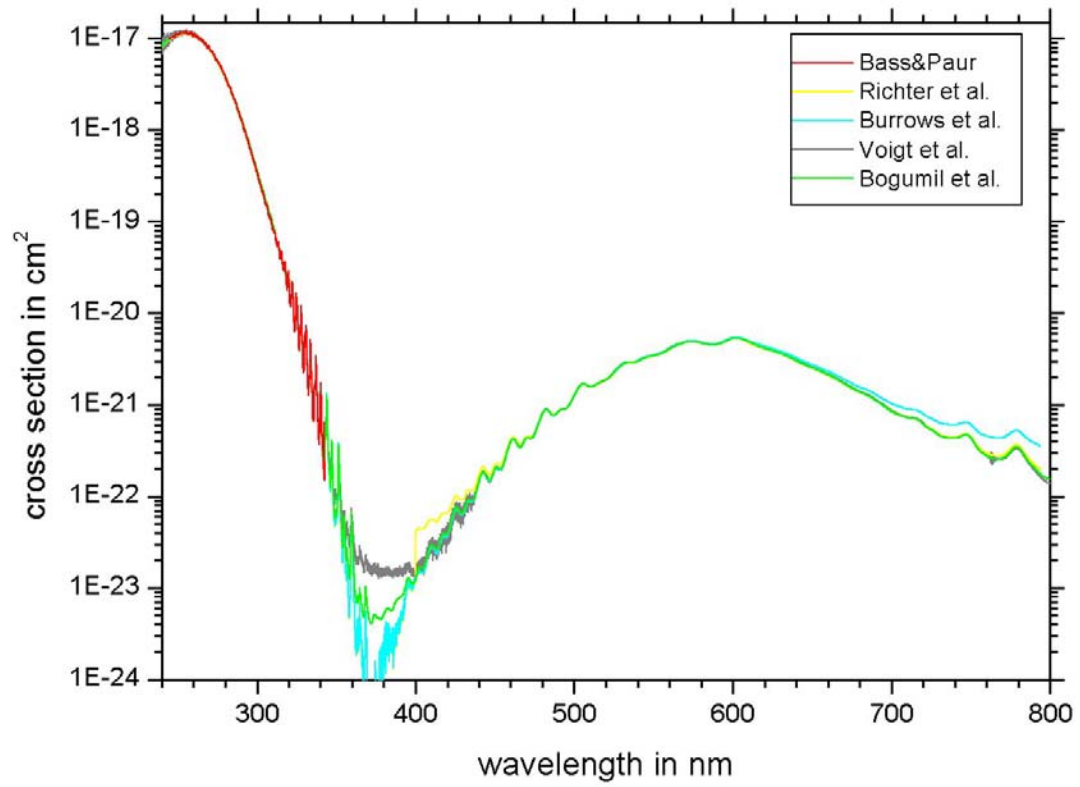


Figure 7-38: Comparison of O₃ absorption cross-sections at 203±1 K: 240–270 nm

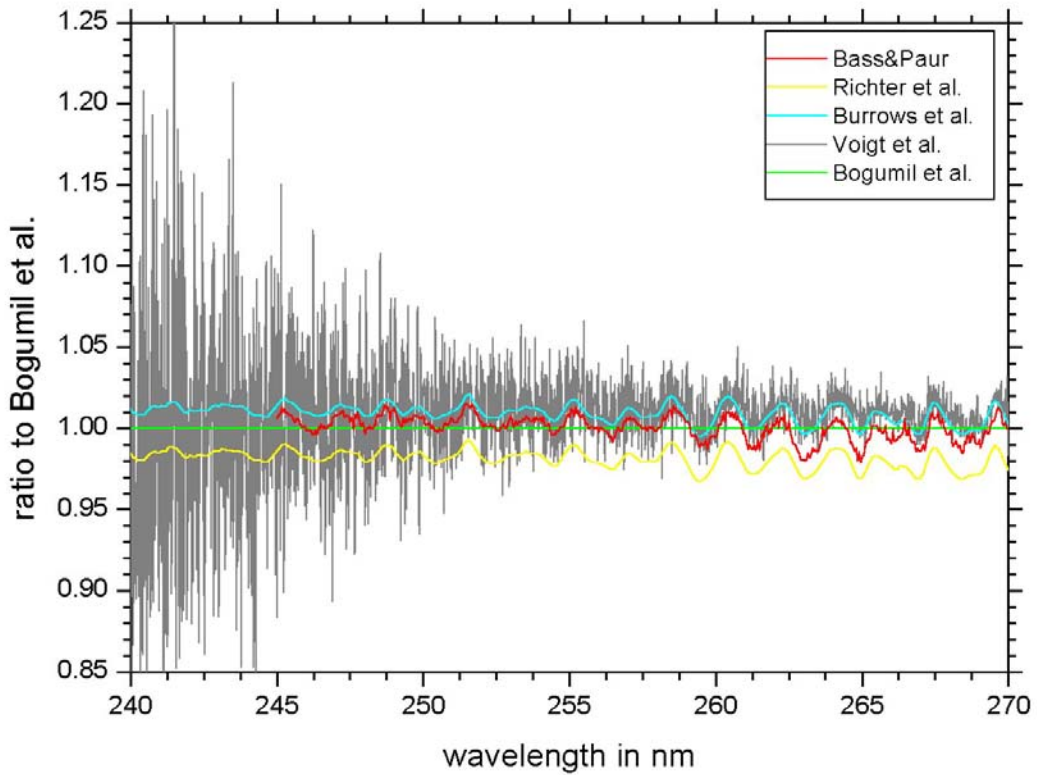
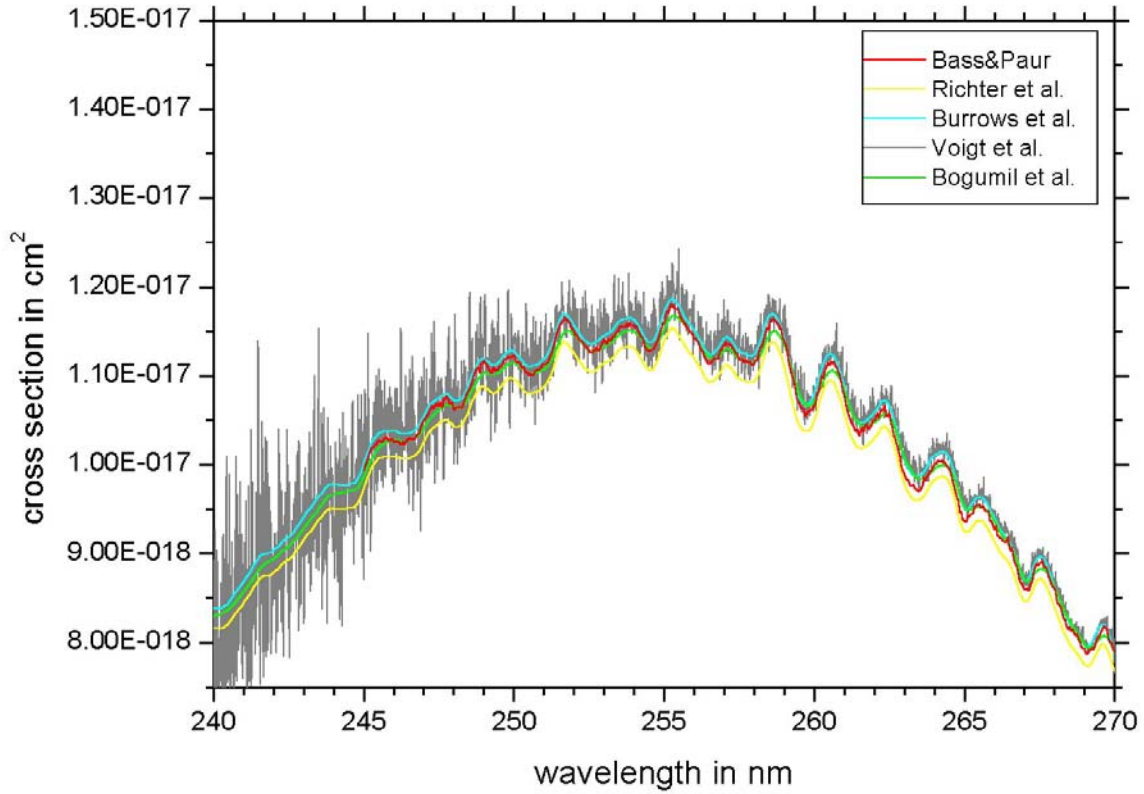


Figure 7-39: Comparison of O₃ absorption cross-sections at 203±1 K: 270–310 nm

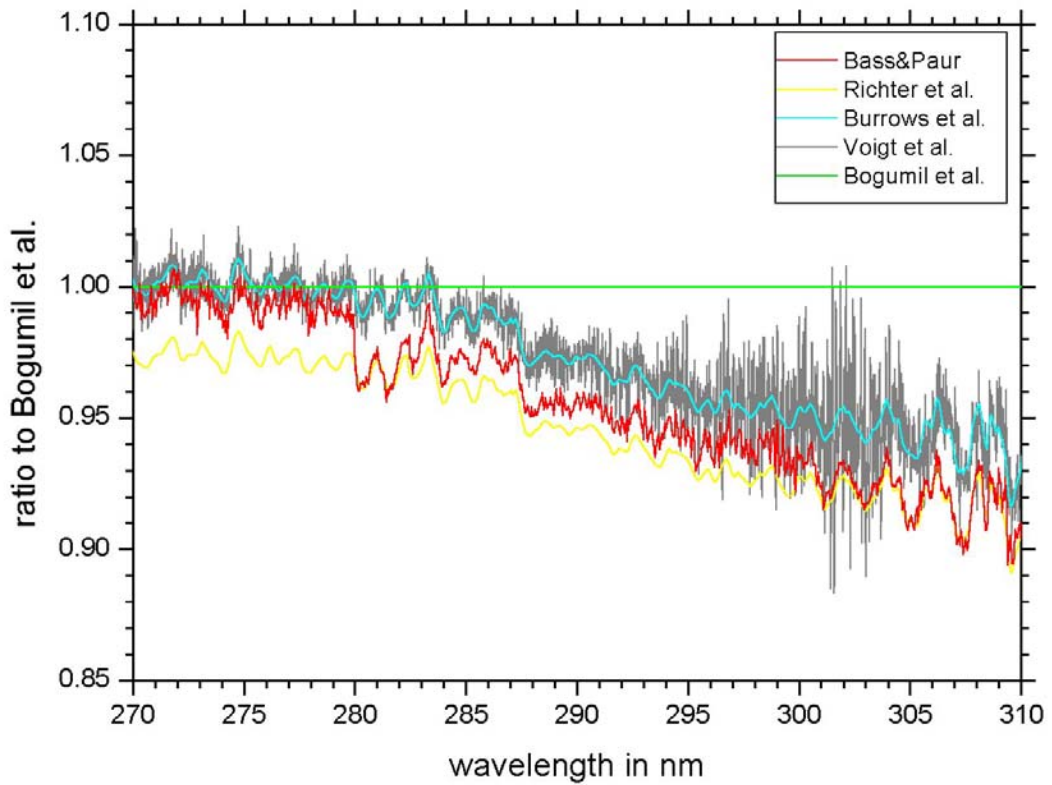
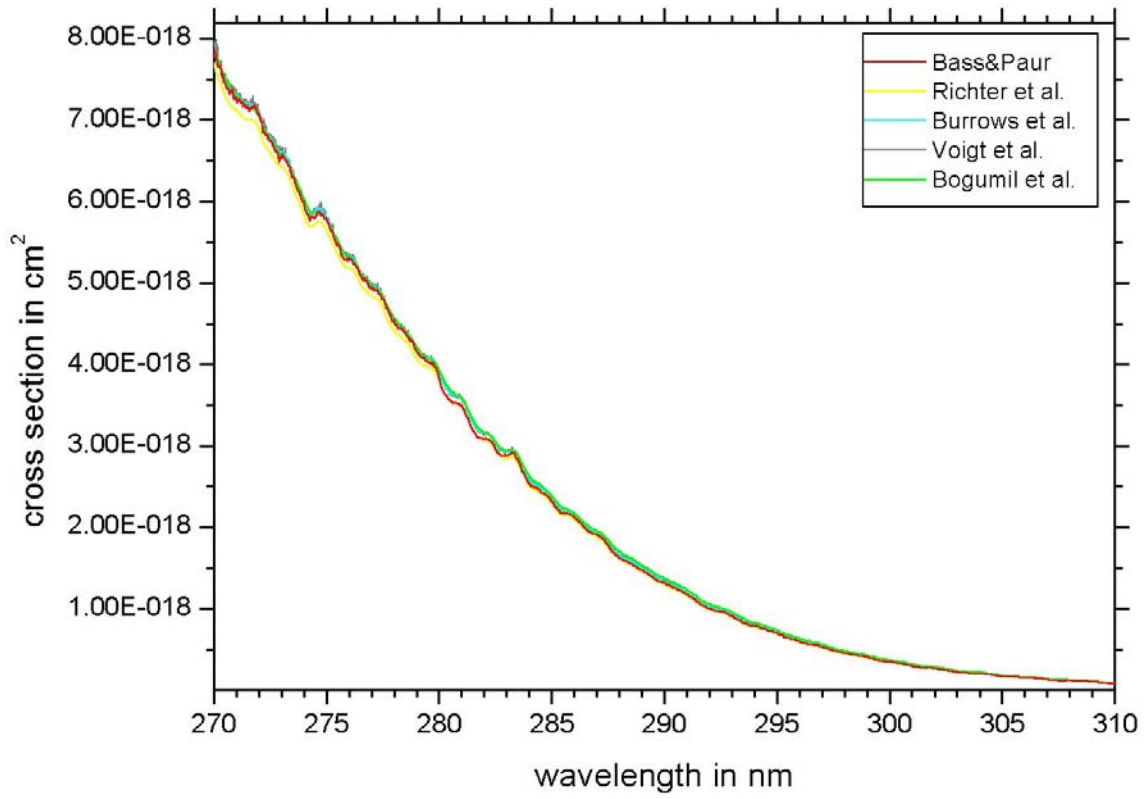


Figure 7-40: Comparison of O₃ absorption cross-sections at 203±1 K: 310–340 nm

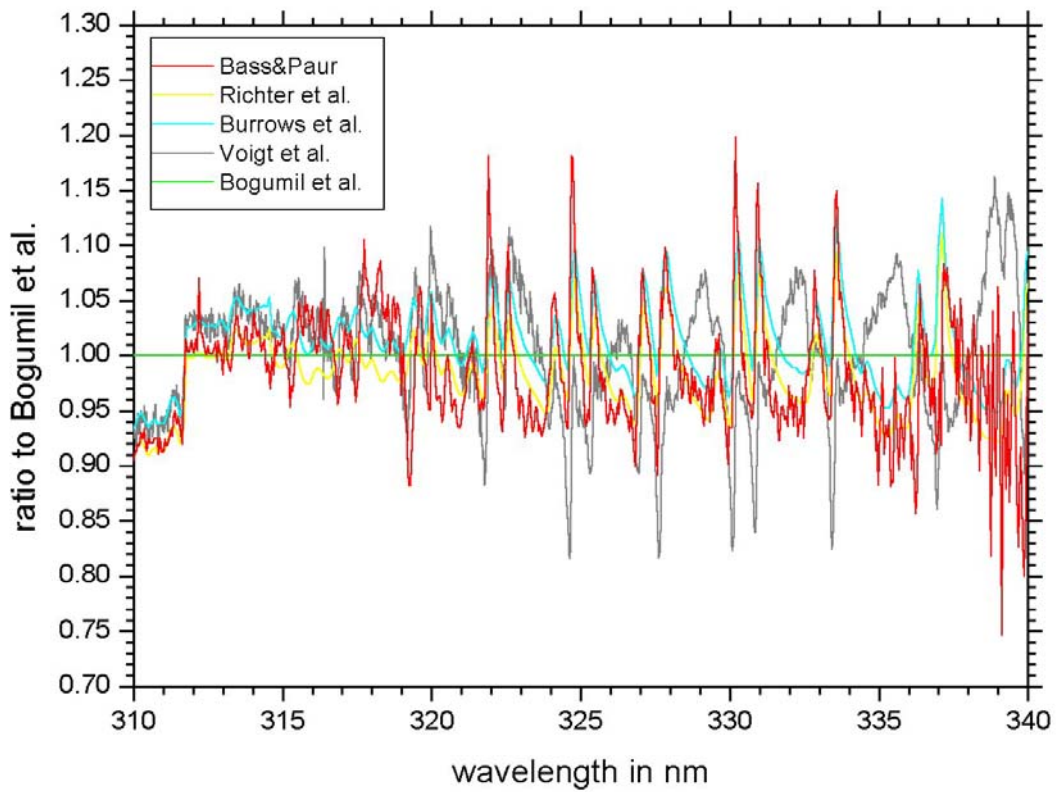
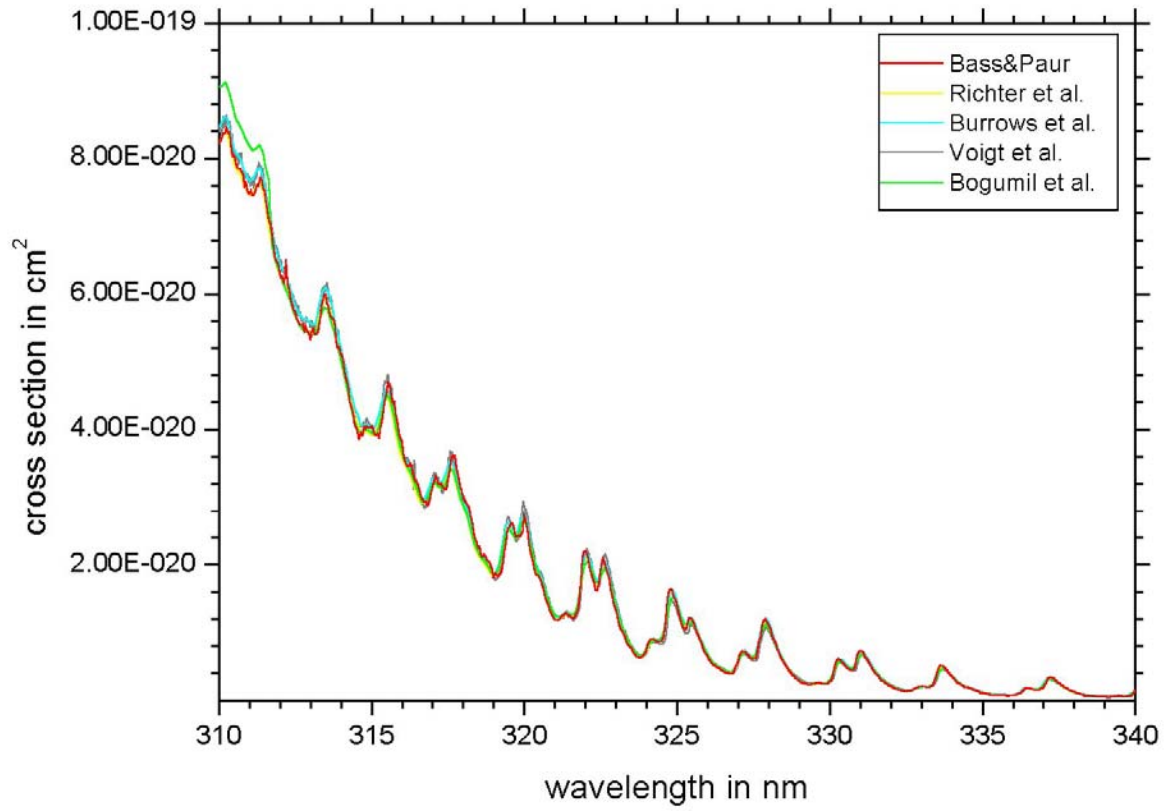


Figure 7-41: Comparison of O₃ absorption cross-sections at 203±1 K: 340–380 nm

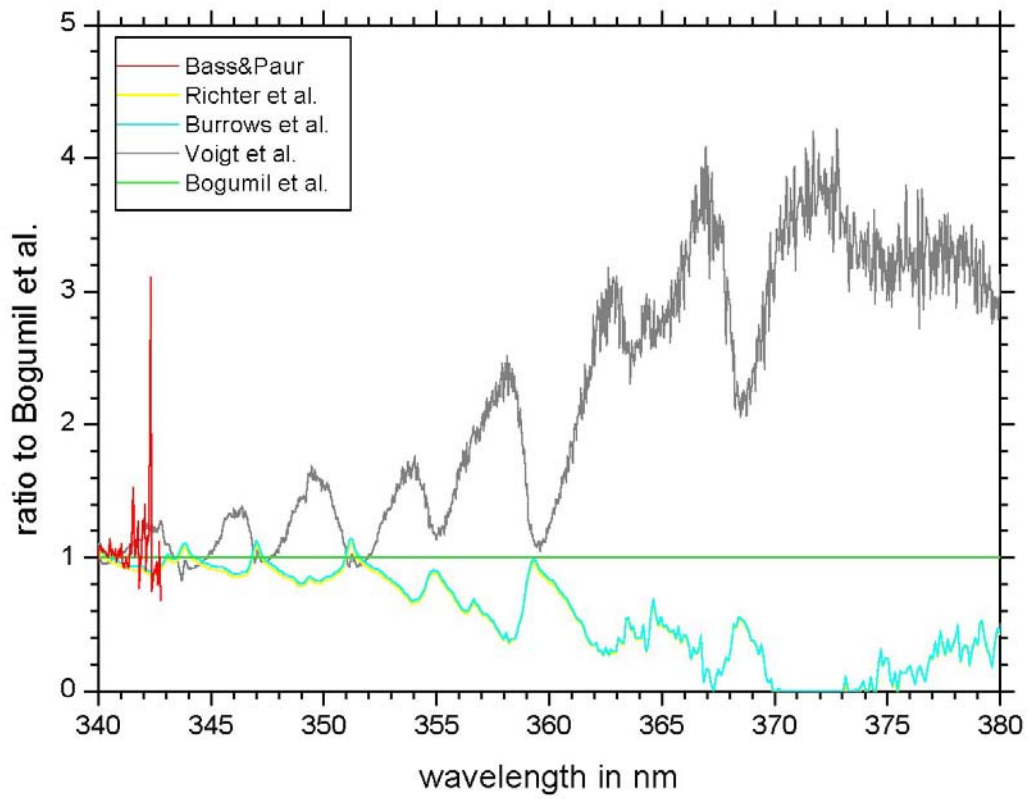
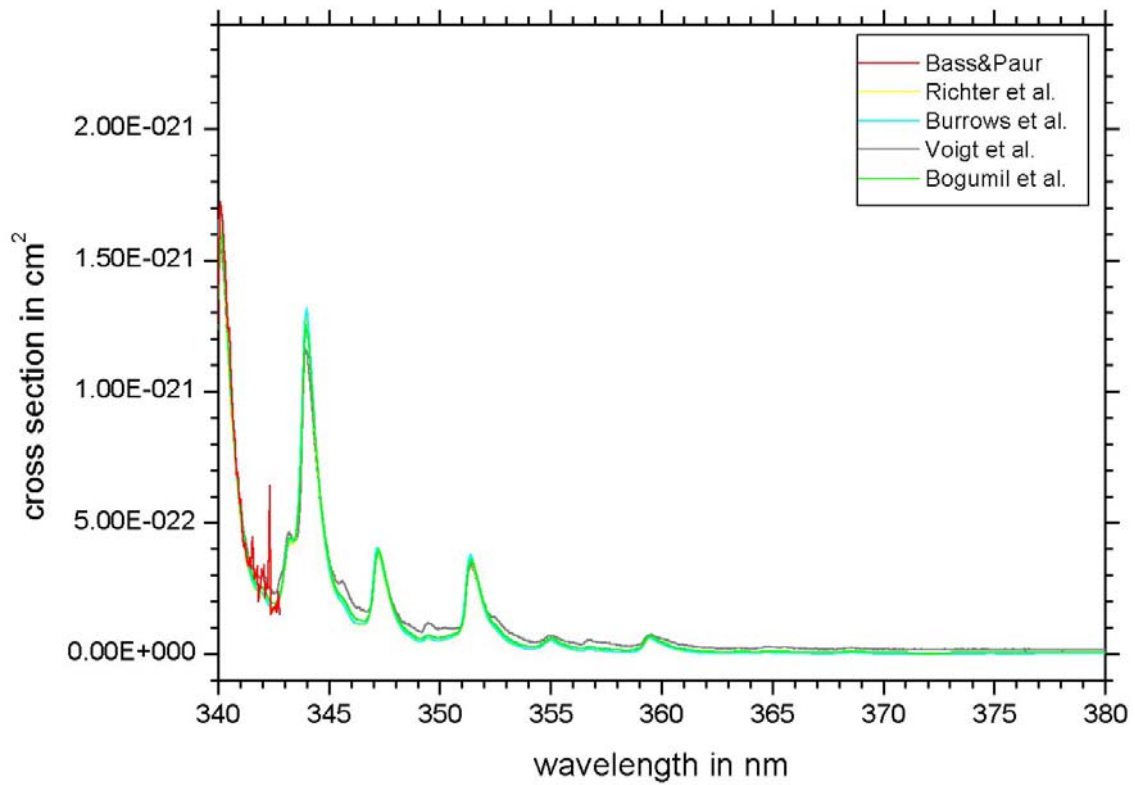


Figure 7-42: Comparison of O₃ absorption cross-sections at 203±1 K: 380–510 nm

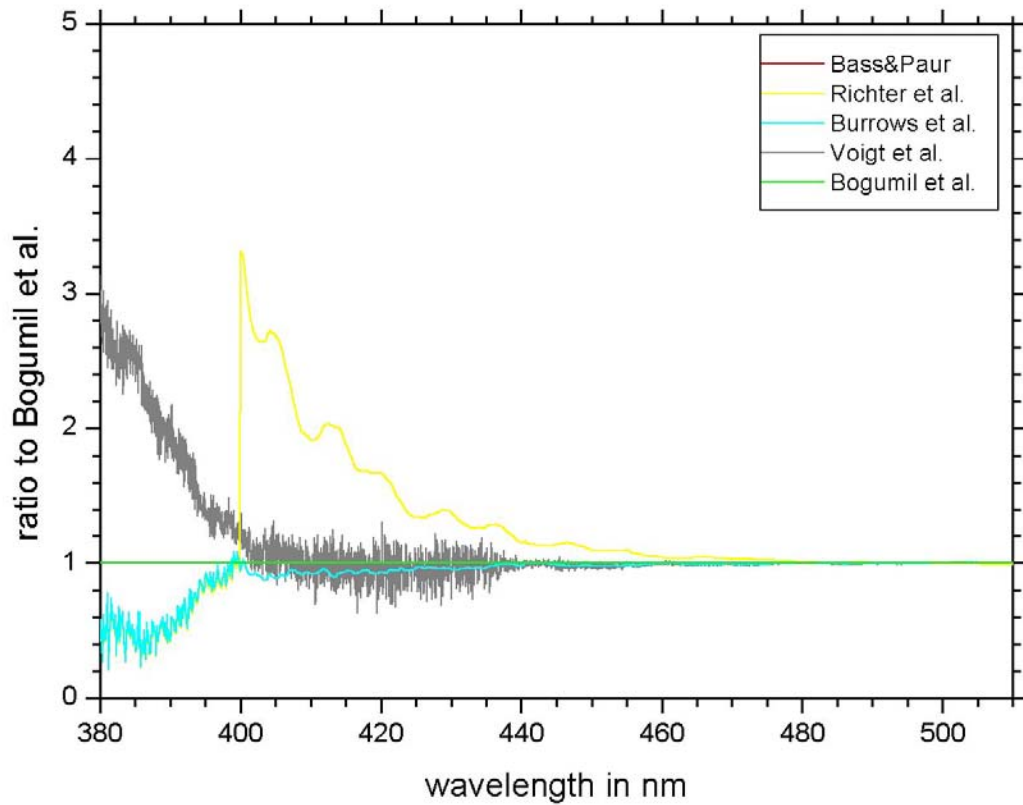
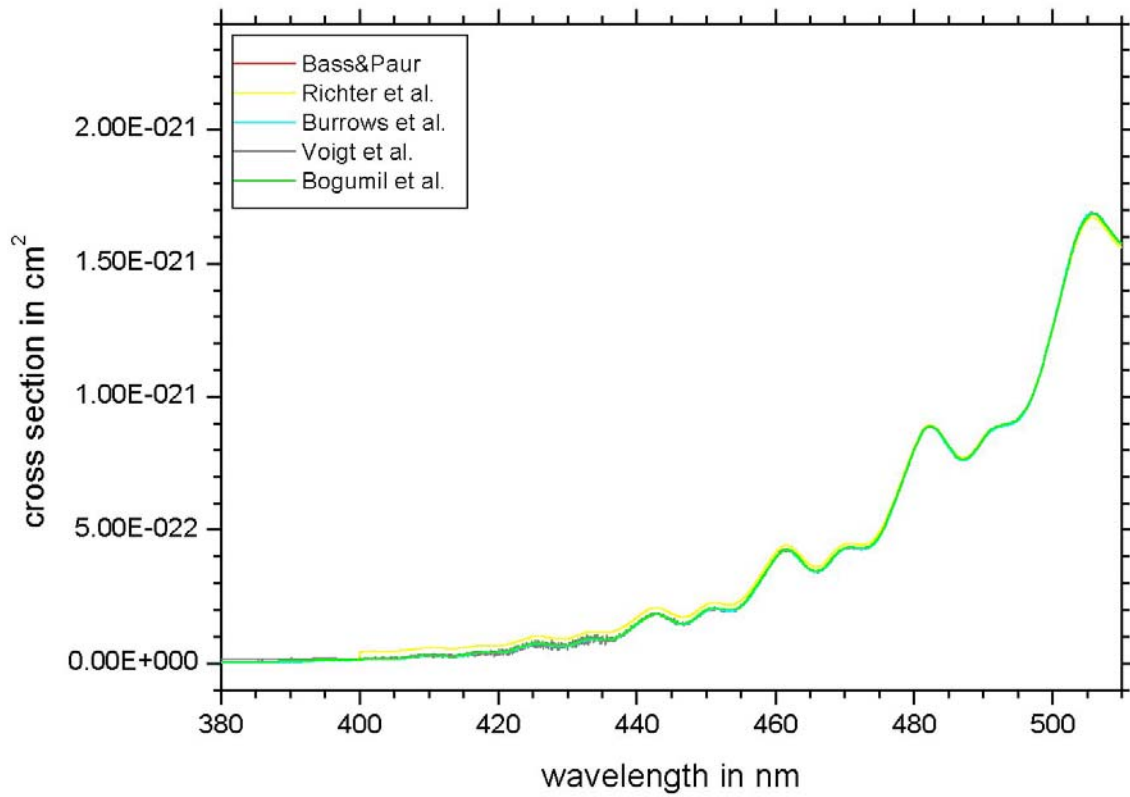


Figure 7-43: Comparison of O₃ absorption cross-sections at 203±1 K: 510–650 nm

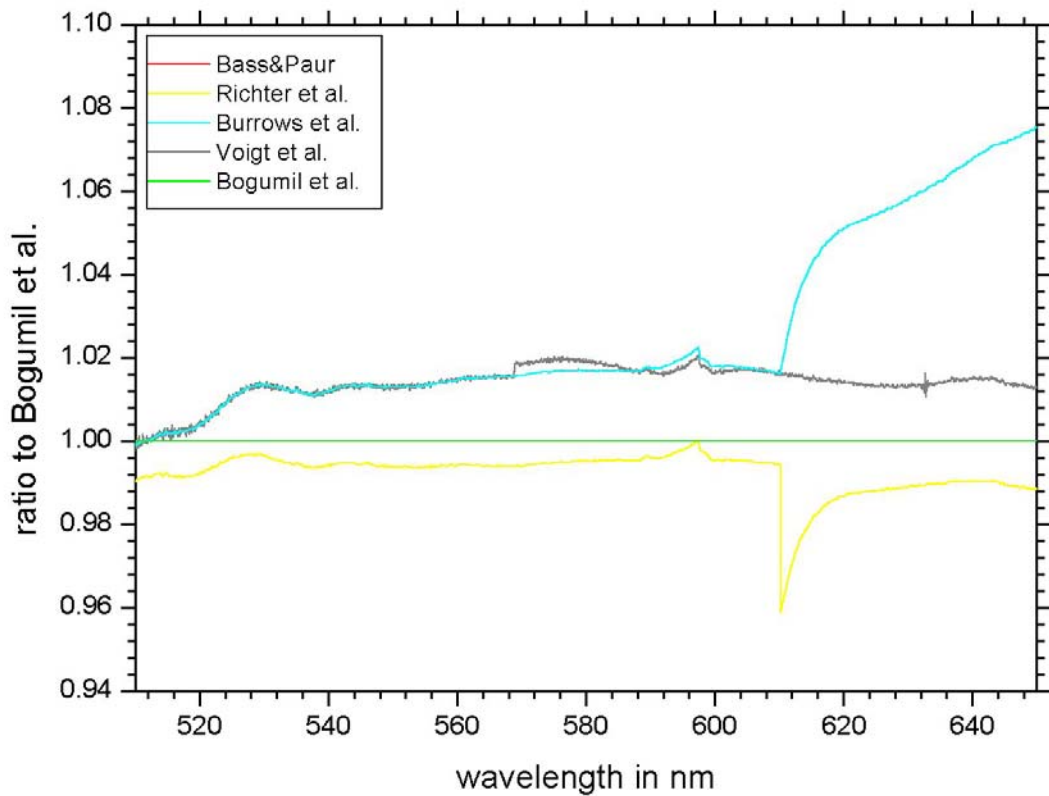
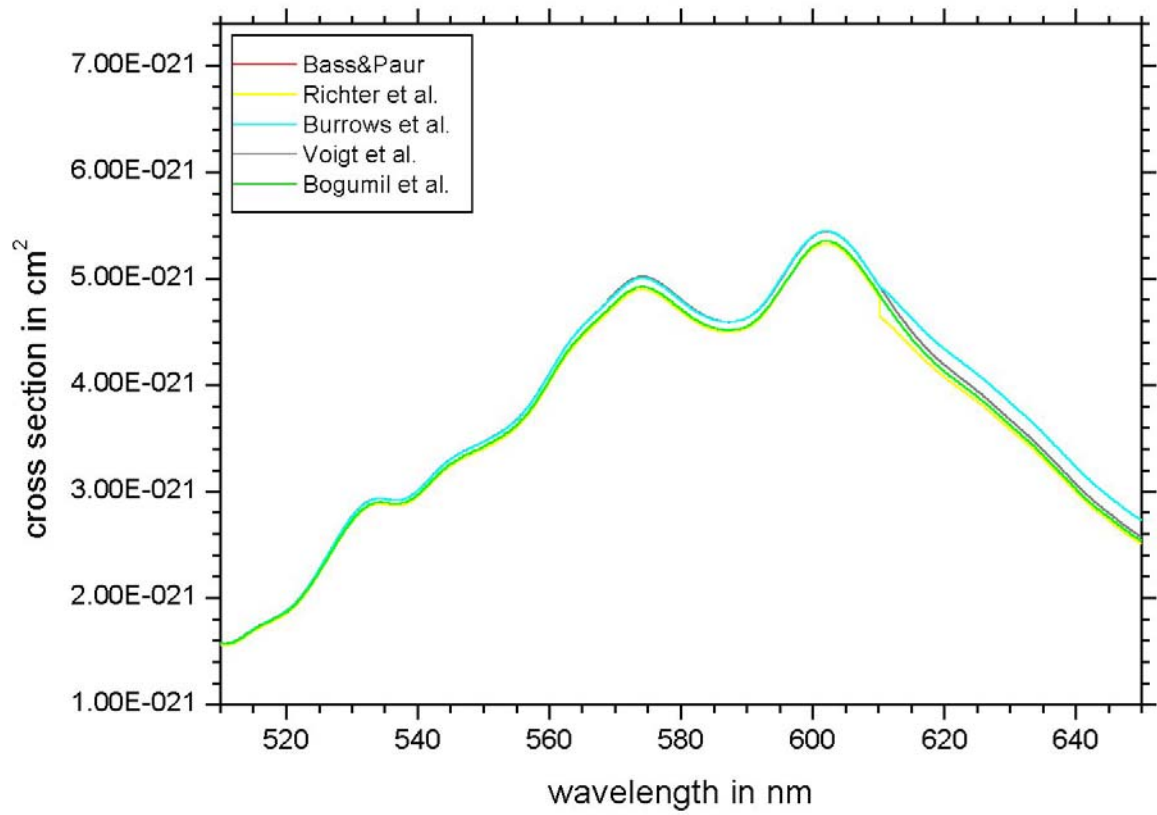
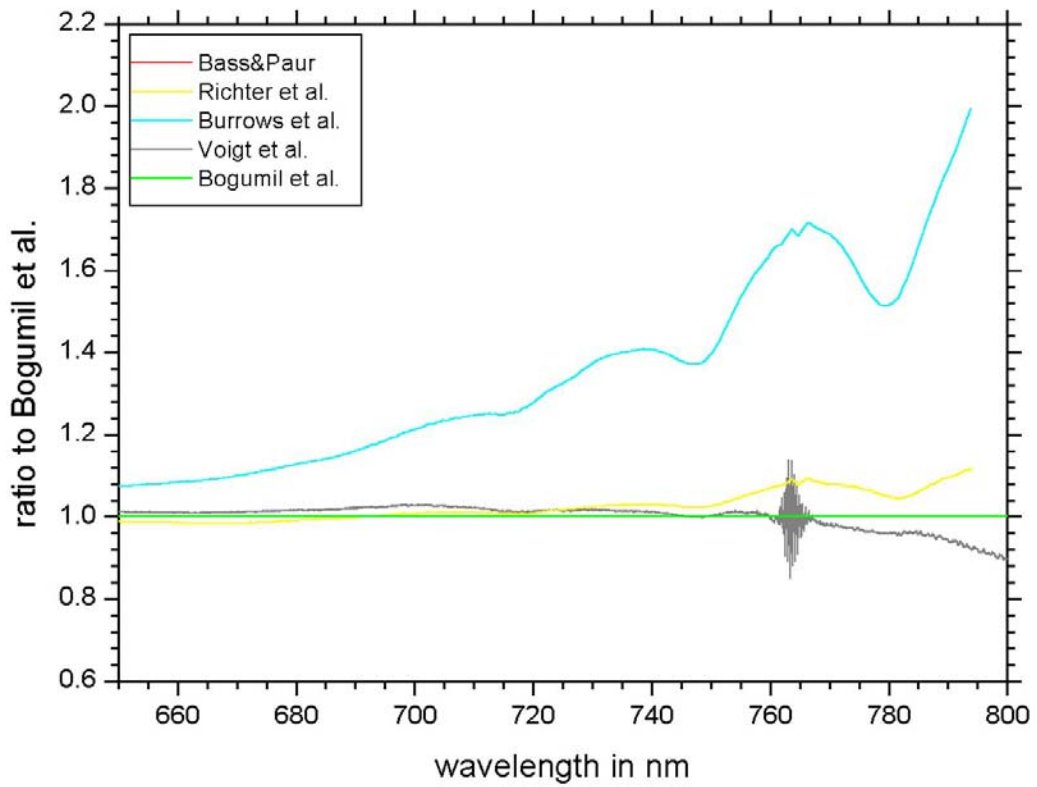
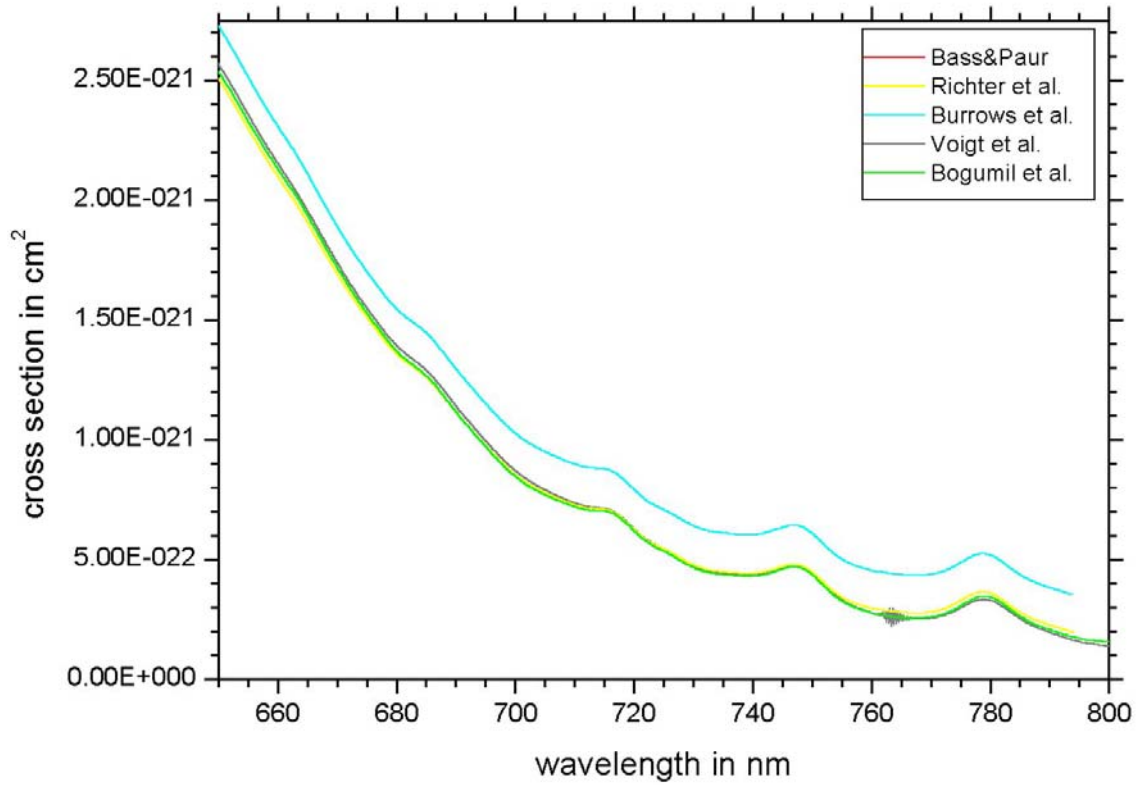


Figure 7-44: Comparison of O₃ absorption cross-sections at 203±1 K: 650–800 nm



7.3. Comparison of the integrated O₃ cross-sections at temperatures below ambient: 276±4 K, 243±3 K, 221±3 K, and 203±1 K

As for the cross-sections at room temperature, we will compare the integrated cross-sections since they are rather insensitive to small wavelength shifts and the ILS. We will first give the integrated cross-sections for every temperature and then summarize the results at all temperatures (including room temperature) for the following spectral regions:

- the Hartley band (245–340 nm),
- the Chappuis band (410–690 nm),
- the Huggins bands (325–340 nm), and
- the blue tail of the Chappuis band (410–520 nm).

The latter two windows are currently used for atmospheric O₃ retrieval.

Table 7-1: Integrated absorption cross-sections of O₃⁽¹⁾ at 276±4 K

Reference	Hartley band	Chappuis band	Huggins band	Blue tail of the Chappuis band
<i>Bass and Paur</i>	3.54×10 ⁻¹⁶ -0.1%	–	7.27×10 ⁻²⁰ -2.1%	–
<i>Brion et al.</i>	–	–	7.16×10 ⁻²⁰ -3.6%	–
<i>Richter et al.</i>	3.49×10 ⁻¹⁶ -1.6%	6.45×10 ⁻¹⁹ +0.2%	7.55×10 ⁻²⁰ +1.7%	7.00×10 ⁻²⁰ +4.3%
<i>Burrows et al.</i>	3.58×10 ⁻¹⁶ +0.8%	6.58×10 ⁻¹⁹ +2.3%	7.73×10 ⁻²⁰ +4.1%	6.91×10 ⁻²⁰ +3.1%
<i>Voigt et al.</i>	3.57×10 ⁻¹⁶ +0.6%	6.52×10 ⁻¹⁹ +1.3%	7.31×10 ⁻²⁰ -1.5%	6.77×10 ⁻²⁰ +0.9%
<i>Bogumil et al.</i>	3.56×10 ⁻¹⁶ +0.4%	6.43×10 ⁻¹⁹ -0.1%	7.51×10 ⁻²⁰ +1.3%	6.57×10 ⁻²⁰ +0.9%
<i>Burkholder and Talukdar</i>	–	6.20×10 ⁻¹⁹ -3.7%	–	6.29×10 ⁻²⁰ -6.2%
Average value	3.55×10 ⁻¹⁶	6.44×10 ⁻¹⁹	7.42×10 ⁻²⁰	6.71×10 ⁻²⁰
Relative uncertainty	±1.0%	±2.3%	±2.9%	±4.2%

⁽¹⁾ The integrated cross sections are given in units of cm²×nm.

Table 7-2: Integrated absorption cross-sections of O₃⁽¹⁾ at 243±3 K

Reference	Hartley band	Chappuis band	Huggins band	Blue tail of the Chappuis band
<i>Bass and Paur</i>	3.54×10 ⁻¹⁶ -0.2%	–	6.21×10 ⁻²⁰ -1.4%	–
<i>Brion et al.</i>	3.50×10 ⁻¹⁶ -1.1%	–	6.23×10 ⁻²⁰ -1.1%	–
<i>Richter et al.</i>	3.49×10 ⁻¹⁶ -1.4%	6.38×10 ⁻¹⁹ +0.2%	6.28×10 ⁻²⁰ -0.2%	6.90×10 ⁻²⁰ +5.9%
<i>Burrows et al.</i>	3.58×10 ⁻¹⁶ +1.0%	6.44×10 ⁻¹⁹ +2.3%	6.41×10 ⁻²⁰ +1.9%	6.57×10 ⁻²⁰ +0.8%
<i>Voigt et al.</i>	3.59×10 ⁻¹⁶ +1.2%	6.42×10 ⁻¹⁹ +1.3%	6.18×10 ⁻²⁰ -1.8%	6.55×10 ⁻²⁰ +0.4%
<i>Bogumil et al.</i>	3.56×10 ⁻¹⁶ +0.5%	6.36×10 ⁻¹⁹ -0.1%	6.46×10 ⁻²⁰ +2.6%	6.44×10 ⁻²⁰ -1.2%
<i>Burkholder and Talukdar</i>	–	6.17×10 ⁻¹⁹ -3.7%	–	6.13×10 ⁻²⁰ -6.0%
Average value	3.54×10 ⁻¹⁶	6.35×10 ⁻¹⁹	6.30×10 ⁻²⁰	6.52×10 ⁻²⁰
Relative uncertainty	±1.1%	±1.7%	±1.8%	±4.3%

⁽¹⁾ The integrated cross sections are given in units of cm²×nm.

Table 7-3: Integrated absorption cross-sections of O₃⁽¹⁾ at 221±3 K

Reference	Hartley band	Chappuis band	Huggins band	Blue tail of the Chappuis band
<i>Bass and Paur</i>	3.53×10 ⁻¹⁶ ±0.0%	–	5.70×10 ⁻²⁰ –3.4%	–
<i>Brion et al.</i> ⁶	3.50×10 ⁻¹⁶ –1.0%	–	5.65×10 ⁻²⁰ –4.2%	–
<i>Richter et al.</i>	3.47×10 ⁻¹⁶ –1.6%	6.29×10 ⁻¹⁹ –1.0%	6.03×10 ⁻²⁰ +2.3%	6.45×10 ⁻²⁰ +0.6%
<i>Burrows et al.</i>	3.56×10 ⁻¹⁶ +0.7%	6.55×10 ⁻¹⁹ +3.1%	6.16×10 ⁻²⁰ +4.4%	6.55×10 ⁻²⁰ +2.2%
<i>Voigt et al.</i>	3.56×10 ⁻¹⁶ +1.0%	6.45×10 ⁻¹⁹ +1.4%	5.87×10 ⁻²⁰ –0.4%	6.53×10 ⁻²⁰ +1.9%
<i>Bogumil et al.</i>	3.56×10 ⁻¹⁶ +0.8%	6.33×10 ⁻¹⁹ –0.3%	5.96×10 ⁻²⁰ +1.2%	6.54×10 ⁻²⁰ +2.0%
<i>Burkholder and Talukdar</i>	–	6.15×10 ⁻¹⁹ –3.2%	–	5.99×10 ⁻²⁰ –6.5%
Average value	3.53×10 ⁻¹⁶	6.35×10 ⁻¹⁹	5.89×10 ⁻²⁰	6.41×10 ⁻²⁰
Relative uncertainty	±1.1%	±2.4%	±3.3%	±3.7%

⁽¹⁾ The integrated cross sections are given in units of cm²×nm.

⁶ The cross-sections of *Brion et al.* at 218 K cover only the region between 515-650 nm and could therefore not be included in the comparison.

Table 7-4: Integrated absorption cross-sections of O₃⁽¹⁾ at 203±1 K

Reference	Hartley band	Chappuis band	Huggins band	Blue tail of the Chappuis band
<i>Bass and Paur</i>	3.52×10 ⁻¹⁶ -0.3%	–	5.44×10 ⁻²⁰ -3.5%	–
<i>Richter et al.</i>	3.47×10 ⁻¹⁶ -2.0%	6.39×10 ⁻¹⁹ -1.5%	5.75×10 ⁻²⁰ +2.0%	6.79×10 ⁻²⁰ +1.3%
<i>Burrows et al.</i>	3.56×10 ⁻¹⁶ +0.8%	6.62×10 ⁻¹⁹ +2.1%	5.93×10 ⁻²⁰ +5.2%	6.69×10 ⁻²⁰ -0.3%
<i>Voigt et al.</i>	3.56×10 ⁻¹⁶ +0.8%	6.51×10 ⁻¹⁹ +0.4%	5.63×10 ⁻²⁰ -3.5%	6.67×10 ⁻²⁰ -0.5%
<i>Bogumil et al.</i>	3.56×10 ⁻¹⁶ +0.7%	6.42×10 ⁻¹⁹ -1.0%	5.44×10 ⁻²⁰ ±0.0%	6.68×10 ⁻²⁰ -0.4%
Average value	3.53×10 ⁻¹⁶	6.48×10 ⁻¹⁹	5.64×10 ⁻²⁰	6.71×10 ⁻²⁰
Relative uncertainty	±1.2%	±1.6%	±3.7%	±0.8%

⁽¹⁾ The integrated cross sections are given in units of cm²×nm.

At all temperatures, the agreement of the integrated cross-sections in the Hartley band is better than 2%.

The agreement in the Chappuis band is somewhat worse, in particular the integrated cross-sections of *Burkholder and Talukdar* lie systematically below the other measurements by about 3%, and the data of *Burrows et al.* are always higher than the other measurements by about 2%.

In the Huggins bands, the integrated cross-sections scatter by several percent, indicating systematic differences between the available data, and also in the blue tail of the Chappuis band.

In the following tables we will compare the temperature-dependence of the integrated cross-sections for each spectral region.

Again one can state a very good agreement for the Hartley band (less than 2% uncertainty), less good agreement for the Chappuis band (3-4%), and even less agreement for the Huggins bands and the blue tail of the Chappuis band (up to 5%).

Note that within the experimental uncertainties, the integrated cross-sections of the Hartley and Chappuis bands remain constant in the temperature range considered, with less accuracy however for the Chappuis band.

Table 7-5: Integrated cross-sections⁽¹⁾ of O₃ at different temperatures in the Hartley band (245–340 nm)

Reference	295±3 K	276±4 K	243±3 K	221±3 K	203±1 K
<i>Bass and Paur</i>	3.55	3.54	3.54	3.53	3.52
<i>Brion et al.</i>	3.52	–	3.50	3.50	–
<i>Richter et al.</i>	3.53	3.49	3.49	3.47	3.47
<i>Burrows et al.</i>	3.57	3.58	3.58	3.56	3.56
<i>Voigt et al.</i>	3.58	3.57	3.59	3.56	3.56
<i>Bogumil et al.</i>	3.55	3.56	3.56	3.56	3.56
Average value	3.55	3.55	3.54	3.53	3.53
Relative uncertainty	±0.6%	±1.0%	±1.1%	±1.1%	±1.2%

⁽¹⁾ The integrated cross sections are given in units of 10⁻¹⁶ cm²×nm.

Table 7-6: Integrated cross-sections⁽¹⁾ of O₃ at different temperatures in the Huggins bands (325–340 nm)

Reference	295±3 K	276±4 K	243±3 K	221±3 K	203 K
<i>Bass and Paur</i>	8.20	7.27	6.21	5.70	5.44
<i>Brion et al.</i>	8.32	7.16	6.23	5.65	–
<i>Richter et al.</i>	8.25	7.55	6.28	6.03	5.75
<i>Burrows et al.</i>	8.35	7.73	6.41	6.16	5.93
<i>Voigt et al.</i>	8.35	7.31	6.18	5.87	5.63
<i>Bogumil et al.</i>	8.33	7.51	6.46	5.96	5.44
Average value	8.30	7.42	6.30	5.89	5.64
Relative uncertainty	±0.7%	±2.9%	±1.8%	±3.3%	±3.7%

⁽¹⁾ The integrated cross sections are given in units of 10⁻²⁰ cm²×nm.

Table 7-7: Integrated cross-sections⁽¹⁾ of O₃ at different temperatures in the Chappuis band (410–690 nm)

Reference	295±3 K	276±4 K	243±3 K	221±3 K	203 K
<i>Burkholder et al.</i>	6.21	6.20	6.17	6.15	–
<i>Brion et al.</i>	6.29	–	–	–	–
<i>Richter et al.</i>	6.47	6.45	6.38	6.29	6.39
<i>Burrows et al.</i>	6.45	6.58	6.44	6.55	6.62
<i>Voigt et al.</i>	6.42	6.52	6.42	6.45	6.51
<i>Bogumil et al.</i>	6.41	6.43	6.36	6.33	6.42
Average value	6.38	6.44	6.35	6.35	6.48
Relative uncertainty	±1.6%	±2.3%	±1.7%	±2.4%	±1.6%

⁽¹⁾ The integrated cross sections are given in units of 10⁻¹⁹ cm²×nm.

Table 7-8: Integrated cross-sections⁽¹⁾ of O₃ at different temperatures in the blue tail of the Chappuis band (410–520 nm)

Reference	295±3 K	276±4 K	243±3 K	221±3 K	203 K
<i>Burkholder et al.</i>	6.35	6.29	6.13	5.99	–
<i>Brion et al.</i>	6.43	–	–	–	–
<i>Richter et al.</i>	7.23	7.00	6.90	6.45	6.79
<i>Burrows et al.</i>	6.75	6.91	6.57	6.55	6.69
<i>Voigt et al.</i>	6.75	6.77	6.55	6.53	6.67
<i>Bogumil et al.</i>	6.52	6.57	6.44	6.54	6.68
Average value	6.67	6.71	6.52	6.41	6.71
Relative uncertainty	±4.8%	±4.2%	±4.3%	±3.7%	±0.8%

⁽¹⁾ The integrated cross sections are given in units of 10⁻²⁰ cm²×nm.

7.4. Non-linear least-squares fits of the O₃ cross-sections in the Huggins bands at temperatures below ambient: 276±4 K, 243±3 K, 221±3 K, and 203±1 K

In the following tables, we show the results of non-linear least-squares fits of the O₃ cross-sections in the Huggins bands at temperatures below room-temperature. Note that the data of *Brion et al.* are only available down to 218 K

The fits were performed using the same software as used in Section 6.2.3. We will not give individual plots for these fits (total number 19). The results of every fit can be obtained in digital form upon request to the author.

Table 7-9: Non-linear least-squares fits in the Huggins bands at 276±4 K

Reference 1	Reference 2	Shift in nm	Scaling Factor	Scale to Mean
–	<i>Bass and Paur</i>	–	1.000	0.985
<i>Bass and Paur</i>	<i>Brion et al.</i>	–0.027	0.998	0.983
<i>Bass and Paur</i>	<i>Voigt et al.</i>	–0.030	1.040	1.025
<i>Bass and Paur</i>	<i>Richter et al.</i>	–0.007	1.013	0.998
<i>Bass and Paur</i>	<i>Burrows et al.</i>	–0.007	0.989	0.974
<i>Bass and Paur</i>	<i>Bogumil et al.</i>	–0.014	1.050	1.034
Mean: 1.015 ± 0.025				

Table 7-10: Non-linear least-squares fits in the Huggins bands at 243±3 K

Reference 1	Reference 2	Shift in nm	Scaling Factor	Scale to Mean
–	<i>Bass and Paur</i>	–	1.000	0.979
<i>Bass and Paur</i>	<i>Brion et al.</i>	–0.022	0.995	0.974
<i>Bass and Paur</i>	<i>Voigt et al.</i>	–0.032	1.063	1.040
<i>Bass and Paur</i>	<i>Richter et al.</i>	–0.007	1.016	0.994
<i>Bass and Paur</i>	<i>Burrows et al.</i>	–0.007	0.992	0.971
<i>Bass and Paur</i>	<i>Bogumil et al.</i>	–0.017	1.065	1.042
Mean: 1.022 ± 0.034				

Table 7-11: Non-linear least-squares fits in the Huggins bands at 221±3 K

Reference 1	Reference 2	Shift in nm	Scaling Factor	Scale to Mean
–	<i>Bass and Paur</i>	–	1.000	0.973
<i>Bass and Paur</i>	<i>Brion et al.</i>	–0.026	0.992	0.966
<i>Bass and Paur</i>	<i>Voigt et al.</i>	–0.037	1.079	1.050
<i>Bass and Paur</i>	<i>Richter et al.</i>	–0.012	1.018	0.991
<i>Bass and Paur</i>	<i>Burrows et al.</i>	–0.012	0.995	0.969
<i>Bass and Paur</i>	<i>Bogumil et al.</i>	–0.025	1.080	1.051

Mean: 1.027 ± 0.041

Table 7-12: Non-linear least-squares fits in the Huggins bands at 203±1 K

Reference 1	Reference 2	Shift in nm	Scaling Factor	Scale to Mean
–	<i>Bass and Paur</i>	–	1.000	0.949
<i>Bass and Paur</i>	<i>Voigt et al.</i>	–0.047	1.195	1.135
<i>Bass and Paur</i>	<i>Richter et al.</i>	–0.015	1.011	0.960
<i>Bass and Paur</i>	<i>Burrows et al.</i>	–0.015	0.983	0.933
<i>Bass and Paur</i>	<i>Bogumil et al.</i>	–0.021	1.077	1.023

Mean: 1.053 ± 0.087

On the next page, we will provide two tables to summarize the results from the non-linear least-squares fits.

At all temperatures including room temperature, the cross-sections of *Burrows et al.* are the highest, followed by the data of *Bass and Paur*, *Brion et al.*, and *Richter et al.* The cross-sections of *Voigt et al.* and of *Bogumil et al.* are significantly perturbed by baseline drifts (as also observed when comparing the relative temperature dependence, see above). At all temperatures where data are available, the agreement between the cross-sections of *Bass and Paur* and *Brion et al.* is good (better than 0.5%), and both sets of data need only small baseline corrections.

Concerning the wavelength shifts, the results at lower temperatures confirm the observations at room temperature: the wavelength scale of *Brion et al.* is non-linear, and high-order shift-and-squeeze is required for an agreement of better than 0.01 nm. The data of *Bass and Paur* need significant wavelength shifts of 0.03–0.05 nm.

Table 7-13: Relative differences in the cross-sections of O₃ at different temperatures in the Huggins bands (323–343 nm)

Reference 1	Reference 2	295 K	273 K	243 K	223 K	203 K
–	<i>Bass and Paur</i>	1.000	1.000	1.000	1.000	1.000
<i>Bass and Paur</i>	<i>Brion et al.</i>	1.001	0.998	0.995	0.992	–
<i>Bass and Paur</i>	<i>Voigt et al.</i>	0.956	1.040	1.063	1.079	1.195
<i>Bass and Paur</i>	<i>Richter et al.</i>	1.014	1.013	1.016	1.018	1.011
<i>Bass and Paur</i>	<i>Burrows et al.</i>	1.002	0.989	0.992	0.995	0.983
<i>Bass and Paur</i>	<i>Bogumil et al.</i>	1.049	1.050	1.065	1.080	1.077

Table 7-14: Wavelength shifts (in nm) in the cross-sections of O₃ at different temperatures in the Huggins bands (323–343 nm)

Reference 1	Reference 2	295 K	273 K	243 K	223 K	203 K
–	<i>Bass and Paur</i>	0.000	0.000	0.000	0.000	0.000
<i>Bass and Paur</i>	<i>Brion et al.</i>	–0.043	–0.027	–0.022	–0.026	–
<i>Bass and Paur</i>	<i>Voigt et al.</i>	–0.029	–0.030	–0.032	–0.037	–0.047
<i>Bass and Paur</i>	<i>Richter et al.</i>	–0.013	–0.007	–0.007	–0.012	–0.015
<i>Bass and Paur</i>	<i>Burrows et al.</i>	–0.013	–0.007	–0.007	–0.012	–0.015
<i>Bass and Paur</i>	<i>Bogumil et al.</i>	–0.015	–0.014	–0.017	–0.025	–0.021

8. Empirical models for the temperature-dependence of the O₃ cross-sections in the 240–790 nm region

First, we want to point out that from the results of Chapter 7, we concluded that the integrated cross-sections change only significantly in the region of the Huggins bands. This is consistent with the Born-Oppenheimer approximation which is applicable for O₃ since there is no low-lying electronic state that couples the electronic and vibrational wavefunctions for energies corresponding to the temperature range that is considered here 202–300 K. In the Huggins bands, however, the integrated cross-sections become lower with decreasing temperature due to the decreasing absorption of the “red” tail of the Hartley band.

Second, it was concluded that there are relative changes of the spectrum which are observed in the peak region of the Hartley band, in the Huggins bands, and in the Chappuis band. These changes are strongest in the Huggins bands.

The most difficult region is therefore the region of the Huggins bands where two effects are present: an overall decrease of the cross-sections together with strong changes in the differential structure of the bands.

Generally, three different models have been proposed in the past to reproduce the temperature-dependence of the absorption cross-sections of O₃.

- The first model [*Adler-Golden*] uses an exponential function:

$$\sigma(\lambda, T)/\sigma(\lambda, T_0) = c_1(\lambda) \times \exp[-1300/T] + c_2(\lambda)$$

where T is the temperature in K, T₀ is 295 K, and c₁(λ) and c₂(λ) are wavelength-dependent coefficients. The factor 1300 in the exponential term arises from the Boltzmann factor for a vibrational energy of 900 cm⁻¹ which is close to the average energy of the ν₁, ν₂, and ν₃ vibrations of ozone in the electronic ground state. This model was only applied to the temperature-dependence of the O₃ absorption cross-sections in the Hartley band.

- The second model [*Bass and Paur*] use a quadratic polynomial:

$$\sigma(\lambda, T)/\sigma(\lambda, T_0) = c_0(\lambda) + c_1(\lambda) \times T + c_2(\lambda) \times T^2$$

where T is the temperature in K and c₀(λ), c₁(λ), and c₂(λ) are wavelength-dependent coefficients. Although there is no physical interpretation of this model it was concluded by several authors in the past that this function can reproduce the temperature-dependence of the O₃ absorption cross-sections within the experimental uncertainties, even in the Huggins bands.

- The third model [*Voigt et al.*] uses a double exponential function:

$$\sigma(\lambda, T)/\sigma(\lambda, T_0) = c_0(\lambda)/\lambda \times \exp[-c_1(\lambda)/T + c_2(\lambda)*T]$$

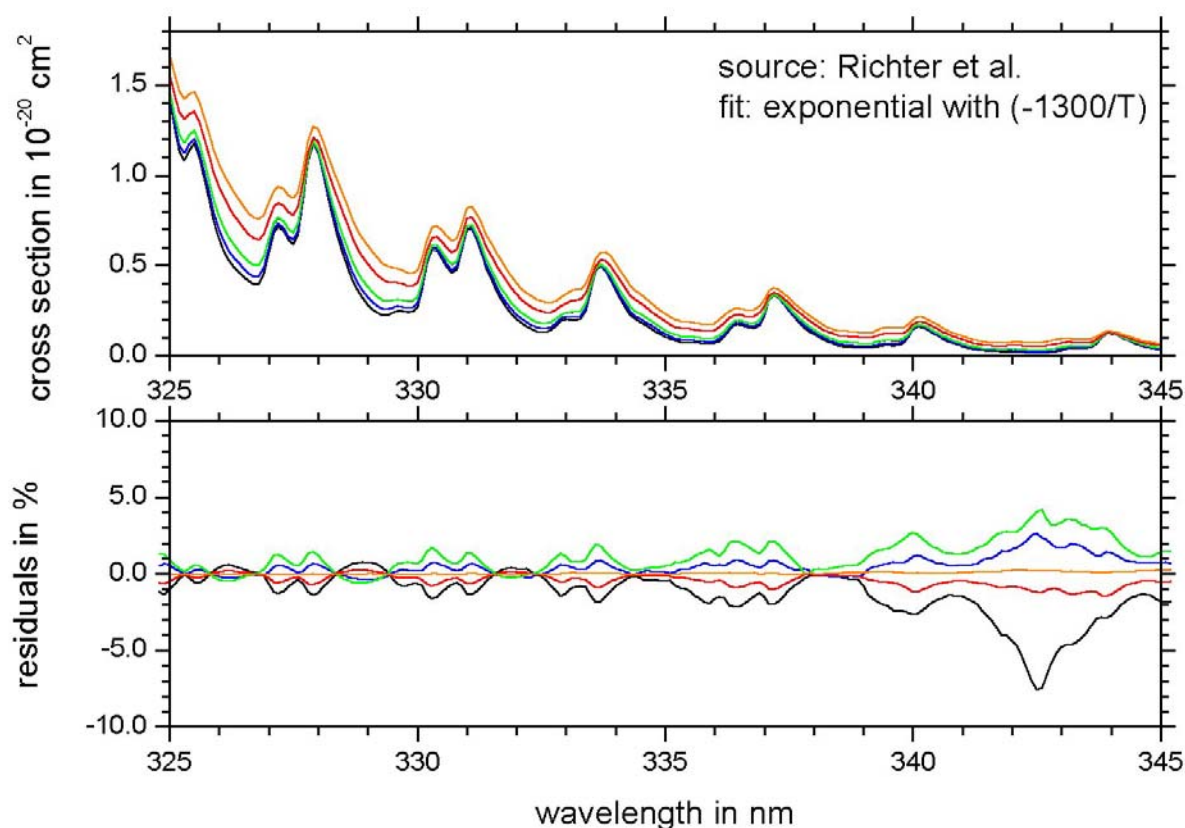
where T is the temperature in K and $c_0(\lambda)$, $c_1(\lambda)$, and $c_2(\lambda)$ are wavelength-dependent coefficients. The latter coefficients are proportional to the temperature-independent transition moment and to the Boltzmann factor of the lower states involved in the transitions.

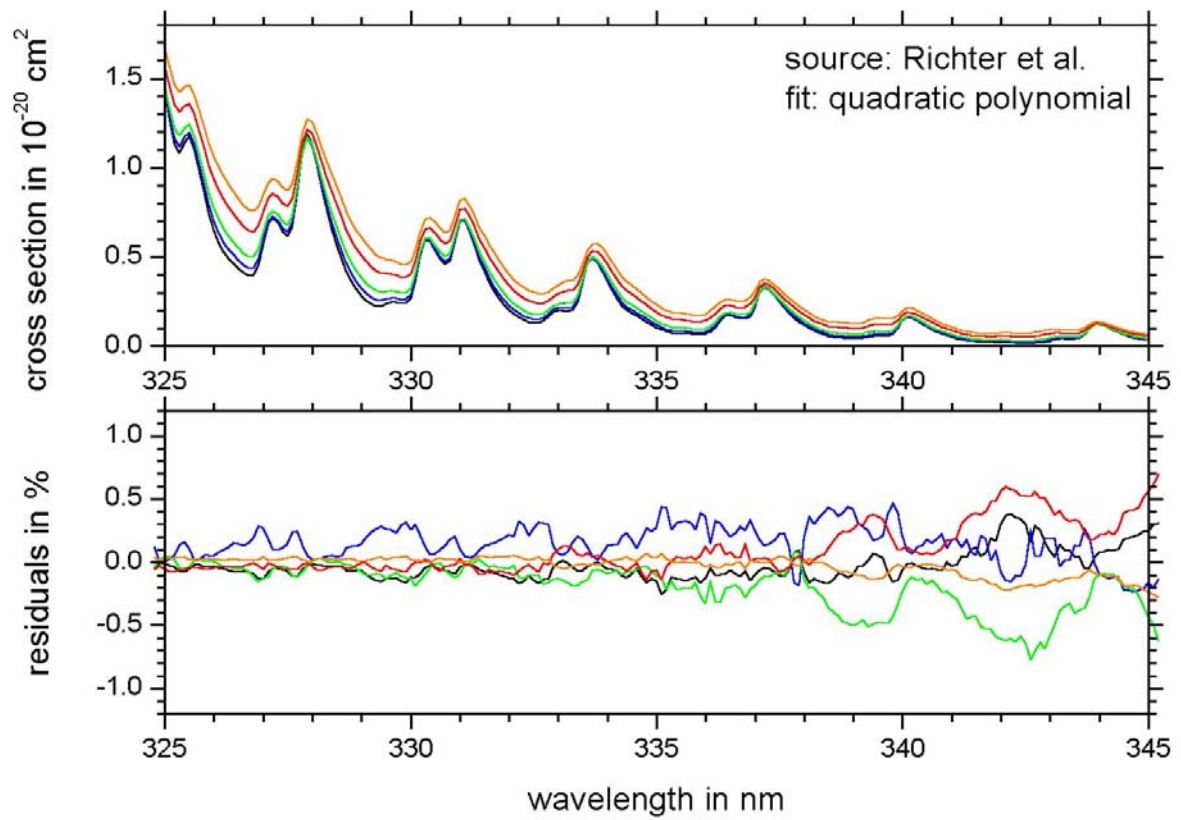
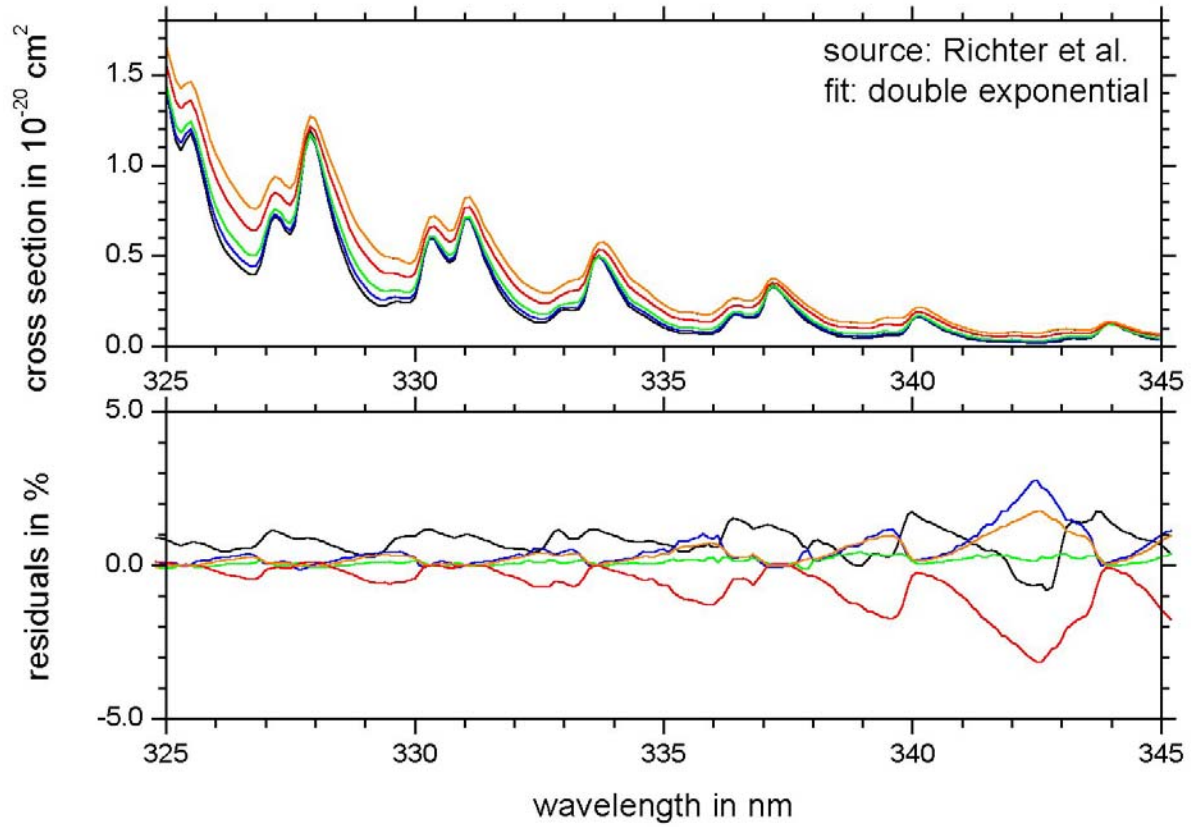
We have investigated the accuracy of the three models using the experimental data of *Richter et al.* Because the effect of temperature is most important in the Huggins bands, we show only the region between 325–345 nm (although the calculations have been performed in the entire region between 240–790 nm). Before the calculations, the experimental data at 5 temperatures were interpolated to a new grid with a spacing of 0.1 nm.

The results are displayed in the three plots below.

One can conclude that the exponential models are both very sensitive to baseline uncertainties, so that the experimental data are better reproduced using a quadratic polynomial. The latter reproduced the experiments to better than 1%.

In the absence of any theoretical model for the temperature-dependence of the O_3 cross-sections, we would therefore recommend to use the quadratic polynomial to interpolate the experimental data for other temperatures.





9. Pressure-dependence of the O₃ cross-sections in the 240–790 nm region

The pressure-dependence of the O₃ absorption cross-sections in the 240–790 nm region was investigated by *Hearn* in the Hartley band and by *Voigt et al.* in the entire region. Both concluded that, within the limits of their experimental uncertainties, there was no effect of total pressure on the O₃ absorption cross-sections.

This is consistent with the theoretical interpretation of the O₃ spectrum in this region. Collisional broadening requires considerably longer timescales (10^{-8} – 10^{-10} s) than the dissociative lifetimes (10^{-12} – 10^{-15} s) of the upper electronic states that are involved in the transitions observed in the 240–790 nm region.

Recently, it has been proposed that a weakly-bound complex of O₂ and O₃ might exist at low temperatures (*Voigt et al.*), and that this complex might absorb at wavelengths between 350–450 nm.

There are a few theoretical and infrared matrix studies on the O₃ dimer (Z. Slanina and L. Adamowicz, *J. Atmos. Chem.* 16, 41, 1993; M. Bahou et al, *J. Chem. Phys.* 114, 4045, 2001).

However, there is no experimental evidence for the presence of these species in the UV-visible cross-sections available for this study.

We conclude that there is no experimental or theoretical support for any pressure dependence of the O₃ cross-sections in the entire spectral region 240–790 nm.

10. Conclusions of the O₃ review

10.1. Influence of spectral resolution and wavelength shifts

In the 240–790 nm region (except between 310–410 nm), the O₃ spectrum changes by less than 1% for wavelength shifts of 0.05 nm or less.

In the 240–790 nm region (except between 310–410 nm), the O₃ spectrum changes by less than 0.2% when the spectrum is convoluted with a Gaussian of 0.1 nm FWHM, and by less than 0.05% when the spectrum is convoluted with a Gaussian of 0.01 nm FWHM.

In the 310–410 nm region, the O₃ spectrum (at spectral resolutions of 0.025 nm or better) changes by up to 20% for wavelength shifts of 0.05 nm and by up to 7% for wavelength shifts of 0.01 nm. In this region (310–410 nm) the changes in the O₃ spectrum for different wavelength shifts are resolution-dependent: For lower resolution (e.g. for the GOME-FM spectra at a spectral resolution of about 0.2 nm) wavelength shifts of 0.05 nm introduce changes in the O₃ spectrum of up to 9% and even shifts of only 0.01 nm still introduce changes of up to 1.5%.

In the 310–410 nm region, the O₃ spectrum changes by up to 9% after convolution with a Gaussian of 0.1 nm FWHM by up to 0.2% after convolution with a Gaussian of 0.01 nm.

10.2. Influence of total pressure

At present, there is no experimental or theoretical support for a pressure dependence of the O₃ cross-sections in the entire spectral region 240–790 nm.

10.3. Room-temperature cross-sections at single wavelengths

At room temperature, the O₃ absorption cross-sections were compared at 10 discrete wavelengths between 253.65–632.82 nm (corresponding to strong Hg-emission or HeNe-laser lines). The results of all available laboratory experiments agree within 0.7–2.0%.

At the wavelengths used for the comparison, the influence of spectral resolution and wavelength shifts is smaller than 1% for the data considered in this review.

The cross-sections of *Bass and Paur* show the smallest deviations from the average values (in the Hartley and Huggins bands).

In the visible, either the cross-sections by *Burkholder and Talukdar* (calibrated using the measurements of *Anderson and Mauersberger*) and by *Brion et al.* are too low by

at least 2%, or all recent broad-band measurements produce systematically too high O₃ cross-sections in the entire Chappuis band.

10.4. Room temperature cross-sections over large spectral regions

At room temperature, comparisons of the available cross-sections over the spectral region 240–790 nm show that the cross-sections agree within better than 2% in the Hartley band (240–310 nm), and within 4% in the Chappuis band (510–650 nm).

In the Huggins bands (310–345 nm), there are important differences (up to 13%) due to wavelength shifts and spectral resolution.

Even larger differences are observed in the regions 340–510 nm and 650–790 nm where the cross-sections are small, probably due to baseline drifts and/or straylight in the experimental data.

10.5. Room temperature integrated cross-sections

At room temperature, the integrated absorption cross-sections of all available experiments agree within 0.6% for the Hartley band (245–340 nm) and within 1.6% for the Chappuis band (410–690 nm).

In the Huggins bands (325–340 nm) the agreement of the integrated absorption cross-sections is 0.7%.

In the blue tail of the Chappuis band (410–520 nm) the agreement is only 4.8%.

10.6. Room temperature cross-sections in the Huggins bands

At room temperature, the available cross-sections in the Huggins bands vary by up to 5%. The data of *Bass and Paur*, *Brion et al.*, and *Burrows et al.* are very close to each other (less than 0.2%) difference and to the average value. The data of *Bass and Paur* and of *Brion et al.* show wavelength shifts of more than 0.02 nm. The data of *Voigt et al.* and of *Bogumil et al.* contain systematic baseline drifts.

In addition to the differences in wavelength calibration and in the cross-section amplitudes, accurate modelling of the instrumental line shapes is required to eliminate systematic residuals when comparing different experiments in this region.

Note that the cross-sections measured with the GOME-FM (*Richter et al.*, *Burrows et al.*) and with the SCIAMACHY-FM (*Bogumil et al.*) are not perfectly reproduced by the convolution of the relevant ILS with laboratory cross-sections measured at higher spectral resolution (*Bass and Paur*, *Brion et al.*, *Voigt et al.*) [K. Bogumil, personal

communication], see Annex A for examples. The remaining residuals are in the order of 10^{-2} which is substantial in regions where weak absorbers have to be detected. This effect is probably due to the limited accuracy of the ILS available for the GOME and SCIAMACHY instruments, and possibly also partly due to the non-linearity of the convolution. Further work is required to elucidate this problem.¹

On the long-wavelength part of the Huggins bands (above 350 nm) the four sets of temperature-dependent cross-sections show large differences due to the small cross sections in this region.

10.7. Temperature dependence of the cross-sections over large spectral regions

There are less measurements of the O₃ cross sections over large spectral regions at temperatures below ambient. Comparing the available data shows systematic differences through the entire region 240–790 nm which are strongest in regions with small cross-sections. There are also significant artefacts around wavelengths where spectra from different measurements had to be concatenated.

The relative change of the cross-sections is small (less than 2%) in the Hartley band, but very strong in the Huggins bands. In the central region of the Chappuis band (550–650 nm), the cross-sections seem to be nearly independent of temperature, but there are discrepancies concerning the temperature-dependence of the cross-sections in the wings of the Chappuis band (400–550 nm and 650–790 nm).

10.8. Temperature dependence of the integrated cross-sections

The Hartley-band integrated cross-sections remain constant in the temperature range 203–293 K, within the experimental uncertainties.

At lower temperatures, the integrated cross-sections in the Huggins bands decrease by more than 30% between 298 K and 203 K. The differential cross-sections increase significantly.

The integrated cross-sections of the Chappuis band also seem to be independent of temperature within the limits of experimental uncertainties, but the agreement between the different sets of data is less satisfactory than for the Hartley and Huggins bands (over 4% differences at all temperatures). The cross-sections of *Burkholder et al.* are always significantly lower (up to 6%) than the other broad-band

¹ It is reported that using the cross-sections of *Bass and Paur* convoluted to GOME FM resolution leads to lower uncertainties and RMS values than using the cross-sections of *Burrows et al.* [K. V. Chance, personal communication, 2001]. This issue needs obviously a more detailed investigation.

measurements (*Richter et al.*, *Burrows et al.*, *Voigt et al.*, and *Bogumil et al.*), as already observed for the cross-sections at room temperature.

10.9. Temperature dependence of the cross-sections in the Huggins bands

At all temperatures, the cross-sections of *Bass and Paur* and *Brion et al.* agree within less than 0.5%. The cross-sections of *Richter et al.* are always smaller than those of *Burrows et al.* by 2.4–2.8%, but both sets agree with those of *Bass and Paur* and of *Brion et al.* within 1.8%. The cross-sections of *Bogumil et al.* and of *Voigt et al.* are always below the others by several percent and show systematic baseline drifts.

The cross-sections of *Bass and Paur* and *Brion et al.* show systematic wavelength shifts of more than 0.01 nm. The cross-sections of *Bass and Paur* contain more noise than the other data.

10.10. Empirical models for the O₃ cross-sections

For modelling the temperature-dependence of the absorption cross-sections in the 240–790 nm region, a quadratic polynomial can reproduce the experimental values within less than 0.5%.

Other models (simple or double exponentials) show larger differences in the Huggins bands (up to 8%), possibly due to their higher sensitivity to baseline drifts.

11. Recommendations for atmospheric remote-sensing

The following recommendations are based on the results of the present report and discussions with scientists involved in laboratory spectroscopy and atmospheric remote-sensing. We want to underline that these recommendation are open for discussion and we wish to encourage all scientists who are concerned to send us their suggestions and questions.

1. **Cross-section standard.** We recommend to establish a standard of temperature-dependent O₃ cross-sections for the region 240–790 nm, based on available laboratory data. We have been informed that the Bureau International des Poids et Mesures in Sèvres (France)¹ and the National Institute for Standards and Technology in Gaithersburg (USA) have started activities to define such a standard. An intermediate solution is however required.^{2,3} We propose to use:

- In the Hartley and Huggins bands: The modified cross-sections of *Bass and Paur* (240–340 nm), which have been corrected for the 1% increase of the cross-sections at 253.65 nm between 298K and 203K. Note that these cross-sections have to be corrected for the wavelength calibration errors (in particular in the Huggins bands). A recent investigation⁴ has led to the conclusion that the *Bass and Paur* cross-sections shall be shifted in the entire spectral region by 0.015 nm, which is probably not sufficiently accurate to achieve an accuracy of better than 0.01 nm in the Huggins bands. But despite of the limited spectral range and the wavelength calibration errors, these cross-sections are well suited because (1) they cover all relevant atmospheric temperatures, (2) they are very close to the average value of all available laboratory data at all temperatures, (3) they have been recorded at sufficiently high resolution, and (4) they show only small systematic errors (baseline drifts) concerning the magnitude of the cross-sections. In addition, they have been indirectly validated through the ground-based measurements of the Dobson and Brewer instruments and the TOMS satellite measurements.

¹ R. Wielgosz, personal communication, 2001.

² The “Quality Assurance Committee” of the International Ozone Association (IOA) recommends the value of $(3000 \pm 30) \text{ l} / (\text{mol} \times \text{cm})$ for the O₃ absorption cross-section at 253.65 nm (this is the value of *Hearn*) [P. Uhlig, personal communication, 2001].

³ The “IUPAC Subcommittee on Gas Kinetic Data Evaluation” recommends the data of *Brion et al.* (*Malicet et al.*) for high-resolution work (<http://www.iupac-kinetic.ch.cam.ac.uk/>). The NASA Panel “Chemical Kinetics and Photochemical Data for Stratospheric Modelling” recommends the evaluation of the WMO Report No.16 (Geneva, 1985), see <http://jpldataeval.jpl.nasa.gov/>. Note that both panels do not focus on reference data for atmospheric remote-sensing.

⁴ K. V. Chance, personal communication, 2000.

Note that the cross-sections of *Brion et al.* – that are available at all temperatures except for the lowest one, 203 K – show very good agreement (differences of less than 1%) with the cross-sections of *Bass and Paur*. In addition, this data set shows smaller wavelength calibration errors and less noise in the long wavelength region (up to 345 nm). For all purposes where cross-sections at the lowest temperature of 203 K are not required, the use of the data of *Brion et al.* is recommended.

- In the long-wavelength part including the Chappuis band (340–790 nm): The cross-sections of *Bogumil et al.* (after calibration of the absolute values to the cross-sections of *Bass and Paur* in the region 320–340 nm). The most significant problems with this data are the limited spectra resolution (which is only important in the region below 410 nm) and the obvious baseline errors in the UV (below 310 nm). However, these cross-sections cover nearly all atmospheric temperatures and show much less systematic baseline errors in the visible than the cross-sections recorded with the GOME (*Richter et al.*, *Burrows et al.*) and with the FTS (*Voigt et al.*). The data of *Burkholder et al.* are always lower than the other available laboratory measurements, are recorded at relatively low spectral resolution, and – as the data of *Brion et al.* – do not extend down to 203 K. There is good agreement between the data of *Bogumil et al.* and *Brion et al.* at the temperatures available for the latter set in the Chappuis band (515–650 nm), better than 1% at 218 K and better than 2% at 295 K.

2. **Using other cross-sections as the standard.** When other cross-sections than the recommended standard set are used (e.g. because of better fitting results using cross-sections recorded with the same instrument as employed for the atmospheric spectra or due to the limited resolution of the propose standard set at wavelengths above 340 nm), it is recommended that these cross-sections be scaled to the standard set in the relevant spectral region (e.g. using a non-linear least-squares fit), and to verify the influence of using other laboratory cross-sections than the standard set on the retrieved O₃ concentrations.

For instance, in the Huggins bands, the data of *Burrows et al.* recorded with the GOME-FM agree very well (differences of less than 1-2%) with the cross-sections of *Bass and Paur* and *Brion et al.* at all available temperatures (203–295 K) and show very high signal/noise ratio in the cross-sections. Therefore, for GOME data analysis, the use of the cross-sections by *Burrows et al.* should lead to the same ozone amounts (within 1–2 % or better) as when using the cross-sections of *Bass and Paur* or *Brion et al.* for the retrieval (besides differences in residuals and

estimated errors).⁵ Note that one has to take into account the fact that the cross-sections of *Burrows et al.* were recorded at a spectral resolution larger than the O₃ absorption features, and that there are small wavelength calibration errors in this data set (similar to those in the data of *Bass and Paur*).

3. **Interpolating the temperature dependence.** It is recommended to use a quadratic polynomial for interpolating cross-sections at different temperatures.⁶
4. **Influence of the Instrumental Line Shape.** We recommend studying in great detail the ILS for the atmospheric instruments, by comparing laboratory spectra recorded with the same instruments with those recorded at high resolution (e.g. *Bass and Paur*, *Brion et al.*, or *Voigt et al.*), after proper convolution and wavelength shifting, in particular in the Huggins bands. As long as the ILS is not known with sufficient accuracy, it might be necessary to use reference spectra recorded with the atmospheric instruments, but the errors introduced by this approach (due to the convolution non-linearity) need to be assessed. This comparison with high-resolution laboratory data should be part of the calibration and characterisation of all atmospheric instruments.
5. **Recording O₃ spectra with the field instruments.** We recommend recording laboratory cross-sections, or at least a few relative absorption spectra, with those instruments that are used for atmospheric remote-sensing, for – at least – one or several relevant temperatures, in order to make these comparisons.
6. **Spectral regions with large cross-section uncertainties.** At all wavelengths above 350 nm, the available laboratory cross-sections show more differences than at shorter wavelengths (up to more than 5%). The blue wing of the Chappuis band is currently used for atmospheric O₃ retrieval from ground. The retrieval should be validated through simultaneous measurements in the UV and visible spectral regions (e.g. in solar or stellar occultation or using satellite instruments), and recommendations on the used cross-section standard should be derived and made available.
7. **New laboratory measurements.** The need for laboratory absorption cross-sections of O₃ in the UV-visible with an absolute accuracy of better than 2% is becoming more and more urgent. We recommend new laboratory high-resolution measurements to be undertaken, in particular focusing on:
 - The absolute values of the O₃ cross-sections in the Huggins bands at all atmospheric temperatures (ca. 190–298 K), in order to validate the

⁵ We would encourage the GOME users to perform such a test using the same cross-sections also for the air mass factor calculations.

⁶ Note however that extrapolation to lower temperatures (e.g. ≤ 200 K) could lead to significant errors.

available standard and to achieve an absolute accuracy of better than 2%. This requires – at least – two independent sets of measurements from different laboratories.

- The temperature dependence (ca. 190–298 K) of the O₃ cross-sections in the wings of the Chappuis band (400–550 nm and 650–790 nm).
- The ratio of the O₃ cross-sections in the Chappuis band and in the Huggins bands (e.g. using simultaneous laboratory measurements in the most relevant spectral regions, 310–350 nm and 400–790 nm), to achieve an absolute accuracy of better than 2% also for the Chappuis band.
- Simultaneous measurements in the UV (Huggins bands), visible (Chappuis band), and mid-infrared (10 μm bands): In the latter spectral region, three independent laboratory measurements of the O₃ absorption coefficients have led to results which are consistent to within 1.8% (J.-M. Flaud, 2001), and the temperature dependence of the infrared absorption coefficients can be predicted with a theoretical model within experimental accuracy.

It is important to stress the fact that an increasing overall accuracy of the atmospheric measurements requires not only the development of better algorithms and more sensitive atmospheric instruments, but also ongoing activities to improve the quality of the laboratory data.

If absolute accuracies of better than 1% for the UV-visible cross-sections of O₃ over large spectra regions are required, one needs many independent laboratory measurements or new experimental techniques to achieve this goal.

Annex A: Influence of the convolution and the ILS in the Huggins bands

In order to give an example of the importance of performing the convolution with the correct ILS, we have used the ILS of SCIAMACHY (as determined by industry during the calibration) to convolute the FTS cross-sections of *Voigt et al.* The resulting cross-sections are compared to those recorded with the SCIAMACHY PFM during the Delta PI-Period (*Bogumil et al.*) at 203 K (upper plot) and at 223 K (lower plot). The residuals are smaller at 223 K but a number of features remain (several %) indicating a non-perfect ILS and/or non-linear effects.

